Model reduction for variational inequalities

Idrissa Niakh

École des Ponts ParisTech

THÈSE DE DOCTORAT
de l'École des Ponts ParisTech

Réduction de modèle pour les inéquations variationnelles

École doctorale N°532, Mathématiques et Sciences et Technologies de l'Information et de la Communication (MSTIC)

Mathématiques Appliquées

Thèse préparée au Centre d'Enseignement et de Recherche en Mathématiques et Calcul Scientifique (CERMICS)

Thèse soutenue le 14 décembre 2022 par
Idrissa NIAKH

Composition du jury:

Franz CHOULY Professeur, Université de Bourgogne	*Examinateur*
Guillaume DROUET Docteur, EDF R&D	*Encadrant industriel*
Virginie EHRLACHER Docteure, ENPC - Université Paris Est	*Co-directrice de thèse*
Alexandre ERN Professeur, ENPC - Université Paris Est	*Directeur de thèse*
Yvon MADAY Professeur, Sorbonne Université	*Examinateur*
Isabelle RAMIÈRE Docteure, CEA Cadarache	*Examinatrice*
Yves RENARD Professeur, INSA de Lyon	*Rapporteur*
Karen VEROY-GREPL Professeure, Eindhoven University of Technology	*Rapportrice*

À ma défunte mère,
à qui tout le mérite revient.

"Toi qui veux acquérir le savoir, révises à chaque fois, à chaque instant..."
Cheikh Ahmadou Bamba

Résumé

Dans cette thèse, nous nous intéressons à la réduction de modèle pour les inéquations variationnelles dépendant d'un paramètre. Dans un premier temps, nous considérons le cas où le problème est formulé par une méthode mixte où la difficulté est que le modèle réduit doit satisfaire une condition de stabilité inf-sup. Pour ce faire, nous avons établi un algorithme glouton, basé sur un résultat théorique, qui permet de construire efficacement un modèle réduit stable. Nous avons également développé une méthode de construction de la base duale permettant de générer un cône de plus grande ouverture. Dans le cas du frottement, des nouveaux résultats concernent l'imposition des contraintes tangentielles dans le modèle réduit par une méthode de collocation. Des résultats numériques sont présentés pour le problème de contact avec et sans frottement, et une première intégration dans le code de calcul industriel `code_aster` a été réalisée pour le cas sans frottement. Dans un deuxième temps, nous étudions la méthode des bases réduites appliquée au problème de contact formulé avec la méthode de Nitsche. Cette méthode, purement primale, conduit à un modèle réduit inefficace en raison de la non-linéarité. Pour pallier ce problème, nous proposons une procédure de réduction de modèle s'appuyant sur la méthode d'interpolation empirique. Des tests numériques confirment la robustesse et l'efficacité de l'approche.

Mot-clés : Inéquations variationnelles, Réduction de modèles, Méthode des bases réduites, Condition inf-sup, Problème de contact, Frottement de Coulomb, Frottement de Tresca, Méthode de Nitsche.

Abstract

In this thesis, we investigate model reduction for parameter-dependent variational inequalities. First, we consider the case where the problem is formulated by a mixed method, where the challenge is that the reduced model must satisfy an inf-sup stability condition. For this purpose, we have devised a new greedy algorithm, based on a theoretical result, which allows to efficiently build a stable reduced model. In addition, we have also devised a method to construct the dual basis leading to a larger aperture. In the case of friction, a new idea deals with the enforcement of the tangential constraints in the reduced model by means of a collocation method. Numerical results are presented for the problem of contact with and without friction. A first integration in the industrial software `code_aster` has been achieved in the frictionless case. In a second step, we study the reduced basis method applied to the contact problem formulated with Nitsche's method. This method, which is purely primal, leads to an inefficient reduced model owing to the nonlinearity in the formulation. To overcome this problem, we propose a model reduction procedure based on the empirical interpolation method. Numerical tests confirm the robustness and efficiency of the approach.

Keywords: Variational Inequalities, Model reduction, Reduced Basis Method, Inf-sup condition, Contact problem, Coulomb friction, Tresca friction, Nitsche's method.

Remerciements

Après trois années de thèse riches d'enseignements qui m'ont permis de réaliser l'un de mes plus précieux rêves, je me dois de témoigner ma profonde gratitude à toutes les personnes qui de près ou de loin l'ont rendu possible.

Naturellement, je commencerais par mon directeur de thèse Alexandre qui a toujours été disponible pour m'orienter et s'est régulièrement intéressé à l'avancée de mes travaux. Son humanisme, sa pédagogie, son expérience, sa pertinence ainsi que ses qualités scientifiques sont beaucoup pour le résultat final de cette thèse. Enfin, je ne pourrais jamais assez le remercier pour tout son investissement afin de me mettre dans les meilleures dispositions pour finir cette thèse.

Au même titre qu'Alexandre, je témoigne ma reconnaissance à Virginie co-directrice de cette thèse qui m'a également accompagné avec beaucoup d'investissement tout au long de ces trois années. Sa capacité d'écoute, ses encouragements, ses qualités humaines, ses compétences scientifiques ainsi que ses brillantes idées sont également beaucoup pour la réalisation de ce travail.

Je tiens particulièrement à remercier Guillaume pour son encadrement industriel. Son recul ainsi que sa vision d'ingénieur m'ont permis de mieux appréhender certains aspects de mon sujet de thèse et d'avancer dans l'implémentation avec `code_aster`. Ses qualités humaines exceptionnelles ainsi que sa capacité à tirer du positif dans toutes les situations m'ont permis de garder la confiance et de surmonter les moments les plus difficiles de cette thèse. Pour cela, je lui témoigne ma reconnaissance absolue.

Mes remerciements vont également à Karen Veroy-Grepl et Yves Renard pour m'avoir fait l'honneur d'accepter d'être rapporteurs de ma thèse. Je remercie également Yvon Maday, Franz Chouly et Isabelle Ramière d'avoir accepté d'être membre de mon jury de thèse.

Je voudrais également remercier Mickaël et Guilhem de leur présence à chacune de mes réunions de comité suivi de thèse. Les discussions ont été importantes dans l'orientation et l'accomplissement de ce travail.

J'ai passé la majeure partie de ces trois années de thèse à EDF R&D et en particulier dans le groupe T6A qui m'a accueilli et parfaitement intégré. Je commencerais par remercier mes collègues doctorants Zouhair et Youri avec qui j'ai démarré cette aventure et qui ont rendu mon séjour à EDF beaucoup plus enthousiasme. Je n'oublierais certainement pas les moments passés à discuter de tout et de rien, les voyages et surtout les séances de blagues avec Eliass. Je tiens également à remercier Hao avec qui j'ai souvent eu des discussions scientifiques très pertinentes entre autres sur la méthode de Nitsche. Mes remerciements vont également à tous les autres doctorants en particulier Ana et Amine, et à tous les membres du groupe T6A que je n'ai pas cité.

Je remercie également l'équipe SERENA de l'INRIA Paris qui m'a accueilli en son sein et m'a fourni un deuxième lieu de travail dans lequel j'ai également passé beaucoup de temps. Je remercie en particulier Zhaonan pour les encouragements et les agréables petites discussions du petit matin.

Je voudrais également remercier l'équipe d'entrainement de Vo Vietnam en particulier le dirigeant Frederic qui m'a encouragé à rejoindre l'équipe et de reprendre le sport. Je regrette que la pandémie ait freiner ma progression parce que j'ai eu beaucoup de plaisir à faire ce sport, à découvrir d'autres cultures et à passer des moments agréables

avec des personnes sympathiques.

Je remercie solennellement tous les membres de ma famille en particulier mon oncle Sidy et mon grand frère Ibra qui ont su toujours être présents et m'encadrer depuis mon enfance afin que je puisse réussir dans mes études et dans ma vie d'une manière générale. Je leur témoigne ma profonde gratitude.

Enfin, je souhaite remercier ma femme Mariama qui a su me soutenir, me supporter et s'occuper de notre famille durant ces dernières années et en particulier ces derniers mois de thèse qui n'ont pas été très faciles. Je n'ai nul doute que sans sa présence à mes côtés cette thèse aurait été très difficile. Merci beaucoup.

CONTENTS

CHAPITRE 1

INTRODUCTION

Dans ce chapitre, nous commençons par exposer le contexte ainsi que les enjeux industriels des travaux présentés dans ce manuscrit. Puis, nous définissons les objectifs de la thèse. Ensuite, nous rappelons le cadre général des inéquations variationnelles puis nous présentons la réduction de modèle d'une manière générale et la méthode des bases réduites en particulier. Pour finir, nous présentons le plan du manuscrit en décrivant les contributions apportées dans chaque chapitre.

Sommaire

1.1 Contexte industriel

La simulation numérique est aujourd'hui un outil incontournable dans le milieu industriel notamment dans les industries de fabrication, de production et de maintenance. Une composante essentielle de la simulation numérique est la modélisation numérique car

elle permet d'établir les modèles utilisés avant d'en réaliser la simulation. De manière générale, les modèles sont souvent très complexes et par conséquent leur simulation nécessite de grosses ressources de calculs afin d'obtenir des résultats en des temps raisonnables. À cette complexité s'ajoute le fait que les modèles dépendent très souvent de plusieurs paramètres qui peuvent être connus ou non. Dans certaines situations, il est nécessaire de simuler ces modèles pour un grand nombre de valeurs du paramètre. Par exemple, dans le cadre de la maintenance, on souhaite connaître l'état des installations en temps réel. Dans ce cas, le temps est considéré comme un paramètre (connu) du modèle. En outre, dans les études réalisées en ingénierie, il est très fréquent de rencontrer des problèmes de calibration de données. Dans ce type d'études, on cherche à trouver la valeur optimale des paramètres de sorte que les résultats des simulations numériques soient aussi proches que possible de résultats expérimentaux. Ce qui nécessite d'évaluer le modèle pour plusieurs valeurs des paramètres.
Dès lors, on voit que dans le contexte de modèles dépendant d'un paramètre, le coût de calcul peut très vite devenir prohibitif. Pour répondre à cette problématique, on distingue globalement deux techniques :

- **Calcul de Haute Performance** : l'idée est d'implémenter les modèles numériques de manière efficace notamment par l'utilisation du calcul parallèle. Cette technique présuppose que l'on dispose de grosses ressources de calculs (supercalculateur) et donc nécessite un gros investissement financier. Ce qui n'est pas toujours possible.

- **Réduction de Modèle** : l'idée est de réduire le coût des calculs en remplaçant le modèle initial dit de haute fidélité par un autre modèle dit d'ordre réduit qui est beaucoup moins coûteux en temps de calcul. Afin d'obtenir le modèle réduit, il est nécessaire de passer par une phase d'apprentissage sur le modèle de haute fidélité. Une fois le modèle réduit mis en place, sa simulation numérique ne nécessite pas de disposer de grosses ressources de calculs.

Dans cette thèse, nous utilisons la technique de réduction de modèle dans le cadre des inéquations variationnelles dépendant de paramètres. Ces inéquations sont présentes dans plusieurs domaines tels que la mécanique, la finance et la biologie [66, 67, 82]. En particulier, on les retrouve dans de nombreux problèmes industriels en mécanique mettant en jeu des phénomènes de contact, de frottement, etc. Par exemple, l'étude de l'étanchéité des assemblages à brides boulonnés est très courant dans les industries du pétrole, du gaz, de l'hydraulique et du nucléaire. Pour s'assurer de l'étanchéité des assemblages boulonnés, on utilise le plus souvent des joints (cf. Figure 1.1). La problématique étudiée dans ce contexte est la tenue de l'étanchéité en situation d'utilisation normale et particulière (par exemple haute pression interne). Dans ce but, on étudie le problème de contact au niveau de la bride (entre la zone en jaune et les zones en bleu et en gris sur la figure) et au niveau des joints (entre les zones en rouge et en bleu, et entre les zones en rouge et en gris). La modélisation du problème de contact conduit à une inéquation variationnelle. Le chargement (pressions interne et externe), le niveau de serrage des joints, les paramètres matériaux, ou encore la géométrie jouent le rôle de paramètres du modèle. Il est clair que pour réaliser une telle étude, il est nécessaire d'évaluer le modèle pour un grand nombre de configurations en tenant compte de la complexité et de la précision nécessaire pour la modélisation au niveau des zones de

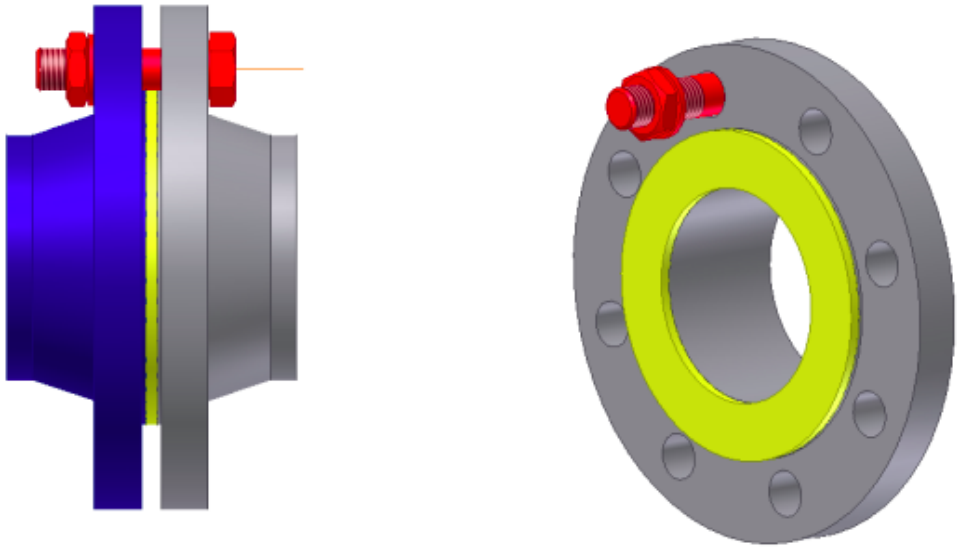

FIGURE 1.1 – Assemblages à brides boulonnés.

contact. D'où l'utilisation de la réduction de modèle pour réaliser une telle étude en temps raisonnable.

1.2 Objectifs

Dans le cadre de la réduction de modèle, les objectifs de la thèse peuvent être regroupés principalement en trois points autour des inéquations variationnelles avec des contraintes qui dépendent de paramètres :

- **Contraintes linéaires** : une méthode souvent utilisée pour la résolution d'inéquations variationnelles est la formulation primale-duale (ou formulation mixte) par le biais du Lagrangien. Notre objectif est de partir de travaux antérieurs sur la réduction de modèle pour les inéquations variationnelles [12, 55, 105] et de les étendre au cas où les contraintes dépendent du paramètre tout en garantissant la stabilité du modèle réduit de manière efficace. Puis, d'intégrer les développements dans le logiciel de simulation numérique d'EDF `code_aster` pour une application au problème de contact sans frottement en hypothèse de petites déformations.

- **Contraintes non-linéaires** : dans le cas du problème de contact en hypothèse de grandes déformations et dans le cas du frottement, en plus de dépendre d'un ou plusieurs paramètres, les contraintes de l'inéquation variationnelle sont non-linéaires. L'objectif ici est de généraliser les travaux réalisés pour le cas linéaire au cas non-linéaire en s'assurant toujours de la stabilité du modèle réduit et de l'efficacité des calculs.

- **Méthode purement primale** : dans `code_aster`, toutes les formulations disponibles pour le problème de contact sont sous la forme primale-duale, ce qui justifie notre intérêt pour l'utilisation de cette formulation. Ces dernières années, des formulations purement primales basées sur la méthode de Nitsche [85] ont reçu une attention croissante afin de formuler le problème de contact avec ou sans frottement en hypothèse de petites et grandes déformations. Contrairement aux méthodes sous forme primale-duale où l'on introduit une nouvelle variable, ces méthodes ne nécessitent d'introduire aucune inconnue supplémentaire. C'est pourquoi elles sont plus simples à mettre en œuvre dans le cadre de la réduction de modèle. En particulier, on ne rencontre pas de problèmes de stabilité du modèle réduit contrairement aux formulations de type primale-duale.

1.3 Inéquations variationnelles

Les inéquations variationnelles se rencontrent dans de nombreux domaines de l'ingénierie. Les fondements de la théorie ont été posés dans [41, 98] dans le cadre des problèmes de contact unilatéraux. Les bases de la théorie mathématique ont été obtenues grâce aux contributions apportées notamment dans [74, 100]. Elles seront ensuite développées au fil des cinquante dernières années grâce à de nombreux travaux [16, 65, 73, 81, 101]. L'approximation des inéquations variationnelles a également fait l'objet de nombreuses études comme par exemple dans [49, 51, 52, 60, 64, 71, 80, 86]. Dans cette thèse, nous nous intéressons particulièrement aux inéquations variationnelles dites elliptiques [20]. Soit $\mathcal{V}$ un espace de Hilbert muni d'un produit scalaire $\langle\cdot,\cdot\rangle_{\mathcal{V}}$ induisant une norme $\|\cdot\|_{\mathcal{V}}$, et soit $\mathcal{K}$ un sous-ensemble de $\mathcal{V}$ non vide, convexe, et fermé. On considère $a : \mathcal{V}\times\mathcal{V}\to\mathbb{R}$, une forme bilinéaire, continue et coercive, *i.e.*,

$$\begin{aligned} \exists C<\infty, \quad |a(u,v)| &\le C\|u\|_{\mathcal{V}}\|v\|_{\mathcal{V}}, \quad \forall u,v\in\mathcal{V},\\ \exists \alpha>0, \quad a(v,v) &\ge \alpha\|v\|^2_{\mathcal{V}}, \qquad \forall v\in\mathcal{V}. \end{aligned} \tag{1.1}$$

Soit $f : \mathcal{V}\to\mathbb{R}$ une forme linéaire continue sur $\mathcal{V}$. On distingue deux types d'inéquations variationnelles :

- **première espèce** : Trouver $u\in\mathcal{K}$ tel que

$$a(u, v-u) \ge f(v-u), \quad \forall v\in\mathcal{K}. \tag{1.2}$$

- **deuxième espèce** : Trouver $u\in\mathcal{K}$ tel que

$$a(u, v-u) + j(v) - j(u) \ge f(v-u), \quad \forall v\in\mathcal{K}, \tag{1.3}$$

où $j : \mathcal{V}\to\bar{\mathbb{R}} := \mathbb{R}\cup\{\pm\infty\}$ est une fonctionnelle convexe, semi-continue inférieurement et propre, *i.e.* ,

$$\begin{aligned} &\forall t\in[0,1], \quad j(tu+(1-t)v) \le tj(u)+(1-t)j(v), \quad \forall u,v\in\mathcal{V},\\ &\text{Si } (v_n)_{n\in\mathbb{N}}\subset\mathcal{K} \text{ converge fortement vers } v\in\mathcal{K}, \text{ alors } \liminf_{n\to+\infty} j(v_n)\ge j(v),\\ &j \text{ non identiquement égale à } +\infty \text{ et } j(v)>-\infty\ \forall v\in\mathcal{V}. \end{aligned} \tag{1.4}$$

1.3.1 Résultats d'existence

On a le résultat d'existence suivant sur les inéquations variationnelles :

Théorème 1.3.1. *Le problème (1.3) admet une unique solution $u \in \mathcal{K}$. De plus, si la forme bilinéaire a est symétrique, alors u est l'unique élément de $\mathcal{K}$ qui minimise la fonctionnelle $J : \mathcal{V} \to \mathbb{R}$ définie par*

$$J(v) := \frac{1}{2}a(v,v) + j(v) - f(v), \quad \forall v \in \mathcal{V}. \tag{1.5}$$

En particulier,

$$\exists! u \in \mathcal{K}, \quad u = \underset{v\in\mathcal{K}}{\operatorname{argmin}}\ J(v). \tag{1.6}$$

Dans le cas d'une inéquation variationnelle de première espèce ($j \equiv 0$), ce résultat est connu sous le nom de théorème de Stampacchia. Pour l'inéquation variationnelle de seconde espèce, une preuve est donnée dans [20, 51].

1.3.2 Formulation duale

Soit $\mathcal{W}$ un espace de Hilbert muni d'un produit scalaire $\langle\cdot,\cdot\rangle_{\mathcal{W}}$ induisant une norme $\|\cdot\|_{\mathcal{W}}$ et $\mathcal{W}^+ \subset \mathcal{W}$ un cône convexe et non vide.

1.3.2.1 Contraintes linéaires

On considère $b : \mathcal{V} \times \mathcal{W} \to \mathbb{R}$ une forme bilinéaire continue et inf-sup stable par rapport à la paire $(\mathcal{V}, \mathcal{W}^+)$, *i.e.*,

$$\begin{aligned} \exists M < \infty, \quad & |b(v,\eta)| \le M\|v\|_{\mathcal{V}}\|\eta\|_{\mathcal{W}}, \\ \exists \beta > 0, \quad & \inf_{v\in\mathcal{V}} \sup_{\eta\in\mathcal{W}^+} \frac{b(v,\eta)}{\|v\|_{\mathcal{V}}\|\eta\|_{\mathcal{W}}} > \beta. \end{aligned} \tag{1.7}$$

Soit $g : \mathcal{W} \to \mathbb{R}$ une forme linéaire continue continue sur $\mathcal{W}$. On suppose que l'ensemble admissible $\mathcal{K}$ s'écrit comme suit :

$$\mathcal{K} := \{v \in \mathcal{V} \mid b(v,\eta) \le g(\eta)\ \forall \eta \in \mathcal{W}^+\}. \tag{1.8}$$

Pour résoudre le problème (1.2), on utilise une formulation mixte. On introduit le Lagrangien $\mathcal{L} : \mathcal{V} \times \mathcal{W}^+ \to \mathbb{R}$ défini par

$$\mathcal{L}(v,\eta) := J(v) + b(v,\eta) - g(\eta), \quad \forall (v,\eta) \in \mathcal{V} \times \mathcal{W}^+. \tag{1.9}$$

Un résultat classique montre que l'inéquation (1.3) est équivalente au problème de point-selle : Trouver $(u,\lambda) \in \mathcal{V} \times \mathcal{W}^+$ tel que

$$(u,\lambda) = \arg \inf_{v\in\mathcal{V}} \sup_{\eta\in\mathcal{W}^+} \mathcal{L}(v,\eta). \tag{1.10}$$

Théorème 1.3.2. *Le problème (1.10) admet une unique solution $(u,\lambda) \in \mathcal{V} \times \mathcal{W}^+$.*

La preuve de l'existence et de l'unicité de la solution est très classique, voir [36, 51, 61, 65]. En écrivant les conditions d'optimalité du premier ordre associées à (1.10), on obtient

$$\begin{cases} a(u,v) + b(v,\lambda) = f(v), & \forall v \in \mathcal{V}, \\ b(u,\eta-\lambda) \leq g(\eta-\lambda), & \forall \eta \in \mathcal{W}^+. \end{cases} \tag{1.11}$$

En prenant $\eta = 0$ et $\eta = 2\lambda$, on trouve $b(u,\lambda) = g(\lambda)$. Par conséquent, (1.11) est équivalent à

$$\begin{cases} a(u,v) + b(v,\lambda) = f(v), & \forall v \in \mathcal{V}, \\ b(u,\eta) \leq g(\eta), & \forall \eta \in \mathcal{W}^+. \end{cases} \tag{1.12}$$

1.3.2.2 Contraintes non-linéaires

On considère une forme $b : \mathcal{V} \times \mathcal{V} \times \mathcal{W} \to \mathbb{R}$ continue, non-linéaire par rapport à sa première variable et qui vérifie qu'il existe $\beta_0 > 0$ tel que pour tout $w \in \mathcal{W}$,

$$\inf_{v\in\mathcal{V}} \sup_{\eta\in\mathcal{W}^+} \frac{b(w;v,\eta)}{\|v\|_{\mathcal{V}}\|\eta\|_{\mathcal{W}}} \geq \beta_0. \tag{1.13}$$

Soit $g : \mathcal{V} \times \mathcal{W} \to \mathbb{R}$ une forme continue et non-linéaire par rapport à sa première variable. On suppose que l'ensemble admissible $\mathcal{K}$ s'écrit

$$\mathcal{K} := \{v \in \mathcal{V} \mid b(v;v,\eta) \leq g(v;\eta)\ \forall \eta \in \mathcal{W}^+\}. \tag{1.14}$$

Le Lagrangien $\mathcal{L} : \mathcal{V} \times \mathcal{V} \times \mathcal{W}^+ \to \mathbb{R}$ associé au problème (1.2) s'écrit comme suit :

$$\mathcal{L}(w;v,\eta) := J(v) + b(w;v,\eta) - g(w;\eta), \quad \forall (w,v,\eta) \in \mathcal{V} \times \mathcal{V} \times \mathcal{W}^+. \tag{1.15}$$

On considère le problème de point-selle : Trouver $(u,\lambda) \in \mathcal{V} \times \mathcal{W}^+$ tel que

$$(u,\lambda) \in \arg \inf_{v\in\mathcal{V}} \sup_{\eta\in\mathcal{W}^+} \mathcal{L}(v;v,\eta). \tag{1.16}$$

Une possibilité pour résoudre ce problème de manière itérative est de linéariser le Lagrangien en utilisant l'algorithme de Kačanov [45]. Concrètement, pour $u^0 \in \mathcal{V}$ donné, on résout à l'itération $k+1$, $k \in \mathbb{N}$, le problème suivant : Trouver $(u^{k+1},\lambda^{k+1}) \in \mathcal{V} \times \mathcal{W}^+$ tel que

$$(u^{k+1},\lambda^{k+1}) = \arg \inf_{v\in\mathcal{V}} \sup_{\eta\in\mathcal{W}^+} \mathcal{L}(u^k;v,\eta). \tag{1.17}$$

1.4 Réduction de modèle

La réduction de modèle consiste à réduire le coût de calcul de la simulation numérique en utilisant des connaissances a priori sur le modèle, soit par simplification du problème soit par la réduction de la complexité du problème lorsque les paramètres varient. Les premières méthodes de réduction de modèle sont issues du domaine de la dynamique des structures [37, 53, 79]. Ces dernières années, elles se sont beaucoup développées dans d'autres domaines tels que la mécanique des milieux continus [23, 91, 97]. Parmi les différentes techniques de réduction de modèle, nous nous intéressons aux méthodes des bases réduites. L'idée générale repose sur l'organisation des calculs en une première

phase dite hors-ligne (`offline`) où des calculs coûteux sont effectués en utilisant le modèle de haute fidélité sur un petit nombre de valeurs du paramètre sélectionné dans un ensemble d'entrainement. Les résultats de ces calculs sont ensuite utilisés pour construire le modèle dit réduit. Puis, dans une deuxième phase dite en-ligne (`online`), un grand nombre de nouvelles valeurs du paramètre sont considérées. Pour ces nouvelles valeurs, le modèle réduit est utilisé à la place du modèle de haute fidélité. On note $\mathcal{D} \subset \mathbb{R}^m$, $m \in \mathbb{N}^*$, le domaine paramétrique et μ le paramètre. Dans le contexte des inéquations variationnelles, nous considérons le problème paramétrique suivant : Pour tout $\mu \in \mathcal{D}$, trouver $(u(\mu), \lambda(\mu)) \in \mathcal{V} \times \mathcal{W}^+$ tel que

$$\begin{cases} a(\mu; u(\mu), v) + b(\mu; v, \lambda(\mu)) = f(\mu; v), & \forall v \in \mathcal{V}, \\ b(\mu; u(\mu), \eta) \leq g(\mu; \eta), & \forall \eta \in \mathcal{W}^+, \end{cases} \tag{1.18}$$

comme problème de haute fidélité. On notera que les formes bilinéaires a et b, ainsi que les formes linéaires f et g, dépendent maintenant du paramètre μ. On suppose que les espaces de haute fidélité $\mathcal{V}$ et $\mathcal{W}$ sont de dimension finie $\mathcal{N}$ et $\mathcal{R}$ respectivement avec

$$\mathcal{V} := \boldsymbol{Span}\Big(\{\varphi_n\}_{n\in\{1:\mathcal{N}\}}\Big), \quad \mathcal{W}^+ := \boldsymbol{Span}^+\Big(\{\psi_r\}_{r\in\{1:\mathcal{R}\}}\Big), \tag{1.19}$$

où $\boldsymbol{Span}$ (resp. $\boldsymbol{Span}^+$) désigne toute combinaison linéaire (resp. à coefficients positifs). Les espaces $\mathcal{V}$ et $\mathcal{W}$ sont typiquement obtenus par discrétisation éléments finis [14, 15, 30, 38] d'espaces de Hilbert.

1.4.1 Méthode des bases réduites

La méthode des bases réduites est une méthode de réduction de modèle où l'on remplace les espaces de haute fidélité (supposés être de grande dimension) par des sous-espaces de petite dimension obtenus en échantillonnant le modèle de haute fidélité. Cette approche a été développée depuis plusieurs décennies ; on pourra citer les travaux pionniers [87, 89], les travaux [76, 90] qui en ont précisé le cadre mathématique, [13] pour des résultats de convergence, et [58, 92] pour deux monographies relativement récentes sur le sujet.

Introduisons la notion de variété de solutions (en anglais, solution manifold) qui désigne l'ensemble des solutions du problème pour tout le domaine paramétrique. On note par $\mathcal{M}^{\mathrm{pr}}$ (resp. $\mathcal{M}^{\mathrm{du}}$) la variété de solutions associée à la variable primale (resp. duale), définies comme suit :

$$\mathcal{M}^{\mathrm{pr}} := \Big\{u(\mu), \quad \forall \mu \in \mathcal{D}\Big\} \subset \mathcal{V}, \tag{1.20a}$$

$$\mathcal{M}^{\mathrm{du}} := \Big\{\lambda(\mu), \quad \forall \mu \in \mathcal{D}\Big\} \subset \mathcal{W}^+ \subset \mathcal{W}. \tag{1.20b}$$

L'objectif est alors de construire (sous-hypothèse d'existence) un sous-espace primal réduit $V_N \subset \mathcal{V}$ de dimension $N \ll \mathcal{N}$ et un sous-cône dual $W_R^+ \subset \mathcal{W}^+$ de dimension $R \ll \mathcal{R}$ qui fournissent des approximations suffisamment précises des variétés de solutions $\mathcal{M}^{\mathrm{pr}}$ et $\mathcal{M}^{\mathrm{du}}$, respectivement. Le problème réduit s'écrit alors : Pour tout $\mu \in \mathcal{D}$, trouver $(u_N(\mu), \lambda_R(\mu)) \in V_N \times W_R^+$ tel que

$$\begin{cases} a(\mu; u_N(\mu), v) + b(\mu; v, \lambda_R(\mu)) = f(\mu; v), & \forall v \in V_N, \\ b(\mu; u_N(\mu), \eta) \leq g(\mu; \eta), & \forall \eta \in W_R^+. \end{cases} \tag{1.21}$$

Soit $\{\xi_n\}_{n\in\{1:N\}} \subset V_N$ et $\{\chi_r\}_{r\in\{1:R\}} \subset W_R^+$ tels que :

$$V_N := \boldsymbol{Span}\Big(\{\xi_n\}_{n\in\{1:N\}}\Big), \quad W_R^+ := \boldsymbol{Span}^+\Big(\{\chi_r\}_{r\in\{1:R\}}\Big). \tag{1.22}$$

On note par $U_N(\mu) = (U_N^n(\mu))_{n\in\{1:N\}} \subset \mathbb{R}^N$ (resp. $\Lambda_R(\mu) = (\Lambda_R^r(\mu))_{r\in\{1:R\}} \subset \mathbb{R}_+^R$) les coordonnées de $u_N(\mu)$ (resp. $\lambda_R(\mu)$) dans la base $\{\xi_n\}_{n\in\{1:N\}}$ (resp. $\{\chi_r\}_{r\in\{1:R\}}$). En supposant les contraintes linéaires, le problème réduit (1.21) peut se réécrire : Pour tout $\mu \in \mathcal{D}$, trouver $(U_N(\mu), \Lambda_R(\mu)) \in \mathbb{R}^N \times \mathbb{R}_+^R$ tel que

$$\begin{cases} A_N(\mu)U_N(\mu) + B_{N,R}(\mu)\Lambda_R(\mu) = F_N(\mu), \\ \qquad\qquad\qquad\qquad B_{N,R}^\top U_N(\mu) \leq G_R(\mu), \end{cases} \tag{1.23}$$

avec les matrices et les vecteurs

$$\begin{aligned} (A_N(\mu))_{nm} &:= a(\mu;\xi_n,\xi_m), \quad F_N^n(\mu) := f(\mu;\xi_n), \quad \forall n,m \in \{1{:}N\} \\ (B_{N,R}(\mu))_{nr} &:= b(\mu;\xi_n,\chi_r), \quad G_R^r(\mu) := g(\mu;\chi_r), \quad n \in \{1{:}N\},\ \forall r \in \{1{:}R\}. \end{aligned} \tag{1.24}$$

À ce stade, la méthode des bases réduites se résume à :

- `Phase offline` : construire les bases réduites primale et duale $\{\xi_n\}_{n\in\{1:N\}}$ et $\{\chi_r\}_{r\in\{1:R\}}$.
- `Phase online` : Pour tout paramètre $\mu \in \mathcal{D}$,
  1. calculer $A_N(\mu)$, $F_N(\mu)$, $B_{N,R}(\mu)$ et $G_R(\mu)$
  2. résoudre le problème (1.23).

On explicitera dans la Section 1.4.2 comment construire dans la phase `offline` les bases réduites primale et duale. Dans la phase `online`, les matrices et vecteurs $A_N(\mu)$, $F_N(\mu)$, $B_{N,R}(\mu)$ et $G_R(\mu)$ sont facilement calculables. En effet, en définissant les matrices

$$Z := \Big[\xi_1 \cdots \xi_N\Big] \in \mathbb{R}^{\mathcal{N}\times N}, \quad Q := \Big[\chi_1 \cdots \chi_R\Big] \in \mathbb{R}_+^{\mathcal{R}\times R}, \tag{1.25}$$

on obtient

$$A_N(\mu) := Z^\top A(\mu) Z, \quad F_N(\mu) := Z^\top F(\mu), \tag{1.26a}$$

$$B_{N,R}(\mu) := Z^\top B(\mu) Q, \quad G_R(\mu) := Q^\top G(\mu), \tag{1.26b}$$

où $A(\mu)$, $F(\mu)$, $B(\mu)$ et $G(\mu)$ sont respectivement les représentants algébriques des opérateurs $a(\mu;\cdot,\cdot)$, $f(\mu;\cdot)$, $b(\mu;\cdot,\cdot)$ et $g(\mu;\cdot)$ dans les espaces de haute fidélité $\mathcal{V}$ et $\mathcal{W}$.

Il est crucial d'obtenir un problème indépendant de la dimension du problème de haute fidélité afin d'obtenir une phase `online` peu coûteuse. Cette condition n'est pas remplie avec le formalisme actuel conduisant à (1.26). Pour satisfaire cette condition, on fait l'hypothèse que les opérateurs $A(\mu)$, $F(\mu)$, $B(\mu)$ et $G(\mu)$ admettent chacun une décomposition (dite affine) de la forme suivante :

$$\begin{aligned} A(\mu) &:= \sum_{s\in\{1:S^a\}} \alpha_s^a(\mu) A^s, \quad F(\mu) := \sum_{s\in\{1:S^f\}} \alpha_s^f(\mu) F^s, \\ B(\mu) &:= \sum_{s\in\{1:S^b\}} \alpha_s^b(\mu) B^s, \quad G(\mu) := \sum_{s\in\{1:S^g\}} \alpha_s^g(\mu) G^s, \end{aligned} \tag{1.27}$$

où pour tout $z \in \{a, f, b, g\}$, $P^z \in \mathbb{N}^*$, $\alpha_s^z : \mathcal{D} \to \mathbb{R}$ dépend uniquement du paramètre et pour tout $s \in \mathbb{N}^*$, $A^s \in \mathbb{R}^{\mathcal{N}\times\mathcal{N}}$, $F^s \in \mathbb{R}^{\mathcal{N}}$, $B^s \in \mathbb{R}^{\mathcal{N}\times\mathcal{R}}$ et $G^s \in \mathbb{R}^{\mathcal{R}}$ sont indépendants du paramètre. L'idée fondamentale se conçoit plus clairement en explicitant les indices des matrices et vecteurs. Par exemple, (1.29a) se réécrit

$$(A_N(\mu))_{nm} = \sum_{s\in\{1:S^a\}} \alpha_s^a(\mu)(A_N^s)_{nm}, \quad \forall n, m \in \{1{:}N\}, \tag{1.28}$$

où le membre de droite a permis de séparer la dépendance en μ de la dépendance en n, m. En remplaçant dans (1.26), on obtient

$$A_N(\mu) = \sum_{s\in\{1:S^a\}} \alpha_s^a(\mu)A_N^s, \qquad A_N^s := Z^\top A^s Z \in \mathbb{R}^{N\times N}, \tag{1.29a}$$

$$F_N(\mu) = \sum_{s\in\{1:S^f\}} \alpha_s^f(\mu)F_N^s, \qquad F^s := Z^\top F^s \in \mathbb{R}^N, \tag{1.29b}$$

$$B_{N,R}(\mu) = \sum_{s\in\{1:S^b\}} \alpha_s^b(\mu)B_{N,R}^s, \quad B_{N,R}^s := Z^\top B^s Q \in \mathbb{R}^{N\times R}, \tag{1.29c}$$

$$G_R(\mu) = \sum_{s\in\{1:S^g\}} \alpha_s^g(\mu)G_R^s, \qquad G_R^s := Q^\top G^s \in \mathbb{R}^R. \tag{1.29d}$$

Avec cette nouvelle formulation, la méthode des bases réduites est organisée comme suit :

- `Phase offline` :
  1. construire les bases réduites primale et duale $\{\xi_n\}_{n\in\{1:N\}}$ et $\{\chi_r\}_{r\in\{1:R\}}$.
  2. calculer les matrices et vecteurs A_N^s, F_N^s, $B_{N,R}^s$ et G_R^s pour tout s.
- `Phase online` : Pour tout paramètre $\mu \in \mathcal{D}$,
  1. évaluer $\alpha_s^a(\mu)$, $\alpha_s^f(\mu)$, $\alpha_s^b(\mu)$ et $\alpha_s^g(\mu)$.
  2. évaluer $A_N(\mu)$, $F_N(\mu)$, $B_{N,R}(\mu)$ et $G_R(\mu)$ en utilisant (1.29).
  3. résoudre le problème (1.23).

Ainsi, grâce à la décomposition affine, le calcul des matrices et vecteurs réduits $A_N(\mu)$, $F_N(\mu)$, $B_{N,R}(\mu)$ et $G_R(\mu)$ ne fait intervenir que les tailles réduites N et R. Ce qui permet de réduire de manière très conséquente le coût des calculs de la phase `online`. Dans le cas où la décomposition affine n'est pas donnée a priori, il existe des techniques permettant de construire une décomposition approchée. Par exemple, on peut citer la méthode d'interpolation empirique (EIM) [10, 75].

1.4.2 Construction des bases réduites

La méthode des bases réduites repose sur l'hypothèse que la variété de solutions peut être approchée par des sous-espaces de faible dimension. Ceci se formalisme en supposant que l'épaisseur de Kolmogorov (en anglais, Kolmogorov n-width) décroît suffisamment vite par rapport à la dimension du sous-espace [13]. On note $d_N(\mathcal{M}^{\mathrm{pr}})$ (resp. $d_R(\mathcal{M}^{\mathrm{du}})$)

l'épaisseur de Kolmogorov d'ordre N (resp. R) de la variété $\mathcal{M}^{\mathrm{pr}}$ (resp. $\mathcal{M}^{\mathrm{du}}$). Ces quantités sont définies comme suit :

$$d_N(\mathcal{M}^{\mathrm{pr}}) := \inf_{\dim(V)=N} \sup_{\mu\in\mathcal{D}} \inf_{v\in V} \|u(\mu) - v\|_{\mathcal{V}}, \tag{1.30a}$$

$$d_R(\mathcal{M}^{\mathrm{du}}) := \inf_{\dim(W^+)=R} \sup_{\mu\in\mathcal{D}} \inf_{\eta\in W^+} \|\lambda(\mu) - \eta\|_{\mathcal{W}}. \tag{1.30b}$$

En théorie, le meilleur sous-espace (resp. sous-cône) approchant $\mathcal{M}^{\mathrm{pr}}$ (resp. $\mathcal{M}^{\mathrm{du}}$) est celui qui réalise le minimum de $d_N(\mathcal{M}^{\mathrm{pr}})$ (resp. $d_R(\mathcal{M}^{\mathrm{du}})$). En pratique, il est souvent très difficile de calculer ce minimiseur. C'est pourquoi pour construire les espaces réduits on utilise d'autres techniques qui permettent de générer les bases réduites. Dans le cas où on dispose d'un estimateur d'erreur *a posteriori* par exemple, il est possible d'utiliser des algorithmes de type glouton [18] pour échantillonner la variété des solutions. Ces algorithmes sont adaptés pour les deux types de base (primale et duale). Outre les algorithmes glouton, il existe d'autres méthodes pour construire des bases réduites. Par exemple, on peut citer entre autres la décomposition orthogonale aux valeurs propres (POD) [54, 69] pour la base primale et l'algorithme glouton de projection conique (CPG) [12] pour la base duale. Ces algorithmes sont brièvement rappelés dans l'appendice B.

1.5 Organisation du manuscrit et contributions

Après ce chapitre introductif, le manuscrit de thèse est principalement composé de trois chapitres techniques (Chapitre 2 à 4). Dans le Chapitre 2, nous traitons la réduction de modèle pour les inéquations variationnelles dépendant d'un paramètre avec des contraintes linéaires dualisées par le biais du Lagrangien. Dans le Chapitre 3, nous utilisons la méthodes des bases réduites pour la réduction du problème de contact avec frottement en formulation mixte. Dans le Chapitre 4, nous appliquons la méthodes des bases réduites au problème de contact avec et sans frottement formulé avec la méthode de Nitsche.

1.5.1 Réduction de modèle pour les inéquations variationnelles avec des contraintes linéaires

La réduction de modèle pour les inéquations variationnelles a déjà fait l'objet de quelques travaux [55, 50, 105]. Dans le Chapitre 2, nous nous intéressons au cas où les contraintes dépendent d'un paramètre et sont formulées par l'introduction de multiplicateurs de Lagrange (stratégie dite primale-duale). Dans ce contexte, l'utilisation de la méthode des bases réduites nécessite une base primale pour la variable primale et une base duale pour la variable duale. Une première possibilité consiste à créer de manière décorrélée les deux bases. C'est par exemple le cas dans [8] où les espaces primal et dual sont échantillonnés par le biais de snapshots calculés en considérant des valeurs du paramètre choisies dans un ensemble d'entraînement, puis la POD est utilisée pour compresser la base primale et la factorisation matricielle non négative (NMF) [72] pour la base duale. Pour la compression de la base duale, des algorithmes de type glouton comme CPG ou "Angle greedy" [55, 19] peuvent être utilisés à la place de la NMF. On peut

également mentionner la méthode d'hyper-réduction utilisée dans [40] pour le problème de contact. Cependant, indépendamment de la méthode de compression utilisée, si la compression des bases primale et duale est faite de manière décorrélée, on ne peut garantir que l'opérateur associé aux contraintes satisfasse une condition de stabilité inf-sup par rapport aux bases réduites primale et duale. Une stratégie visant à garantir la stabilité inf-sup du modèle en enrichissant la base primale en fonction de la base duale par le biais de "supremizers" [9, 2] a été proposée dans [96, 46, 55, 95] dans le cas où les contraintes sont indépendantes du paramètre. Dans cette situation, les supremizers sont aussi indépendants du paramètre de sorte que l'enrichissement peut être réalisé une fois pour toutes dans la phase `offline`. Cependant, dans le cas des contraintes dépendantes du paramètre, les supremizers héritent de cette dépendance de sorte que l'enrichissement doit être réalisé dans la phase `online`. Ce qui diminue considérablement l'efficacité de la phase `online`.

Dans ce contexte, notre principale contribution est une stratégie permettant d'enrichir l'espace primal de façon à garantir la condition de stabilité inf-sup par un espace indépendant du paramètre pouvant être construit une fois pour toutes dans la phase `offline`. De plus, une condition suffisante pour garantir la stabilité inf-sup du modèle réduit est fournie pour les valeurs du paramètre dans l'espace d'entrainement. Une deuxième contribution est une version modifiée de l'algorithme CPG appelée mCPG (en anglais, modified CPG). Cette nouvelle version permet de construire un cône dual avec une plus grande ouverture par rapport à l'algorithme CPG et par conséquent d'obtenir de meilleures propriétés d'approximation de la base duale réduite. Enfin, nous appliquons ces développements au problème de contact sans frottement. Les résultats numériques obtenus sur le problème des sphères de Hertz et d'une membrane avec obstacle confirment l'efficacité de l'approche proposée. Les travaux présentés dans le Chapitre 2 ont fait l'objet d'une publication [84].

1.5.2 Méthode des bases réduites pour le problème de contact avec frottement en formulation mixte

Le Chapitre 3 porte sur la réduction de modèle pour le problème de contact avec frottement (Tresca ou Coulomb). La formulation mathématique du problème conduit à une inéquation variationnelle de seconde espèce. Comme dans le Chapitre 2, nous nous intéressons au cas où le problème est formulé par le biais d'une stratégie primale-duale. La différence principale par rapport au problème de contact sans frottement est que dans le cas du frottement, la formulation mixte conduit à l'introduction de deux multiplicateurs de Lagrange (au lieu d'un) : un multiplicateur associé à la composante normale des efforts de contact et un multiplicateur tangentiel associé à leur composante tangentielle. Dans la littérature, la réduction de modèle pour le problème de contact avec frottement n'est que très peu étudiée. On peut citer quelques travaux existants portant sur l'utilisation de la méthode de décomposition propre généralisée (PGD) et de la méthode LATIN (en anglais, LArge Time INcrement) en mécanique des structures [70, 48, 47]. À notre connaissance, il n'existe pas de travaux sur la méthode des bases réduites appliqués au problème de contact avec frottement.

Notre première contribution est ainsi d'étendre le champ d'application de la méthode des bases réduites au problème de contact avec frottement en formulation mixte.

L'application de la méthode soulève principalement deux difficultés : la stabilité du modèle réduit et le caractère non-linéaire de la formulation duale des contraintes de frottement. Pour traiter le premier point, nous utilisons la stratégie développée dans le Chapitre 2 en stabilisant conjointement la base primale par rapport aux deux bases duales (composantes normale et tangentielle). Pour le deuxième point, nous utilisons une méthode de collocation afin de discrétiser les contraintes associées aux conditions de frottement dans le problème de haute fidélité. Pour le modèle réduit, nous proposons un algorithme permettant d'imposer les contraintes tangentielles en des points de collocation choisis de manière gloutonne dans l'ensemble des points de collocations utilisés pour le modèle de haute fidélité. Comme l'illustre nos résultats numériques, ceci permet de construire un modèle réduit efficace en terme de calcul.

1.5.3 Méthode des bases réduites pour le problème de contact formulé par la méthode de Nitsche

Outre les méthodes mixtes, il existe d'autres méthodes purement primales, *i.e.*, qui ne nécessitent pas l'introduction d'inconnues supplémentaires afin de traiter les inéquations variationnelles en mécanique comme les problèmes de contact avec et sans frottement. L'avantage de ces méthodes est qu'elles conduisent à des problèmes d'optimisation sans contraintes qu'on peut donc résoudre plus facilement. De plus, elles ne nécessitent aucune condition de stabilité inf-sup. Cependant, elles ne permettent pas de garantir le strict respect des conditions de contact et de frottement contrairement aux méthodes mixtes. Comme exemple, on peut citer les méthodes de pénalisation [99]. Dans le Chapitre 4, nous nous intéressons à une approche primale basée sur la méthode de Nitsche [85]. Cette méthode a été originellement introduite pour la reformulation des conditions de Dirichlet dans les problèmes elliptiques. Ces dernières années, la méthode de Nitsche a reçu beaucoup d'attention et a fait l'objet de plusieurs travaux dans le cadre de la reformulation des conditions de contact et de frottement en mécanique. On peut citer les travaux pionniers [27] qui ont permis une première extension de la méthode au problème de contact sans frottement dans le cadre de la méthode des éléments finis ; [24] qui traite le problème de contact avec frottement de Tresca ; [29] qui en présente des versions symétrique et non symétrique ; [77] qui étend la méthode au frottement de Coulomb et aux grandes déformations ; [25] qui fournit une application au cas d'une discrétisation non conforme d'ordre élevé ; [28] qui fournit des résultats d'existence pour le problème de contact avec frottement de Coulomb dans le cadre des formulations éléments finis statique et dynamique. La caractéristique principale de la méthode de Nitsche est qu'elle est consistante contrairement aux méthodes de pénalisation classiques. À notre connaissance, il n'existe aucun travail sur la réduction de modèle pour le problème de contact avec ou sans frottement formulé avec la méthode de Nitsche.

Notre première contribution est ainsi d'appliquer la méthode des bases réduites au problème de contact formulé par la méthode de Nitsche. La difficulté principale est que la méthode des bases réduites classique conduit à un modèle réduit inefficace à cause du caractère non-linéaire de la formulation de Nitsche (même en petites déformations). Pour pallier ce problème, nous proposons de combiner la méthode des bases réduites et la méthode d'interpolation empirique (EIM) brièvement décrite ci-dessus. Nous

effectuons également une comparaison des approches Nitsche et mixte en termes de précision et d'efficacité.

1.5.4 Développements informatiques

Dans `code_aster`, toutes les méthodes de résolution du problème de contact avec frottement et sans frottement sont actuellement en formulation primale-duale. Avant cette thèse, il n'existait aucune méthode de réduction de modèle pour le problème de contact avec ou sans frottement. Plusieurs mois de la thèse ont été dédiés à la prise en main de `code_aster` et à l'intégration de la méthode de réduction de modèle développée dans la thèse d'Amina Benaceur [11] et appliquée au problème de contact sans frottement en grandes déformations. Ces premiers développements ont permis de munir `code_aster` de sa première méthode de réduction de modèle pour le problème de contact sans frottement. Ce travail a été réalisé après une appropriation et une adaptation des développements de [12] en levant les différentes contraintes liées au caractère industriel de `code_aster`.

Le développement informatique des méthodes introduites dans les Chapitres 2 et 3 a également été réalisé dans une maquette python combinée avec la bibliothèque éléments finis `FreeFEM` [56]. Ce choix a été fait dans l'optique d'avancer plus rapidement dans la validation de ces méthodes tenant compte des contraintes présentes dans `code_aster`. Une intégration de ces développements dans `code_aster` est en cours. En particulier, la méthode d'enrichissement dite `online` est maintenant complètement intégrée.

Dans `code_aster`, la méthode de Nitsche n'est pas encore disponible. Une implémentation de la méthode est prévue dans la nouvelle architecture du code. Les développements informatiques du Chapitre 4 portant sur la méthode de Nitsche pour le contact sont donc réalisés en python avec l'utilisation de la bibliothèque élément finis `getfem` [93] qui est parfaitement adaptée à la méthode de Nitsche. Une partie des développements sont issus du stage de Yoan Gorschka encadré par l'auteur du manuscrit.

CHAPTER 2

STABLE MODEL REDUCTION FOR LINEAR VARIATIONAL INEQUALITIES WITH PARAMETER-DEPENDENT CONSTRAINTS

Abstract

We consider model reduction for linear variational inequalities with parameter-dependent constraints. We study the stability of the reduced problem in the context of a dualized formulation of the constraints using Lagrange multipliers. Our main result is an algorithm that guarantees inf-sup stability of the reduced problem. The algorithm is computationally effective since it can be performed in the offline phase even for parameter-dependent constraints. Moreover, we also propose a modification of the Cone Projected Greedy algorithm so as to avoid ill-conditioning issues when manipulating the reduced dual basis. Our results are illustrated numerically on the frictionless Hertz contact problem between two half-disks with parameter-dependent radius and on the membrane obstacle problem with parameter-dependent obstacle geometry.

The contents of this chapter have been published in [84].

Contents

2.1 Introduction

Model reduction is a method for reducing computational costs by approximating a high-fidelity (HF) parameter-dependent model that is computationally expensive by another model that is much cheaper to solve; see [79, 90, 76, 102, 3, 21] and the more recent textbooks [58, 92]. The principle is to organize the calculations in a first offline phase which is a learning phase where expensive calculations are carried out on the HF model for a small number of values of the parameter drawn from a training set. The output of the offline phase is used to build the reduced-order model. Then, in the online phase, a large number of new instances of the parameter are considered for which the reduced model is solved instead of the HF model. Such studies are often carried out, for example, in the context of model calibration, where the aim is to find the optimal value for certain parameters so that the results of numerical simulations are as close as possible to those of the experiments.

The work developed herein is concerned with model reduction for linear parameter-dependent variational inequalities [55, 50, 105]. These inequalities are, for instance, encountered in several problems in computational mechanics [67]. As example of applications, we will study the frictionless Hertz contact problem [57, 103] and the membrane obstacle problem [42, 43, 65, 78, 51]. We are particularly interested in the case where the problem is formulated by introducing Lagrange multipliers. This formulation leads to a so-called primal-dual strategy, whereby reduced bases are created for both the primal and the dual variables.

A first possibility in the primal-dual context is to generate the reduced primal and dual bases in a decorrelated manner. This is for instance the case in [8] where, after sampling pairs of primal and dual solutions for parameter values taken from a training set, the Proper Orthogonal Decomposition (POD) [22, 69] is used to compress the primal basis and a Non-negative Matrix Factorization (NMF) [72] is used to compress the dual basis. Let us also mention [40] where a hypereduction method for contact problems is proposed. Instead of the NMF, one can also consider the Angle Greedy [55, 19] and the Cone Projected Greedy (CPG) [12] algorithms for the compression of the dual basis. However, whatever the compression technique, if the primal and dual reduced bases are generated in a decorrelated way, the stability of the reduced problem is not guaranteed a priori. Specifically, it cannot be guaranteed that the resulting reduced bases are such that the operator associated with the constraint satisfies an inf-sup condition for the reduced primal and dual spaces.

In order to satisfy this inf-sup condition, a strategy for constructing the reduced primal basis according to the reduced dual basis has been proposed in [96, 46, 55, 95] in various contexts. The idea is to complete the reduced primal basis with as many functions as there are in the reduced dual basis, each of these functions being determined by a maximization problem in order to control the corresponding element of the reduced dual basis. These functions are often called supremizers; see, e.g., [9, 2]. In the case where the constraints are parameter-independent (which is the case in the above references), the completion of the reduced primal basis can be calculated only once in

the offline phase. However, in the case where the constraints are parameter-dependent, the supremizers become parameter-dependent so that the reduced primal space has to be constructed during the online phase. This considerably reduces the efficiency of the online phase. An example of this situation is the Hertz frictionless contact problem between two spheres, even under the assumption of small deformations, when the radius of one of the spheres depends on the parameter.

In this paper, we propose a strategy to approximate the parameter-dependent primal space ensuring inf-sup stability by a parameter-independent space. This latter space can thus be constructed only once in the offline phase. In addition, we establish a criterion to be checked during the construction in the offline phase so as to guarantee uniform inf-sup stability condition for the reduced problem (at least for all the parameters in the training set). We notice that an algorithm to build supremizers in the context of parameter-dependent constraints has also been devised in [32]; we discuss below the differences between this contribution and the present one.

A second, distinct contribution of the present work is a modified version of the CPG algorithm to build a cone with a wider aperture. The motivation is to achieve better approximation properties compared to the ones provided by the plain CPG algorithm. In our numerical experiments, this modification turned out to be instrumental in order to avoid ill-conditioning issues when manipulating the reduced dual basis. Another algorithm to enhance the aperture of a given cone has been recently devised in [7]; we discuss below the differences between this contribution and the present one.

The rest of this paper is organized as follows. In Section 2.2, we introduce the mathematical framework for parameter-dependent variational inequalities. Then, we formulate the reduced model in the standard cases where the reduced primal basis is decorrelated from the reduced dual basis or enriched by parameter-dependent supremizers to be computed online. In Section 2.3, we present our main result, namely the strategy to achieve stability by enriching the primal basis in the offline phase. In Section 2.4, we describe the new version of the CPG algorithm to enhance the aperture of the cone associated with the reduced dual basis. In Section 2.5, numerical results illustrating the efficiency of our approach are reported for the frictionless Hertz contact problem between two half-disks with parameter-dependent radius and the membrane obstacle problem with parameter-dependent obstacle geometry. In future work, we plan to extend our work to the case of nonlinear problems such as the contact problem under large deformations and the contact problem with Coulomb friction.

2.2 Setting

2.2.1 High-fidelity model

Let $\mathcal{V}$ and $\mathcal{W}$ be two finite-dimensional high-fidelity (HF) subspaces typically resulting from the finite element discretization of some Hilbert spaces. We denote by $\langle\cdot,\cdot\rangle_{\mathcal{V}}$ (resp. $\langle\cdot,\cdot\rangle_{\mathcal{W}}$) the inner product equipping $\mathcal{V}$ (resp. $\mathcal{W}$) and inducing the norm $\|\cdot\|_{\mathcal{V}}$ (resp. $\|\cdot\|_{\mathcal{W}}$). We denote by $\mathcal{V}'$ the dual space of $\mathcal{V}$ equipped with the duality product $\langle\cdot,\cdot\rangle_{\mathcal{V}',\mathcal{V}}$, and by $\|\cdot\|_{\mathcal{V}'}$ the associated norm. Let $\mathcal{W}^+ \subset \mathcal{W}$ be a positive cone containing 0. Let $\mathcal{D} \subset \mathbb{R}^m, m \in \mathbb{N}^* := \mathbb{N} \setminus \{0\}$, be the parameter domain. We consider two uniformly bounded bilinear forms $a(\mu;\cdot,\cdot) : \mathcal{V} \times \mathcal{V} \to \mathbb{R}$ and $b(\mu;\cdot,\cdot) : \mathcal{V} \times \mathcal{W} \to \mathbb{R}$ for

all $\mu \in \mathcal{D}$, and two uniformly bounded linear forms $f(\mu;\cdot) : \mathcal{V} \to \mathbb{R}$ and $g(\mu;\cdot) : \mathcal{W} \to \mathbb{R}$ for all $\mu \in \mathcal{D}$. We assume that $a(\mu;\cdot,\cdot)$ is symmetric and uniformly coercive for all $\mu \in \mathcal{D}$. We consider the following well-posed constrained minimization problem: For all $\mu \in \mathcal{D}$, find $u(\mu) \in \mathcal{V}$ such that

$$u(\mu) = \underset{v \in \mathcal{K}(\mu)}{\operatorname{argmin}} \frac{1}{2} a(\mu; v, v) - f(\mu; v), \tag{2.1}$$

where the admissible set is defined as

$$\mathcal{K}(\mu) := \Big\{ v \in \mathcal{V} \;\Big|\; b(\mu; v, \eta) \leq g(\mu; \eta), \quad \forall \eta \in \mathcal{W}^+ \Big\}, \tag{2.2}$$

and is assumed to be non-empty for all $\mu \in \mathcal{D}$.

We denote the boundedness and inf-sup stability coefficients of the bilinear form $b(\mu;\cdot,\cdot)$ with respect to the high-fidelity pair $\left(\mathcal{V}, \mathcal{W}^+\right)$ as follows:

$$c_{\mathrm{HF}}(\mu) := \sup_{\eta \in \mathcal{W}^+} \sup_{v \in \mathcal{V}} \frac{b(\mu; v, \eta)}{\|v\|_{\mathcal{V}} \|\eta\|_{\mathcal{W}}}, \qquad \beta_{\mathrm{HF}}(\mu) := \inf_{\eta \in \mathcal{W}^+} \sup_{v \in \mathcal{V}} \frac{b(\mu; v, \eta)}{\|v\|_{\mathcal{V}} \|\eta\|_{\mathcal{W}}}. \tag{2.3}$$

By the above assumption on $b(\mu;\cdot,\cdot)$, there exists a real number C_0 such that $c_{\mathrm{HF}}(\mu) \leq C_0$ for all $\mu \in \mathcal{D}$, and we additionally assume that the HF pair $\left(\mathcal{V}, \mathcal{W}^+\right)$ is such that

$$\exists \beta_0 > 0, \quad \forall \mu \in \mathcal{D}, \quad \beta_{\mathrm{HF}}(\mu) \geq \beta_0 > 0. \tag{2.4}$$

One possibility to solve the optimization problem (2.1) is to use a dual formulation. Let $\mathcal{L}(\mu;\cdot,\cdot) : \mathcal{V} \times \mathcal{W}^+ \to \mathbb{R}$ be the Lagrangian associated with (2.1) and defined as follows: For all $\mu \in \mathcal{D}$,

$$\mathcal{L}(\mu; v, \eta) := \frac{1}{2} a(\mu; v, v) - f(\mu; v) + b(\mu; v, \eta) - g(\mu; \eta), \quad \forall\, (v, \eta) \in \mathcal{V} \times \mathcal{W}^+. \tag{2.5}$$

Then, for all $\mu \in \mathcal{D}$, we can rewrite (2.1) as the following saddle-point problem: Find $\left(u(\mu), \lambda(\mu)\right) \in \mathcal{V} \times \mathcal{W}^+$ such that

$$\left(u(\mu), \lambda(\mu)\right) = \arg \min_{v \in \mathcal{V}} \max_{\eta \in \mathcal{W}^+} \mathcal{L}(\mu; v, \eta). \tag{2.6}$$

Owing to the above assumptions (in particular (2.4) and the coercivity of $a(\mu;\cdot,\cdot)$), the pair $\left(u(\mu), \lambda(\mu)\right) \in \mathcal{V} \times \mathcal{W}^+$ is uniquely defined and can be found as the critical point of the Lagrangian $\mathcal{L}(\mu;\cdot,\cdot)$ by solving for all $\mu \in \mathcal{D}$,

$$\begin{cases} a(\mu; u(\mu), v) + b(\mu; v, \lambda(\mu)) = f(\mu; v), & \forall v \in \mathcal{V}, \\ b(\mu; u(\mu), \eta) \leq g(\mu; \eta), & \forall \eta \in \mathcal{W}^+. \end{cases} \tag{2.7}$$

2.2.2 Decorrelated model reduction

Let $P \in \mathbb{N}^*$ and consider a family $\{(u(\mu_p), \lambda(\mu_p))\}_{p \in \{1:P\}} \subset \mathcal{V} \times \mathcal{W}^+$ of solutions to (2.7) which are computed by using a training subset $\mathcal{D}_{\texttt{train}} := \{\mu_p\}_{p \in \{1:P\}} \subset \mathcal{D}$ of cardinality

P. In practice, the sampling of the parameter domain can be driven by a posteriori error estimates, as in [55, 5, 105]. Let us set

$$V := \boldsymbol{Span}\Big(\{u(\mu_p)\}_{p\in\{1:P\}}\Big) \subset \mathcal{V}, \qquad W^+ := \boldsymbol{Span}^+\Big(\{\lambda(\mu_p)\}_{p\in\{1:P\}}\Big) \subset \mathcal{W}^+, \quad (2.8)$$

where, for an arbitrary family $\{\theta_q\}_{q\in\{1:Q\}} \subset \mathcal{W}^+$ with $Q \in \mathbb{N}^*$, $\boldsymbol{Span}^+$ denotes the positive cone generated by setting

$$\boldsymbol{Span}^+\Big(\{\theta_q\}_{q\in\{1:Q\}}\Big) := \left\{ \sum_{q\in\{1:Q\}} \alpha_q\theta_q,\ (\alpha_1,\cdots,\alpha_Q) \in \mathbb{R}^Q_+ \right\}. \quad (2.9)$$

Given a positive real number $\delta_{\texttt{POD}} > 0$, one can construct using POD an orthonormal family of $N \in \mathbb{N}^*$ ($N \le P$) elements of V,

$$\{v_n\}_{n\in\{1:N\}} := \texttt{POD}\Big(\{u(\mu_p)\}_{p\in\{1:P\}};\ \mathcal{V},\ \delta_{\texttt{POD}}\Big),$$

such that

$$V_N := \boldsymbol{Span}\Big(\{v_n\}_{n\in\{1:N\}}\Big) \subset V, \quad (2.10)$$

$$e_{\texttt{POD}}(N) := \frac{\left(\sum\limits_{p\in\{1:P\}} \|\Big(\mathbb{I}^{\mathcal{V}} - \Pi^{\mathcal{V}}_{V_N}\Big)(u(\mu_p))\|^2_{\mathcal{V}}\right)^{\frac{1}{2}}}{\left(\sum\limits_{p\in\{1:P\}} \|u(\mu_p)\|^2_{\mathcal{V}}\right)^{\frac{1}{2}}} \le \delta_{\texttt{POD}}, \quad (2.11)$$

where $\Pi^{\mathcal{H}}_Z$ denotes the projection onto a generic closed convex subset Z of the generic Hilbert space $\mathcal{H}$ ($\Pi^{\mathcal{H}}_Z$ is the orthogonal projection if $\mathcal{Z}$ is a linear subspace) and $\mathbb{I}^{\mathcal{H}}$ denotes the identity operator in $\mathcal{H}$. Moreover, given a positive real number $\delta_{\texttt{CPG}} > 0$, one can construct using the CPG algorithm a subset $\{\chi_r\}_{r\in\{1:R\}}$ of $\{\lambda(\mu_p)\}_{p\in\{1:P\}}$ composed of $R \in \mathbb{N}^*$ ($R \le P$) vectors of W^+,

$$\{\chi_r\}_{r\in\{1:R\}} := \texttt{CPG}\Big(\{\lambda(\mu_p)\}_{p\in\{1:P\}};\ \mathcal{W},\ \delta_{\texttt{CPG}}\Big),$$

satisfying

$$W^+_R := \boldsymbol{Span}^+\Big(\{\chi_r\}_{r\in\{1:R\}}\Big) \subset W^+, \quad (2.12)$$

$$e_{\texttt{CPG}}(R) := \frac{\max\limits_{p\in\{1:P\}} \|\Big(\mathbb{I}^{\mathcal{W}} - \Pi^{\mathcal{W}}_{W^+_R}\Big)(\lambda(\mu_p))\|_{\mathcal{W}}}{\max\limits_{p\in\{1:P\}} \|\lambda(\mu_p)\|_{\mathcal{W}}} \le \delta_{\texttt{CPG}}. \quad (2.13)$$

For all $\mu \in \mathcal{D}$ and $N, R \le P$, we define

$$\beta^{\text{dec}}_{N,R}(\mu) := \inf_{\eta\in W^+_R} \sup_{v\in V_N} \frac{b(\mu; v, \eta)}{\|v\|_{\mathcal{V}}\|\eta\|_{\mathcal{W}}}, \quad (2.14)$$

where the superscript refers to the decorrelated construction of the reduced bases. Since the primal reduced space V_N and the dual reduced cone W^+_R are constructed in a decorrelated manner, one cannot guarantee that $\beta^{\text{dec}}_{N,R}(\mu) > 0$ for all $\mu \in \mathcal{D}$, *i.e.*, the pair (V_N, W^+_R) may not satisfy an inf-sup condition.

2.2.3 Online enhancement of the reduced primal basis

A strategy for enriching the reduced primal basis in order to achieve inf-sup stability has been proposed in [96, 46, 55, 95]. The idea is to complete the reduced primal basis $\{v_n\}_{n\in\{1:N\}}$ with as many functions as there are in the reduced dual basis $\{\chi_r\}_{r\in\{1:R\}}$. To this purpose, one proceeds as follows: For all μ in $\mathcal{D}$, one defines the operator $\mathbb{T}(\mu) : \mathcal{W}^+ \to \mathcal{V}$ such that

$$\mathbb{T}(\mu) := J \circ \mathcal{B}_{\mathrm{HF}}(\mu), \tag{2.15}$$

where $J : \mathcal{V}' \to \mathcal{V}$ is the Riesz isomorphism between $\mathcal{V}'$ and $\mathcal{V}$ and where the operator $\mathcal{B}_{\mathrm{HF}}(\mu) : \mathcal{W}^+ \to \mathcal{V}'$ is defined such that

$$\langle \mathcal{B}_{\mathrm{HF}}(\mu)(\eta), v\rangle_{\mathcal{V}',\mathcal{V}} := b(\mu; v, \eta), \quad \forall (v,\eta) \in \mathcal{V}\times\mathcal{W}^+. \tag{2.16}$$

Then, for all $\mu \in \mathcal{D}$, the enriched reduced primal space $V^{\mathrm{on}}_{N,R}(\mu)$ is defined as

$$V^{\mathrm{on}}_{N,R}(\mu) := V_N + S_R(\mu) \subset \mathcal{V}, \quad S_R(\mu) := \boldsymbol{Span}\Big(\{\mathbb{T}(\mu)\chi_r\}_{r\in\{1:R\}}\Big). \tag{2.17}$$

The superscript refers to the online construction of the enriched basis. The main motivation for (2.17) is that it ensures that the bilinear form $b(\mu;\cdot,\cdot)$ is uniformly inf-sup stable with respect to the pair $\Big(V^{\mathrm{on}}_{N,R}(\mu), W^+_R\Big)$, *i.e.*, we have

$$\forall \mu \in \mathcal{D}, \quad \beta^{\mathrm{on}}_{N,R}(\mu) := \inf_{\eta\in W^+_R} \sup_{v\in V^{\mathrm{on}}_{N,R}(\mu)} \frac{b(\mu; v, \eta)}{\|v\|_{\mathcal{V}}\|\eta\|_{\mathcal{W}}} \geq \beta_{\mathrm{HF}}(\mu) \geq \beta_0 > 0. \tag{2.18}$$

Indeed, for all $\eta \in W^+_R$, we have

$$\begin{aligned}\sup_{v\in V^{\mathrm{on}}_{N,R}(\mu)} \frac{b(\mu; v, \eta)}{\|v\|_{\mathcal{V}}} &\geq \frac{b(\mu; \mathbb{T}(\mu)(\eta), \eta)}{\|\mathbb{T}(\mu)(\eta)\|_{\mathcal{V}}} = \frac{\|\mathbb{T}(\mu)(\eta)\|^2_{\mathcal{V}}}{\|\mathbb{T}(\mu)(\eta)\|_{\mathcal{V}}} = \|\mathbb{T}(\mu)(\eta)\|_{\mathcal{V}} \\ &= \|J\Big(\mathcal{B}_{\mathrm{HF}}(\mu)(\eta)\Big)\|_{\mathcal{V}} = \|\mathcal{B}_{\mathrm{HF}}(\mu)(\eta)\|_{\mathcal{V}'} \geq \beta_{\mathrm{HF}}(\mu)\|\eta\|_{\mathcal{W}}.\end{aligned} \tag{2.19}$$

In the case where the operator $\mathcal{B}_{\mathrm{HF}}$ is parameter-independent, the space $V^{\mathrm{on}}_{N,R}$ is also parameter-independent. This space can thus be constructed once and for all in the offline phase. However, when the operator $\mathcal{B}_{\mathrm{HF}}(\mu)$ is parameter-dependent, the enriched space $V^{\mathrm{on}}_{N,R}(\mu)$ shares the same feature, and thus has to be constructed in the online phase, which is computationally inefficient. We overcome this problem in the next section.

2.3 Computationally efficient, stable model reduction

In this section, the reduced subspaces V_N and W^+_R obtained respectively by (2.10) and (2.12) are fixed. Our goal is to construct a parameter-independent subspace of $\mathcal{V}$ that provides a sufficiently accurate approximation of $V^{\mathrm{on}}_{N,R}(\mu)$ for all $\mu \in \mathcal{D}$ to preserve inf-sup stability. The crucial advantage is that this parameter-independent subspace

can be constructed once and for all in the offline phase. The idea is to approximate the linear space

$$S_R := \underset{\mu\in\mathcal{D}_{\mathtt{train}}}{+} S_R(\mu), \tag{2.20}$$

by a subspace $S_R^{\mathrm{red}} \subset S_R$, so that the bilinear form $b(\mu;\cdot,\cdot)$ is inf-sup stable with respect to the pair $(V_N + S_R^{\mathrm{red}}, W_R^+)$ for all $\mu \in \mathcal{D}_{\mathtt{train}}$. We will see in our numerical experiments that it is possible to achieve this property by a proper subspace $S_R^{\mathrm{red}} \subset S_R$ having a much smaller dimension than S_R. To realize this strategy, we rely on the following theoretical result which gives a sufficient condition on a subspace S of S_R to guarantee the above inf-sup stability.

Proposition 2.3.1 (Inf-sup stability)**.** *Let S be any finite-dimensional subspace of S_R. For all $\mu \in \mathcal{D}$, we define*

$$\sigma_S(\mu) := \sup_{\substack{v\in S_R(\mu)\\ \|v\|_{\mathcal{V}}\le 1}} \|(\mathbb{I}^{\mathcal{V}} - \Pi^{\mathcal{V}}_{V_N+S})(v)\|_{\mathcal{V}} = \|\left(\mathbb{I}^{\mathcal{V}} - \Pi^{\mathcal{V}}_{V_N+S}\right)|_{S_R(\mu)}\|_{\mathcal{L}(\mathcal{V})}, \tag{2.21}$$

and the boundedness constant

$$c_S(\mu) := \sup_{\eta\in W_R^+} \sup_{v\in V_N+S_R(\mu)+S} \frac{b(\mu;v,\eta)}{\|v\|_{\mathcal{V}}\|\eta\|_{\mathcal{W}}} \le C_0. \tag{2.22}$$

For all $\mu \in \mathcal{D}$, if

$$\sigma_S(\mu) < \frac{\beta^{\mathrm{on}}_{N,R}(\mu)}{c_S(\mu)}, \tag{2.23}$$

then the following inf-sup condition holds:

$$\inf_{\eta\in W_R^+} \sup_{v\in V_N+S} \frac{b(\mu;v,\eta)}{\|v\|_{\mathcal{V}}\|\eta\|_{\mathcal{W}}} \ge \beta^*_S(\mu) := \frac{\beta^{\mathrm{on}}_{N,R}(\mu) - c_S(\mu)\sigma_S(\mu)}{1+\sigma_S(\mu)} > 0. \tag{2.24}$$

Proof. Let $\mu \in \mathcal{D}$ and let $\eta \in W_R^+$ with $\|\eta\|_{\mathcal{W}} = 1$. The inf-sup stability of $b(\mu;\cdot,\cdot)$ with respect to the pair $\left(V^{\mathrm{on}}_{N,R}(\mu), W_R^+\right)$ (see (2.18)) implies that there exists $v_\eta \in S_R(\mu)$ such that

$$b(\mu;v_\eta,\eta) \ge 1, \qquad \beta^{\mathrm{on}}_{N,R}(\mu)\|v_\eta\|_{\mathcal{V}} \le 1. \tag{2.25}$$

Letting $u_\eta := \Pi^{\mathcal{V}}_{V_N+S}(v_\eta)$, the definition of $\sigma_S(\mu)$ implies that

$$\|v_\eta - u_\eta\|_{\mathcal{V}} = \|(\mathbb{I}^{\mathcal{V}} - \Pi^{\mathcal{V}}_{V_N+S})(v_\eta)\|_{\mathcal{V}} \le \sup_{\substack{v\in S_R(\mu)\\ \beta^{\mathrm{on}}_{N,R}(\mu)\|v\|_{\mathcal{V}}\le 1}} \|(\mathbb{I}^{\mathcal{V}} - \Pi^{\mathcal{V}}_{V_N+S})(v)\|_{\mathcal{V}} = \frac{\sigma_S(\mu)}{\beta^{\mathrm{on}}_{N,R}(\mu)}. \tag{2.26}$$

On the one hand, we have

$$b(\mu;u_\eta,\eta) = b(\mu;u_\eta - v_\eta,\eta) + b(\mu;v_\eta,\eta),$$

and the definition (2.22) of $c_S(\mu)$ implies that

$$\big|b(\mu; u_\eta - v_\eta, \eta)\big| \le c_S(\mu)\|u_\eta - v_\eta\|_{\mathcal{V}}\|\eta\|_{\mathcal{W}} = c_S(\mu)\|u_\eta - v_\eta\|_{\mathcal{V}}.$$

Hence, recalling that $b(\mu; v_\eta, \eta) \ge 1$ owing to (2.25), we have

$$\begin{aligned} b(\mu; u_\eta, \eta) &= b(\mu; u_\eta - v_\eta, \eta) + b(\mu; v_\eta, \eta) \\ &\ge 1 - c_S(\mu)\|u_\eta - v_\eta\|_{\mathcal{V}} \ge 1 - \frac{c_S(\mu)}{\beta^{\mathrm{on}}_{N,R}(\mu)}\sigma_S(\mu), \end{aligned}$$

where the last bound follows from the inequality (2.26). On the other hand, we have

$$\|u_\eta\|_{\mathcal{V}} \le \|v_\eta - u_\eta\|_{\mathcal{V}} + \|v_\eta\|_{\mathcal{V}} \le \frac{\sigma_S(\mu)}{\beta^{\mathrm{on}}_{N,R}(\mu)} + \frac{1}{\beta^{\mathrm{on}}_{N,R}(\mu)} = \frac{1 + \sigma_S(\mu)}{\beta^{\mathrm{on}}_{N,R}(\mu)}.$$

We conclude that

$$\frac{b(\mu; u_\eta, \eta)}{\|u_\eta\|_{\mathcal{V}}} \ge \frac{\beta^{\mathrm{on}}_{N,R}(\mu)}{1 + \sigma_S(\mu)}\left(1 - \frac{c_S(\mu)}{\beta^{\mathrm{on}}_{N,R}(\mu)}\sigma_S(\mu)\right) = \frac{\beta^{\mathrm{on}}_{N,R}(\mu) - c_S(\mu)\sigma_S(\mu)}{1 + \sigma_S(\mu)} > 0,$$

where the last bound follows from the assumption (2.23). Since $u_\eta \in V_N + S$, this implies the inf-sup condition (2.24). □

Using the result of Prop. 2.3.1, we design in Algo. 1 a so-called Projected Greedy Algorithm (PGA) that, given a training subset $\mathcal{D}_{\mathtt{train}} \subset \mathcal{D}$, the vector space V_N, and a tolerance $\delta > 0$, returns a subspace $S_R^{\mathrm{red}} \subset S_R$ such that

$$\sup_{\mu \in \mathcal{D}_{\mathtt{train}}} \sigma_{S_R^{\mathrm{red}}}(\mu) \le \delta. \tag{2.27}$$

Notice that since $\sigma_{S_R}(\mu) = 0$ for all $\mu \in \mathcal{D}$, it is possible to construct a subspace S_R^{red} of S_R satisfying (2.27). Our numerical results presented in Section 2.5 indicate that it is reasonable to expect that S_R^{red} has a (much) smaller dimension than S_R. In practice, the space S_R^{red} is constructed in a progressive way by means of a greedy algorithm. The PGA algorithm involves the following two main steps at iteration n:

- seek the parameter μ_n by solving an eigenvalue problem (line 2 and line 9).
- seek the supremizer $v_{n+1}^{(1)} \in S_R(\mu_n)$ by solving a linear system (line 5).

In conclusion, we define the enriched reduced primal space $V_{N,R}^{\mathrm{off}}$ as follows:

$$S_R^{\mathrm{red}} := \mathtt{PGA}\big(\mathcal{D}_{\mathtt{train}}, V_N, \delta_{\mathtt{PGA}}\big) \subset S_R \subset \mathcal{V}, \tag{2.28}$$

$$V_{N,R}^{\mathrm{off}} := V_N + S_R^{\mathrm{red}} \subset \mathcal{V}, \tag{2.29}$$

where the tolerance $\delta_{\mathtt{PGA}} > 0$ is small enough so that (2.23) is satisfied for all $\mu \in \mathcal{D}_{\mathtt{train}}$. In practice, a simple choice is $\delta_{\mathtt{PGA}} < \beta_0 C_0^{-1}$ since $\beta^{\mathrm{on}}_{N,R}(\mu) \ge \beta_0$ and $c_S(\mu) \le C_0$ for all $\mu \in \mathcal{D}_{\mathtt{train}}$. The superscript in the notation $V_{N,R}^{\mathrm{off}}$ refers to the offline construction of the enriched reduced primal basis. For all $\mu \in \mathcal{D}$, we define

$$\beta^{\mathrm{off}}_{N,R}(\mu) := \inf_{\eta \in W_R^+} \sup_{v \in V_{N,R}^{\mathrm{off}}} \frac{b(\mu; v, \eta)}{\|v\|_{\mathcal{V}}\|\eta\|_{\mathcal{W}}}. \tag{2.30}$$

Algorithm 1 `PGA: Projected Greedy Algorithm` | $\texttt{PGA}(\mathcal{D}_{\texttt{train}}, V_N, \delta)$

Require: $\mathcal{D}_{\texttt{train}} \subset \mathcal{D}$: `training subset`
$V_N \subset \mathcal{V}$: `reduced primal space`
$\delta > 0$: `tolerance`
Ensure: S: `subspace of` S_R

$S^0 := \{0\}$
$\mu_0 \in \underset{\mu \in \mathcal{D}_{\texttt{train}}}{\texttt{argmax}}\ \sigma_{S^0}(\mu)$
$n := 0$
while $\sigma_{S^n}(\mu_n) > \delta$ **do**
  $v_{n+1}^{(1)} \in \underset{\substack{v \in S_R(\mu_n) \\ \|v\|_{\mathcal{V}} \leq 1}}{\texttt{argmax}}\ \|(\mathbb{I}^{\mathcal{V}} - \Pi^{\mathcal{V}}_{V_N + S^n})(v)\|_{\mathcal{V}}$
  $v_{n+1}^{(2)} := (\mathbb{I}^{\mathcal{V}} - \Pi^{\mathcal{V}}_{V_N + S^n})(v_{n+1}^{(1)})$
  $v_{n+1} := \frac{v_{n+1}^{(2)}}{\|v_{n+1}^{(2)}\|_{\mathcal{V}}}$
  $S^{n+1} := S^n + \boldsymbol{Span}\{v_{n+1}\}$
  $\mu_{n+1} \in \underset{\mu \in \mathcal{D}_{\texttt{train}}}{\texttt{argmax}}\ \sigma_{S^{n+1}}(\mu)$
  $n = n + 1$
end while
return $S := S^n$

Notice that we only guarantee that $\beta^{\text{off}}_{N,R}(\mu) > 0$ for all $\mu \in \mathcal{D}_{\texttt{train}}$. It is reasonable to expect inf-sup stability for all $\mu \in \mathcal{D}$ if the training subset is sufficiently rich.

Let us now show that Algo. 1 necessarily terminates in a finite number of iterations.

Lemma 2.3.1 (Convergence of PGA algorithm)**.** *The sequence* $\left(\max_{\mu \in \mathcal{D}_{train}} \sigma_{S^n}(\mu)\right)_{n \geq 0}$ *is (non-strictly) decreasing. Moreover, there is* $n_0 \leq \min(m_{\mathcal{D}_{train}} R, \dim(\mathcal{V}) - \dim(V_N))$ *with* $m_{\mathcal{D}_{train}} := \#(\mathcal{D}_{train})$ *such that*

$$\max_{\mu \in \mathcal{D}_{train}} \sigma_{S^n}(\mu) = 0, \qquad \forall n \geq n_0. \tag{2.31}$$

Proof. (1) Line 8 of Algo. 1 implies that $S^n \subseteq S^{n+1}$ for all $n \geq 0$. Hence, for all $\mu \in \mathcal{D}_{\texttt{train}}$,

$$\max_{v \in S_R(\mu)} \|(\mathbb{I}^{\mathcal{V}} - \Pi^{\mathcal{V}}_{V_N + S^{n+1}})(v)\|_{\mathcal{V}} \leq \max_{v \in S_R(\mu)} \|(\mathbb{I}^{\mathcal{V}} - \Pi^{\mathcal{V}}_{V_N + S^n})(v)\|_{\mathcal{V}},$$

which implies that

$$\max_{\mu \in \mathcal{D}_{\texttt{train}}} \sigma_{S^{n+1}}(\mu) \leq \max_{\mu \in \mathcal{D}_{\texttt{train}}} \sigma_{S^n}(\mu).$$

This proves the first assertion.

(2) Let us now prove the second assertion. To this purpose, let us first prove by induction that for all $n \geq 0$, if $\max_{\mu \in \mathcal{D}_{\texttt{train}}} \sigma_{S^n}(\mu) > 0$, then $S^n \subsetneq S^{n+1}$ and

$$\dim\,(V_N + S^{n+1}) = \dim\,(V_N + S^n) + 1. \tag{2.32}$$

Indeed, since $\mu_n \in \texttt{argmax}_{\mu\in\mathcal{D}_{\texttt{train}}}\sigma_{S^n}(\mu)$, we have $\sigma_{S^n}(\mu_n) = \max_{\mu\in\mathcal{D}_{\texttt{train}}}\sigma_{S^n}(\mu) > 0$. Hence, $v_{n+1}^{(1)}$ from line 5 satisfies

$$v_{n+1}^{(2)} := (\mathbb{I}^{\mathcal{V}} - \Pi^{\mathcal{V}}_{V_N+S^n})(v_{n+1}^{(1)}) \neq 0.$$

Thus, $v_{n+1}^{(2)}$ is nonzero and orthogonal to the space $V_N + S^n$. Since $S^{n+1} := S^n + \boldsymbol{Span}\{v_{n+1}\}$, this proves (2.32). We are now in a position to prove the second assertion. We first observe that if there is $n_0 \geq 0$ such that $\max_{\mu\in\mathcal{D}_{\texttt{train}}}\sigma_{S^{n_0}}(\mu) = 0$, then $\max_{\mu\in\mathcal{D}_{\texttt{train}}}\sigma_{S^n}(\mu) = 0$ for all $n \geq n_0$. Moreover, since $S^n \subseteq S_R$ and $\dim(S_R) \leq m_{\mathcal{D}_{\texttt{train}}}R$, we infer from (2.21) that $\max_{\mu\in\mathcal{D}_{\texttt{train}}}\sigma_{S^n}(\mu) = 0$ whenever $n \geq m_{\mathcal{D}_{\texttt{train}}}R$. Finally, reasoning by induction and using (2.32) shows that $\dim(V_N+S^n) = \dim(V_N)+n$ for all $n \geq 0$ such that $\max_{\mu\in\mathcal{D}_{\texttt{train}}}\sigma_{S^n}(\mu) > 0$. Since $V_N + S^n \subset \mathcal{V}$, we must have $n \leq \dim(\mathcal{V}) - \dim(V_N)$. This completes the proof of (2.31). □

Remark 2.3.1 (Finite termination). Lemma 2.3.1 provides two upper bounds on the maximum number of iterations of the PGA algorithm. The first upper bound, $n_0 \leq m_{\mathcal{D}_{\texttt{train}}}R$ is, in particular, independent of the dimension of the HF space $\mathcal{V}$.

Remark 2.3.2 (Comparison with [32]). The PGA algorithm is similar in spirit to the Algorithms 2 and 3 proposed in [32] in the context of Petrov–Galerkin reduced basis approximations of transport equations (the adaptation to saddle-point problems is discussed in Section 7 therein). The overall organization of the reduced basis method is, however, different. Indeed, in contrast to [32] where a double greedy algorithm is proposed, we do not enrich here the reduced dual space in a greedy way and adapt the reduced primal space to guarantee inf-sup stability at each iteration of the greedy algorithm. Instead, we fix once and for all the reduced dual space (which can be obtained as the output of a greedy algorithm, see Section 2.4), and then enrich the reduced primal space following the strategy highlighted in Algo. 1. A computational comparison of the performances of both algorithms is postponed to future work. Moreover, we notice that Proposition 3.1 relates the inf-sup constant of the pair of reduced spaces to some approximation property of the subspace $V_N + S$ in $\mathcal{V}$. This idea is similar to [32, Prop. 3.7] which relates inf-sup stability to the notion of δ-proximality.

2.4 Modified CPG algorithm

In this section, we propose a modified version of the plain CPG algorithm (see Remark 2.4.4 for a comparison with the algorithm from [7]). The goal is to promote the generation of a cone having a larger aperture than the one built by the plain CPG algorithm. Indeed, a problem that arises numerically when working with a positive cone is to be able to generate a basis such that the corresponding Gram matrix is as well-conditioned as possible. In practice, one has often to deal with bases composed of vectors which are almost collinear. In this context, ill-conditioning issues can arise, in particular when performing projections onto the cone. To overcome this difficulty, it is not possible to perform an orthogonalization process (such as Gram–Schmidt) since this would lead to a departure from the positive cone $\mathcal{W}^+$. Instead, one possibility is to promote the aperture of the cone produced by the plain CPG algorithm.

Specifically, we introduce the mCPG (modified CPG) algorithm (see Algo. 2) which, given a set of $Q \in \mathbb{N}^*$ vectors $\{\theta_q\}_{q\in\{1:Q\}}$ of $\mathcal{W}^+$, and a positive real number δ, produces a set of $R \in \mathbb{N}^*(R \leq Q)$ vectors of $\mathcal{W}^+$,

$$\{\nu_r\}_{r\in\{1:R\}} := \texttt{mCPG}\Big(\{\theta_q\}_{q\in\{1:Q\}};\ \mathcal{W},\ \delta\Big),$$

satisfying

$$W_R^+ := \boldsymbol{Span}^+\Big(\{\nu_r\}_{r\in\{1:R\}}\Big) \subset \mathcal{W}^+, \tag{2.33}$$

$$e_{\texttt{mCPG}}(R) := \frac{\max\limits_{q\in\{1:Q\}} \|\Big(\mathbb{I}^{\mathcal{W}} - \Pi^{\mathcal{W}}_{W_R^+}\Big)(\theta_q)\|_{\mathcal{W}}}{\max\limits_{q\in\{1:Q\}} \|\theta_q\|_{\mathcal{W}}} \leq \delta. \tag{2.34}$$

Algorithm 2 `mCPG: modified CPG algorithm` | $\texttt{mCPG}(\{\theta_q\}_{q\in\{1:Q\}}; \mathcal{W}, \delta)$

Require: $\{\theta_q\}_{q\in\{1:Q\}}, Q \in \mathbb{N}^*$: `set of vectors`
$\mathcal{W}$: `Hilbert space`
$\delta > 0$: `tolerance`
Ensure: $\{\nu_r\}_{r\in\{1:R\}} \subset \mathcal{W}^+, R \leq Q$
1: $r := 0$
2: $I_0 := \emptyset$
3: $K_0 := \{0\} \subset \mathcal{W}^+$
4: $e_0 := 1 + \delta$
5: $q_1 := \underset{q\in\{1:Q\}}{\texttt{argmax}} \|\theta_q\|_{\mathcal{W}}$
6: **while** $(e_r > \delta)$ **and** $(r < Q)$ **do**
7: $r := r + 1$
8: $I_r := I_{r-1} \cup \{q_r\}$
9: $\Upsilon_r := \underset{\Upsilon\in K_{r-1}\cap(\theta_{q_r}-\mathcal{W}^+)}{\texttt{argmin}} \|\theta_{q_r} - \Upsilon\|_{\mathcal{W}}$
10: $\nu_r := \frac{\theta_{q_r}-\Upsilon_r}{\|\theta_{q_r}-\Upsilon_r\|_{\mathcal{W}}}$
11: $K_r := K_{r-1} + \boldsymbol{Span}^+\{\nu_r\}$
12: $q_{r+1} := \underset{q\in\{1:Q\}\setminus I_r}{\texttt{argmax}} \frac{\|(\mathbb{I}^{\mathcal{W}}-\Pi^{\mathcal{W}}_{K_r})(\theta_q)\|_{\mathcal{W}}}{\|\theta_{q_1}\|_{\mathcal{W}}}$
13: $e_r := \frac{\|(\mathbb{I}^{\mathcal{W}}-\Pi^{\mathcal{W}}_{K_r})(\theta_{q_{r+1}})\|_{\mathcal{W}}}{\|\theta_{q_1}\|_{\mathcal{W}}}$
14: **end while**
15: $R := r$
16: **return** $\{\nu_n\}_{n\in\{1:R\}}$

Remark 2.4.1 (Cone aperture). For all $n \in \mathbb{N}^*$, we have $\boldsymbol{Span}^+\Big(\Big\{\theta_{q_n}\Big\}_{n\in\{1:r\}}\Big) \subset \boldsymbol{Span}^+\Big(\Big\{\nu_n\Big\}_{n\in\{1:r\}}\Big)$. Indeed, reasoning by induction, since we have $\nu_r := \frac{\theta_{q_r}-\Upsilon_r}{\Big\|\theta_{q_r}-\Upsilon_r\Big\|_{\mathcal{W}}}$ with $\Upsilon_r \in K_{r-1}$, we infer that $\theta_{q_r} = \Big\|\theta_{q_r} - \Upsilon_r\Big\|_{\mathcal{W}} \times \nu_r + \Upsilon_r \in \boldsymbol{Span}^+\Big(\Big\{\nu_n\Big\}_{n\in\{1:r\}}\Big)$.

Remark 2.4.2 (Proper termination). In the mCPG algorithm, we observe that line 10 is only executed if $\nu_r \neq 0$. Indeed, if $\nu_r = 0$, then $\theta_{q_r} = \Upsilon_r \in K_{r-1}$ and consequently $e_{r-1} = \frac{\|(\mathbb{I}^{\mathcal{W}} - \Pi^{\mathcal{W}}_{K_{r-1}})(\theta_{q_r})\|_{\mathcal{W}}}{\|\theta_{q_1}\|_{\mathcal{W}}} = 0 < \delta$. This means that we do not continue the loop since the condition $e_{r-1} > \delta$ is not satisfied.

Remark 2.4.3 (Comparison with CPG). The main difference between the CPG and mCPG algorithms is that at each iteration $r \geq 1$, the CPG algorithm does not execute line 9 and simply sets $\nu_r = \frac{\theta_{q_r}}{\|\theta_{q_r}\|_{\mathcal{W}}}$. Instead, the mCPG algorithm computes ν_r as a member of $\mathcal{W}^+$ (in fact of $\boldsymbol{Span}^+\Big(\big\{\theta_{q_n}\big\}_{n\in\{1:r\}}\Big)$). We will show in the numerical experiments of Section 2.5 that the mCPG algorithm has the advantage of providing a set of vectors whose Gram matrix is better conditioned compared to the one obtained with the CPG algorithm. This property comes from the fact that at iteration r of the mCPG algorithm, the element r of the basis is constructed by removing all the information contained in the basis constructed at iteration $r-1$. Figure 2.1 presents an illustration of how the CPG and mCPG algorithms operate on the first two iterations.

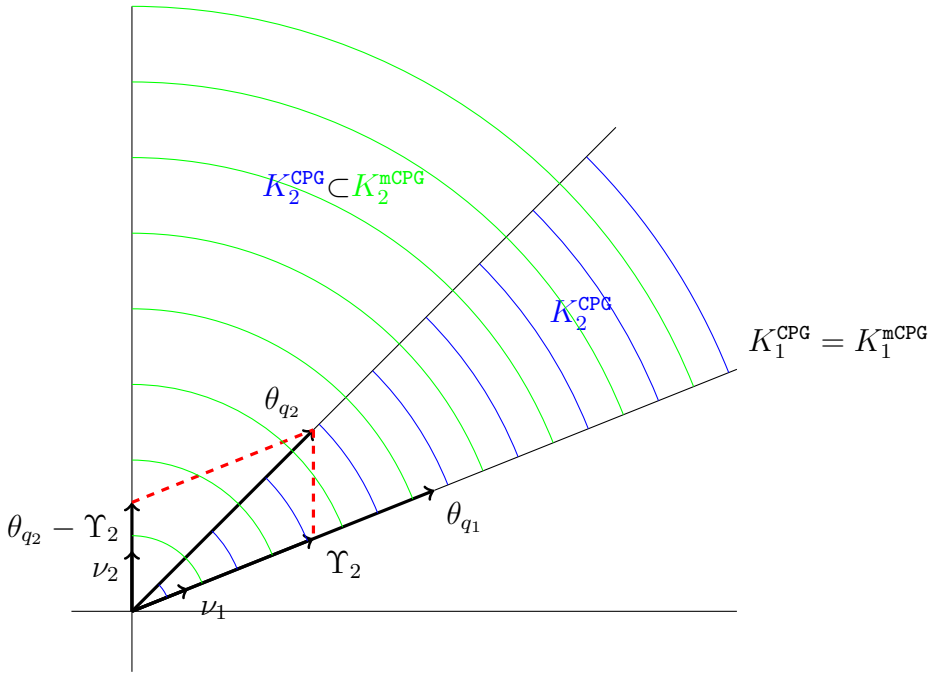

Figure 2.1 – Comparison of the first two iterations of the CPG and mCPG algorithms.

Remark 2.4.4 (Comparison with [7]). The algorithm proposed in [7] consists in constructing from a given family of functions $\{\nu_r\}_{r\in\{1:R\}}$ (which can be obtained, for instance, as the output of the CPG algorithm from an original family of functions $\{\theta_q\}_{q\in\{1:Q\}}$), a new family of modified functions $\{\widetilde{\nu}_r\}_{r\in\{1:R\}}$ so that

$$\boldsymbol{Span}^+\Big(\{\nu_r\}_{r\in\{1:R\}}\Big) \subset \boldsymbol{Span}^+\Big(\{\widetilde{\nu}_r\}_{r\in\{1:R\}}\Big).$$

In other words, the approach proposed in [7] allows one to construct an enlarged cone from a reduced cone which has to be given as an input, and which is spanned by the same number of functions as the orginal reduced cone. In contrast, the mCPG algorithm

proposed herein consists in constructing an enlarged cone directly from the original family of functions $\{\theta_q\}_{q\in\{1:Q\}}$ as an output of a greedy algorithm, by enlarging the current reduced cone at each step of the greedy algorithm. This has, in our opinion, two advantages. First, it avoids ill-conditioning issues raised by the standard CPG algorithm and which are then also encountered in the approach proposed in [7]. Second, considering enlarged reduced cones at each iteration of a greedy algorithm yields a tighter control on the accuracy of the results given by the corresponding reduced-order model. Finally, we observe that our numerical experiments indicate that the accuracy of the reduced-order approximation is better when using the mCPG algorithm than the CPG algorithm. A more detailed computational comparison with the approach from [7] is left to future work.

Finally, the following result states that Algo. 2 terminates in a finite number of iterations.

Lemma 2.4.1 (Finite termination)**.** *The sequence $(e_r)_{1\leq r\leq Q}$ is (non-strictly) decreasing and $e_Q = 0$.*

Proof. Let $1 \leq r \leq Q-1$ and let us prove that $e_{r+1} \leq e_r$. First, we have $K_r \subset K_{r+1}$. Hence,

$$e_{r+1} := \frac{\|(\mathbb{I}^{\mathcal{W}} - \Pi^{\mathcal{W}}_{K_{r+1}})(\theta_{q_{r+2}})\|_{\mathcal{W}}}{\|\theta_{q_1}\|_{\mathcal{W}}} \leq \frac{\|(\mathbb{I}^{\mathcal{W}} - \Pi^{\mathcal{W}}_{K_r})(\theta_{q_{r+2}})\|_{\mathcal{W}}}{\|\theta_{q_1}\|_{\mathcal{W}}}.$$

In addition, since

$$q_{r+1} := \underset{q\in\{1:Q\}\setminus I_r}{\texttt{argmax}} \frac{\|(\mathbb{I}^{\mathcal{W}} - \Pi^{\mathcal{W}}_{K_r})(\theta_q)\|_{\mathcal{W}}}{\|\theta_{q_1}\|_{\mathcal{W}}},$$

we infer that

$$\frac{\|(\mathbb{I}^{\mathcal{W}} - \Pi^{\mathcal{W}}_{K_r})(\theta_{q_{r+2}})\|_{\mathcal{W}}}{\|\theta_{q_1}\|_{\mathcal{W}}} \leq \frac{\|(\mathbb{I}^{\mathcal{W}} - \Pi^{\mathcal{W}}_{K_r})(\theta_{q_{r+1}})\|_{\mathcal{W}}}{\|\theta_{q_1}\|_{\mathcal{W}}} =: e_r.$$

This proves that the sequence $(e_r)_{1\leq r\leq Q}$ is (non-strictly) decreasing. Finally, since necessarily $\boldsymbol{Span}^+\Big(\{\theta_q\}_{q\in\{1:Q\}}\Big) \subset K_Q$, we infer that $e_Q = 0$. This completes the proof. □

2.5 Numerical results

In this section, we numerically illustrate our theoretical results on the membrane obstacle problem and on the frictionless Hertz contact problem. In both examples, we compare the computational performance of the different methods for building the reduced primal space (decorrelated, online and offline) and the reduced dual basis (CPG and mCPG). The HF computations use a combination of `Freefem++` [56] and `Python`, whereas the algorithms presented herein have been developed in `Python` using the convex optimization package `cvxopt` [4].

2.5.1 Membrane obstacle problem

In this section, we study the membrane obstacle problem. We consider a square, elastic membrane $\Omega \subset \mathbb{R}^2$ of side $A = 1\text{m}$, located at some distance from an obstacle represented by a circular sub-domain $\omega(\mu) \subset \Omega$ of radius $r := \mu_1$ and centre $c := (\mu_2, \mu_3)$ with

$$\mu = (\mu_1, \mu_2, \mu_3) \in \mathcal{D} := \Big[0.16, 0.24\Big] \times \Big[-0.05, 0.05\Big] \times \Big[-0.05, 0.05\Big](\text{m}). \tag{2.35}$$

For all $\mu \in \mathcal{D}$, we assume that there is a smooth invertible geometric mapping $h(\mu) : \widehat{\Omega} := \Omega \longrightarrow \Omega$ such that there is a reference domain $\widehat{\omega} \subset \Omega$ satisfying $h(\mu)(\widehat{\omega}) = \omega(\mu)$. We set $h_1(\mu) := h(\mu)|_{\widehat{\omega}}$. Moreover, the function $\widehat{\psi} : \widehat{\omega} \to \mathbb{R}$ prescribes the elevation of the obstacle in the reference domain, and we set $\psi(\mu) := \widehat{\psi} \circ h_1(\mu)^{-1}$. We apply to the membrane a vertical load $\widehat{\ell} : \widehat{\Omega} \to \mathbb{R}$, with $\widehat{\ell} \in L^2(\widehat{\Omega})$ and we set $\ell(\mu) := \widehat{\ell} \circ h(\mu)^{-1}$. The membrane is fixed on the boundary Γ of Ω (see Figure 2.2). Thus, we consider the following model problem:

$$\begin{cases} -\Delta u = \ell(\mu), & \text{in } \Omega, \\ \quad u \geq \psi(\mu), & \text{in } \omega(\mu), \\ \quad u = 0, & \text{on } \Gamma. \end{cases} \tag{2.36}$$

In what follows, we take $\widehat{\psi}$ so that $\psi(\mu)(x, y) := -1.25\frac{(x-\mu_2)^2+(y-\mu_3)^2}{\mu_1^2}$ for all $\mu \in \mathcal{D}$ and all $(x, y) \in \omega(\mu)$, and $\widehat{\ell}(x, y) = -1$ for all $(x, y) \in \widehat{\Omega}$. The coefficient -1.25 in front of the obstacle function is chosen so that the constraints at the boundary of $\omega(\mu)$ are inactive in order to avoid oscillations of the Lagrange multiplier at the transition zone. The training set is chosen as $\mathcal{D}_{\texttt{train}} := \Big\{0.8 + 0.1i, 0 \leq i \leq 4\Big\} \times \Big\{-0.05 + 0.025i, 0 \leq i \leq 4\Big\}^2$ (altogether 125 points) and the validation set $\mathcal{D}_{\texttt{valid}}$ is generated by choosing 64 elements in $\mathcal{D}$ randomly with a uniform distribution.

We consider the HF subspace $\widehat{\boldsymbol{\mathcal{V}}} \subset H_0^1(\widehat{\Omega}; \mathbb{R})$ and the HF subcone $\widehat{\mathcal{W}}^+ \subset L^2(\widehat{\omega}; \mathbb{R}_+)$ built using $\mathbb{P}_1$ finite elements for the displacement and the Lagrange multiplier [39, 17]. Notice that the displacement and the Lagrange multiplier are now defined on the reference domains $\widehat{\Omega}$ and $\widehat{\omega}$, respectively. The reference mesh of $\widehat{\Omega}$ is fitted to the boundary of $\widehat{\omega}$ and is composed of 3594 nodes with 467 nodes in $\widehat{\omega}$. Thus, we have $\mathcal{N} := \dim(\widehat{\mathcal{V}}) = 3594$ primal and $\mathcal{R} := \dim(\widehat{\mathcal{W}}) = 467$ dual degrees of freedom. For all $\mu \in \mathcal{D}$, the mesh of Ω fitted to the boundary of $\omega(\mu)$ is built using the geometric mapping $h(\mu)$. We have verified that all the meshes maintain satisfactory regularity properties by using the aspect ratio quality criterion from the Salome platform [94]. Figure 2.3 displays the maximum aspect ratio of the meshes for all $\mu \in \mathcal{D}_{\texttt{train}} \cup \mathcal{D}_{\texttt{valid}}$.

The variational formulation of (2.36) leads to a minimization problem of the form (2.1) with the bilinear form $\widehat{a}(\mu; \cdot, \cdot) : \widehat{\mathcal{V}} \times \widehat{\mathcal{V}} \to \mathbb{R}$ defined by

$$\widehat{a}(\mu; \widehat{u}, \widehat{v}) := \int_{\Omega} \nabla(\widehat{u} \circ h(\mu)^{-1}) \cdot \nabla(\widehat{v} \circ h(\mu)^{-1})\, d\Omega, \tag{2.37}$$

and the linear form $\widehat{f}(\mu; \cdot) : \widehat{\mathcal{V}} \to \mathbb{R}$ defined by

$$\widehat{f}(\mu; \widehat{v}) := \int_{\Omega} \Big(\widehat{\ell} \circ h(\mu)^{-1}\Big)\Big(\widehat{v} \circ h(\mu)^{-1}\Big)\, d\Omega. \tag{2.38}$$

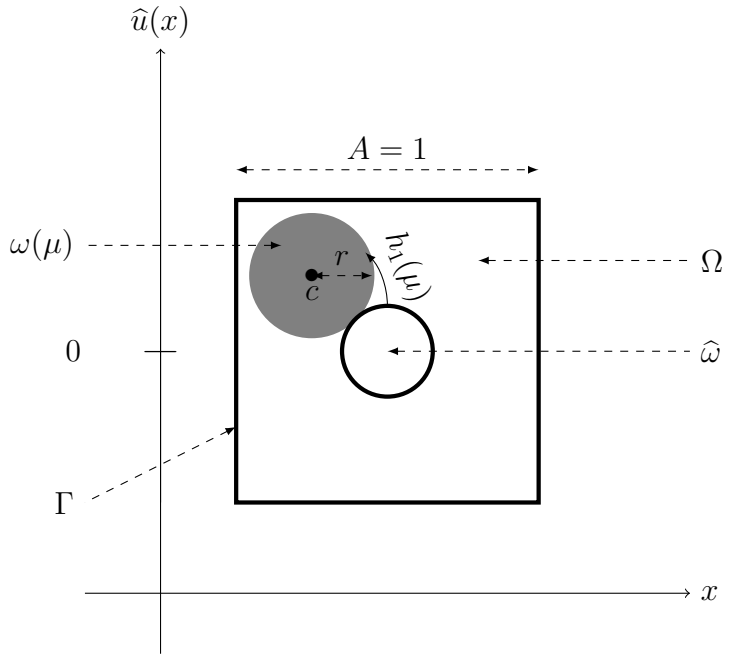

Figure 2.2 – Obstacle test case: Configuration.

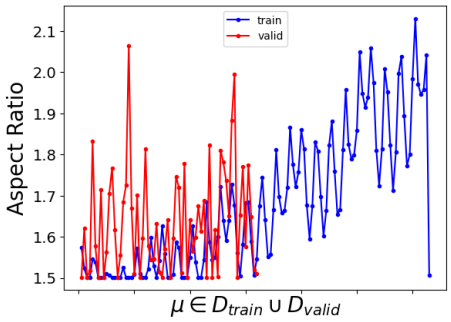

Figure 2.3 – Obstacle test case: Maximum aspect ratio for $\mu \in \mathcal{D}_{\texttt{train}} \cup \mathcal{D}_{\texttt{valid}}$.

The admissible set $\widehat{\mathcal{K}}(\mu)$ associated with the obstacle condition is defined as follows:

$$\widehat{\mathcal{K}}(\mu) := \left\{ \widehat{v} \in \widehat{\mathcal{V}} \;\middle|\; \widehat{b}(\mu; \widehat{v}, \widehat{\eta}) \leq \widehat{g}(\mu; \widehat{\eta}),\ \forall \widehat{\eta} \in \widehat{\mathcal{W}}^+ \right\}, \tag{2.39}$$

where

$$\widehat{b}(\mu; \widehat{v}, \widehat{\eta}) := \int_{\omega(\mu)} \left(\widehat{v} \circ h_1(\mu)^{-1}\right)\left(\widehat{\eta} \circ h_1(\mu)^{-1}\right) d\Gamma, \tag{2.40a}$$

$$\widehat{g}(\mu; \widehat{\eta}) := \int_{\omega(\mu)} \left(\widehat{\psi} \circ h_1(\mu)^{-1}\right)\left(\widehat{\eta} \circ h_1(\mu)^{-1}\right) d\Gamma. \tag{2.40b}$$

Figure 2.4 displays the deformed configuration resulting from the HF displacement field $u(\mu) := \widehat{u}(\mu) \circ h(\mu)^{-1}$ (left panel) and the Lagrange multiplier $\lambda(\mu) := \widehat{\lambda}(\mu) \circ h(\mu)^{-1}$ (right panel) for $\mu = (0.18, 0.025, -0.025)$(m). Figure 2.5 shows on its left (resp. right) panel the projection error $\widehat{e}_{\texttt{POD}}$ (resp. $\widehat{e}_{\texttt{CPG}}$ and $\widehat{e}_{\texttt{mCPG}}$) defined in (2.11) (resp. (2.13) and (2.34)) produced by the POD (resp. CPG and mCPG) algorithms as a function of the number of vectors composing the reduced primal (resp. dual) bases. In all cases,

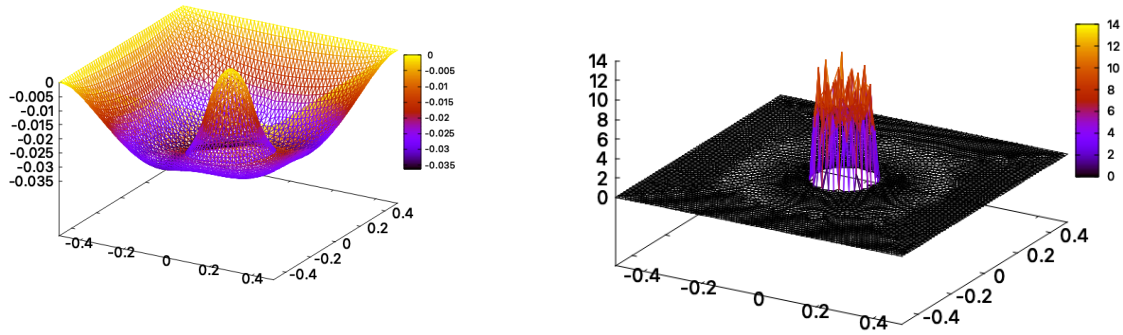

Figure 2.4 – Obstacle test case: HF solution for $\mu = (0.18, 0.025, -0.025)$. Left: $u(\mu)$. Right: $\lambda(\mu)$.

the projection errors decrease sufficiently fast so that the linear spaces generated by the primal and dual snapshots can be approximated by small-dimensional subspaces. We also notice that the projection error for the mCPG algorithm is smaller than that

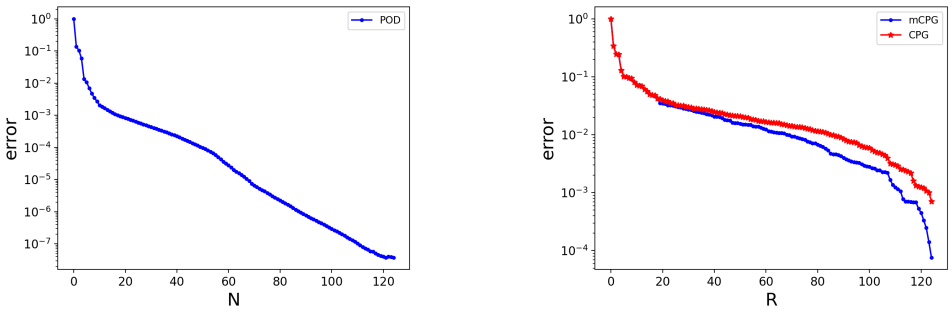

Figure 2.5 – Obstacle test case: projection errors for the POD, CPG and mCPG algorithms. Left: POD. Right: CPG and mCPG.

for the CPG algorithm. This indicates that the cone constructed using the mCPG algorithm yields more accurate approximations than the one obtained by means of the CPG algorithm. To further compare the CPG and the mCPG algorithms, we introduce for all $r \geq 0$, the quantity $\widehat{e}_{\mathrm{orth}}(r)$ which measures the orthogonality of the vector $\widehat{\nu}_{r+1}$, constructed by either the CPG or the mCPG algorithm, with respect to the cone $\widehat{K}_r$. This quantity is defined as

$$\widehat{e}_{\mathrm{orth}}(r) := \|\left(\mathbb{I}^{\widehat{\mathcal{W}}} - \Pi^{\widehat{\mathcal{W}}}_{\widehat{K}_r}\right)(\widehat{\nu}_{r+1})\|_{\widehat{\mathcal{W}}} \leq 1. \tag{2.41}$$

Notice that by definition, the larger $\widehat{e}_{\mathrm{orth}}(r)$ (i.e., close to 1), the closer $\widehat{\nu}_{r+1}$ to being orthogonal to the cone. It can be seen in Figure 2.6 that $\widehat{e}^{\mathtt{CPG}}_{\mathrm{orth}}(r) \leq \widehat{e}^{\mathtt{mCPG}}_{\mathrm{orth}}(r)$ for all $r \geq 0$, which illustrates that the basis constructed with the mCPG algorithm is of better quality than the one constructed with the CPG algorithm.

Considering the three tolerance pairs $(\delta_{\mathtt{POD}} = 10^{-3}, \delta_{\mathtt{mCPG}} = 10^{-2})$, $(\delta_{\mathtt{POD}} = 10^{-4}, \delta_{\mathtt{mCPG}} = 10^{-3})$, and $(\delta_{\mathtt{POD}} = 10^{-6}, \delta_{\mathtt{mCPG}} = 10^{-2})$, we obtain respectively the following pairs for the

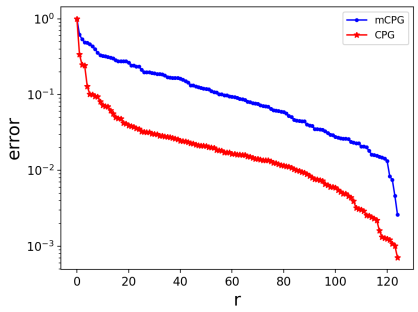

Figure 2.6 – Obstacle test case: Comparison between $\widehat{e}^{\texttt{CPG}}_{\text{orth}}(r)$ and $\widehat{e}^{\texttt{mCPG}}_{\text{orth}}(r)$.

dimensions of the reduced bases: $(N, R) = (19, 50)$, $(N, R) = (51, 70)$, $(N, R) = (89, 50)$. With these choices, we cover the two possible settings, namely $N < R$ where we are sure that for all $\mu \in \mathcal{D}$, the bilinear form $\widehat{b}(\mu; \cdot, \cdot)$ is not inf-sup stable ($\widehat{\beta}^{\text{dec}}_{N,R}(\mu) = 0$) and $N \geq R$ where inf-sup stability cannot be asserted a priori. Our numerical results for the pair $(N, R) = (89, 50)$ show that the plain construction of the reduced model does not guarantee inf-sup stability in this case. Indeed, the value of the inf-sup constant $\widehat{\beta}^{\text{dec}}_{N,R}(\mu)$ for the pair $(N, R) = (89, 50)$ is almost zero (of the order of 10^{-7}) for all $\mu \in \mathcal{D}_{\texttt{valid}}$.

Let us now consider the results obtained with the strategy proposed in Section 2.3. For all $\mu \in \mathcal{D}$, we define

$$\widehat{\beta}_{\widehat{S}^n}(\mu) := \inf_{\widehat{\eta} \in \widehat{W}_R^+} \sup_{\widehat{v} \in \widehat{V}_N + \widehat{S}^n} \frac{b(\mu; \widehat{v}, \widehat{\eta})}{\|\widehat{v}\|_{\widehat{\mathcal{V}}} \|\widehat{\eta}\|_{\widehat{\mathcal{W}}}}, \quad \forall n \in \mathbb{N}. \tag{2.42}$$

Figures 2.7c, 2.7f and 2.7i, respectively, show the values of $\widehat{\beta}^{\text{off}}_{N,R}(\mu)$ as a function of $\mu \in \mathcal{D}_{\texttt{valid}}$ for the pairs $(N, R) = (19, 50)$, $(N, R) = (51, 70)$, $(N, R) = (89, 50)$. For each pair, we consider the tight tolerance $\delta_{\texttt{PGA}} = 10^{-3}$ as well as the loose tolerance $\delta_{\texttt{PGA}} = 0.5$, 0.6, 0.95, respectively. These results illustrate the fact that the PGA algorithm does indeed recover the expected stability property. Notice that the values of $\mu \in \mathcal{D}_{\texttt{valid}}$ have been sorted in increasing order with respect to the inf-sup constant $\widehat{\beta}^{\text{off}}_{N,R}(\mu)$. The panels in column 1 (resp. 2) of Figure 2.7 report the values of $\widehat{\sigma}_{\widehat{S}^n}(\mu_n)$ (see (2.23)) (resp. $\min_{\mu \in \mathcal{D}_{\texttt{train}}} \widehat{\beta}_{\widehat{S}^n}(\mu)$) as a function of n for the pairs $(N, R) = (19, 50)$, $(N, R) = (51, 70)$ and $(N, R) = (89, 50)$ with $\delta_{\texttt{PGA}} = 10^{-3}$. The results show that the PGA algorithm converges and employs an effective greedy selection of supremizers in order to recover inf-sup stability for the reduced model. Figure 2.8 shows a comparison between the inf-sup constants $\widehat{\beta}_{\text{HF}}(\mu)$, $\widehat{\beta}^{\text{dec}}_{N,R}(\mu)$, $\widehat{\beta}^{\text{on}}_{N,R}(\mu)$, and $\widehat{\beta}^{\text{off}}_{N,R}(\mu)$ for each of the reduced basis dimension pairs $(N, R) = (19, 50)$, $(N, R) = (51, 70)$ and $(N, R) = (89, 50)$ with respectively $\delta_{\texttt{PGA}} = 0.5$, $\delta_{\texttt{PGA}} = 0.6$ and $\delta_{\texttt{PGA}} = 0.95$. On the one hand, we see that in all cases, in agreement with the theoretical results, $\widehat{\beta}^{\text{on}}_{N,R}(\mu) \geq \widehat{\beta}^{\text{off}}_{N,R}(\mu) \geq \widehat{\beta}^{\text{dec}}_{N,R}(\mu)$ and $\widehat{\beta}^{\text{on}}_{N,R}(\mu) \geq \widehat{\beta}_{\text{HF}}(\mu)$ for all $\mu \in \mathcal{D}_{\texttt{valid}}$. On the other hand, we notice that there is no established order between $\widehat{\beta}^{\text{off}}_{N,R}(\mu)$ and $\widehat{\beta}_{\text{HF}}(\mu)$.

Table 2.1 shows that the offline phase of the offline enrichment method is approximately up to two times more expensive than the online enrichment method for the three reduced basis dimension pairs (N, R) with $\delta_{\texttt{PGA}} = 10^{-3}$. We see the opposite effect concerning the cost of the online phase. This is explained on the one hand by the fact

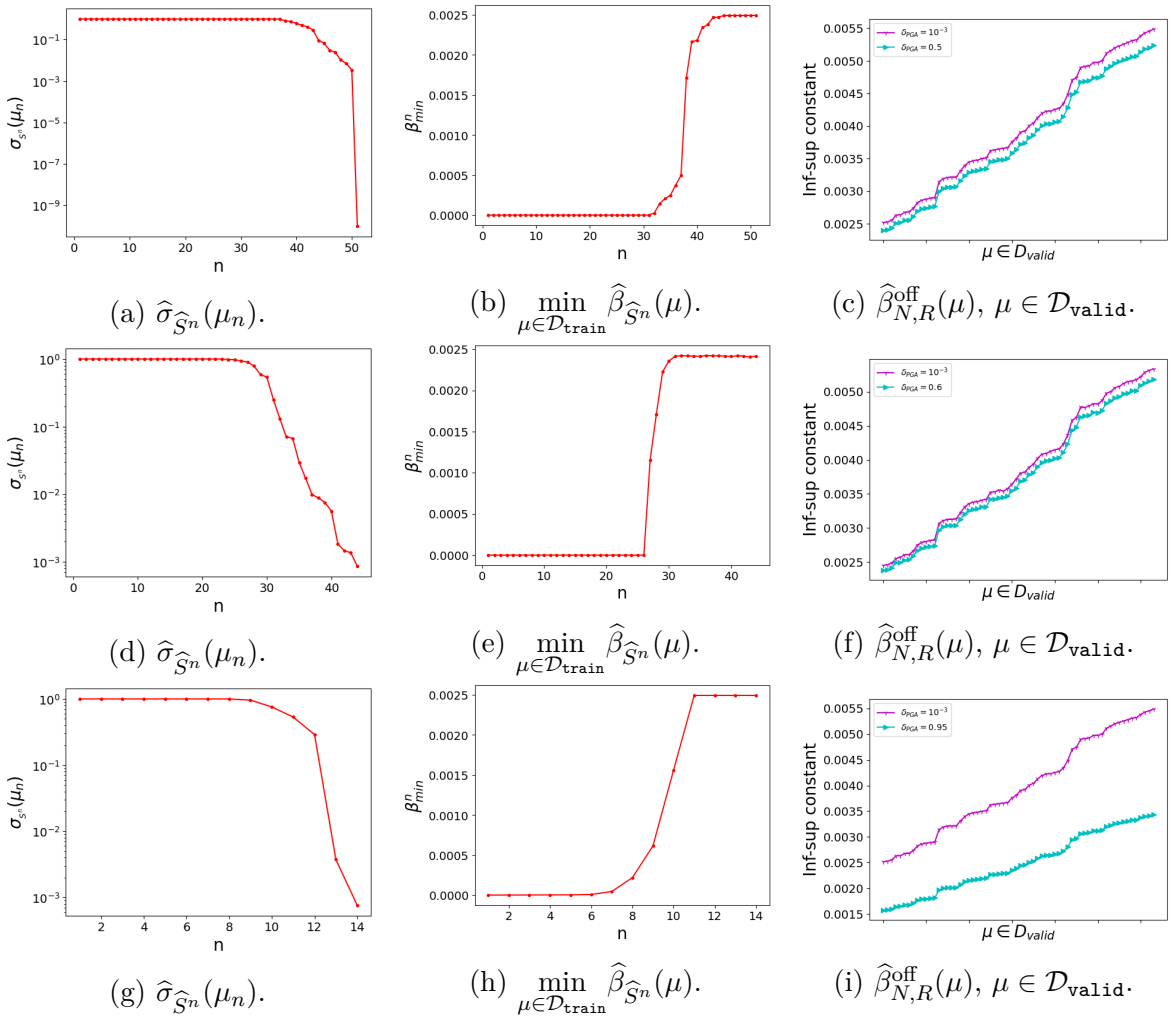

(a) $\widehat{\sigma}_{\widehat{S}^n}(\mu_n)$. (b) $\min_{\mu \in \mathcal{D}_{\texttt{train}}} \widehat{\beta}_{\widehat{S}^n}(\mu)$. (c) $\widehat{\beta}^{\text{off}}_{N,R}(\mu)$, $\mu \in \mathcal{D}_{\texttt{valid}}$.

(d) $\widehat{\sigma}_{\widehat{S}^n}(\mu_n)$. (e) $\min_{\mu \in \mathcal{D}_{\texttt{train}}} \widehat{\beta}_{\widehat{S}^n}(\mu)$. (f) $\widehat{\beta}^{\text{off}}_{N,R}(\mu)$, $\mu \in \mathcal{D}_{\texttt{valid}}$.

(g) $\widehat{\sigma}_{\widehat{S}^n}(\mu_n)$. (h) $\min_{\mu \in \mathcal{D}_{\texttt{train}}} \widehat{\beta}_{\widehat{S}^n}(\mu)$. (i) $\widehat{\beta}^{\text{off}}_{N,R}(\mu)$, $\mu \in \mathcal{D}_{\texttt{valid}}$.

Figure 2.7 – Obstacle test case: PGA algorithm. Row 1: $(N, R) = (19, 50)$. Row 2: $(N, R) = (51, 70)$. Row 3 $(N, R) = (89, 50)$. Column 1 and Column 2: $\delta_{\texttt{PGA}} = 10^{-3}$. Column 3: $\delta_{\texttt{PGA}} \in \{0.95, 0.6, 0.5, 10^{-3}\}$.

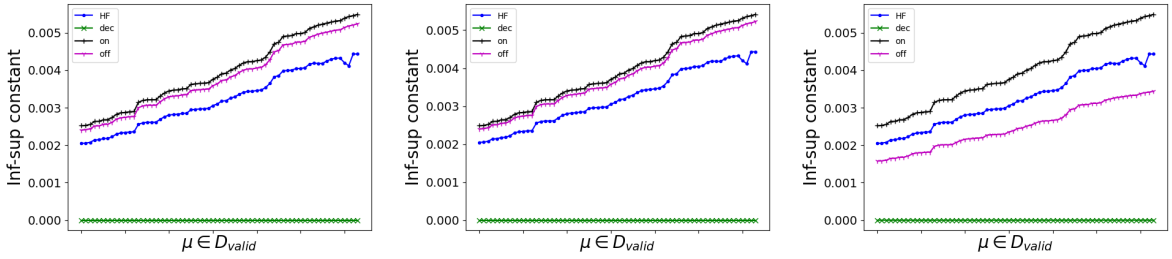

(a) $(N, R) = (19, 50), \delta_{\texttt{PGA}} = 0.5$. (b) $(N, R) = (51, 70), \delta_{\texttt{PGA}} = 0.6$. (c) $(N, R) = (89, 50), \delta_{\texttt{PGA}} = 0.95$.

Figure 2.8 – Obstacle test case: Inf-sup constant $\widehat{\beta}_{\text{HF}}(\mu)$, $\widehat{\beta}^{\text{dec}}_{N,R}(\mu)$, $\widehat{\beta}^{\text{on}}_{N,R}(\mu)$, and $\widehat{\beta}^{\text{off}}_{N,R}(\mu)$ for $\mu \in \mathcal{D}_{\texttt{valid}}$.

that in the case of the online enrichment strategy, the primal basis is reconstructed for each calculation of the reduced model. On the other hand, it is also explained by

the fact that in the present test case, the dimension of the primal basis is smaller in the case of an offline enrichment strategy because the PGA algorithm converges in at most R iterations. We notice that the larger R, the more advantageous the offline strategy compared to the online strategy. It can also be seen that in the case of the offline strategy, the cost of the online phase is practically the same for all the three reduced basis dimension pairs, although the dimensions are different. This is explained by the fact that, once the reduced model is constructed, the cost of solving the resulting system varies quite moderately as a function of the dimension of the reduced bases. Comparing the overall cost in computation time between the two enrichment strategies, we conclude that the offline enrichment strategy is more advantageous than the online enrichment strategy if more than 102, 83, 52 online calculations are required with the reduced model for the reduced basis dimension pairs $(N, R) = (19, 50)$, $(N, R) = (51, 70)$, $(N, R) = (89, 50)$, respectively. These numbers are called benefit threshold in Table 2.1.

(N, R)	$(19, 50)$		$(51, 70)$		$(89, 50)$	
Phase \ Method	on	off	on	off	on	off
Offline time(s)	1112	2296	1193	2395	1272	1884
Online time(s)	14	2.4	17	2.5	14	2.3
Benefit threshold	102		83		52	

Table 2.1 – Obstacle test case: The cost in seconds of the offline and online phases of the reduced model for the online (on) and offline (off) enrichment cases for the pairs $(N, R) = (19, 50)$, $(N, R) = (51, 70)$ and $(N, R) = (89, 50)$ with $\delta_{\texttt{PGA}} = 10^{-3}$.

2.5.2 Hertz contact between two half-disks

We consider two half-disks as shown in Figure 2.9. The first half-disk occupies a domain $\Omega_1 \subset \mathbb{R}^2$ of fixed radius $R_1 = 1\text{m}$, and the second a domain $\Omega_2(\mu) \subset \mathbb{R}^2$ of parametric radius $R_2 := \mu$ with

$$\mu \in \mathcal{D} := \Big[0.7, 1.3\Big](\text{m}). \tag{2.43}$$

For reasons of symmetry, only quarter-disks are discretized. The initial gap between the two disks is equal to $\gamma_0 > 0$. We impose a displacement of $-d$ (resp. d) on $\Gamma_1^{\texttt{top}}$ (resp. $\Gamma_2^{\texttt{bot}}$) of Ω_1 (resp. of $\Omega_2(\mu)$), with $d \geq \frac{1}{2}\gamma_0$. We set $\Omega(\mu) := \Omega_1 \cup \Omega_2(\mu)$ as well as $E := 15\text{Pa}$ (resp. $\nu := 0.35$) for the Young modulus (resp. the Poisson coefficient). For all $\mu \in \mathcal{D}$, we assume that there is a smooth invertible geometric mapping $h(\mu) : \widehat{\Omega} \to \Omega(\mu)$ defined on a reference domain $\widehat{\Omega} := \widehat{\Omega}_1 \cup \widehat{\Omega}_2$ such that $\Big\{\widehat{\Omega}_1, \widehat{\Omega}_2\Big\}$ is a partition of $\widehat{\Omega}$, $h(\mu)(\widehat{\Omega}_1) = \Omega_1$, $h(\mu)(\widehat{\Omega}_2) = \Omega_2(\mu)$ (notice that $h(\mu)|_{\widehat{\Omega}_1}$ is parameter-independent). We denote by $\widehat{\Gamma}_1^c$ (resp. $\widehat{\Gamma}_2^c$) the potential contact manifold located on $\partial\widehat{\Omega}_1$ (resp. $\partial\widehat{\Omega}_2$), and we set $\Gamma_1^c := h(\mu)(\widehat{\Gamma}_1^c)$ and $\Gamma_2^c(\mu) := h(\mu)(\widehat{\Gamma}_2^c)$. The training set is chosen as $\mathcal{D}_{\texttt{train}} := \Big\{0.7 + 0.0075i, 0 \leq i \leq 80\Big\}(\text{m})$ (altogether 81 points)

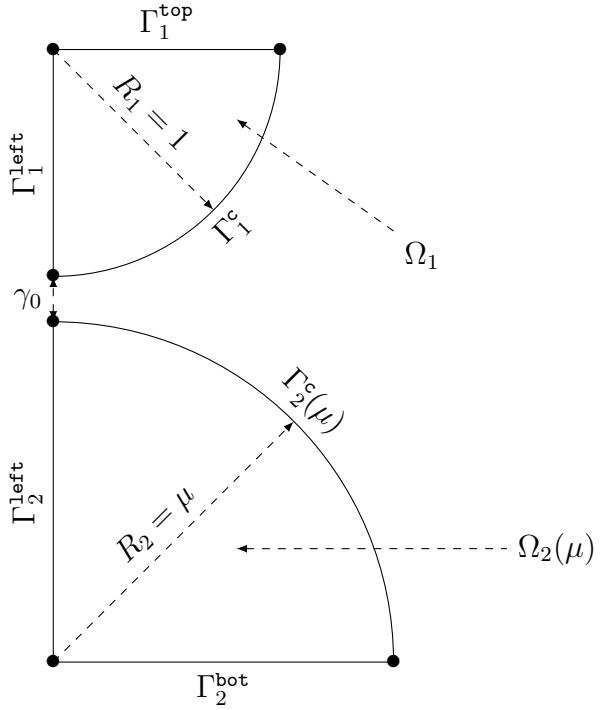

Figure 2.9 – Hertz test case: Configuration.

and the validation set $\mathcal{D}_{\mathtt{valid}}$ is generated by choosing 30 elements in $\mathcal{D}$ randomly with a uniform distribution.

We consider the HF subspace $\widehat{\mathcal{V}} \subset H^1(\widehat{\Omega}; \mathbb{R}^2)$ and the HF subcone $\widehat{\mathcal{W}}^+ \subset L^2(\widehat{\Gamma}_1^c, \mathbb{R}_+)$ built using $\mathbb{P}_1$ finite elements for displacement and the LAC (Local Average Contact) method [1] with $\mathbb{P}_0$ finite elements for the Lagrange multiplier on a mesh composed of 6130 nodes with 560 nodes on the potential contact manifold $\widehat{\Gamma}_1^{\mathtt{c}}$. Thus, we have $\mathcal{N} := \dim(\widehat{\mathcal{V}}) = 12260$ primal and $\mathcal{R} := \dim(\widehat{\mathcal{W}}) = 280$ dual degrees of freedom. We equip the space $\widehat{\mathcal{V}}$ with the norm $\|\cdot\|_{\widehat{\mathcal{V}}}$ defined as follows (we use boldface notation for vector-valued fields):

$$\|\widehat{\boldsymbol{v}}\|_{\widehat{\mathcal{V}}} := \left(\|\widehat{\boldsymbol{v}}\|_{L^2}^2 + \hat{\ell}^2 \|\nabla \widehat{\boldsymbol{v}}\|_{L^2}^2\right)^{\frac{1}{2}}, \quad \forall \widehat{\boldsymbol{v}} \in \widehat{\mathcal{V}}, \tag{2.44}$$

where $\hat{\ell}$ is a characteristic length of $\widehat{\Omega}$ which is introduced for dimensional consistency. The variational formulation of the contact problem leads to a minimization problem of the form (2.1) subject to a so-called non-interpenetration condition which can be written either under the small deformation assumption (linear) or under the large deformation assumption (nonlinear). The bilinear form $\widehat{a}(\mu; \cdot, \cdot) : \widehat{\mathcal{V}} \times \widehat{\mathcal{V}} \to \mathbb{R}$ associated with the equilibrium equation in $\Omega(\mu)$ is defined by

$$\widehat{a}(\mu; \widehat{\boldsymbol{u}}, \widehat{\boldsymbol{v}}) := \int_{\Omega(\mu)} \sigma(\varepsilon(\widehat{\boldsymbol{u}} \circ h(\mu)^{-1})) : \varepsilon(\widehat{\boldsymbol{v}} \circ h(\mu)^{-1}) \, d\Omega(\mu), \tag{2.45}$$

where the linearized strain tensor $\varepsilon(\boldsymbol{v})$ is given by

$$\varepsilon(\boldsymbol{v}) := \frac{1}{2}\left(\nabla \boldsymbol{v} + \nabla \boldsymbol{v}^\top\right), \tag{2.46}$$

and the stress tensor $\sigma(\varepsilon)$ is given by

$$\sigma(\varepsilon) := \frac{E\nu}{(1+\nu)(1-2\nu)} tr(\varepsilon)\mathbb{I}_2 + \frac{E}{(1+\nu)}\varepsilon, \tag{2.47}$$

with $\mathbb{I}_2$ the identity matrix of order 2. The linear form $\widehat{f}(\mu;\cdot) : \widehat{\mathcal{V}} \to \mathbb{R}$ associated with the external load $\boldsymbol{\ell}(\mu) : \Omega(\mu) \to \mathbb{R}^2$ applied to $\Omega(\mu)$ is defined as

$$\widehat{f}(\mu;\widehat{\boldsymbol{v}}) := \int_{\Omega(\mu)} \boldsymbol{\ell}(\mu) \cdot \left(\widehat{\boldsymbol{v}} \circ h(\mu)^{-1}\right) d\Omega(\mu). \tag{2.48}$$

We consider here the first situation where we make the assumption of small deformations so that $\widehat{\Omega}$ deviates very little from its initial configuration. This allows us to assume that the normal vector is constant on the whole contact manifold. We denote by $\boldsymbol{n} := \boldsymbol{e}_y = (0,1)^\top$ the outward normal vector in $\widehat{\Gamma}_1^c$ and by $\widehat{\boldsymbol{\phi}} : \widehat{\Gamma}_1^c \to \widehat{\Gamma}_2^c$ the pairing function. The non-interpenetration condition is written as follows:

$$\left(\widehat{\boldsymbol{u}}_1(\mu)(\widehat{\boldsymbol{x}}) - \widehat{\boldsymbol{u}}_2(\mu) \circ \widehat{\boldsymbol{\phi}}(\widehat{\boldsymbol{x}})\right) \cdot \boldsymbol{e}_y \leq \left(\widehat{\boldsymbol{\phi}}(\widehat{\boldsymbol{x}}) - \widehat{\boldsymbol{x}}\right) \cdot \boldsymbol{e}_y, \quad \forall \widehat{\boldsymbol{x}} \in \widehat{\Gamma}_1^c. \tag{2.49}$$

Thus, the admissible set $\widehat{\mathcal{K}}(\mu)$ becomes

$$\widehat{\mathcal{K}}(\mu) := \left\{ \widehat{\boldsymbol{v}} \in \widehat{\mathcal{V}} \;\middle|\; \widehat{b}(\mu;\widehat{\boldsymbol{v}},\widehat{\eta}) \leq \widehat{g}(\mu;\widehat{\eta}),\ \forall \widehat{\eta} \in \widehat{\mathcal{W}}^+ \right\}, \tag{2.50}$$

where

$$\widehat{b}(\mu;\widehat{\boldsymbol{v}},\widehat{\eta}) := \int_{\widehat{\Gamma}_1^c} \left(\widehat{\boldsymbol{v}}_1(\mu)(\widehat{\boldsymbol{x}}) - (\widehat{\boldsymbol{v}}_2(\mu) \circ \widehat{\boldsymbol{\phi}})(\widehat{\boldsymbol{x}})\right) \cdot \boldsymbol{e}_y \widehat{\eta}(\widehat{\boldsymbol{x}})\, d\widehat{\boldsymbol{x}}, \tag{2.51}$$

$$\widehat{g}(\mu;\widehat{\eta}) = \widehat{g}(\widehat{\eta}) := \int_{\widehat{\Gamma}_1^c} (\widehat{\boldsymbol{\phi}}(\widehat{\boldsymbol{x}}) - \widehat{\boldsymbol{x}}) \cdot \boldsymbol{e}_y \widehat{\eta}(\widehat{\boldsymbol{x}})\, d\widehat{\boldsymbol{x}}. \tag{2.52}$$

The initial gap γ_0 and the imposed displacement d are, respectively, set to $\gamma_0 := 0.001$m and $d := 0.09$m. This latter value, which is less than 10% of the maximum value between R_1 and R_2, allows us to remain within the validity of the small deformation assumption.

Figure 2.10 displays the deformed configuration resulting from the HF displacement field $\boldsymbol{u}(\mu) := \widehat{\boldsymbol{u}}(\mu) \circ h(\mu)^{-1}$ for $\mu = 0.9$m on its left panel and the Lagrange multiplier $\lambda(\mu) := \widehat{\lambda}(\mu) \circ h(\mu)^{-1}$ as a function of the abscissa along $\widehat{\Gamma}_1^c$ for $\mu \in \left\{0.7, 0.8, 1.0, 1.1, 1.3\right\}(m)$ on its right panel. We notice that the non-interpenetration condition is respected on the deformed configuration as expected. We can also notice some small oscillations in the Lagrange multipliers. This is due to the fact that for the evaluation of the contact contributions, a direct projection of the integration scheme is used instead of a projection-intersection of the master cells onto the slave cells. Figure 2.11 shows on its left (resp. right) panel the projection error $\widehat{e}_{\texttt{POD}}$ (resp. $\widehat{e}_{\texttt{CPG}}$ and $\widehat{e}_{\texttt{mCPG}}$) defined in (2.11) (resp. (2.13) and (2.34)) produced by the POD (resp. CPG and mCPG) algorithms as a function of the number of vectors composing the primal (resp. dual) reduced bases. In all cases, the projection errors decrease sufficiently fast so that the linear spaces generated by the primal and dual snapshots can be approximated by small-dimensional subspaces. We also notice that the projection error for the mCPG

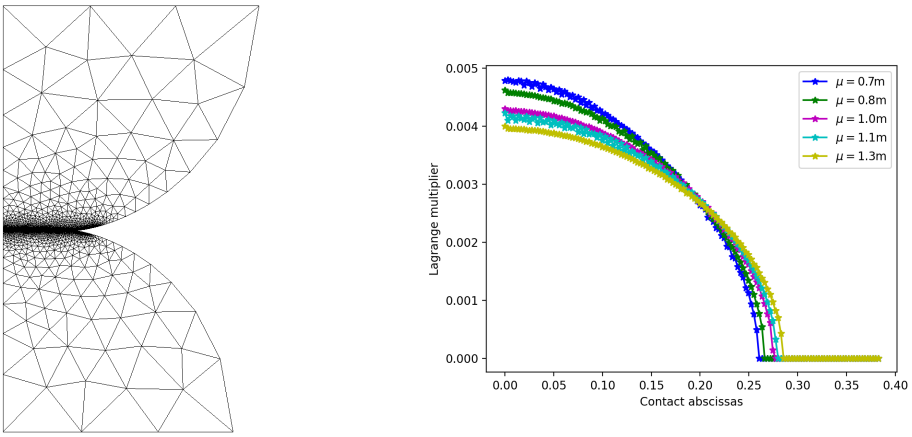

Figure 2.10 – Hertz test case: HF solution. Left: $\boldsymbol{u}(\mu)$ for $\mu = 0.9m$. Right: $\lambda(\mu)$ for $\mu \in \{0.7, 0.8, 1.0, 1.1, 1.3\}(m)$.

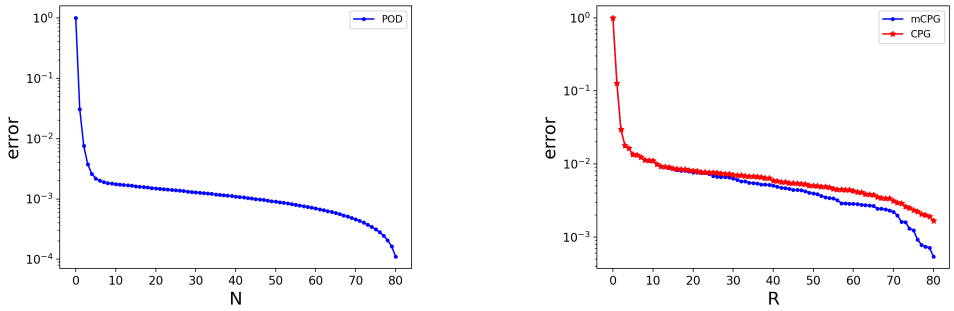

Figure 2.11 – Hertz test case: projection errors for the POD, CPG and mCPG algorithms. Left: POD. Right: CPG and mCPG.

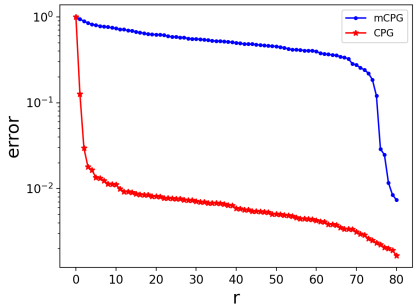

Figure 2.12 – Hertz test case: Comparison between $\widehat{e}^{\texttt{CPG}}_{\text{orth}}(r)$ and $\widehat{e}^{\texttt{mCPG}}_{\text{orth}}(r)$.

algorithm is smaller than that for the CPG algorithm. This numerically indicates that the cone constructed using the mCPG algorithm yields more accurate approximations than the one obtained by means of the CPG algorithm.

As before, it can be seen in Figure 2.12 that $\widehat{e}^{\texttt{CPG}}_{\text{orth}}(r) \leq \widehat{e}^{\texttt{mCPG}}_{\text{orth}}(r)$ for all $r \geq 0$, which illustrates that the basis constructed with the mCPG algorithm is of better quality than the one constructed with the CPG algorithm.

Considering the three tolerance pairs $(\delta_{\texttt{POD}} = 10^{-3}, \delta_{\texttt{mCPG}} = 10^{-2})$, $(\delta_{\texttt{POD}} = 10^{-3}, \delta_{\texttt{mCPG}} =$

10^{-3}), and ($\delta_{\texttt{POD}} = 10^{-2}, \delta_{\texttt{mCPG}} = 10^{-2}$), we obtain respectively the following pairs for the dimensions of the reduced bases: $(N = 46, R = 12)$, $(N = 46, R = 70)$, $(N = 3, R = 12)$. With these choices, we cover the two possible settings, namely $N < R$ where we are sure that for all $\mu \in \mathcal{D}$, the bilinear form $\widehat{b}(\mu; \cdot, \cdot)$ is not inf-sup stable ($\widehat{\beta}^{\text{dec}}_{N,R}(\mu) = 0$) and $N \geq R$ where inf-sup stability cannot be asserted a priori. Figure 2.13 shows the coefficient $\widehat{\beta}^{\text{dec}}_{N,R}(\mu)$ as a function of $\mu \in \mathcal{D}_{\texttt{valid}}$ for the pair $(N, R) = (46, 12)$. Contrary to the results obtained in the obstacle test case, the value of the inf-sup constant $\widehat{\beta}^{\text{dec}}_{N,R}(\mu)$ is non-zero although it remains very small compared with $\widehat{\beta}_{\text{HF}}(\mu)$ (which is of the order of 8).

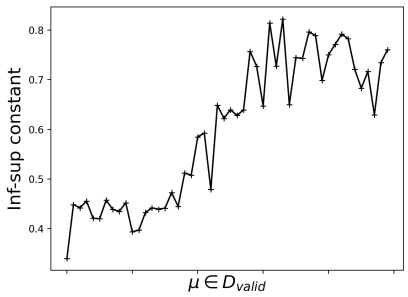

Figure 2.13 – Hertz test case: Inf-sup constant $\widehat{\beta}^{\text{dec}}_{N,R}(\mu)$ with $(N, R) = (46, 12)$.

Let us now consider the results obtained with the strategy proposed in Section 2.3. Figures 2.14c, 2.14f and 2.14i, respectively, show the values of $\widehat{\beta}^{\text{off}}_{N,R}(\mu)$ as a function of $\mu \in \mathcal{D}_{\texttt{valid}}$ for the pairs $(N, R) = (3, 12)$, $(N, R) = (46, 70)$, $(N, R) = (46, 12)$. For each of the above pairs, we consider the tighter tolerance $\delta_{\texttt{PGA}} = 0.3$ as well as the looser tolerance $\delta_{\texttt{PGA}} = 0.5$, 0.6, 0.4, respectively. These results illustrate the fact that the PGA algorithm does indeed recover the expected stability property. The panels in column 1 (resp. 2) of Figure 2.14, report the values of $\widehat{\sigma}_{\widehat{S}^n}(\mu_n)$ (see (2.23)) (resp. $\min_{\mu \in \mathcal{D}_{\texttt{train}}} \widehat{\beta}_{\widehat{S}^n}(\mu)$ (see (2.42))) as a function of n for the pairs $(N, R) = (3, 12)$, $(N, R) = (46, 70)$, $(N, R) = (46, 12)$ with $\delta_{\texttt{PGA}} = 0.3$. The results show that the PGA algorithm converges and employs an effective greedy selection of supremizers in order to recover inf-sup stability for the reduced model. Another interesting observation is that the decrease of $\widehat{\sigma}_{\widehat{S}^n}(\mu^n)$ with respect to n is much slower than for the previous test case.

Figure 2.15 shows a comparison between the inf-sup constants $\widehat{\beta}_{\text{HF}}(\mu)$, $\widehat{\beta}^{\text{dec}}_{N,R}(\mu)$, $\widehat{\beta}^{\text{on}}_{N,R}(\mu)$, and $\widehat{\beta}^{\text{off}}_{N,R}(\mu)$ for each of reduced basis dimension pairs $(N = 46, R = 12)$, $(N = 46, R = 70)$, and $(N = 3, R = 12)$ with respectively $\delta_{\texttt{PGA}} = 0.5$, $\delta_{\texttt{PGA}} = 0.6$ and $\delta_{\texttt{PGA}} = 0.4$. On the one hand, we see that in all cases, in agreement with the theoretical results, $\widehat{\beta}^{\text{on}}_{N,R}(\mu) \geq \widehat{\beta}^{\text{off}}_{N,R}(\mu) \geq \widehat{\beta}^{\text{dec}}_{N,R}(\mu)$ and $\widehat{\beta}^{\text{on}}_{N,R}(\mu) \geq \widehat{\beta}_{\text{HF}}(\mu)$ for all $\mu \in \mathcal{D}_{\texttt{valid}}$. On the other hand, we notice that there is no established order between $\widehat{\beta}^{\text{off}}_{N,R}(\mu)$ and $\widehat{\beta}_{\text{HF}}(\mu)$.

Finally, Table 2.2 shows that the offline phase of the offline enrichment method is up to two times more expensive than the online enrichment method for the three reduced basis dimension pairs (N, R) with $\delta_{\texttt{PGA}} = 0.3$. Overall, the same conclusions can be reached as those related to the previous test case in Table 2.1.

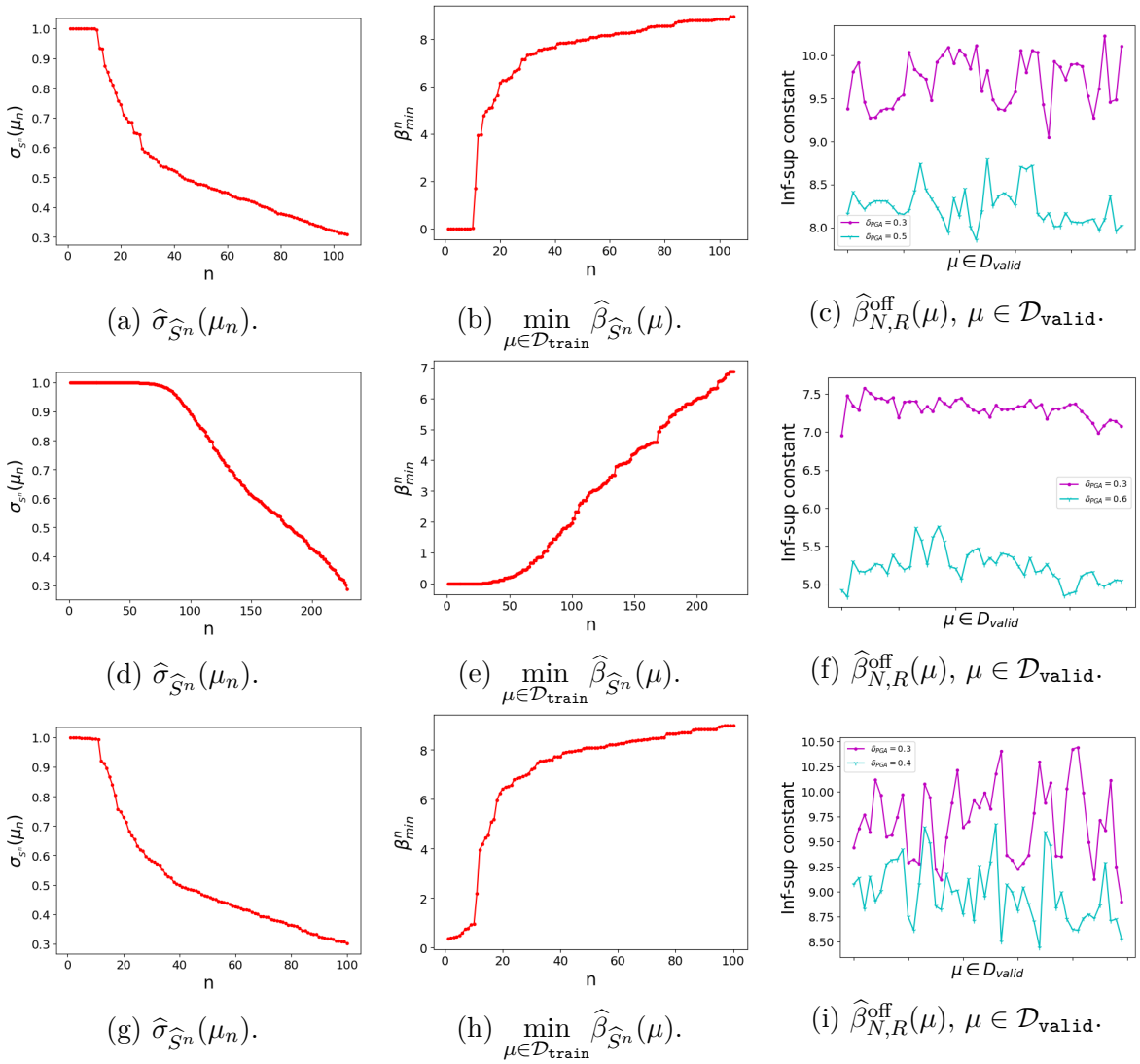

(a) $\widehat{\sigma}_{\widehat{S}^n}(\mu_n)$. (b) $\min_{\mu \in \mathcal{D}_{\texttt{train}}} \widehat{\beta}_{\widehat{S}^n}(\mu)$. (c) $\widehat{\beta}^{\text{off}}_{N,R}(\mu)$, $\mu \in \mathcal{D}_{\texttt{valid}}$.

(d) $\widehat{\sigma}_{\widehat{S}^n}(\mu_n)$. (e) $\min_{\mu \in \mathcal{D}_{\texttt{train}}} \widehat{\beta}_{\widehat{S}^n}(\mu)$. (f) $\widehat{\beta}^{\text{off}}_{N,R}(\mu)$, $\mu \in \mathcal{D}_{\texttt{valid}}$.

(g) $\widehat{\sigma}_{\widehat{S}^n}(\mu_n)$. (h) $\min_{\mu \in \mathcal{D}_{\texttt{train}}} \widehat{\beta}_{\widehat{S}^n}(\mu)$. (i) $\widehat{\beta}^{\text{off}}_{N,R}(\mu)$, $\mu \in \mathcal{D}_{\texttt{valid}}$.

Figure 2.14 – Hertz test case: PGA algorithm. Row 1: $(N, R) = (3, 12)$. Row 2: $(N, R) = (46, 70)$. Row 3 $(N, R) = (46, 12)$. Column 1 and Column 2: $\delta_{\texttt{PGA}} = 0.3$. Column 3: $\delta_{\texttt{PGA}} \in \{0.6, 0.5, 0.4, 0.3\}$.

(N, R)	$(3, 12)$		$(46, 70)$		$(46, 12)$	
Phase \ Method	on	off	on	off	on	off
Offline time(s)	8490	18098	10889	19750	10874	18312
Online time(s)	75	18	162	20	78	19
Benefit threshold	169		62		126	

Table 2.2 – Hertz test case: The cost in seconds of the offline and online phases of the reduced model for the online (on) and offline (off) enrichment cases for the pairs $(N, R) = (3, 12)$, $(N, R) = (46, 70)$ and $(N, R) = (46, 12)$ with $\delta_{\texttt{PGA}} = 0.3$.

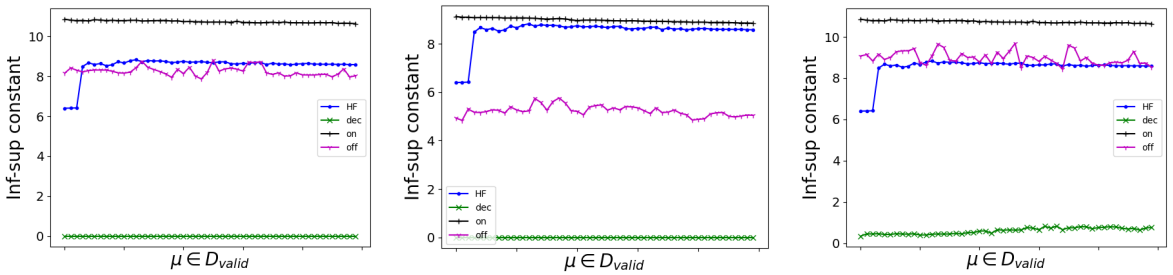

(a) $(N, R) = (3, 12), \delta_{\texttt{PGA}} = 0.5$.

(b) $(N, R) = (46, 70), \delta_{\texttt{PGA}} = 0.6$.

(c) $(N, R) = (46, 12), \delta_{\texttt{PGA}} = 0.4$.

Figure 2.15 – Hertz test case: Inf-sup constant $\widehat{\beta}_{\mathrm{HF}}(\mu)$, $\widehat{\beta}^{\mathrm{dec}}_{N,R}(\mu)$, $\widehat{\beta}^{\mathrm{on}}_{N,R}(\mu)$, and $\widehat{\beta}^{\mathrm{off}}_{N,R}(\mu)$ for $\mu \in \mathcal{D}_{\texttt{valid}}$.

CHAPTER 3

MODEL REDUCTION FOR FRICTIONAL CONTACT PROBLEMS IN MIXED FORMULATION

Abstract

In this work, we propose a new reduced-basis method to construct a reduced-order model for parametric mechanical contact problems with friction. We consider a mixed formulation of the problem, and reduced bases are constructed separately for the displacement field, and the normal and tangential stress components. The main novelty lies in the way the friction condition is imposed on the reduced-order model: we propose here a greedy algorithm, which shares common features with cutting-plane algorithms, in order to appropriately select a set of collocation nodes where the friction condition is enforced in the reduced-order model. We provide numerical evidence of the efficiency of the proposed algorithm on the Hertz contact problem between two half-disks with Coulomb friction.

Contents

3.1 Introduction

The aim of model reduction methods is to reduce the computational cost of the resolution of models which depend on some parameters for a large number of values of these parameters. Indeed, standard numerical approaches for the resolution of such models, like finite elements for instance, lead to a high-fidelity (HF) approximation of the parametric model of interest that is usually very expensive to compute. The objective of reduced-order modelling is to build another, *reduced*, model that is much cheaper to solve for any values of the parameters and, at the same time, yields approximations of the original HF model with good accuracy; see [79, 90, 76, 102, 3, 21] and the more recent textbooks [58, 92]. Such a task is usually performed by organizing the calculations in a first offline phase which is a learning phase where expensive calculations are carried out on the HF model for a small number of values of the parameter drawn from a training set. The output of the offline phase is used to build the reduced-order model. Then, in the online phase, a large number of new instances of the parameter are considered for which the reduced model is solved instead of the HF model. The obtained reduced-order model can then be used instead of the original HF model in any context where intensive parametric studies are needed, thus saving substantial amounts of computational time. This strategy can be useful for instance in design optimization, inverse problems, and real-time control applications.

The aim of the present contribution is to investigate a new Reduced Basis (RB) method for the resolution of parametric contact problems with friction (Tresca or Coulomb) in computational mechanics [67]. We are particularly interested in the mixed formulation [34, 59] where the constraints are taken into account through the use of Lagrange multipliers. Model-order reduction methods for parametric contact problems without friction, and in particular RB methods, has been a very active research area in the past decade. More generally, several contributions have been concerned with model reduction for linear parameter-dependent variational inequalities of the first kind [55, 50, 105]. The mixed formulation leads to a so-called primal-dual strategy, whereby reduced bases must be created for both the primal and the dual variables. In the case of mechanical contact problems without friction, the primal variable is the displacement field, whereas the dual variable is the normal component of the contact stress. Various strategies can be adopted in order to build reduced spaces for the primal and dual variables, including Proper Orthogonal Decomposition (POD) [8, 22, 69] for the primal variable and Non-negative Matrix Factorization (NMF) [72] for the dual variable. Let us also mention [40] where a hypereduction method for contact problems is proposed. Instead of the NMF, one can also consider the Angle Greedy [55, 19] and the Cone Projected Greedy (CPG) [12, 84] algorithms for the compression of the dual basis.

Much fewer works have dealt with the reduction of contact problems in the presence of friction and, more generally, of variational inequalities of the second kind. We are only aware of reduced-order modelling methods for this type of problems using the Progressive Generalized Decomposition (PGD) approach [83]. Here, we propose and investigate a new RB method where reduced spaces have to be built for the displacement field, the normal component of the contact stress and the tangential component of the contact stress, the latter being the Lagrange multiplier associated with the friction

condition in (Tresca or Coulomb) friction models. The construction of reduced spaces for the displacement field and the normal component of the contact stress are done here following the approach presented in [84]. In the case of friction, the construction of a reduced-order model taking into account the friction constraints requires two additional ingredients:

(i) the construction of a reduced space for the approximation of the tangential component of the contact stress: this is done here by means of a classical POD method;

(ii) the construction of a reduced set of collocation points on which the friction constraints have to be enforced at the level of the reduced-order model.

It appears that the second item mentioned above is not a trivial task: indeed, for a given reduced space in which the tangential stress components are computed, enforcing friction constraints at the same number of collocation points than in the HF model may lead to reduced tangential stresses that are computed to be zero, because of the disproportion between the number of basis functions used to discretize the tangential stresses, and the number of constraints imposed in the reduced model. One novel contribution of our work is to propose a greedy algorithm, which shares similarities with cutting-plane algorithms [63], for the selection of a relevant subset of collocation points to be used in the reduced-order model, depending on the choice of the reduced basis in which the tangential stress components are computed.

The outline of the paper is as follows. In Section 3.2, we present the HF model used here for the resolution of mechanical contact problems with (Tresca or Coulomb) friction. The RB method together with the Greedy Collocation Node Selection procedure we propose is presented in Section 3.3. Finally, in Section 3.4, numerical results illustrating the behaviour of the proposed algorithms are presented for the Hertz contact problem [57, 103] between two half-disks.

3.2 High-fidelity model

In this section, we present the HF problem in mixed form and introduce an approximate HF problem using collocation.

3.2.1 Mixed formulation in general form

For all $\mu \in \mathcal{D}$ (the parametric domain), we consider an elastic body whose reference configuration is the domain $\Omega(\mu) \subset \mathbb{R}^d$, with $d \in \{2, 3\}$. The boundary $\Gamma(\mu) := \partial\Omega(\mu)$ is partitioned as $\Gamma(\mu) = \Gamma^{\mathrm{D}}(\mu) \cup \Gamma^{\mathrm{N}}(\mu) \cup \Gamma^{\mathrm{c}}(\mu)$. The body is clamped at the boundary $\Gamma^{\mathrm{D}}(\mu)$, free of traction at the boundary $\Gamma^{\mathrm{N}}(\mu)$, and $\Gamma^{\mathrm{c}}(\mu)$ denotes the potential contact boundary with a given rigid support. The body in its reference configuration is located at some distance from the rigid support. An external load $\boldsymbol{\ell}(\mu) : \Omega(\mu) \to \mathbb{R}^d$ is applied to the body. We denote by $\boldsymbol{u}(\mu) : \Omega(\mu) \to \mathbb{R}^d$ the resulting displacement field, by $\boldsymbol{n}(\mu)$ the unit outward normal on $\Gamma(\mu)$ and by $\boldsymbol{\tau}(\mu) := \left[\boldsymbol{\tau}_1(\mu) \cdots \boldsymbol{\tau}_{d-1}(\mu)\right] \in \mathbb{R}^{d\times(d-1)}$ an orthonormal basis of the hyperplane orthogonal to $\boldsymbol{n}(\mu)$ in $\mathbb{R}^d$. For simplicity, we just

write $\boldsymbol{n}$ and $\boldsymbol{\tau}$ whenever there is no ambiguity. For a generic $\mathbb{R}^d$-valued displacement field $\boldsymbol{v}$, the $\mathbb{R}^{d\times d}$-valued linearized strain tensor $\varepsilon(\boldsymbol{v})$ and the $\mathbb{R}^{d\times d}$-valued stress tensor $\sigma(\boldsymbol{v})$ are given by

$$\varepsilon(\boldsymbol{v}) := \frac{1}{2}\Big(\nabla \boldsymbol{v} + \nabla \boldsymbol{v}^\top\Big), \quad \sigma(\boldsymbol{v}) := \mathbb{C}\varepsilon(\boldsymbol{v}), \tag{3.1}$$

with $\mathbb{C}$ the elastic coefficient tensor. At the boundary, we decompose the displacement field, $\boldsymbol{v}$, and the normal component of the stress tensor, $\sigma(\boldsymbol{v})\boldsymbol{n}$, in normal and tangential components as follows:

$$\boldsymbol{v} = v_{\boldsymbol{n}}\boldsymbol{n} + \boldsymbol{\tau}\boldsymbol{v}_{\boldsymbol{\tau}}, \quad \sigma(\boldsymbol{v})\boldsymbol{n} = \sigma_{\boldsymbol{nn}}(\boldsymbol{v})\boldsymbol{n} + \boldsymbol{\tau}\boldsymbol{\sigma}_{\boldsymbol{n\tau}}(\boldsymbol{v}), \tag{3.2}$$

with $v_{\boldsymbol{n}} \in \mathbb{R}$, $\boldsymbol{v}_{\boldsymbol{\tau}} \in \mathbb{R}^{d-1}$, $\sigma_{\boldsymbol{nn}}(\boldsymbol{v}) \in \mathbb{R}$ and $\boldsymbol{\sigma}_{\boldsymbol{n\tau}}(\boldsymbol{v}) \in \mathbb{R}^{d-1}$. We consider the following problem: For all $\mu \in \mathcal{D}$, find the displacement field $\boldsymbol{u}(\mu) : \Omega(\mu) \to \mathbb{R}^d$ such that

$$-\mathrm{div}(\sigma(\boldsymbol{u}(\mu))) = \boldsymbol{\ell}(\mu), \quad \text{in } \Omega(\mu), \tag{3.3a}$$
$$\boldsymbol{u}(\mu) = \boldsymbol{0}, \quad \text{on } \Gamma^{\mathrm{D}}(\mu), \tag{3.3b}$$
$$\sigma(\boldsymbol{u}(\mu))\boldsymbol{n} = \boldsymbol{0}, \quad \text{on } \Gamma^{\mathrm{N}}(\mu), \tag{3.3c}$$

together with the non-interpenetration and friction conditions on $\Gamma^{\mathrm{c}}(\mu)$ which we now detail. We denote by $\boldsymbol{\phi}(\mu) : \Gamma^{\mathrm{c}}(\mu) \to \Gamma^{\mathrm{c}}_r$ the contact pairing function where Γ^{c}_r refers to the potential contact zone on the rigid support. Under the assumption of small deformations, the non-interpenetration condition is written using the normal from the reference configuration and reads

$$u_{\boldsymbol{n}}(\mu)(\boldsymbol{x}) \le d^{\boldsymbol{n}}(\mu)(\boldsymbol{x}) := \Big(\boldsymbol{\phi}(\mu)(\boldsymbol{x}) - \boldsymbol{x}\Big) \cdot \boldsymbol{n}(\mu)(\boldsymbol{x}), \quad \forall \boldsymbol{x} \in \Gamma^{\mathrm{c}}(\mu). \tag{3.4}$$

Notice that $d^{\boldsymbol{n}}(\mu) \ge 0$ by construction. The Signorini contact conditions on $\Gamma^{\mathrm{c}}(\mu)$ are then formulated as

$$u_{\boldsymbol{n}}(\mu) \le d^{\boldsymbol{n}}(\mu), \quad \sigma_{\boldsymbol{nn}}(\boldsymbol{u}(\mu)) \le 0, \quad \sigma_{\boldsymbol{nn}}(\boldsymbol{u}(\mu))\Big(u_{\boldsymbol{n}}(\mu) - d^{\boldsymbol{n}}(\mu)\Big) = 0. \tag{3.5}$$

The formulation of the friction conditions on $\Gamma^{\mathrm{c}}(\mu)$ depends on the friction law. In this work, we consider the Coulomb friction law:

$$\begin{cases} \|\boldsymbol{\sigma}_{\boldsymbol{n\tau}}(\boldsymbol{u}(\mu))\| \le \nu_{\mathcal{F}}|\sigma_{\boldsymbol{nn}}(\boldsymbol{u}(\mu))|, & \text{if } \boldsymbol{u}_{\boldsymbol{\tau}}(\mu) = \boldsymbol{0}, \\ \boldsymbol{\sigma}_{\boldsymbol{n\tau}}(\boldsymbol{u}(\mu)) = -\nu_{\mathcal{F}}|\sigma_{\boldsymbol{nn}}(\boldsymbol{u}(\mu))|\dfrac{\boldsymbol{u}_{\boldsymbol{\tau}}(\mu)}{\|\boldsymbol{u}_{\boldsymbol{\tau}}(\mu)\|}, & \text{otherwise,} \end{cases} \tag{3.6}$$

where $\nu_{\mathcal{F}} > 0$ is a given nondimensional coefficient, taken to be constant for simplicity. The Coulomb frictional contact problem consists in finding the displacement field $\boldsymbol{u}(\mu) : \Omega(\mu) \to \mathbb{R}^d$ satisfying (3.3a)-(3.3b)-(3.3c), (3.5) and (3.6).

Let $\boldsymbol{\mathcal{V}}(\mu)$, $\mathcal{W}(\mu)$ and $\boldsymbol{\mathcal{X}}(\mu)$ be three finite-dimensional high-fidelity (HF) spaces typically resulting from the finite element discretization of Hilbert spaces and such that

$$\boldsymbol{\mathcal{V}}(\mu) \subset \Big\{\boldsymbol{v} \in H^1(\Omega(\mu);\mathbb{R}^d) \mid \boldsymbol{v} = \boldsymbol{0} \text{ on } \Gamma^{\mathrm{D}}(\mu)\Big\}, \tag{3.7a}$$
$$\mathcal{W}(\mu) \subset L^2(\Gamma^{\mathrm{c}}(\mu);\mathbb{R}), \tag{3.7b}$$
$$\boldsymbol{\mathcal{X}}(\mu) \subset L^2(\Gamma^{\mathrm{c}}(\mu);\mathbb{R}^{d-1}), \tag{3.7c}$$

and let $\mathcal{W}^{\boldsymbol{n}}(\mu) \subset \mathcal{W}(\mu)$ be the positive cone defined as

$$\mathcal{W}^{\boldsymbol{n}}(\mu) := \left\{\eta^{\boldsymbol{n}} \in \mathcal{W}(\mu) \mid \eta^{\boldsymbol{n}} \geq 0\right\} \subset L^2(\Gamma^{\mathrm{c}}(\mu); \mathbb{R}_+). \tag{3.8}$$

The bilinear form $a(\mu; \cdot, \cdot) : \boldsymbol{\mathcal{V}}(\mu) \times \boldsymbol{\mathcal{V}}(\mu) \to \mathbb{R}$ associated with the equilibrium equation (3.3a) in $\Omega(\mu)$ is defined as

$$a(\mu; \boldsymbol{u}, \boldsymbol{v}) := \int_{\Omega(\mu)} \sigma(\boldsymbol{u}) : \varepsilon(\boldsymbol{v})\, d\Omega(\mu), \tag{3.9}$$

and the linear form $f(\mu; \cdot) : \boldsymbol{\mathcal{V}}(\mu) \to \mathbb{R}$ associated with the external load $\boldsymbol{\ell}(\mu)$ is defined as

$$f(\mu; \boldsymbol{v}) := \int_{\Omega(\mu)} \boldsymbol{\ell}(\mu) \cdot \boldsymbol{v}\, d\Omega(\mu). \tag{3.10}$$

The admissible set $\boldsymbol{\mathcal{K}}(\mu)$ is defined as

$$\boldsymbol{\mathcal{K}}(\mu) := \left\{\boldsymbol{v} \in \boldsymbol{\mathcal{V}}(\mu) \;\middle|\; b^{\boldsymbol{n}}(\mu; \boldsymbol{v}, \eta^{\boldsymbol{n}}) \leq g^{\boldsymbol{n}}(\mu; \eta^{\boldsymbol{n}}), \quad \forall \eta^{\boldsymbol{n}} \in \mathcal{W}^{\boldsymbol{n}}(\mu)\right\}, \tag{3.11}$$

with the bilinear form $b^{\boldsymbol{n}}(\mu; \cdot, \cdot) : \boldsymbol{\mathcal{V}}(\mu) \times \mathcal{W}(\mu) \to \mathbb{R}$ and the linear form $g^{\boldsymbol{n}}(\mu; \cdot) : \mathcal{W}(\mu) \to \mathbb{R}$ such that

$$b^{\boldsymbol{n}}(\mu; \boldsymbol{v}, \eta^{\boldsymbol{n}}) := \langle v_{\boldsymbol{n}}, \eta^{\boldsymbol{n}} \rangle_{\Gamma^{\mathrm{c}}(\mu)}, \tag{3.12a}$$

$$g^{\boldsymbol{n}}(\mu; \eta^{\boldsymbol{n}}) := \langle d^{\boldsymbol{n}}(\mu), \eta^{\boldsymbol{n}} \rangle_{\Gamma^{\mathrm{c}}(\mu)}, \tag{3.12b}$$

where $\langle \cdot, \cdot \rangle_{\Gamma^{\mathrm{c}}(\mu)}$ denotes the inner product of $L^2(\Gamma^{\mathrm{c}}(\mu); \mathbb{R})$ or $L^2(\Gamma^{\mathrm{c}}(\mu); \mathbb{R}^{d-1})$ depending on the context. Notice that $\boldsymbol{\mathcal{K}}(\mu)$ is a non-empty convex set. Finally, the friction functional $\mathcal{F}$ is defined as

$$\mathcal{F}(\mu; \boldsymbol{w}, \boldsymbol{v}) := \langle -\nu_{\mathcal{F}} |\sigma_{\boldsymbol{nn}}(\boldsymbol{w})|, \|\boldsymbol{v}_{\boldsymbol{\tau}}\| \rangle_{\Gamma^{\mathrm{c}}(\mu)}. \tag{3.13}$$

The classical weak formulation of frictional contact problems [34, 59] consists of solving the following variational inequality: For all $\mu \in \mathcal{D}$, find $\boldsymbol{u}(\mu) \in \boldsymbol{\mathcal{K}}(\mu)$ such that

$$a(\mu; \boldsymbol{u}(\mu), \boldsymbol{v} - \boldsymbol{u}(\mu)) + \mathcal{F}(\mu; \boldsymbol{u}(\mu), \boldsymbol{v}) - \mathcal{F}(\mu; \boldsymbol{u}(\mu), \boldsymbol{u}(\mu)) \geq f(\mu; \boldsymbol{v} - \boldsymbol{u}(\mu)), \quad \forall \boldsymbol{v} \in \boldsymbol{\mathcal{K}}(\mu). \tag{3.14}$$

To solve (3.14), we use a primal-dual formulation. We introduce the set of admissible tangential stresses $\boldsymbol{\mathcal{X}}^{\boldsymbol{\tau}}(\mu; \eta^{\boldsymbol{n}})$, for a given $\eta^{\boldsymbol{n}} \in \mathcal{W}^{\boldsymbol{n}}(\mu)$, defined as follows:

$$\boldsymbol{\mathcal{X}}^{\boldsymbol{\tau}}(\mu; \eta^{\boldsymbol{n}}) := \left\{\boldsymbol{\theta}^{\boldsymbol{\tau}} \in \boldsymbol{\mathcal{X}}(\mu) \mid \langle \boldsymbol{\theta}^{\boldsymbol{\tau}}, \boldsymbol{\rho}^{\boldsymbol{\tau}} \rangle_{\Gamma^{\mathrm{c}}(\mu)} - \langle \eta^{\boldsymbol{n}}, \|\boldsymbol{\rho}^{\boldsymbol{\tau}}\| \rangle_{\Gamma^{\mathrm{c}}(\mu)} \leq 0, \ \forall \boldsymbol{\rho}^{\boldsymbol{\tau}} \in \boldsymbol{\mathcal{X}}(\mu)\right\}. \tag{3.15}$$

Notice that $\boldsymbol{\theta}^{\boldsymbol{\tau}} \in \boldsymbol{\mathcal{X}}^{\boldsymbol{\tau}}(\mu; \eta^{\boldsymbol{n}})$ weakly means that $\|\boldsymbol{\theta}^{\boldsymbol{\tau}}\| \leq \eta^{\boldsymbol{n}}$ a.e on $\Gamma^{\mathrm{c}}(\mu)$.

Remark 3.2.1 (Notation). For the sake of clarity, we point out that the use of $\boldsymbol{n}$ and $\boldsymbol{\tau}$ as superscripts is generic and refers to the connection with the normal and tangential components of dual variables, whereas their use as subscripts corresponds to the definition of normal and tangential components introduced in (3.2).

According to [59], the Coulomb frictional problem (3.14) is equivalent to the following mixed problem: Find $(\boldsymbol{u}(\mu), \lambda^{\boldsymbol{n}}(\mu), \boldsymbol{\lambda}^{\boldsymbol{\tau}}(\mu)) \in \boldsymbol{\mathcal{V}}(\mu) \times \mathcal{W}^{\boldsymbol{n}}(\mu) \times \boldsymbol{\mathcal{X}}^{\boldsymbol{\tau}}(\mu; \nu_{\mathcal{F}}\lambda^{\boldsymbol{n}}(\mu))$ such that

$$\begin{cases} a(\mu; \boldsymbol{u}(\mu); \boldsymbol{v}) + b^{\boldsymbol{n}}(\mu; \boldsymbol{v}, \lambda^{\boldsymbol{n}}(\mu)) + b^{\boldsymbol{\tau}}(\mu; \boldsymbol{v}, \boldsymbol{\lambda}^{\boldsymbol{\tau}}(\mu)) = f(\mu; \boldsymbol{v}), \quad \forall \boldsymbol{v} \in \boldsymbol{\mathcal{V}}(\mu), \\ \qquad\qquad b^{\boldsymbol{n}}(\mu; \boldsymbol{u}(\mu), \eta^{\boldsymbol{n}} - \lambda^{\boldsymbol{n}}(\mu)) \leq g^{\boldsymbol{n}}(\mu; \eta^{\boldsymbol{n}} - \lambda^{\boldsymbol{n}}(\mu)), \quad \forall \eta^{\boldsymbol{n}} \in \mathcal{W}^{\boldsymbol{n}}(\mu), \\ \qquad\qquad b^{\boldsymbol{\tau}}(\mu; \boldsymbol{u}(\mu), \boldsymbol{\eta}^{\boldsymbol{\tau}} - \boldsymbol{\lambda}^{\boldsymbol{\tau}}(\mu)) \leq 0, \quad \forall \boldsymbol{\eta}^{\boldsymbol{\tau}} \in \boldsymbol{\mathcal{X}}^{\boldsymbol{\tau}}(\mu; \nu_{\mathcal{F}}\lambda^{\boldsymbol{n}}(\mu)), \end{cases} \tag{3.16}$$

where the bilinear form $b^{\boldsymbol{\tau}}(\mu; \cdot, \cdot) : \boldsymbol{\mathcal{V}}(\mu) \times \boldsymbol{\mathcal{X}}(\mu) \to \mathbb{R}$ is defined as

$$b^{\boldsymbol{\tau}}(\mu; \boldsymbol{v}, \boldsymbol{\theta}^{\boldsymbol{\tau}}) := \langle \boldsymbol{v}_{\boldsymbol{\tau}}, \boldsymbol{\theta}^{\boldsymbol{\tau}} \rangle_{\Gamma^c(\mu)}. \tag{3.17}$$

Let us denote by $\Pi_Z^{\mathcal{H}}$ the orthogonal projection onto a generic closed convex subset Z in the generic Hilbert space $\mathcal{H}$ (we drop the superscript whenever the context is unambiguous). In practice, one solves (3.16) using a Uzawa-type algorithm for some parameter $\rho > 0$. Given $\left(\lambda_0^{\boldsymbol{n}}(\mu), \boldsymbol{\lambda}_0^{\boldsymbol{\tau}}(\mu)\right) \in \mathcal{W}^{\boldsymbol{n}}(\mu) \times \boldsymbol{\mathcal{X}}^{\boldsymbol{\tau}}(\mu; \nu_{\mathcal{F}}\lambda_0^{\boldsymbol{n}}(\mu))$ and a pair of tolerances $\left(\delta^{\boldsymbol{n}}, \delta^{\boldsymbol{\tau}}\right) \in \mathbb{R}_+ \times \mathbb{R}_+$, the algorithm consists of solving the following sequence of problems: For all $k \geq 0$, find $\left(\boldsymbol{u}_{k+1}(\mu), \lambda_{k+1}^{\boldsymbol{n}}(\mu), \boldsymbol{\lambda}_{k+1}^{\boldsymbol{\tau}}(\mu)\right) \in \boldsymbol{\mathcal{V}}(\mu) \times \mathcal{W}^{\boldsymbol{n}}(\mu) \times \boldsymbol{\mathcal{X}}^{\boldsymbol{\tau}}(\mu; \nu_{\mathcal{F}}\lambda_{k+1}^{\boldsymbol{n}}(\mu))$ such that

$$\begin{cases} a(\mu; \boldsymbol{u}_{k+1}(\mu); \boldsymbol{v}) + b^{\boldsymbol{n}}(\mu; \boldsymbol{v}, \lambda_k^{\boldsymbol{n}}(\mu)) + b^{\boldsymbol{\tau}}(\mu; \boldsymbol{v}, \boldsymbol{\lambda}_k^{\boldsymbol{\tau}}(\mu)) = f(\mu; \boldsymbol{v}), \quad \forall \boldsymbol{v} \in \boldsymbol{\mathcal{V}}(\mu), \\ \lambda_{k+1}^{\boldsymbol{n}}(\mu) = \Pi_{\mathcal{W}^{\boldsymbol{n}}(\mu)}^{\mathcal{W}(\mu)}(\lambda_k^{\boldsymbol{n}}(\mu) - \rho\left(u_{k+1,\boldsymbol{n}}(\mu) - d^{\boldsymbol{n}}(\mu)\right)), \\ \boldsymbol{\lambda}_{k+1}^{\boldsymbol{\tau}}(\mu) = \Pi_{\boldsymbol{\mathcal{X}}^{\boldsymbol{\tau}}(\mu; \nu_{\mathcal{F}}\lambda_{k+1}^{\boldsymbol{n}}(\mu))}^{\boldsymbol{\mathcal{X}}(\mu)}(\boldsymbol{\lambda}_k^{\boldsymbol{\tau}}(\mu) - \rho \boldsymbol{u}_{k+1,\boldsymbol{\tau}}(\mu)). \end{cases} \tag{3.18}$$

One iterates on k until the following convergence criterion is reached:

$$\frac{\|\lambda_{k+1}^{\boldsymbol{n}}(\mu) - \lambda_k^{\boldsymbol{n}}(\mu)\|_{\mathcal{W}(\mu)}}{\|\lambda_{k+1}^{\boldsymbol{n}}(\mu)\|_{\mathcal{W}(\mu)}} \leq \delta^{\boldsymbol{n}} \quad \text{and} \quad \frac{\|\boldsymbol{\lambda}_{k+1}^{\boldsymbol{\tau}}(\mu) - \boldsymbol{\lambda}_k^{\boldsymbol{\tau}}(\mu)\|_{\boldsymbol{\mathcal{X}}(\mu)}}{\|\boldsymbol{\lambda}_{k+1}^{\boldsymbol{\tau}}(\mu)\|_{\boldsymbol{\mathcal{X}}(\mu)}} \leq \delta^{\boldsymbol{\tau}}. \tag{3.19}$$

Remark 3.2.2 (Tresca friction). The methodology presented in this work for the Coulomb frictional contact problem applies also to the Tresca frictional contact problem for which the friction law reads as

$$\begin{cases} \|\boldsymbol{\sigma}_{\boldsymbol{n}\boldsymbol{\tau}}(\boldsymbol{u}(\mu))\| \leq s, & \text{if } \boldsymbol{u}_{\boldsymbol{\tau}}(\mu) = \boldsymbol{0}, \\ \boldsymbol{\sigma}_{\boldsymbol{n}\boldsymbol{\tau}}(\boldsymbol{u}(\mu)) = -s\dfrac{\boldsymbol{u}_{\boldsymbol{\tau}}(\mu)}{\|\boldsymbol{u}_{\boldsymbol{\tau}}(\mu)\|}, & \text{otherwise}, \end{cases} \tag{3.20}$$

and the friction functional reads as

$$\mathcal{F}(\mu; \boldsymbol{v}) := \langle s, \|\boldsymbol{v}_{\boldsymbol{\tau}}\| \rangle_{\Gamma^c(\mu)}, \tag{3.21}$$

where $\|\cdot\|$ denotes the Euclidean norm in $\mathbb{R}^{d-1}$ and $s > 0$ is a given threshold (units in Pa). To derive the mixed formulation of the Tresca frictional contact problem, one simply replaces the set of admissible tangential stresses $\boldsymbol{\mathcal{X}}^{\boldsymbol{\tau}}(\mu; \nu_{\mathcal{F}}\lambda^{\boldsymbol{n}}(\mu))$ by $\boldsymbol{\mathcal{X}}^{\boldsymbol{\tau}}(\mu; s)$ in (3.16). The Uzawa algorithm (3.18)-(3.19) can still be used.

3.2.2 Mixed formulation with collocation

Owing to the nonlinearity of the friction conditions (see (3.20)-(3.6)), the set of admissible tangential stresses $\boldsymbol{\mathcal{X}}^{\boldsymbol{\tau}}(\mu;\eta^{\boldsymbol{n}})$ is not a linear space (see (3.15)). We approximate $\boldsymbol{\mathcal{X}}^{\boldsymbol{\tau}}(\mu;\eta^{\boldsymbol{n}})$ by using a set

$$\boldsymbol{\mathcal{C}}^{\mathrm{HF}}(\mu) := \{\boldsymbol{c}_s(\mu)\}_{s\in\{1:\mathcal{S}_0^{\mathrm{HF}}\}} \subset \Gamma^{\mathrm{c}}(\mu) \tag{3.22}$$

composed of $\mathcal{S}_0^{\mathrm{HF}} \in \mathbb{N}^*$ collocation nodes. This leads to the approximate manifold $\boldsymbol{\mathcal{X}}^{\boldsymbol{\tau}}_{\boldsymbol{\mathcal{C}}^{\mathrm{HF}}(\mu)}(\mu;\eta^{\boldsymbol{n}})$ defined as follows:

$$\boldsymbol{\mathcal{X}}^{\boldsymbol{\tau}}_{\boldsymbol{\mathcal{C}}^{\mathrm{HF}}(\mu)}(\mu;\eta^{\boldsymbol{n}}) := \Big\{\boldsymbol{\theta}^{\boldsymbol{\tau}} \in \boldsymbol{\mathcal{X}}(\mu) \mid \|\boldsymbol{\theta}^{\boldsymbol{\tau}}(\boldsymbol{c}_s(\mu))\| \le \eta^{\boldsymbol{n}}(\boldsymbol{c}_s(\mu)),\ \forall s \in \{1{:}\mathcal{S}_0^{\mathrm{HF}}\}\Big\}. \tag{3.23}$$

Using this approximation in (3.18) (for simplicity, we keep the same notation as in (3.18) although the problems (3.18) and (3.24) have in general different solutions), we consider the following sequence of approximate problems: For all $k \ge 0$, find $(\boldsymbol{u}_{k+1}(\mu), \lambda^{\boldsymbol{n}}_{k+1}(\mu), \boldsymbol{\lambda}^{\boldsymbol{\tau}}_{k+1}(\mu)) \in \boldsymbol{\mathcal{V}}(\mu) \times \mathcal{W}^{\boldsymbol{n}}(\mu) \times \boldsymbol{\mathcal{X}}^{\boldsymbol{\tau}}_{\boldsymbol{\mathcal{C}}^{\mathrm{HF}}(\mu)}(\mu;\nu_{\mathcal{F}}\lambda^{\boldsymbol{n}}_{k+1}(\mu))$ such that

$$\begin{cases} a(\mu;\boldsymbol{u}_{k+1}(\mu);\boldsymbol{v}) + b^{\boldsymbol{n}}(\mu;\boldsymbol{v},\lambda^{\boldsymbol{n}}_k(\mu)) + b^{\boldsymbol{\tau}}(\mu;\boldsymbol{v},\boldsymbol{\lambda}^{\boldsymbol{\tau}}_k(\mu)) = f(\mu;\boldsymbol{v}), \quad \forall \boldsymbol{v} \in \boldsymbol{\mathcal{V}}(\mu), \\ \lambda^{\boldsymbol{n}}_{k+1}(\mu) = \Pi^{\mathcal{W}(\mu)}_{\mathcal{W}^{\boldsymbol{n}}(\mu)}(\lambda^{\boldsymbol{n}}_k(\mu) - \rho(u_{k+1,\boldsymbol{n}}(\mu) - d^{\boldsymbol{n}}(\mu))), \\ \boldsymbol{\lambda}^{\boldsymbol{\tau}}_{k+1}(\mu) = \Pi^{\boldsymbol{\mathcal{X}}(\mu)}_{\boldsymbol{\mathcal{X}}^{\boldsymbol{\tau}}_{\boldsymbol{\mathcal{C}}^{\mathrm{HF}}(\mu)}(\mu;\nu_{\mathcal{F}}\lambda^{\boldsymbol{n}}_{k+1}(\mu))}(\boldsymbol{\lambda}^{\boldsymbol{\tau}}_k(\mu) - \rho\boldsymbol{u}_{k+1,\boldsymbol{\tau}}(\mu)), \end{cases} \tag{3.24}$$

until the convergence criterion (3.19) is reached. We denote the converged solution to the problem (3.24) as the triple $(\boldsymbol{u}_{\mathrm{cv}}(\mu), \lambda^{\boldsymbol{n}}_{\mathrm{cv}}(\mu), \boldsymbol{\lambda}^{\boldsymbol{\tau}}_{\mathrm{cv}}(\mu)) \in \boldsymbol{\mathcal{V}}(\mu) \times \mathcal{W}^{\boldsymbol{n}}(\mu) \times \boldsymbol{\mathcal{X}}^{\boldsymbol{\tau}}_{\boldsymbol{\mathcal{C}}^{\mathrm{HF}}(\mu)}(\mu;\nu_{\mathcal{F}}\lambda^{\boldsymbol{n}}_{\mathrm{cv}}(\mu))$.

3.2.3 Algebraic formulation

To introduce the algebraic formulation, we assume that for all $\mu \in \mathcal{D}$, the HF spaces $\boldsymbol{\mathcal{V}}(\mu)$, $\mathcal{W}(\mu)$ and $\boldsymbol{\mathcal{X}}(\mu)$ are such that

$$\boldsymbol{\mathcal{V}}(\mu) := \boldsymbol{Span}\Big(\{\boldsymbol{\varphi}_n(\mu)\}_{n\in\{1:\mathcal{N}^{\mathrm{HF}}\}}\Big), \tag{3.25a}$$

$$\mathcal{W}(\mu) := \boldsymbol{Span}\Big(\{\psi^{\boldsymbol{n}}_r(\mu)\}_{r\in\{1:\mathcal{R}^{\mathrm{HF}}\}}\Big), \tag{3.25b}$$

$$\boldsymbol{\mathcal{X}}(\mu) := \boldsymbol{Span}\Big(\{\boldsymbol{\psi}^{\boldsymbol{\tau}}_s(\mu)\}_{s\in\{1:\mathcal{S}^{\mathrm{HF}}\}}\Big). \tag{3.25c}$$

Notice that the dimensions $\mathcal{N}^{\mathrm{HF}}$, $\mathcal{R}^{\mathrm{HF}}$ and $\mathcal{S}^{\mathrm{HF}}$ of $\boldsymbol{\mathcal{V}}(\mu)$, $\mathcal{W}(\mu)$ and $\boldsymbol{\mathcal{X}}(\mu)$, respectively, are parameter-independent. We discuss in Section 3.3.1 how to accomplish this property. Assuming that

$$\{\psi^{\boldsymbol{n}}_r(\mu)\}_{r\in\{1:\mathcal{R}^{\mathrm{HF}}\}} \subset \mathcal{W}^{\boldsymbol{n}}(\mu), \quad \forall r \in \{1{:}\mathcal{R}^{\mathrm{HF}}\}, \tag{3.26}$$

the positive cone $\mathcal{W}^{\boldsymbol{n}}(\mu)$ becomes

$$\mathcal{W}^{\boldsymbol{n}}(\mu) := \boldsymbol{Span}^+\Big(\{\psi^{\boldsymbol{n}}_r(\mu)\}_{r\in\{1:\mathcal{R}^{\mathrm{HF}}\}}\Big), \tag{3.27}$$

where, for a generic family $\{\theta_q\}_{q\in\{1:Q\}} \subset \mathcal{W}^{\boldsymbol{n}}(\mu)$ with $Q \in \mathbb{N}^*$, $\boldsymbol{Span}^+\Big(\{\theta_q\}_{q\in\{1:Q\}}\Big)$ denotes the positive cone generated by setting

$$\boldsymbol{Span}^+\Big(\{\theta_q\}_{q\in\{1:Q\}}\Big) := \Big\{\sum_{q\in\{1:Q\}} \alpha_q\theta_q,\ (\alpha_1,\cdots,\alpha_Q) \in \mathbb{R}^Q_+\Big\}. \tag{3.28}$$

The property (3.26) is realized whenever the basis functions $\psi_r^{\boldsymbol{n}}$ take positive values. In what follows, we consider the $\mathbb{P}_1$ finite element shape functions $\psi_r^{\boldsymbol{n}}(\mu)$ so that (3.26) indeed holds true. Furthermore, we use the same scalar-valued and $\mathbb{R}^{d-1}$-valued finite elements on the same mesh for the discretization of the Lagrange multipliers $\lambda^{\boldsymbol{n}}(\mu)$ and $\boldsymbol{\lambda}^{\boldsymbol{\tau}}(\mu)$, respectively. Hence, we have

$$\mathcal{S}^{\mathrm{HF}} = (d-1) \times \mathcal{R}^{\mathrm{HF}}. \tag{3.29}$$

Finally, we use as collocation nodes the nodes associated with the discretization of $\lambda^{\boldsymbol{n}}(\mu)$, so that we have

$$\mathcal{S}_0^{\mathrm{HF}} = \mathcal{R}^{\mathrm{HF}}. \tag{3.30}$$

We adopt the following decompositions for the sequence of solutions to (3.24):

$$\boldsymbol{u}_k(\mu) := \sum_{n\in\{1:\mathcal{N}^{\mathrm{HF}}\}} u_k^n(\mu)\boldsymbol{\varphi}_n(\mu), \quad \boldsymbol{U}_k(\mu) := (u_k^n(\mu))_{n\in\{1:\mathcal{N}^{\mathrm{HF}}\}} \in \mathbb{R}^{\mathcal{N}^{\mathrm{HF}}}, \tag{3.31a}$$

$$\lambda_k^{\boldsymbol{n}}(\mu) := \sum_{r\in\{1:\mathcal{R}^{\mathrm{HF}}\}} \lambda_k^{\boldsymbol{n},r}(\mu)\psi_r^{\boldsymbol{n}}(\mu), \quad \Lambda_k^{\boldsymbol{n}}(\mu) := (\lambda_k^{\boldsymbol{n},r}(\mu))_{r\in\{1:\mathcal{R}^{\mathrm{HF}}\}} \in \mathbb{R}_+^{\mathcal{R}^{\mathrm{HF}}}, \tag{3.31b}$$

$$\boldsymbol{\lambda}_k^{\boldsymbol{\tau}}(\mu) := \sum_{s\in\{1:\mathcal{S}^{\mathrm{HF}}\}} \boldsymbol{\lambda}_k^{\boldsymbol{\tau},s}(\mu)\boldsymbol{\psi}_s^{\boldsymbol{\tau}}(\mu), \quad \boldsymbol{\Lambda}_k^{\boldsymbol{\tau}}(\mu) := (\boldsymbol{\lambda}_k^{\boldsymbol{\tau},s}(\mu))_{s\in\{1:\mathcal{S}^{\mathrm{HF}}\}} \in \mathbb{R}^{\mathcal{S}^{\mathrm{HF}}}. \tag{3.31c}$$

The algebraic formulation of the sequence of problems (3.24) then reads as follows: For all $k \geq 0$, find $(\boldsymbol{U}_{k+1}(\mu), \Lambda_{k+1}^{\boldsymbol{n}}(\mu), \boldsymbol{\Lambda}_{k+1}^{\boldsymbol{\tau}}(\mu)) \in \mathbb{R}^{\mathcal{N}^{\mathrm{HF}}} \times \mathbb{R}_+^{\mathcal{R}^{\mathrm{HF}}} \times \boldsymbol{X}^{\boldsymbol{\tau}}_{\boldsymbol{\mathcal{C}}^{\mathrm{HF}}(\mu)}(\mu; \nu_{\mathcal{F}}\Lambda_{k+1}^{\boldsymbol{n}}(\mu))$ such that

$$\begin{cases} A(\mu)\boldsymbol{U}_{k+1}(\mu) + B^{\boldsymbol{n}}(\mu)^\top \Lambda_{k+1}^{\boldsymbol{n}}(\mu) + B^{\boldsymbol{\tau}}(\mu)^\top \boldsymbol{\Lambda}_{k+1}^{\boldsymbol{\tau}}(\mu) = F(\mu), \\ \Lambda_{k+1}^{\boldsymbol{n}}(\mu) = \Pi_{\mathbb{R}_+^{\mathcal{R}^{\mathrm{HF}}}}(\Lambda_{k+1}^{\boldsymbol{n}}(\mu) - \rho(B^{\boldsymbol{n}}(\mu)\boldsymbol{U}_{k+1}(\mu) - G^{\boldsymbol{n}}(\mu))), \\ \boldsymbol{\Lambda}_{k+1}^{\boldsymbol{\tau}}(\mu) = \Pi_{\boldsymbol{X}^{\boldsymbol{\tau}}_{\boldsymbol{\mathcal{C}}^{\mathrm{HF}}(\mu)}(\mu;\nu_{\mathcal{F}}\Lambda_{k+1}^{\boldsymbol{n}}(\mu))}(\boldsymbol{\Lambda}_{k+1}^{\boldsymbol{\tau}}(\mu) - \rho B^{\boldsymbol{\tau}}(\mu)\boldsymbol{U}_{k+1}(\mu)), \end{cases} \tag{3.32}$$

where for all $n, m \in \{1:\mathcal{N}^{\mathrm{HF}}\}$, all $r \in \{1:\mathcal{R}^{\mathrm{HF}}\}$ and all $s \in \{1:\mathcal{S}^{\mathrm{HF}}\}$,

$$(A(\mu))_{mn} := a(\mu; \boldsymbol{\varphi}_n(\mu), \boldsymbol{\varphi}_m(\mu)), \quad F_m(\mu) := f(\mu; \boldsymbol{\varphi}_m(\mu)), \tag{3.33a}$$

$$(B^{\boldsymbol{n}}(\mu))_{rm} := b^{\boldsymbol{n}}(\mu; \boldsymbol{\varphi}_m(\mu), \psi_r^{\boldsymbol{n}}(\mu)), \quad G_r^{\boldsymbol{n}}(\mu) := g^{\boldsymbol{n}}(\mu; \psi_r^{\boldsymbol{n}}(\mu)), \tag{3.33b}$$

$$(B^{\boldsymbol{\tau}}(\mu))_{sm} := b^{\boldsymbol{\tau}}(\mu; \boldsymbol{\varphi}_m(\mu), \boldsymbol{\psi}_s^{\boldsymbol{\tau}}(\mu)). \tag{3.33c}$$

Moreover, using (3.29)-(3.30) the set

$$\boldsymbol{X}^{\boldsymbol{\tau}}_{\boldsymbol{\mathcal{C}}^{\mathrm{HF}}(\mu)}(\mu; \nu_{\mathcal{F}}\Lambda_{k+1}^{\boldsymbol{n}}(\mu)) := \Big\{ \boldsymbol{\Theta}^{\boldsymbol{\tau}} \in \mathbb{R}^{(d-1)\times\mathcal{R}^{\mathrm{HF}}} \mid \|\boldsymbol{\Theta}^{\boldsymbol{\tau},r}\| \leq \nu_{\mathcal{F}}\Lambda_{k+1}^{\boldsymbol{n},r}(\mu),\ \forall r \in \{1:\mathcal{R}^{\mathrm{HF}}\} \Big\}, \tag{3.34}$$

is the algebraic counterpart of the set $\boldsymbol{\mathcal{X}}^{\boldsymbol{\tau}}_{\boldsymbol{\mathcal{C}}^{\mathrm{HF}}(\mu)}(\mu; \nu_{\mathcal{F}}\lambda_{k+1}^{\boldsymbol{n}}(\mu))$ defined in (3.23). Notice that in (3.34), we used that $\{\psi_r^{\boldsymbol{n}}(\mu)\}_{r\in\{1:\mathcal{R}^{\mathrm{HF}}\}}$ and $\{\boldsymbol{\psi}_s^{\boldsymbol{\tau}}(\mu)\}_{s\in\{1:\mathcal{S}^{\mathrm{HF}}\}}$ are nodal basis functions associated with the same set of nodes which are the collocation nodes. The convergence criterion for (3.32) is still (3.19) using the reconstructed functions. We denote the converged solution to the problem (3.32) as the triple $(\boldsymbol{U}_{\mathrm{cv}}(\mu), \Lambda_{\mathrm{cv}}^{\boldsymbol{n}}(\mu), \boldsymbol{\Lambda}_{\mathrm{cv}}^{\boldsymbol{\tau}}(\mu)) \in \mathbb{R}^{\mathcal{N}^{\mathrm{HF}}} \times \mathbb{R}_+^{\mathcal{R}^{\mathrm{HF}}} \times \boldsymbol{X}^{\boldsymbol{\tau}}_{\boldsymbol{\mathcal{C}}^{\mathrm{HF}}(\mu)}(\mu; \nu_{\mathcal{F}}\Lambda_{\mathrm{cv}}^{\boldsymbol{n}}(\mu))$.

3.3 Model reduction

In this section, we derive the RB method for the contact problem with friction.

3.3.1 Geometric mapping

We recall that the dimensions $\mathcal{N}^{\mathrm{HF}}$, $\mathcal{R}^{\mathrm{HF}}$ and $\mathcal{S}^{\mathrm{HF}}$ of the finite-dimensional spaces $\boldsymbol{\mathcal{V}}(\mu)$, $\mathcal{W}(\mu)$ and $\boldsymbol{\mathcal{X}}(\mu)$ are parameter-independent. This is important since, in order to compress the spaces generated by the snapshots, it is necessary that all the snapshots live in the same space. For this purpose, since the geometry is parameter-dependent, we use a parameter-independent reference domain $\widehat{\Omega}$. We assume that for all $\mu \in \mathcal{D}$, there is a smooth invertible geometric mapping $h(\mu) : \widehat{\Omega} \to \Omega(\mu)$. We denote by $\widehat{\Gamma} := \partial\widehat{\Omega}$ the boundary of $\widehat{\Omega}$, and we assume that it can be partitioned as $\widehat{\Gamma} = \widehat{\Gamma}^{\mathrm{D}} \cup \widehat{\Gamma}^{\mathrm{N}} \cup \widehat{\Gamma}^{\mathrm{c}}$ in such a way that, for all $\mu \in \mathcal{D}$,

$$\widehat{\Gamma}^{\mathrm{D}} := h_d^{-1}(\mu)(\Gamma^{\mathrm{D}}(\mu)), \quad \widehat{\Gamma}^{\mathrm{N}} := h_n^{-1}(\mu)(\Gamma^{\mathrm{N}}(\mu)), \quad \widehat{\Gamma}^{\mathrm{c}} := h_c^{-1}(\mu)(\Gamma^{\mathrm{c}}(\mu)), \tag{3.35}$$

with $h_d(\mu) := h(\mu)_{|\widehat{\Gamma}^{\mathrm{D}}}$, $h_n(\mu) := h(\mu)_{|\widehat{\Gamma}^{\mathrm{N}}}$ and $h_c(\mu) := h(\mu)_{|\widehat{\Gamma}^{\mathrm{c}}}$. Then, the mesh of $\Omega(\mu)$ is generated by generating a mesh of $\widehat{\Omega}$ matching the partition of the boundary $\widehat{\Gamma}$ and applying the mapping $h(\mu)$ to the mesh of the reference domain $\widehat{\Omega}$. We use $\mathbb{P}_2$ finite elements for the primal space $\boldsymbol{\mathcal{V}}(\mu)$ and scalar-valued or $\mathbb{R}^{d-1}$-valued $\mathbb{P}_1$ finite elements for the dual spaces $\mathcal{W}(\mu)$ and $\boldsymbol{\mathcal{X}}(\mu)$, respectively. The collocation nodes $\boldsymbol{\mathcal{C}}^{\mathrm{HF}}(\mu) := \{\boldsymbol{c}_s(\mu)\}_{s\in\{1:\mathcal{S}_0^{\mathrm{HF}}\}} \subset \Gamma^{\mathrm{c}}(\mu)$ are generated from a set of nodes $\widehat{\boldsymbol{\mathcal{C}}}^{\mathrm{HF}} := \{\widehat{\boldsymbol{c}}_s\}_{s\in\{1:\mathcal{S}_0^{\mathrm{HF}}\}} \subset \widehat{\Gamma}^{\mathrm{c}}$ by setting $\boldsymbol{c}_s(\mu) := h(\mu)(\widehat{\boldsymbol{c}}_s)$ for all $s \in \{1{:}\mathcal{S}_0^{\mathrm{HF}}\}$ and all $\mu \in \mathcal{D}$. We recall that the collocation nodes in $\boldsymbol{\mathcal{C}}^{\mathrm{HF}}(\mu)$ are the ones associated with the finite element shape functions $\psi_r^{\boldsymbol{n}}(\mu)$.

3.3.2 Naive approach

The aim of this section is to present a naive reduced-order model relying on a plain RB approach and to highlight the problems raised by such a formulation. These problems will be circumvented in the next section, eventually leading to a computationally effective reduced-order model. As we shall see, the major difficulty comes from the approach used in order to implement the friction condition at the level of the reduced-order model.

To build the RB, the starting point is to compute (in the offline phase) a family

$$\{\Big(\boldsymbol{U}_{\mathrm{cv}}(\mu_p), \Lambda_{\mathrm{cv}}^{\boldsymbol{n}}(\mu_p), \boldsymbol{\Lambda}_{\mathrm{cv}}^{\boldsymbol{\tau}}(\mu_p)\Big)\}_{p\in\{1:P\}} \subset \mathbb{R}^{\mathcal{N}^{\mathrm{HF}}} \times \mathbb{R}_+^{\mathcal{R}^{\mathrm{HF}}} \times \mathbb{R}^{\mathcal{S}^{\mathrm{HF}}}, \tag{3.36}$$

of HF solutions to (3.32) by using a training subset $\mathcal{D}_{\mathtt{train}} := \{\mu_p\}_{p\in\{1:P\}} \subset \mathcal{D}$ of cardinality $P \in \mathbb{N}^*$. Using the Proper Orthogonal Decomposition (POD) [54, 69] based on the inner product of $H^1(\widehat{\Omega};\mathbb{R}^d)$ (resp. $L^2(\widehat{\Gamma}^{\mathrm{c}};\mathbb{R}^{d-1})$) and the geometric mapping $h(\mu)$, one can then construct an orthonormal family $\{\boldsymbol{\Xi}_n\}_{n\in\{1:N\}} \subset \mathbb{R}^{\mathcal{N}^{\mathrm{HF}}}$ (resp. $\{\boldsymbol{\Upsilon}_s^{\boldsymbol{\tau}}\}_{s\in\{1:S\}} \subset \mathbb{R}^{\mathcal{S}^{\mathrm{HF}}}$) of $N \in \mathbb{N}^*$ (resp. $S \in \mathbb{N}^*$), $N \le P$ (resp. $S \le P$), vectors. Let us denote by $\boldsymbol{V}_N$ (resp. $\boldsymbol{X}_S^{\boldsymbol{\tau}}$) the reduced primal (resp. tangential dual) space generated by the family $\{\boldsymbol{\Xi}_n\}_{n\in\{1:N\}}$ (resp. $\{\boldsymbol{\Upsilon}_s^{\boldsymbol{\tau}}\}_{s\in\{1:S\}}$), *i.e.*,

$$\boldsymbol{V}_N := \boldsymbol{Span}\Big(\{\boldsymbol{\Xi}_n\}_{n\in\{1:N\}}\Big) \subset \mathbb{R}^{\mathcal{N}^{\mathrm{HF}}}, \quad \boldsymbol{X}_S^{\boldsymbol{\tau}} := \boldsymbol{Span}\Big(\{\boldsymbol{\Upsilon}_s^{\boldsymbol{\tau}}\}_{s\in\{1:S\}}\Big) \subset \mathbb{R}^{\mathcal{S}^{\mathrm{HF}}}. \tag{3.37}$$

Moreover, using the modified Cone Projected Greedy (mCPG) algorithm [12, 84] based on the inner product of $L^2(\widehat{\Gamma}^c;\mathbb{R})$ and the geometric mapping $h(\mu)$, one can construct a family $\{\Upsilon_r^{\boldsymbol{n}}\}_{r\in\{1:R\}} \subset \mathbb{R}_+^{\mathcal{R}^{\mathrm{HF}}}$ of $R \in \mathbb{N}^*$ vectors with nonnegative components. Let us denote by $W_R^{\boldsymbol{n}}$ the reduced dual cone generated by the family $\{\Upsilon_r^{\boldsymbol{n}}\}_{r\in\{1:R\}}$, *i.e.*,

$$W_R^{\boldsymbol{n}} := \boldsymbol{Span}^+\Big(\{\Upsilon_r^{\boldsymbol{n}}\}_{r\in\{1:R\}}\Big) \subset \mathbb{R}_+^{\mathcal{R}^{\mathrm{HF}}}. \tag{3.38}$$

In general, the primal reduced space $\boldsymbol{V}_N$ needs to be enriched to ensure that the reduced problem satisfies an inf-sup stability condition. We stabilize the RB problem using the Projected Greedy Algorithm (PGA) algorithm introduced in [84]. Specifically, we enrich the reduced primal space $\boldsymbol{V}_N$ according to the reduced dual space $W_R^{\boldsymbol{n}} \times \boldsymbol{X}_S^{\boldsymbol{\tau}}$ by computing suitable supremizers using the bilinear form $b(\mu;\cdot,\cdot) : \boldsymbol{\mathcal{V}}(\mu) \times \boldsymbol{\mathcal{Y}}(\mu) \to \mathbb{R}$ defined as

$$b(\mu;\boldsymbol{v},\boldsymbol{\eta}) := b^{\boldsymbol{n}}(\mu;\boldsymbol{v},\eta^{\boldsymbol{n}}) + b^{\boldsymbol{\tau}}(\mu;\boldsymbol{v},\boldsymbol{\eta}^{\boldsymbol{\tau}}), \quad \forall \boldsymbol{v} \in \boldsymbol{\mathcal{V}}(\mu),\ \boldsymbol{\eta} := (\eta^{\boldsymbol{n}},\boldsymbol{\eta}^{\boldsymbol{\tau}}) \in \boldsymbol{\mathcal{Y}}(\mu), \tag{3.39}$$

with $\boldsymbol{\mathcal{Y}}(\mu) := \mathcal{W}(\mu) \times \boldsymbol{\mathcal{X}}(\mu)$. For simplicity, in what follows, we still refer to $\boldsymbol{V}_N$ as the enriched reduced primal space.

In algebraic form, the RB formulation of the sequence of HF problems (3.32) reads as follows: For all $k \geq 0$, find $(\boldsymbol{U}_{N,k+1}(\mu), \Lambda_{R,k+1}^{\boldsymbol{n}}(\mu), \boldsymbol{\Lambda}_{S,k+1}^{\boldsymbol{\tau}}(\mu)) \in \mathbb{R}^N \times \mathbb{R}_+^R \times \boldsymbol{X}_{S,\boldsymbol{\mathcal{C}}^{\mathrm{HF}}(\mu)}^{\boldsymbol{\tau}}(\mu;\nu_{\mathcal{F}}\Lambda_{R,k+1}^{\boldsymbol{n}}(\mu))$ such that

$$\begin{cases} A_N(\mu)\boldsymbol{U}_{N,k+1}(\mu) + B_{R,N}^{\boldsymbol{n}}(\mu)^\top \Lambda_{R,k}^{\boldsymbol{n}}(\mu) + B_{S,N}^{\boldsymbol{\tau}}(\mu)^\top \boldsymbol{\Lambda}_{S,k}^{\boldsymbol{\tau}}(\mu) = F_N(\mu), \\ \Lambda_{R,k+1}^{\boldsymbol{n}}(\mu) = \Pi_{\mathbb{R}_+^R}(\Lambda_{R,k}^{\boldsymbol{n}}(\mu) - \rho(B_{R,N}^{\boldsymbol{n}}(\mu)\boldsymbol{U}_{N,k+1}(\mu) - G_R^{\boldsymbol{n}}(\mu))), \\ \boldsymbol{\Lambda}_{S,k+1}^{\boldsymbol{\tau}}(\mu) = \Pi_{\boldsymbol{X}_{S,\boldsymbol{\mathcal{C}}^{\mathrm{HF}}(\mu)}^{\boldsymbol{\tau}}(\mu;\nu_{\mathcal{F}}\Lambda_{R,k+1}^{\boldsymbol{n}}(\mu))}(\boldsymbol{\Lambda}_{S,k}^{\boldsymbol{\tau}}(\mu) - \rho B_{S,N}^{\boldsymbol{\tau}}(\mu)\boldsymbol{U}_{N,k+1}(\mu)), \end{cases} \tag{3.40}$$

where

$$A_N(\mu) := Z^\top A(\mu) Z, \qquad F_N(\mu) := Z^\top F(\mu), \tag{3.41a}$$
$$B_{R,N}^{\boldsymbol{n}}(\mu) := {Q^{\boldsymbol{n}}}^\top B^{\boldsymbol{n}}(\mu) Z, \quad G_R^{\boldsymbol{n}}(\mu) := {Q^{\boldsymbol{n}}}^\top G^{\boldsymbol{n}}(\mu), \tag{3.41b}$$
$$B_{S,N}^{\boldsymbol{\tau}}(\mu) := {Q^{\boldsymbol{\tau}}}^\top B^{\boldsymbol{\tau}}(\mu) Z, \tag{3.41c}$$

with $Z \in \mathbb{R}^{\mathcal{N}^{\mathrm{HF}} \times N}$, $Q^{\boldsymbol{n}} \in \mathbb{R}^{\mathcal{R}^{\mathrm{HF}} \times R}$ and $Q^{\boldsymbol{\tau}} \in \mathbb{R}^{\mathcal{S}^{\mathrm{HF}} \times S}$ defined as

$$Z := \Big[\boldsymbol{\Xi}_1 \cdots \boldsymbol{\Xi}_N\Big], \quad Q^{\boldsymbol{n}} := \Big[\Upsilon_1^{\boldsymbol{n}} \cdots \Upsilon_R^{\boldsymbol{n}}\Big], \quad Q^{\boldsymbol{\tau}} := \Big[\boldsymbol{\Upsilon}_1^{\boldsymbol{\tau}} \cdots \boldsymbol{\Upsilon}_S^{\boldsymbol{\tau}}\Big], \tag{3.42}$$

and

$$\boldsymbol{X}_{S,\boldsymbol{\mathcal{C}}^{\mathrm{HF}}(\mu)}^{\boldsymbol{\tau}}(\mu;\nu_{\mathcal{F}}\Lambda_{R,k+1}^{\boldsymbol{n}}(\mu)) := \Big\{\boldsymbol{\Theta} \in \mathbb{R}^S \mid \|(Q^{\boldsymbol{\tau}}\boldsymbol{\Theta})^r\| \leq \nu_{\mathcal{F}}(Q^{\boldsymbol{n}}\Lambda_{R,k+1}^{\boldsymbol{n}}(\mu))^r,\ \forall r \in \{1{:}\mathcal{R}^{\mathrm{HF}}\}\Big\}. \tag{3.43}$$

Let us point out that, by construction, we have $(Q^{\boldsymbol{n}}H)^r \geq 0$ for all $r \in \{1{:}\mathcal{R}^{\mathrm{HF}}\}$ and all $H \in \mathbb{R}_+^R$. The convergence criterion for (3.40) is still (3.19) using reconstructed functions (see Remark 3.3.1 for more details). Notice also that the friction condition is imposed on the same collocation nodes as in the HF model, namely $\boldsymbol{\mathcal{C}}^{\mathrm{HF}}(\mu)$.

At this stage, the model reduction procedure basically consists of the following two stages:

— Offline stage

1. Select a training subset $\mathcal{D}_{\texttt{train}} := \{\mu_p\}_{p\in\{1:P\}} \subset \mathcal{D}$.
2. Compute the snapshots $\{\boldsymbol{U}_{\rm cv}(\mu_p), \Lambda^{\boldsymbol{n}}_{\rm cv}(\mu_p), \boldsymbol{\Lambda}^{\boldsymbol{\tau}}_{\rm cv}(\mu_p)\}_{p\in\{1:P\}} \subset \mathbb{R}^{\mathcal{N}^{\rm HF}} \times \mathbb{R}_+^{\mathcal{R}^{\rm HF}} \times \mathbb{R}^{\mathcal{S}^{\rm HF}}$ by solving (3.32).
3. Compute the reduced spaces $\boldsymbol{V}_N$, $W^{\boldsymbol{n}}_R$ and $\boldsymbol{X}^{\boldsymbol{\tau}}_S$ by using POD and mCPG on snapshots.
4. Stabilize the RB problem: enrich $\boldsymbol{V}_N$ by using the PGA.

— Online stage: For any $\mu \in \mathcal{D} \setminus \mathcal{D}_{\texttt{train}}$,

1. Compute $A_N(\mu)$, $F_N(\mu)$, $B^{\boldsymbol{n}}_{R,N}(\mu)$, $B^{\boldsymbol{\tau}}_{S,N}(\mu)$ and $G^{\boldsymbol{n}}_R(\mu)$ by using (3.41).
2. Loop on $k \geq 0$,
   (a) Solve (3.40).
   (b) Check convergence; if not, set $k \leftarrow k+1$ and go back to (2a).

It is crucial to derive a reduced problem that is independent of the high-fidelity dimensions $\mathcal{N}^{\rm HF}$, $\mathcal{R}^{\rm HF}$ and $\mathcal{S}^{\rm HF}$ in order to obtain an inexpensive online stage. This condition is not yet satisfied with the current formalism. There are indeed two issues: on the one hand, the manipulation of large-dimensional arrays in (3.41), and on the other hand the use of a HF set of collocation nodes in (3.43). We propose in Section 3.3.3 a procedure to overcome these two issues in order to construct a computationally efficient RB model.

Remark 3.3.1 (Reconstructed functions). Let us introduce the following reconstructed functions:

$$\boldsymbol{\xi}_n(\mu) := \sum_{i\in\{1:\mathcal{N}^{\rm HF}\}} \Xi^i_n \boldsymbol{\varphi}_i(\mu) \in \boldsymbol{\mathcal{V}}(\mu), \qquad \forall n \in \{1{:}N\}, \tag{3.44a}$$

$$\chi^{\boldsymbol{n}}_r(\mu) := \sum_{i\in\{1:\mathcal{R}^{\rm HF}\}} \Upsilon^{\boldsymbol{n},i}_r \psi^{\boldsymbol{n}}_i(\mu) \in \mathcal{W}(\mu), \quad \forall r \in \{1{:}R\}, \tag{3.44b}$$

$$\boldsymbol{\chi}^{\boldsymbol{\tau}}_s(\mu) := \sum_{i\in\{1:\mathcal{S}^{\rm HF}\}} \boldsymbol{\Upsilon}^{\boldsymbol{\tau},i}_s \boldsymbol{\psi}^{\boldsymbol{\tau}}_i(\mu) \in \boldsymbol{\mathcal{X}}(\mu), \quad \forall s \in \{1{:}S\}. \tag{3.44c}$$

With this notation, solving the RB problem (3.40) in algebraic form leads to the following reconstructed solutions:

$$\boldsymbol{u}_{N,k}(\mu) := \sum_{n\in\{1:N\}} \boldsymbol{u}^n_{N,k}(\mu)\boldsymbol{\xi}_n(\mu) \in \boldsymbol{\mathcal{V}}(\mu), \quad \boldsymbol{U}_{N,k}(\mu) := (\boldsymbol{u}^n_{N,k}(\mu))_{n\in\{1:N\}} \in \mathbb{R}^N, \tag{3.45a}$$

$$\lambda^{\boldsymbol{n}}_{R,k}(\mu) := \sum_{r\in\{1:R\}} \lambda^{\boldsymbol{n},r}_{R,k}(\mu)\chi^{\boldsymbol{n}}_r(\mu) \in \mathcal{W}(\mu), \quad \Lambda^{\boldsymbol{n}}_{R,k}(\mu) := (\lambda^{\boldsymbol{n},r}_{R,k}(\mu))_{r\in\{1:R\}} \in \mathbb{R}^R_+, \tag{3.45b}$$

$$\boldsymbol{\lambda}^{\boldsymbol{\tau}}_{S,k}(\mu) := \sum_{s\in\{1:S\}} \boldsymbol{\lambda}^{\boldsymbol{\tau},s}_{S,k}(\mu)\boldsymbol{\chi}^{\boldsymbol{\tau}}_s(\mu) \in \boldsymbol{\mathcal{X}}(\mu), \quad \boldsymbol{\Lambda}^{\boldsymbol{\tau}}_{S,k}(\mu) := (\boldsymbol{\lambda}^{\boldsymbol{\tau},s}_{S,k}(\mu))_{s\in\{1:S\}} \in \mathbb{R}^S. \tag{3.45c}$$

Notice that $\lambda^{\boldsymbol{n}}_{R,k}(\mu) \in \mathcal{W}^{\boldsymbol{n}}(\mu)$ and $\boldsymbol{\lambda}^{\boldsymbol{\tau}}_{S,k}(\mu) \in \boldsymbol{\mathcal{X}}^{\boldsymbol{\tau}}_{\boldsymbol{\mathcal{C}}^{\rm HF}(\mu)}(\mu; \nu_{\mathcal{F}}\lambda^{\boldsymbol{n}}_{R,k}(\mu))$.

3.3.3 Computationally efficient reduced-basis model

In this section, we describe the strategies to overcome the two obstacles mentioned above. The first ingredient, detailed in Section 3.3.3.1, consists in introducing appropriate affine decompositions of the parameter-dependent operators involved in the problem (3.40) by using the Empirical Interpolation Method (EIM) [10, 75]. The second ingredient, detailed in Section 3.3.3.2, consists in selecting an appropriate subset of collocation nodes in $\boldsymbol{\mathcal{C}}^{\mathrm{HF}}(\mu)$ on which the friction condition is enforced. This subset is selected by means of a greedy algorithm which is close in spirit to the cutting-plane algorithm [63].

3.3.3.1 Affine decompositions

To avoid the manipulation of large-dimensional arrays in (3.40), we need to separate the dependence on μ from the dependence on the indices in the arrays (matrices and vectors). This operation is performed during the offline stage. To this purpose, using the EIM, we obtain the following approximations (see (3.33) for the definition of the left-hand sides):

$$A(\mu) \approx E^a(\mu) := \sum_{j\in\{1:J^a\}} \alpha_j^a(\mu) A_j, \qquad A_j \in \mathbb{R}^{\mathcal{N}^{\mathrm{HF}}\times\mathcal{N}^{\mathrm{HF}}},\ \alpha_j^a(\mu)\in\mathbb{R}, \tag{3.46a}$$

$$B^{\boldsymbol{n}}(\mu) \approx E^{\boldsymbol{n}b}(\mu) := \sum_{j\in\{1:J^{\boldsymbol{n}b}\}} \alpha_j^{\boldsymbol{n}b}(\mu) B_j^{\boldsymbol{n}}, \quad B_j^{\boldsymbol{n}} \in \mathbb{R}^{\mathcal{R}^{\mathrm{HF}}\times\mathcal{N}^{\mathrm{HF}}},\ \alpha_j^{\boldsymbol{n}b}(\mu)\in\mathbb{R}, \tag{3.46b}$$

$$B^{\boldsymbol{\tau}}(\mu) \approx E^{\boldsymbol{\tau}b}(\mu) := \sum_{j\in\{1:J^{\boldsymbol{\tau}b}\}} \alpha_j^{\boldsymbol{\tau}b}(\mu) B_j^{\boldsymbol{\tau}}, \quad B_j^{\boldsymbol{\tau}} \in \mathbb{R}^{\mathcal{S}^{\mathrm{HF}}\times\mathcal{N}^{\mathrm{HF}}},\ \alpha_j^{\boldsymbol{\tau}b}(\mu)\in\mathbb{R}, \tag{3.46c}$$

$$F(\mu) \approx E^f(\mu) := \sum_{j\in\{1:J^f\}} \alpha_j^f(\mu) F_j, \qquad F_j \in \mathbb{R}^{\mathcal{N}^{\mathrm{HF}}},\ \alpha_j^f(\mu)\in\mathbb{R}, \tag{3.46d}$$

$$G^{\boldsymbol{n}}(\mu) \approx E^{\boldsymbol{n}g}(\mu) := \sum_{j\in\{1:J^{\boldsymbol{n}g}\}} \alpha_j^{\boldsymbol{n}g}(\mu) G_j^{\boldsymbol{n}}, \quad G_j^{\boldsymbol{n}} \in \mathbb{R}^{\mathcal{R}^{\mathrm{HF}}},\ \alpha_j^{\boldsymbol{n}g}(\mu)\in\mathbb{R}, \tag{3.46e}$$

where the large-dimensional arrays A_j, $B_j^{\boldsymbol{n}}$, $B_j^{\boldsymbol{\tau}}$, F_j and $G_j^{\boldsymbol{n}}$ are now independent of the parameter μ, whereas the functions α_j^a, $\alpha_j^{\boldsymbol{n}b}$, $\alpha_j^{\boldsymbol{\tau}b}$, α_j^f and $\alpha_j^{\boldsymbol{n}g}$ only depend on μ. To build the large-dimensional arrays A_j, $B_j^{\boldsymbol{n}}$, $B_j^{\boldsymbol{\tau}}$, F_j and $G_j^{\boldsymbol{n}}$, we use the training set $\mathcal{D}_{\mathtt{train}}$ (a different (possibly richer) training set can be used). We introduce the index subsets $\{(n_j^a, m_j^a)\}_{j\in\{1:J^a\}} \subset \{1{:}\mathcal{N}^{\mathrm{HF}}\}\times\{1{:}\mathcal{N}^{\mathrm{HF}}\}$, $\{(n_j^{\boldsymbol{n}b}, m_j^{\boldsymbol{n}b})\}_{j\in\{1:J^{\boldsymbol{n}b}\}} \subset \{1{:}\mathcal{R}^{\mathrm{HF}}\}\times\{1{:}\mathcal{N}^{\mathrm{HF}}\}$, $\{(n_j^{\boldsymbol{\tau}b}, m_j^{\boldsymbol{\tau}b})\}_{j\in\{1:J^{\boldsymbol{\tau}b}\}} \subset \{1{:}\mathcal{S}^{\mathrm{HF}}\}\times\{1{:}\mathcal{N}^{\mathrm{HF}}\}$, $\{m_j^f\}_{j\in\{1:J^f\}} \subset \{1{:}\mathcal{N}^{\mathrm{HF}}\}$ and $\{m_j^{\boldsymbol{n}g}\}_{j\in\{1:J^{\boldsymbol{n}g}\}} \subset \{1{:}\mathcal{R}^{\mathrm{HF}}\}$ of cardinality J^a, $J^{\boldsymbol{n}b}$, $J^{\boldsymbol{\tau}b}$, J^f and $J^{\boldsymbol{n}g}$, respectively, corresponding to the indices selected by the EIM for the approximation of $A(\mu)$, $B^{\boldsymbol{n}}(\mu)$, $B^{\boldsymbol{\tau}}(\mu)$, $F(\mu)$ and $G^{\boldsymbol{n}}(\mu)$. Then, the functions α_j^a, $\alpha_j^{\boldsymbol{n}b}$, $\alpha_j^{\boldsymbol{\tau}b}$, α_j^f and $\alpha_j^{\boldsymbol{n}g}$ are such that, for all $\mu\in\mathcal{D}_{\mathtt{train}}$,

$$(E^a(\mu))_{n_j^a m_j^a} = (A(\mu))_{n_j^a m_j^a}, \qquad \forall j\in\{1{:}J^a\}, \tag{3.47a}$$

$$(E^{\boldsymbol{n}b}(\mu))_{n_j^{\boldsymbol{n}b} m_j^{\boldsymbol{n}b}} = (B^{\boldsymbol{n}}(\mu))_{n_j^{\boldsymbol{n}b} m_j^{\boldsymbol{n}b}}, \qquad \forall j\in\{1{:}J^{\boldsymbol{n}b}\}, \tag{3.47b}$$

$$(E^{\boldsymbol{\tau}b}(\mu))_{n_j^{\boldsymbol{\tau}b} m_j^{\boldsymbol{\tau}b}} = (B^{\boldsymbol{\tau}}(\mu))_{n_j^{\boldsymbol{\tau}b} m_j^{\boldsymbol{\tau}b}}, \qquad \forall j\in\{1{:}J^{\boldsymbol{\tau}b}\}, \tag{3.47c}$$

$$(E^f(\mu))_{m_j^f} = (F(\mu))_{m_j^f}, \qquad \forall j\in\{1{:}J^f\}, \tag{3.47d}$$

$$(E^{\boldsymbol{n}g}(\mu))_{m_j^{\boldsymbol{n}g}} = (G^{\boldsymbol{n}}(\mu))_{m_j^{\boldsymbol{n}g}}, \qquad \forall j\in\{1{:}J^{\boldsymbol{n}g}\}. \tag{3.47e}$$

In the online phase, for every new value of the parameter $\mu \in \mathcal{D} \setminus \mathcal{D}_{\texttt{train}}$, these functions are approximated by the functions α^{a}_{on}, $\alpha^{\boldsymbol{nb}}_{\mathrm{on}}$, $\alpha^{\boldsymbol{\tau b}}_{\mathrm{on}}$, α^{f}_{on}, and $\alpha^{\boldsymbol{ng}}_{\mathrm{on}}$, solving the following linear systems:

$$Q^{a}\alpha^{a}_{\mathrm{on}}(\mu) = T^{a}(\mu), \qquad T^{a}(\mu) := \left((A(\mu))_{n^{a}_{j} m^{a}_{j}}\right)_{j\in\{1:J^{a}\}} \in \mathbb{R}^{J^{a}}, \tag{3.48a}$$

$$Q^{\boldsymbol{nb}}\alpha^{\boldsymbol{nb}}_{\mathrm{on}}(\mu) = T^{\boldsymbol{nb}}(\mu), \quad T^{\boldsymbol{nb}}(\mu) := \left((B^{\boldsymbol{n}}(\mu))_{n^{\boldsymbol{nb}}_{j} m^{\boldsymbol{nb}}_{j}}\right)_{j\in\{1:J^{\boldsymbol{nb}}\}} \in \mathbb{R}^{J^{\boldsymbol{nb}}}, \tag{3.48b}$$

$$Q^{\boldsymbol{\tau b}}\alpha^{\boldsymbol{\tau b}}_{\mathrm{on}}(\mu) = T^{\boldsymbol{\tau b}}(\mu), \quad T^{\boldsymbol{\tau b}}(\mu) := \left((B^{\boldsymbol{\tau}}(\mu))_{n^{\boldsymbol{\tau b}}_{j} m^{\boldsymbol{\tau b}}_{j}}\right)_{j\in\{1:J^{\boldsymbol{\tau b}}\}} \in \mathbb{R}^{J^{\boldsymbol{\tau b}}}, \tag{3.48c}$$

$$Q^{f}\alpha^{f}_{\mathrm{on}}(\mu) = T^{f}(\mu), \qquad T^{f}(\mu) := \left((F(\mu))_{m^{f}_{j}}\right)_{j\in\{1:J^{f}\}} \in \mathbb{R}^{J^{f}}, \tag{3.48d}$$

$$Q^{\boldsymbol{ng}}\alpha^{\boldsymbol{ng}}_{\mathrm{on}}(\mu) = T^{\boldsymbol{ng}}(\mu), \quad T^{\boldsymbol{ng}}(\mu) := \left((G^{\boldsymbol{n}}(\mu))_{m^{\boldsymbol{ng}}_{j}}\right)_{j\in\{1:J^{\boldsymbol{ng}}\}} \in \mathbb{R}^{J^{\boldsymbol{ng}}}, \tag{3.48e}$$

where the vector-valued functions α^{a}_{on}, $\alpha^{\boldsymbol{nb}}_{\mathrm{on}}$, $\alpha^{\boldsymbol{\tau b}}_{\mathrm{on}}$, $\alpha^{f}_{\mathrm{on,j}}$, and $\alpha^{\boldsymbol{ng}}_{\mathrm{on}}$ are such that

$$\alpha^{a}_{\mathrm{on}}(\mu) := (\alpha^{a}_{\mathrm{on,j}}(\mu))_{j\in\{1:J^{a}\}} \in \mathbb{R}^{J^{a}}, \tag{3.49a}$$

$$\alpha^{\boldsymbol{nb}}_{\mathrm{on}}(\mu) := (\alpha^{\boldsymbol{nb}}_{\mathrm{on,j}}(\mu))_{j\in\{1:J^{\boldsymbol{nb}}\}} \in \mathbb{R}^{J^{\boldsymbol{nb}}}, \tag{3.49b}$$

$$\alpha^{\boldsymbol{\tau b}}_{\mathrm{on}}(\mu) := (\alpha^{\boldsymbol{\tau b}}_{\mathrm{on,j}}(\mu))_{j\in\{1:J^{\boldsymbol{\tau b}}\}} \in \mathbb{R}^{J^{\boldsymbol{\tau b}}}, \tag{3.49c}$$

$$\alpha^{f}_{\mathrm{on}}(\mu) := (\alpha^{f}_{\mathrm{on,j}}(\mu))_{j\in\{1:J^{f}\}} \in \mathbb{R}^{J^{f}}, \tag{3.49d}$$

$$\alpha^{\boldsymbol{ng}}_{\mathrm{on}}(\mu) := (\alpha^{\boldsymbol{ng}}_{\mathrm{on,j}}(\mu))_{j\in\{1:J^{\boldsymbol{ng}}\}} \in \mathbb{R}^{J^{\boldsymbol{ng}}}. \tag{3.49e}$$

The parameter-independent interpolation matrices $Q^{a} \in \mathbb{R}^{J^{a}\times J^{a}}$, $Q^{\boldsymbol{nb}} \in \mathbb{R}^{J^{\boldsymbol{nb}}\times J^{\boldsymbol{nb}}}$, $Q^{\boldsymbol{\tau b}} \in \mathbb{R}^{J^{\boldsymbol{\tau b}}\times J^{\boldsymbol{\tau b}}}$, $Q^{f} \in \mathbb{R}^{J^{f}\times J^{f}}$ and $Q^{\boldsymbol{ng}} \in \mathbb{R}^{J^{\boldsymbol{ng}}\times J^{\boldsymbol{ng}}}$ are such that

$$(Q^{a})_{ij} := (A_{j})_{n^{a}_{i} m^{a}_{i}}, \qquad \forall i,j \in \{1{:}J^{a}\}, \tag{3.50a}$$

$$(Q^{\boldsymbol{nb}})_{ij} := (B^{\boldsymbol{n}}_{j})_{n^{\boldsymbol{nb}}_{i} m^{\boldsymbol{nb}}_{i}}, \qquad \forall i,j \in \{1{:}J^{\boldsymbol{nb}}\}, \tag{3.50b}$$

$$(Q^{\boldsymbol{\tau b}})_{ij} := (B^{\boldsymbol{\tau}}_{j})_{n^{\boldsymbol{\tau b}}_{i} m^{\boldsymbol{\tau b}}_{i}}, \qquad \forall i,j \in \{1{:}J^{\boldsymbol{\tau b}}\}, \tag{3.50c}$$

$$(Q^{f})_{ij} := (F_{j})_{m^{f}_{i}}, \qquad \forall i,j \in \{1{:}J^{f}\}, \tag{3.50d}$$

$$(Q^{\boldsymbol{ng}})_{ij} := (G^{\boldsymbol{n}}_{j})_{m^{\boldsymbol{ng}}_{i}}, \qquad \forall i,j \in \{1{:}J^{\boldsymbol{ng}}\}. \tag{3.50e}$$

By construction, these matrices are lower-triangular with unit diagonal. Consequently, these matrices are invertible and their inverse can be easily computed once and for all during the offline phase. Combining (3.41) with (3.46), we obtain the following approximate decompositions:

$$A_{N}(\mu) \approx \quad E^{a}_{N}(\mu) := \sum_{j\in\{1:J^{a}\}} \alpha^{a}_{\mathrm{on,j}}(\mu) A_{N,j}, \qquad A_{N,j} := Z^{\top} A_{j} Z \in \mathbb{R}^{N\times N}, \tag{3.51a}$$

$$B^{\boldsymbol{n}}_{R,N}(\mu) \approx E^{\boldsymbol{nb}}_{R,N}(\mu) := \sum_{j\in\{1:J^{\boldsymbol{nb}}\}} \alpha^{\boldsymbol{nb}}_{\mathrm{on,j}}(\mu) B^{\boldsymbol{n}}_{R,N,j}, \quad B^{\boldsymbol{n}}_{R,N,j} := Q^{\boldsymbol{n}\top} B^{\boldsymbol{n}}_{j} Z \in \mathbb{R}^{R\times N}, \tag{3.51b}$$

$$B^{\boldsymbol{\tau}}_{S,N}(\mu) \approx E^{\boldsymbol{\tau b}}_{S,N}(\mu) := \sum_{j\in\{1:J^{\boldsymbol{\tau b}}\}} \alpha^{\boldsymbol{\tau b}}_{\mathrm{on,j}}(\mu) B^{\boldsymbol{\tau}}_{S,N,j}, \quad B^{\boldsymbol{\tau}}_{S,N,j} := Q^{\boldsymbol{\tau}\top} B^{\boldsymbol{\tau}}_{j} Z \in \mathbb{R}^{S\times N}, \tag{3.51c}$$

$$F_{N}(\mu) \approx \quad E^{f}_{N}(\mu) := \sum_{j\in\{1:J^{f}\}} \alpha^{f}_{\mathrm{on,j}}(\mu) F_{N,j}, \qquad F_{N,j} := Z^{\top} F_{j} \in \mathbb{R}^{N}, \tag{3.51d}$$

$$G^{\boldsymbol{n}}_{R}(\mu) \approx \quad E^{\boldsymbol{ng}}_{R}(\mu) := \sum_{j\in\{1:J^{\boldsymbol{ng}}\}} \alpha^{\boldsymbol{ng}}_{\mathrm{on,j}}(\mu) G^{\boldsymbol{n}}_{R,j}, \qquad G^{\boldsymbol{n}}_{R,j} := Q^{\boldsymbol{n}\top} G^{\boldsymbol{n}}_{j} \in \mathbb{R}^{R}, \tag{3.51e}$$

where the parameter-independent, small-dimensional arrays $A_{N,j}$, $B^{\boldsymbol{n}}_{R,N,j}$, $B^{\boldsymbol{\tau}}_{S,N,j}$, $F_{N,j}$ and $G^{\boldsymbol{n}}_{R,j}$ can be computed once and for all during the offline phase. Finally, using the approximations from (3.51) in (3.40) (for simplicity, we keep the same notation for the unknowns $\boldsymbol{U}_{N,k+1}(\mu)$, $\Lambda^{\boldsymbol{n}}_{R,k+1}(\mu)$ and $\boldsymbol{\Lambda}^{\boldsymbol{\tau}}_{S,k+1}(\mu)$), we consider the following sequence of problems: For all $k \geq 0$, find $(\boldsymbol{U}_{N,k+1}(\mu), \Lambda^{\boldsymbol{n}}_{R,k+1}(\mu), \boldsymbol{\Lambda}^{\boldsymbol{\tau}}_{S,k+1}(\mu)) \in \mathbb{R}^N \times \mathbb{R}^R_+ \times \boldsymbol{X}^{\boldsymbol{\tau}}_{S,\boldsymbol{\mathcal{C}}^{\mathrm{HF}}(\mu)}(\mu; \nu_{\mathcal{F}}\Lambda^{\boldsymbol{n}}_{R,k+1}(\mu))$ such that

$$\begin{cases} E^a_N(\mu)\boldsymbol{U}_{N,k+1}(\mu) + E^{\boldsymbol{n}b}_{R,N}(\mu)^\top \Lambda^{\boldsymbol{n}}_{R,k}(\mu) + E^{\boldsymbol{\tau}b}_{S,N}(\mu)^\top \boldsymbol{\Lambda}^{\boldsymbol{\tau}}_{S,k}(\mu) = E^f_N(\mu), \\ \Lambda^{\boldsymbol{n}}_{R,k+1}(\mu) = \Pi_{\mathbb{R}^R_+}(\Lambda^{\boldsymbol{n}}_{R,k}(\mu) - \rho(E^{\boldsymbol{n}b}_{R,N}(\mu)\boldsymbol{U}_{N,k+1}(\mu) - E^{\boldsymbol{n}g}_R(\mu))), \\ \boldsymbol{\Lambda}^{\boldsymbol{\tau}}_{S,k+1}(\mu) = \Pi_{\boldsymbol{X}^{\boldsymbol{\tau}}_{S,\boldsymbol{\mathcal{C}}^{\mathrm{HF}}(\mu)}(\mu;\nu_{\mathcal{F}}\Lambda^{\boldsymbol{n}}_{R,k+1}(\mu))}(\boldsymbol{\Lambda}^{\boldsymbol{\tau}}_{S,k}(\mu) - \rho E^{\boldsymbol{\tau}b}_{S,N}(\mu)\boldsymbol{U}_{N,k+1}(\mu)). \end{cases} \tag{3.52}$$

The convergence criterion for (3.52) is still (3.19) using the reconstructed functions.

At this stage, the only remaining dependence of the problem (3.52) on the HF dimensions results from the dependence of $\boldsymbol{X}^{\boldsymbol{\tau}}_{S,\boldsymbol{\mathcal{C}}^{\mathrm{HF}}(\mu)}(\mu; \nu_{\mathcal{F}}\Lambda^{\boldsymbol{n}}_{R,k+1}(\mu))$ on $\mathcal{S}^{\mathrm{HF}}_0 = \mathcal{R}^{\mathrm{HF}}$ as a consequence of using the set of HF collocation nodes $\boldsymbol{\mathcal{C}}^{\mathrm{HF}}(\mu)$. We now address this issue.

3.3.3.2 Selection of the collocation nodes

In order to overcome the dependence of the RB model on the cardinality of the HF collocation nodes, we need to construct a subset of collocation nodes that has small enough cardinality and at the same time is representative enough so that the tangential constraints are accurately satisfied in the RB model. This operation is performed during the offline stage.

Here, we propose to construct, in a progressive way, a subset of $\boldsymbol{\mathcal{C}}^{\mathrm{HF}}(\mu)$ by means of a greedy algorithm. Consistently with the approach from Section 3.3.1, this subset is generated from a subset of $\widehat{\boldsymbol{\mathcal{C}}}^{\mathrm{HF}}$ using the geometric mapping $h(\mu)$. How to do this is described below. At this stage, it suffices to know that the proposed algorithm is iterative. Thus, at each iteration $q \geq 0$, a subset of reference collocation nodes $\widehat{\boldsymbol{\mathcal{C}}}(q) \subset \widehat{\boldsymbol{\mathcal{C}}}^{\mathrm{HF}}$ composed of S_q collocation nodes $\{\widehat{\boldsymbol{c}}_{s_j}\}_{j\in\{1:S_q\}}$ is constructed, with the notation $j : \{1{:}S_q\} \to s_j \in \{1{:}\mathcal{S}^{\mathrm{HF}}_0\}$. Using the geometric mapping $h(\mu)$, we then set

$$\boldsymbol{C}(\mu, q) := h(\mu)(\widehat{\boldsymbol{\mathcal{C}}}(q)) \subset \boldsymbol{\mathcal{C}}^{\mathrm{HF}}(\mu). \tag{3.53}$$

Let us first present the RB model with the reduced set of collocation nodes $\boldsymbol{C}(\mu, q)$. We define

$$\boldsymbol{X}^{\boldsymbol{\tau}}_{S,\boldsymbol{C}(\mu,q)}(\mu; \nu_{\mathcal{F}}\Lambda^{\boldsymbol{n}}_{R,k+1}(\mu)) := \left\{\boldsymbol{\Theta} \in \mathbb{R}^S \mid \|(Q^{\boldsymbol{\tau}}\boldsymbol{\Theta})^{s_j}\| \leq \nu_{\mathcal{F}}(Q^{\boldsymbol{n}}\Lambda^{\boldsymbol{n}}_{R,k+1}(\mu))^{s_j},\ \forall j \in \{1{:}S_q\}\right\}. \tag{3.54}$$

Notice that $\boldsymbol{X}^{\boldsymbol{\tau}}_{S,\boldsymbol{C}(\mu,q)}(\mu; \cdot)$ is actually a superset of the set $\boldsymbol{X}^{\boldsymbol{\tau}}_{S,\boldsymbol{\mathcal{C}}^{\mathrm{HF}}(\mu)}(\mu; \cdot)$ defined in (3.43). Using this superset in (3.52) leads to the following sequence of problems: For all $k \geq 0$, find $(\boldsymbol{U}^q_{N,k+1}(\mu), \Lambda^{\boldsymbol{n},q}_{R,k+1}(\mu),$

$\boldsymbol{\Lambda}^{\boldsymbol{\tau},q}_{S,k+1}(\mu)) \in \mathbb{R}^N \times \mathbb{R}^R_+ \times \boldsymbol{X}^{\boldsymbol{\tau}}_{S,\boldsymbol{C}(\mu,q)}(\mu; \nu_{\mathcal{F}} \Lambda^{\boldsymbol{n},q}_{R,k+1}(\mu))$ such that

$$\begin{cases} E^a_N(\mu)\boldsymbol{U}^q_{N,k+1}(\mu) + E^{\boldsymbol{nb}}_{R,N}(\mu)^\top \Lambda^{\boldsymbol{n},q}_{R,k}(\mu) + E^{\boldsymbol{\tau b}}_{S,N}(\mu)^\top \boldsymbol{\Lambda}^{\boldsymbol{\tau},q}_{S,k}(\mu) = E^f_N(\mu), \\ \Lambda^{\boldsymbol{n},q}_{R,k+1}(\mu) = \Pi_{\mathbb{R}^R_+}(\Lambda^{\boldsymbol{n},q}_{R,k}(\mu) - \rho(E^{\boldsymbol{nb}}_{R,N}(\mu)\boldsymbol{U}^q_{N,k+1}(\mu) - E^{\boldsymbol{ng}}_R(\mu))), \\ \boldsymbol{\Lambda}^{\boldsymbol{\tau},q}_{S,k+1}(\mu) = \Pi_{\boldsymbol{X}^{\boldsymbol{\tau}}_{S,\boldsymbol{C}(\mu,q)}(\mu;\nu_{\mathcal{F}}\Lambda^{\boldsymbol{n},q}_{R,k+1}(\mu))}(\boldsymbol{\Lambda}^{\boldsymbol{\tau},q}_{S,k}(\mu) - \rho E^{\boldsymbol{\tau b}}_{S,N}(\mu)\boldsymbol{U}^q_{N,k+1}(\mu)). \end{cases} \tag{3.55}$$

The convergence criterion for (3.55) is still (3.19) using the reconstructed functions. We denote the converged solution to the problem (3.55) as the triple $(\boldsymbol{U}^q_{N,\mathrm{cv}}(\mu), \Lambda^{\boldsymbol{n},q}_{R,\mathrm{cv}}(\mu), \boldsymbol{\Lambda}^{\boldsymbol{\tau},q}_{S,\mathrm{cv}}(\mu)) \in \mathbb{R}^N \times \mathbb{R}^R_+ \times \boldsymbol{X}^{\boldsymbol{\tau}}_{S,\boldsymbol{C}(\mu,q)}(\mu; \nu_{\mathcal{F}} \Lambda^{\boldsymbol{n},q}_{R,\mathrm{cv}}(\mu))$ and the associated reconstructed solution (see Remark 3.3.1) as the triple $(\boldsymbol{u}^q_{N,\mathrm{cv}}(\mu), \lambda^{\boldsymbol{n},q}_{R,\mathrm{cv}}(\mu), \boldsymbol{\lambda}^{\boldsymbol{\tau},q}_{S,\mathrm{cv}}(\mu)) \in \boldsymbol{\mathcal{V}}(\mu) \times \mathcal{W}^{\boldsymbol{n}}(\mu) \times \boldsymbol{\mathcal{X}}^{\boldsymbol{\tau}}_{\boldsymbol{C}(\mu,q)}(\mu; \nu_{\mathcal{F}} \lambda^{\boldsymbol{n}}_{R,\mathrm{cv}}(\mu))$.

To construct the reduced subset of collocation nodes, we design a so-called Greedy Collocation Nodes Selection (GCNS) algorithm that, given the training subset $\mathcal{D}_{\mathtt{train}} \subset \mathcal{D}$, the set of reference HF collocation nodes $\widehat{\boldsymbol{\mathcal{C}}}^{\mathrm{HF}}$, the primal reduced space $\boldsymbol{V}_N$, the dual reduced cone $W^{\boldsymbol{n}}_R$, and the dual reduced space $\boldsymbol{X}^{\boldsymbol{\tau}}_S$, returns a subset $\widehat{\boldsymbol{C}}(q) \subseteq \widehat{\boldsymbol{\mathcal{C}}}^{\mathrm{HF}}$ of S_q reference collocation nodes such that the relative error

$$\max_{\mu \in \mathcal{D}_{\mathtt{train}}} \frac{\|\boldsymbol{\lambda}^{\boldsymbol{\tau}}_{\mathrm{cv}}(\mu) - \boldsymbol{\lambda}^{\boldsymbol{\tau},q}_{S,\mathrm{cv}}(\mu)\|_{\Gamma^{\mathrm{c}}(\mu)}}{\|\boldsymbol{\lambda}^{\boldsymbol{\tau}}_{\mathrm{cv}}(\mu)\|_{\Gamma^{\mathrm{c}}(\mu)}} \tag{3.56}$$

is as small as possible. Our numerical results presented in Section 3.4 indicate that $\widehat{\boldsymbol{C}}(q)$ has indeed a smaller cardinality than $\widehat{\boldsymbol{\mathcal{C}}}^{\mathrm{HF}}$ and that the tangential constraints are satisfied for all the collocation nodes in $\boldsymbol{\mathcal{C}}^{\mathrm{HF}}(\mu)$ with a satisfactory tolerance. The GCNS algorithm is described in Algorithm 3 and involves the following two main steps at iteration $q \geq 0$:

- seek the parameter $\mu_q \in \mathcal{D}_{\mathtt{train}}$ for which the constraints are most violated by solving the problem (3.55) with the subset of collocation nodes $\boldsymbol{C}(\mu, q) := h(\mu)(\widehat{\boldsymbol{C}}(q))$ (line 4).
- seek the reference collocation nodes $\{\widehat{\boldsymbol{c}}_s\}_{s \in \overline{\mathcal{Q}}(q)}$ defining the collocation nodes of $\boldsymbol{\mathcal{C}}^{\mathrm{HF}}(\mu_q)$ at which the constraint is most violated (line 5).

Notice that by construction, the error $e_{\mathtt{GCNS}}(q)$ is such that $e_{\mathtt{GCNS}}(q) := \min_{r \in \{0:q\}} e_{\mathtt{GCNS}}(r)$.

In conclusion, for all $\mu \in \mathcal{D}$, we define the subset $\boldsymbol{C}(\mu, q)$ from $\widehat{\boldsymbol{C}}(q)$ using (3.53) with

$$\widehat{\boldsymbol{C}}(q) := \mathtt{GCNS}(\mathcal{D}_{\mathtt{train}}, \widehat{\boldsymbol{\mathcal{C}}}^{\mathrm{HF}}, \boldsymbol{V}_N, W^{\boldsymbol{n}}_R, \boldsymbol{X}^{\boldsymbol{\tau}}_S). \tag{3.57}$$

Remark 3.3.2 (First step). In the first step of the GCNS algorithm, the problem (3.55) is solved with no friction constraints since $\widehat{\boldsymbol{C}}(0) = \emptyset$. This means that the tangential efforts do not have to respect any a priori upper bound. Equivalently, one solves a Tresca frictional contact problem by formally setting $s = +\infty$.

Remark 3.3.3 (Stopping criterion). There is no guarantee that the GCNS algorithm will reach a fixed tolerance. Therefore, the algorithm is run as long as $e_{\mathtt{GCNS}}(q)$ decreases and then stops.

Algorithm 3 `GCNS: Greedy Collocation Node Selection`

$\texttt{GCNS}(\mathcal{D}_{\texttt{train}}, \widehat{\boldsymbol{C}}, \boldsymbol{V}_N, W_R^{\boldsymbol{n}}, \boldsymbol{X}_S^{\boldsymbol{\tau}})$

Require: $\mathcal{D}_{\texttt{train}} \subset \mathcal{D}$: `training subset`
$\boldsymbol{V}_N \subset \mathbb{R}^{\mathcal{N}^{\mathrm{HF}}}$: `primal reduced space`
$W_R^{\boldsymbol{n}} \subset \mathbb{R}_+^{\mathcal{R}^{\mathrm{HF}}}$: `dual reduced cone`
$\boldsymbol{X}_S^{\boldsymbol{\tau}} \subset \mathbb{R}^{\mathcal{S}^{\mathrm{HF}}}$: `dual reduced space`
Ensure: $\widehat{\boldsymbol{C}}(q)$: `subset of` $\widehat{\boldsymbol{\mathcal{C}}}^{\mathrm{HF}}$

$q := 0$; $\widehat{\boldsymbol{C}}(0) := \emptyset$; $\mathcal{Q}(0) := \emptyset$
while $(q \leq 1)$ or $(e_{\texttt{GCNS}}(q) \leq e_{\texttt{GCNS}}(q-1))$ **do**
  Solve (3.55) for all $\mu \in \mathcal{D}_{\texttt{train}}$ using $\boldsymbol{V}_N$, $W_R^{\boldsymbol{n}}$, and $\boldsymbol{X}_{S,\boldsymbol{C}(\mu,q)}^{\boldsymbol{\tau}}$.
  $\mu_q \in \underset{\mu \in \mathcal{D}_{\texttt{train}}}{\texttt{argmax}} \left\| \left[\|\boldsymbol{\lambda}_{S,\mathrm{cv}}^{\boldsymbol{\tau},q}(\mu)\| - \nu_{\mathcal{F}} \lambda_{R,\mathrm{cv}}^{\boldsymbol{n},q}(\mu) \right]_+ \right\|_{\ell^\infty(\boldsymbol{\mathcal{C}}^{\mathrm{HF}}(\mu))}$
  $\overline{\mathcal{Q}}(q) := \underset{s \in \{1:\mathcal{S}_0^{\mathrm{HF}}\} \setminus \mathcal{Q}(q)}{\texttt{argmax}} \left[\left(\|\boldsymbol{\lambda}_{S,\mathrm{cv}}^{\boldsymbol{\tau},q}(\mu_q)\| - \nu_{\mathcal{F}} \lambda_{R,\mathrm{cv}}^{\boldsymbol{n},q}(\mu_q) \right) (h(\mu_q)(\widehat{\boldsymbol{c}}_s)) \right]_+$
  $e_{\texttt{GCNS}}(q) := \underset{\mu \in \mathcal{D}_{\texttt{train}}}{\texttt{max}} \frac{\|\boldsymbol{\lambda}_{\mathrm{cv}}^{\boldsymbol{\tau}}(\mu) - \boldsymbol{\lambda}_{S,\mathrm{cv}}^{\boldsymbol{\tau},q}(\mu)\|_{\Gamma^{\mathrm{c}}(\mu)}}{\|\boldsymbol{\lambda}_{\mathrm{cv}}^{\boldsymbol{\tau}}(\mu)\|_{\Gamma^{\mathrm{c}}(\mu)}}$
  $\widehat{\boldsymbol{C}}(q+1) := \widehat{\boldsymbol{C}}(q) \cup \{\widehat{\boldsymbol{c}}_s\}_{s \in \overline{\mathcal{Q}}(q)}$
  $\mathcal{Q}(q+1) := \mathcal{Q}(q) \cup \overline{\mathcal{Q}}(q)$
  $q = q + 1$
end while
return $\widehat{\boldsymbol{C}}(q)$

3.3.3.3 An efficient reduced-basis algorithm

Combining the affine decomposition (Section 3.3.3.1) and the GCNS algorithm (Section 3.3.3.2), we obtain a computationally efficient RB procedure organized as follows:

— Offline stage

1. Select a training subset $\mathcal{D}_{\texttt{train}} := \{\mu_p\}_{p \in \{1:P\}} \subset \mathcal{D}$.
2. Compute the HF snapshots $\{\boldsymbol{U}_{\mathrm{cv}}(\mu_p), \Lambda_{\mathrm{cv}}^{\boldsymbol{n}}(\mu_p), \boldsymbol{\Lambda}_{\mathrm{cv}}^{\boldsymbol{\tau}}(\mu_p)\}_{p \in \{1:P\}} \subset \mathbb{R}^{\mathcal{N}^{\mathrm{HF}}} \times \mathbb{R}_+^{\mathcal{R}^{\mathrm{HF}}} \times \mathbb{R}^{\mathcal{S}^{\mathrm{HF}}}$ by solving (3.32).
3. Compute the reduced spaces $\boldsymbol{V}_N$, $W_R^{\boldsymbol{n}}$ and $\boldsymbol{X}_S^{\boldsymbol{\tau}}$ by using POD and mCPG on the snapshots.
4. Stabilize the RB problem: enrich $\boldsymbol{V}_N$ by using the PGA.
5. Compute the high-dimensional arrays A_j, $B_j^{\boldsymbol{n}}$, $B_j^{\boldsymbol{\tau}}$, F_j and $G_j^{\boldsymbol{n}}$ by using the EIM.
6. Invert the interpolation matrices Q^a, $Q^{\boldsymbol{n}b}$, $Q^{\boldsymbol{\tau}b}$, Q^f and $Q^{\boldsymbol{n}g}$ defined in (3.50).
7. Compute the small-dimensional arrays $A_{N,j}$, $B_{R,N,j}^{\boldsymbol{n}}$, $B_{S,N,j}^{\boldsymbol{\tau}}$, $F_{N,j}$ and $G_{R,j}^{\boldsymbol{n}}$ by using (3.51).
8. Compute the reduced subset of collocation nodes $\widehat{\boldsymbol{C}}(q)$ by using the GCNS algorithm.

— Online stage: For any $\mu \in \mathcal{D} \setminus \mathcal{D}_{\texttt{train}}$,

1. Evaluate $T^a(\mu)$, $T^{nb}(\mu)$, $T^{\tau b}(\mu)$, $T^f(\mu)$ and $T^{ng}(\mu)$ and compute $\alpha^a_{\text{on,j}}(\mu)$, $\alpha^{nb}_{\text{on,j}}(\mu)$, $\alpha^{\tau b}_{\text{on,j}}(\mu)$, $\alpha^f_{\text{on,j}}(\mu)$ and $\alpha^{ng}_{\text{on,j}}(\mu)$ by using (3.48).
2. Evaluate $E^a_N(\mu)$, $E^{nb}_{R,N}(\mu)$, $E^{\tau b}_{S,N}(\mu)$, $E^f_N(\mu)$ and $E^{ng}_R(\mu)$ by using (3.51).
3. Loop on $k \geq 0$,
   (a) Solve (3.55).
   (b) Check convergence; if not, set $k \leftarrow k+1$ and go back to (3a).

3.4 Numerical results

In this section, we present numerical results showcasing the accuracy and the robustness of the proposed RB method to solve contact problem with friction.

3.4.1 Hertz contact between two half-disks

We consider the frictional Hertz contact problem between two half-disks as represented in Figure 3.1. The upper half-disk occupies the deformable domain $\Omega_1(\mu) \subset \mathbb{R}^2$ of parametric radius

$$R_1 := \mu \in \mathcal{D} := \Big[0.7, 1.3\Big](\text{m}), \tag{3.58}$$

and the lower half-disk the rigid domain $\Omega_2 \subset \mathbb{R}^2$ of fixed radius $R_2 := 1\text{m}$. The initial gap between the two half-disks is equal to $\gamma_0 > 0$. We impose a displacement of $-d$ on $\Gamma_1^{\texttt{top}}(\mu)$ of $\Omega_1(\mu)$ with $d \geq \gamma_0$. The initial gap γ_0 and the imposed displacement d are, respectively, set to $\gamma_0 := 0.001\text{m}$ and $d := 0.09\text{m}$. This latter value, which is less than 10% of the maximum value of R_1 allows us to remain within the validity of the small deformation assumption. Since Ω_2 is rigid and fixed, we only mesh the domain $\Omega_1(\mu)$ and set $\Omega(\mu) := \Omega_1(\mu)$ to build the HF spaces. The material parameters are $E := 15\text{Pa}$ for the Young modulus and $\nu := 0.35$ for the Poisson coefficient. The friction coefficient $\nu_{\mathcal{F}}$ is set to $\nu_{\mathcal{F}} := 0.2$. The training set is chosen as $\mathcal{D}_{\texttt{train}} := \Big\{0.7 + 0.01i, 0 \leq i \leq 60\Big\}(\text{m})$ (altogether 61 points), and the validation set $\mathcal{D}_{\texttt{valid}}$ is generated by choosing 30 elements in $\mathcal{D}$ randomly with a uniform distribution.

We consider the reference domain $\widehat{\Omega}_1 := \Omega_1(1)$ and introduce the geometric mapping $h_1(\mu) : \widehat{\Omega}_1 \to \Omega_1(\mu)$ defined as $h_1(\mu)(\boldsymbol{x}) := \mu\boldsymbol{x}$, for all $\boldsymbol{x} \in \widehat{\Omega}_1$, with the origin located at the center of $\widehat{\Omega}_1$. We use a mesh composed of 704 nodes with 101 nodes on the potential contact manifold $\widehat{\Gamma}_1^{\text{c}}$ which is the part of the half-circle of angle $\theta \in [-\frac{5\pi}{8}, -\frac{3\pi}{8}]$ with respect to the horizontal axis. For all $\mu \in \mathcal{D}$, we use $\mathbb{P}_2$ finite elements for the primal space $\boldsymbol{\mathcal{V}}(\mu)$ and $\mathbb{P}_1$ finite elements for the dual spaces $\mathcal{W}(\mu)$ and $\boldsymbol{\mathcal{X}}(\mu)$. Thus, we have $\mathcal{N}^{\text{HF}} := 5350$ primal and $\mathcal{R}^{\text{HF}} = \mathcal{S}^{\text{HF}} := 101$ dual degrees of freedom. We equip the space $\boldsymbol{\mathcal{V}}(\mu)$ with the norm $\|\cdot\|_{\boldsymbol{\mathcal{V}}(\mu)}$ defined as follows:

$$\|\boldsymbol{v}\|_{\boldsymbol{\mathcal{V}}(\mu)} := \left(\|\boldsymbol{v}\|^2_{L^2(\Omega(\mu))} + \widehat{\ell}^2\|\nabla\boldsymbol{v}\|^2_{L^2(\Omega(\mu))}\right)^{\frac{1}{2}}, \quad \forall \boldsymbol{v} \in \boldsymbol{\mathcal{V}}(\mu), \tag{3.59}$$

where the characteristic length $\widehat{\ell}$ is the radius of $\widehat{\Omega}_1$ and is introduced for dimensional consistency.

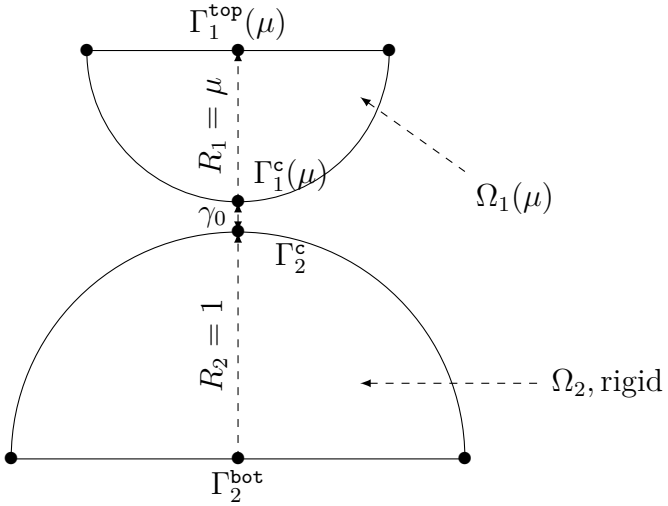

Figure 3.1 – Hertz test case: Configuration.

Figure 3.2 displays the reference configuration of $\Omega_1(\mu)$ for $\mu = 0.7$m (left panel) and the deformed configuration resulting from the HF displacement field $\boldsymbol{u}(\mu)$ (right panel). We can see that we use a symmetric mesh. This is important because it allows us to guarantee the symmetry of the HF snapshots. Indeed, if the snapshots are not symmetric, the resulting POD modes will not be either. Consequently, the reduced model looses this symmetry property, leading to reduced solutions of poorer quality. Moreover, we have discretized a complete half-disk instead of a quarter-disk only to avoid difficulties when enforcing the symmetry condition at the lowest point of $\Omega_1(\mu)$.

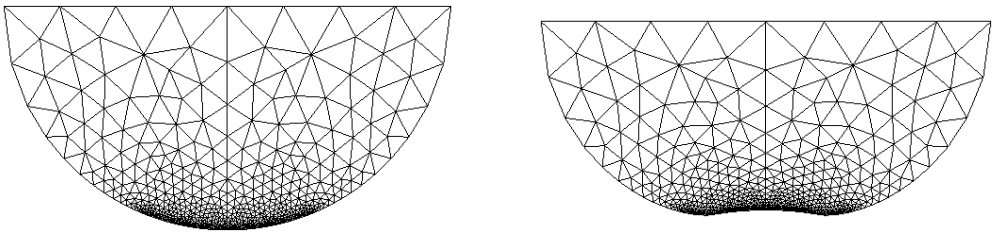

Figure 3.2 – Hertz test case: Configurations for $\mu = 0.7$m. Left: reference; Right: deformed.

Figure 3.3 displays the normal Lagrange multiplier $\lambda^{\boldsymbol{n}}(\mu)$ (Column 1), the tangential Lagrange multiplier $\boldsymbol{\lambda}^{\boldsymbol{\tau}}(\mu)$ (Column 2) and the superposition of $\nu_{\mathcal{F}}|\lambda^{\boldsymbol{n}}(\mu)|$ and $\|\boldsymbol{\lambda}^{\boldsymbol{\tau}}(\mu)\|$ (Column 3) as a function of the abscissa along $\Gamma^{\mathrm{c}}(\mu)$ for $\mu = 0.7$m (Row 1), $\mu = 1$m (Row 2), and $\mu = 1.3$m (Row 3). We notice some slight oscillations on $\lambda^{\boldsymbol{n}}(\mu)$ around the center of the contact boundary where the tangential displacement vanishes. For the tangential Lagrange multiplier, no oscillations are observed. The subfigures in Column 3 show that the Coulomb friction law is well satisfied for all parameters $\mu \in \{0.7, 1.0, 13\}$(m).

Let us consider the POD and mCPG projection errors $e^{\boldsymbol{u}}_{\mathtt{POD}}(N)$, $e^{\lambda^{\boldsymbol{n}}}_{\mathtt{mCPG}}(R)$ and $e^{\boldsymbol{\lambda}^{\boldsymbol{\tau}}}_{\mathtt{POD}}(S)$

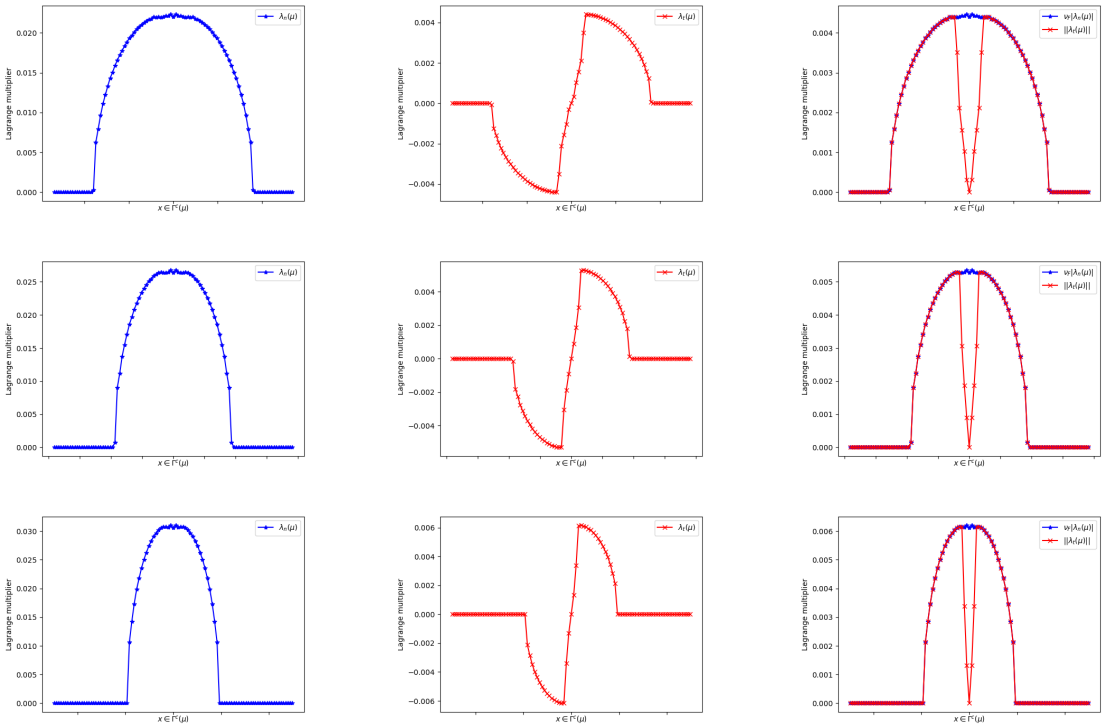

Figure 3.3 – Hertz test case: Lagrange multipliers. Row 1: $\mu = 0.7$m. Row 2: $\mu = 1$m. Row 3 $\mu = 1.3$m. Column 1: $\lambda^{\boldsymbol{n}}(\mu)$(Pa). Column 2: $\boldsymbol{\lambda}^{\boldsymbol{\tau}}(\mu)$(Pa). Column 3: $\nu_{\mathcal{F}}|\lambda^{\boldsymbol{n}}(\mu)|$(Pa) and $\|\boldsymbol{\lambda}^{\boldsymbol{\tau}}(\mu)\|$(Pa).

defined as follows:

$$e^{\boldsymbol{u}}_{\texttt{POD}}(N) := \frac{\left(\sum\limits_{\mu\in\mathcal{D}_{\texttt{train}}} \left\|\left(\mathbb{I}_{\mathbb{R}^{\mathcal{N}^{\mathrm{HF}}}} - \Pi_{\boldsymbol{V}_N}\right)(\boldsymbol{U}_{\mathrm{cv}}(\mu))\right\|^2_{\mathbb{W}^{\boldsymbol{u}}}\right)^{\frac{1}{2}}}{\left(\sum\limits_{\mu\in\mathcal{D}_{\texttt{train}}} \|\boldsymbol{U}_{\mathrm{cv}}(\mu)\|^2_{\mathbb{W}^{\boldsymbol{u}}}\right)^{\frac{1}{2}}}, \tag{3.60a}$$

$$e^{\lambda^{\boldsymbol{n}}}_{\texttt{mCPG}}(R) := \frac{\max\limits_{\mu\in\mathcal{D}_{\texttt{train}}} \left\|\left(\mathbb{I}_{\mathbb{R}^{\mathcal{R}^{\mathrm{HF}}}} - \Pi_{W^{\boldsymbol{n}}_R}\right)(\Lambda^{\boldsymbol{n}}_{\mathrm{cv}}(\mu))\right\|_{\mathbb{W}^{\lambda^{\boldsymbol{n}}}}}{\max\limits_{\mu\in\mathcal{D}_{\texttt{train}}} \|\Lambda^{\boldsymbol{n}}_{\mathrm{cv}}(\mu)\|_{\mathbb{W}^{\lambda^{\boldsymbol{n}}}}}, \tag{3.60b}$$

$$e^{\boldsymbol{\lambda}^{\boldsymbol{\tau}}}_{\texttt{POD}}(S) := \frac{\left(\sum\limits_{\mu\in\mathcal{D}_{\texttt{train}}} \left\|\left(\mathbb{I}_{\mathbb{R}^{\mathcal{S}^{\mathrm{HF}}}} - \Pi_{\boldsymbol{X}^{\boldsymbol{\tau}}_S}\right)(\boldsymbol{\Lambda}^{\boldsymbol{\tau}}_{\mathrm{cv}}(\mu))\right\|^2_{\mathbb{W}^{\boldsymbol{\lambda}^{\boldsymbol{\tau}}}}\right)^{\frac{1}{2}}}{\left(\sum\limits_{\mu\in\mathcal{D}_{\texttt{train}}} \|\boldsymbol{\Lambda}^{\boldsymbol{\tau}}_{\mathrm{cv}}(\mu)\|^2_{\mathbb{W}^{\boldsymbol{\lambda}^{\boldsymbol{\tau}}}}\right)^{\frac{1}{2}}}, \tag{3.60c}$$

where $\mathbb{W}^{\boldsymbol{u}}$, $\mathbb{W}^{\lambda^{\boldsymbol{n}}}$ and $\mathbb{W}^{\boldsymbol{\lambda}^{\boldsymbol{\tau}}}$ denote the Gram matrices associated with the inner product of $H^1(\widehat{\Omega}_1;\mathbb{R}^d)$, $L^2(\widehat{\Gamma}^{\mathrm{c}}_1;\mathbb{R})$ and $L^2(\widehat{\Gamma}^{\mathrm{c}}_1;\mathbb{R}^{d-1})$, respectively. Figure 3.4 shows the POD and mCPG projection errors $e^{\boldsymbol{u}}_{\texttt{POD}}(N)$ (Column 1), $e^{\lambda^{\boldsymbol{n}}}_{\texttt{mCPG}}(R)$ (Column 2) and $e^{\boldsymbol{\lambda}^{\boldsymbol{\tau}}}_{\texttt{POD}}(S)$ (Column 3) for the displacement, the normal Lagrange multiplier and the tangential Lagrange multiplier as a function of the number of vectors composing the reduced bases.

In all cases, the projection errors decrease sufficiently fast so that the sets generated by the primal and dual snapshots can be approximated by small-dimensional linear spaces. We observe a fast decrease of the POD error $e^{\boldsymbol{u}}_{\texttt{POD}}(N)$ for the first 20 modes before a somewhat slower decrease takes over at error levels between 10^{-5} and 10^{-7}. For the mCPG error $e^{\boldsymbol{\lambda^n}}_{\texttt{mCPG}}(R)$, we globally observe a uniform decrease down to 10^{-6} followed by a swifter decrease and some small oscillations toward the end. For the POD error $e^{\boldsymbol{\lambda^\tau}}_{\texttt{POD}}(S)$, we observe an almost uniform decrease for the first 32 modes with error values from 1 down to 10^{-5}, before observing a significant drop of the error at about $S = 30$ before a stagnation of the error between 10^{-8} and 10^{-9}.

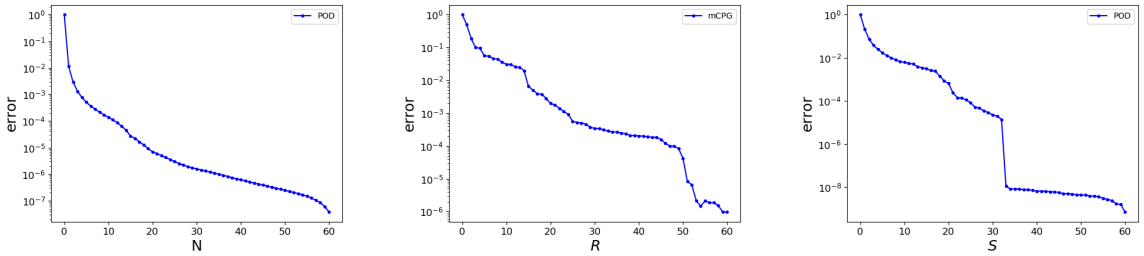

Figure 3.4 – Hertz test case: Projection errors for the POD and mCPG algorithm for $\mu \in \mathcal{D}_{\text{train}}$. Column 1: $e^{\boldsymbol{u}}_{\texttt{POD}}(N)$. Column 2: $e^{\boldsymbol{\lambda^n}}_{\texttt{mCPG}}(R)$. Column 3: $e^{\boldsymbol{\lambda^\tau}}_{\texttt{POD}}(S)$.

To assess our RB procedure, we consider the tolerance triple $(\delta^{\boldsymbol{u}}_{\texttt{POD}}, \delta^{\boldsymbol{\lambda^n}}_{\texttt{mCPG}}, \delta^{\boldsymbol{\lambda^\tau}}_{\texttt{POD}}) := (10^{-6}, 10^{-3}, 10^{-4})$, leading to the dimensions $N = 30$, $R = 20$ and $S = 20$ for $\boldsymbol{V}_N$, $W^{\boldsymbol{n}}_R$ and $\boldsymbol{X}^{\boldsymbol{\tau}}_S$, respectively. Notice that the tolerances $\delta^{\boldsymbol{\lambda^n}}_{\texttt{mCPG}}$ and $\delta^{\boldsymbol{\lambda^\tau}}_{\texttt{POD}}$ are chosen to deliver the same reduced dimensions ($R = S$) for the normal and tangential components of the Lagrange multiplier. This choice was made only to stay in the spirit of the HF model, where $\mathcal{R}^{\text{HF}} = \mathcal{S}^{\text{HF}}$. With these reduced dimensions, we are in the case where $N < R + S$ which means that, the bilinear form $b(\mu; \cdot, \cdot)$ defined in (3.39) is not inf-sup stable. To stabilize the RB model, we use the PGA algorithm introduced in [84] with a tolerance $\delta_{\texttt{PGA}} := \inf_{\mu \in \mathcal{D}_{\texttt{train}}} \frac{\beta_{\text{HF}}(\mu)}{c_{\text{HF}}(\mu)} = 0.072$, so that the stability condition established in [84, Prop 3.1] is fulfilled. Notice that $\beta_{\text{HF}}(\mu)$ and $c_{\text{HF}}(\mu)$ refer to the boundedness and inf-sup stability coefficients of the bilinear form $b(\mu; \cdot, \cdot)$ with respect to the HF pair $\big(\boldsymbol{\mathcal{V}}(\mu), \boldsymbol{\mathcal{Y}}(\mu)\big)$. Figure 3.5 shows the evolution of β_{min}, the minimum over all parameter values in $\mathcal{D}_{\texttt{train}}$ of the RB inf-sup constant as a function of the number of iterations of the PGA algorithm. We notice that with the choice made above for $\delta_{\texttt{PGA}}$, the PGA algorithm converges in $R + S$ iterations. For the first ten iterations, the inf-sup constant remains equal to zero for all $\mu \in \mathcal{D}_{\texttt{train}}$ confirming the necessity to stabilize the RB model. The dimension of the stabilized reduced primal space is equal to $N = 70$, meaning that in total $n = 40$ $(R + S)$ supremizers have been added to $\boldsymbol{V}_N$.

For the EIM approximation, we fix a tolerance $\delta_{\texttt{EIM}} := 10^{-3}$ to bound the errors resulting from (3.46). With this choice, we obtain $J^{\boldsymbol{n}b} = J^{\boldsymbol{\tau}b} = 41$. Notice that in the present test case, we do not need to perform an EIM decomposition on the operators $A(\mu)$, $F(\mu)$ and $G^{\boldsymbol{n}}(\mu)$. Indeed, the stiffness matrix $A(\mu)$ and the gap vector $G^{\boldsymbol{n}}(\mu)$ are already linearly dependent on μ, whereas the vector $F(\mu)$ is null since we only use an imposed displacement for the load. Figure 3.6 shows the EIM interpolation error for

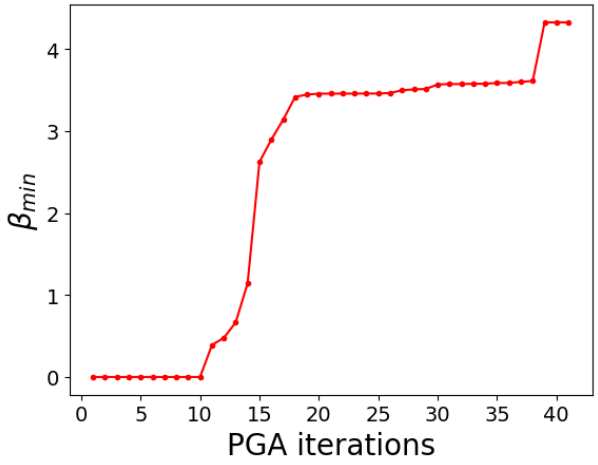

Figure 3.5 – Hertz test case: Stabilization using the PGA algorithm.

the matrix $B^{\boldsymbol{n}}(\mu)$ (Row 1) and the matrix $B^{\boldsymbol{\tau}}(\mu)$ (Row 2), *i.e.*, we plot

$$e^{\boldsymbol{n}b}_{\mathtt{EIM}}(J^{\boldsymbol{n}b}) := \frac{\max\limits_{\mu\in\mathcal{D}_*} \|B^{\boldsymbol{n}}(\mu) - E^{\boldsymbol{n}b}(\mu)\|_{\ell^\infty(ij)}}{\max\limits_{\mu\in\mathcal{D}_*} \|B^{\boldsymbol{n}}(\mu)\|_{\ell^\infty(ij)}}, \tag{3.61a}$$

$$e^{\boldsymbol{\tau}b}_{\mathtt{EIM}}(J^{\boldsymbol{\tau}b}) := \frac{\max\limits_{\mu\in\mathcal{D}_*} \|B^{\boldsymbol{\tau}}(\mu) - E^{\boldsymbol{\tau}b}(\mu)\|_{\ell^\infty(ij)}}{\max\limits_{\mu\in\mathcal{D}_*} \|B^{\boldsymbol{\tau}}(\mu)\|_{\ell^\infty(ij)}}, \tag{3.61b}$$

where for a generic matrix $M \in \mathbb{R}^{\mathcal{N}^{\mathrm{HF}}\times\mathcal{R}^{\mathrm{HF}}}$,

$$\|M\|_{\ell^\infty(ij)} := \max_{(i,j)\in\{1:\mathcal{N}^{\mathrm{HF}}\}\times\{1:\mathcal{R}^{\mathrm{HF}}\}} |M_{ij}|, \tag{3.62}$$

and with $\mathcal{D}_*$ either equal to $\mathcal{D}_{\mathtt{train}}$ or to $\mathcal{D}_{\mathtt{valid}}$. We consider two different training sets to build the EIM approximation, the first with cardinality 61 and the second with cardinality 150. Considering the first training set (the left column in Figure 3.6), we observe that both errors decrease fast enough to allow accurate approximations even if we observe a stagnation of the error at around 10^{-3} after a few iterations. This reflects the fact that the dependencies on μ and on the indices of the matrices $B^{\boldsymbol{n}}(\mu)$ and $B^{\boldsymbol{\tau}}(\mu)$ are particularly hard to separate. Moreover, we observe almost the same behaviour for the error on both matrices. This can be explained by the fact that both matrices exhibit the a similar μ-dependence since the same finite element is used for the normal and tangential components of the Lagrange multiplier. We also observe that we obtain errors on the validation set that are close to, and slightly higher than, those obtained on the training set. This confirms that the approximation obtained with the EIM is of good quality globally over the whole parametric domain. Considering the second training set to build the EIM approximation (the right column in Figure (3.6)), we observe that for the first 60 iterations of the EIM, the errors on $B^{\boldsymbol{n}}(\mu)$ and $B^{\boldsymbol{\tau}}(\mu)$ have a behaviour similar to the ones observed for the first training set. Afterwards, theses errors further decrease down to 10^{-5}. As for the first training set, the errors on the validation set are close to, and slightly higher than those on the training set. Altogether, comparing the left and right columns in Figure (3.6), we can see that even

if we take a training set at least twice as rich, we do not gain much in terms of accuracy on the EIM approximation. This confirms the difficulty to separate the dependence on μ from the dependence on the indices of the matrices $B^{\boldsymbol{n}}(\mu)$ and $B^{\boldsymbol{\tau}}(\mu)$.

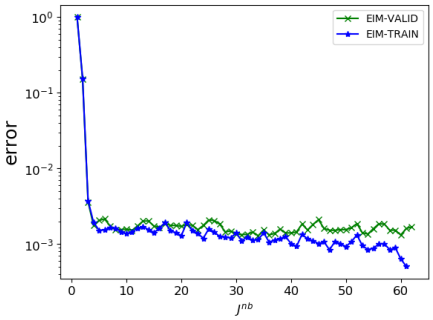

(a) $e^{\boldsymbol{nb}}_{\mathtt{EIM}}(J^{\boldsymbol{nb}})$, $|\mathcal{D}_{\mathtt{train}}| = 61$.

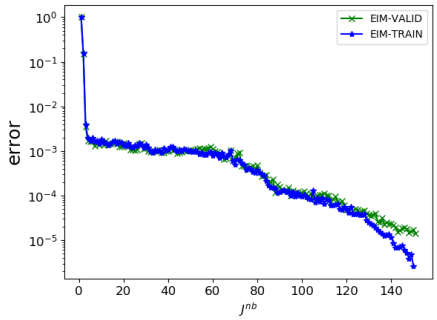

(b) $e^{\boldsymbol{nb}}_{\mathtt{EIM}}(J^{\boldsymbol{nb}})$, $|\mathcal{D}_{\mathtt{train}}| = 150$.

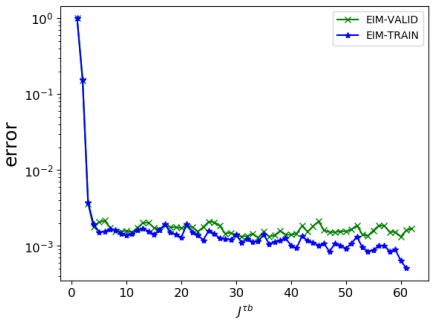

(c) $e^{\boldsymbol{\tau b}}_{\mathtt{EIM}}(J^{\boldsymbol{\tau b}})$, $|\mathcal{D}_{\mathtt{train}}| = 61$.

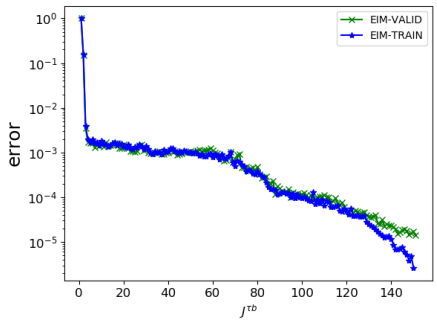

(d) $e^{\boldsymbol{\tau b}}_{\mathtt{EIM}}(J^{\boldsymbol{\tau b}})$, $|\mathcal{D}_{\mathtt{train}}| = 150$.

Figure 3.6 – Hertz test case: EIM ℓ^∞-error as a function of the rank $J^{\boldsymbol{nb}}$ or $J^{\boldsymbol{\tau b}}$ of the approximation. Row 1: $e^{\boldsymbol{nb}}_{\mathtt{EIM}}(J^{\boldsymbol{nb}})$. Row2: $e^{\boldsymbol{\tau b}}_{\mathtt{EIM}}(J^{\boldsymbol{\tau b}})$. Column 1: $|\mathcal{D}_{\mathtt{train}}| = 61$. Column 2: $|\mathcal{D}_{\mathtt{train}}| = 150$.

For the selection of the collocation nodes, the GCNS algorithm stops at $q = 20$ iterations with an error $e_{\mathtt{GCNS}}(q) := 0.39$. At this iteration, the algorithm has selected 40 collocation nodes over the 101 used by the HF model. Note that in this case, the number of selected nodes is the double of the iteration number. Indeed, owing to the symmetry, at each iteration, the GCNS algorithm chooses at least 2 collocation nodes, and no more than two nodes are selected at each iteration of the GCNS algorithm. Figure 3.7 shows the actual location of the reference collocation nodes selected on the reference potential contact manifold $\widehat{\Gamma}_1^{\mathrm{c}}$. For the sake of clarity, we only display the nodes on the right quarter-disk. To quantify the satisfaction of the tangential constraints at the iteration q of the GCNS algorithm, we introduce the error measure

$$e^{\boldsymbol{n\tau}}_{\mathtt{GCNS}}(q) := \max_{\mu\in\mathcal{D}_{\mathtt{train}}} \left\| \left[\|\boldsymbol{\lambda}^{\boldsymbol{\tau},q}_{S,\mathrm{cv}}(\mu)\| - \nu_{\mathcal{F}} \lambda^{\boldsymbol{n},q}_{R,\mathrm{cv}}(\mu) \right]_+ \right\|_{\ell^\infty(\mathcal{C}^{\mathrm{HF}}(\mu))}. \tag{3.63}$$

Figure 3.8 shows the evolution of the errors $e_{\mathtt{GCNS}}(q)$ (see Algo. 3) (left panel) and $e^{\boldsymbol{n\tau}}_{\mathtt{GCNS}}(q)$ (right panel) as a function of the number of iterations of the GCNS algorithm. The stopping criterion is not applied to observe the complete behaviour of the algorithm over all the collocation nodes. Thus, the GCNS algorithm only stops when $S_q = \mathcal{S}_0^{\mathrm{HF}}$.

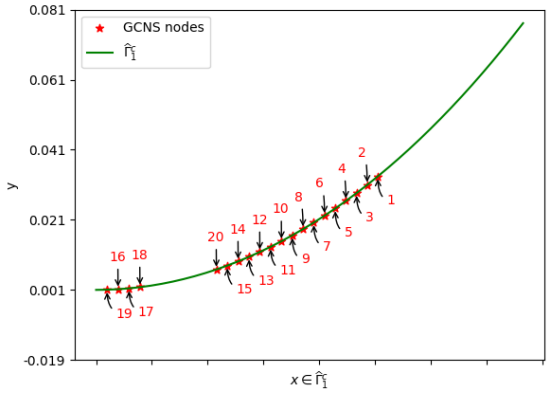

Figure 3.7 – Hertz test case: Selected collocation nodes.

We can see that the algorithm stops after 23 iterations. Specifically, at iteration 23, the algorithm chooses all the remaining collocation nodes. This means that the same error on the tangential constraints is reached at all the collocation nodes which have not yet been chosen. Moreover, we observe a clear decrease of the error $e_{\texttt{GCNS}}(q)$, until iteration 20 and then an increase of the error. This is consistent with the algorithm stopping at 20 iterations when using the stopping criterion on the error decrease. For the error $e^{n\tau}_{\texttt{GCNS}}(q)$, we observe a slow decrease before suddenly dropping to 10^{-6} at iteration 20, and then the error continues dropping until it reaches almost zero (10^{-13}) at iteration 23 when all the collocation nodes have been selected. Thus, we can see that the tangential constraints are respected with a satisfactory accuracy. Figure 3.9 displays the RB

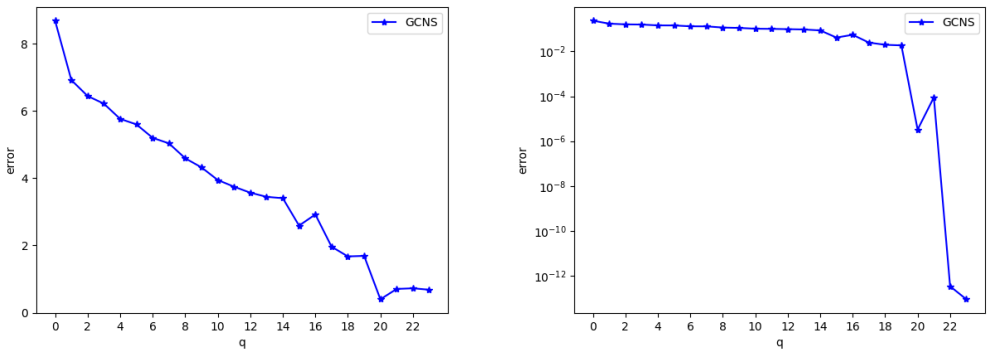

Figure 3.8 – Hertz test case: Selection of the collocation nodes. Left: $e_{\texttt{GCNS}}(q)$ defined in Algo. 3; Right: $e^{n\tau}_{\texttt{GCNS}}(q)$ defined in (3.63).

tangential Lagrange multiplier $\boldsymbol{\lambda}^{\tau,q}_{S,\mathrm{cv}}(\mu)$ superposed with the HF tangential Lagrange multiplier $\boldsymbol{\lambda}^{\tau}_{\mathrm{cv}}(\mu)$ as a function of the abscissa along $\Gamma^c(\mu)$ for $\mu = 0.7$m (Column 1), $\mu = 1$m (Column 2), and $\mu = 1.3$m (Column 3). We notice on the one hand that the effective contact area is exactly determined by the RB model, and on the other hand that the approximation is globally of satisfactory quality.

Table 3.1 provides a comparison of the computational cost in seconds between the HF model and the RB model. We can see that the RB model built with the proposed

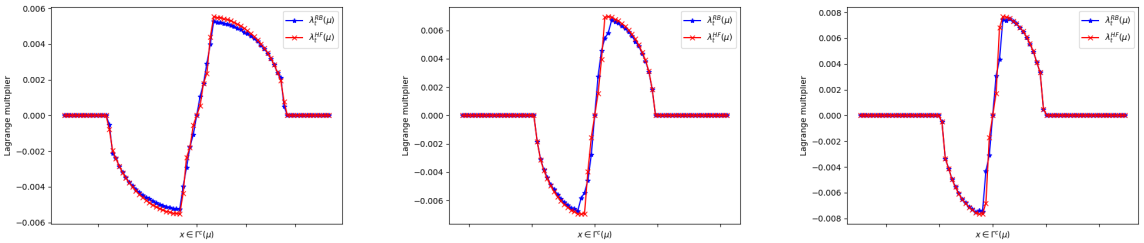

Figure 3.9 – Hertz test case: RB and HF tangential Lagrange multipliers. Column 1: $\mu = 0.7$m. Column 2: $\mu = 1$m. Column 3: $\mu = 1.3$m.

procedure is about 13 times faster than the HF model. Generally, this gap increases very significantly with the number of degrees of freedom. This makes the proposed procedure very relevant for high-dimensional test cases.

(N, R, S)	$(30, 20, 20)$
HF time(s)	450
RB time(s)	35

Table 3.1 – Hertz test case: Comparison of the computational cost between the HF model and the RB model.

CHAPTER 4

A REDUCED BASIS METHOD FOR CONTACT PROBLEMS FORMULATED WITH NITSCHE'S METHOD

Abstract

We develop an efficient reduced basis method for the contact problem with friction formulated with Nitsche's method under the small deformation assumption. The key idea ensuring the computational efficiency of the method is to treat the nonlinearity resulting from the contact conditions by means of the Empirical Interpolation Method. The proposed method is applied to the Hertz contact problem between two half-disks with parameter-dependent radius. We also highlight the benefits of the present approach with respect to the mixed (primal-dual) formulation.

Contents

4.1 Introduction

The reduced basis method (RBM) is a model reduction method. The goal is to reduce the complexity of a parametrized model problem in computational studies where the parameters vary. The idea is to replace the high fidelity (HF) space supposed to be of very large dimension by a small-dimensional subspace called reduced space by sampling the HF model. This allows one to organize the calculations in two phases. The first phase, called offline, is the construction phase of the reduced model. For this purpose, one considers a sample of the parameter space (assumed to be sufficiently representative) for which expensive calculations are performed by solving the HF problem for each parameter of the sample. The results of these calculations are then used to construct a small-dimensional subspace of the HF space, and the reduced model is built by replacing the HF space by the reduced subspace. The second phase, called online, is a phase in which a large number of new values of the parameter are considered, for which accurate approximations of the HF solution are calculated by using the reduced model. The online phase is where substantial computational gains are achieved.

In this work, we are interested in the application of the RBM to the contact problem formulated with Nitsche's method. The problem of mechanical contact [62, 104] with or without friction is present in many structural problems encountered in several industrial fields. The variational formulation of this problem leads to a variational inequality of the first or second kind depending on whether there is friction or not [41, 35]. There are different approaches to solve these variational inequalities. We can mention mixed (primal-dual) methods [44, 64, 6] where Lagrange multipliers are introduced to enforce the contact and friction conditions. In this case, the problem to be solved is a saddle-point problem where one seeks a primal unknown (the displacement) and a dual unknown (the contact forces). One of the difficulties with these methods is that they require the contact operator to satisfy an inf-sup condition. In the literature, there is already some work on model reduction for the frictionless contact problem in the framework of a mixed formulation. For example, [55] derives model reduction methods in the general framework of variational inequalities including the unilateral contact problem. In [8], a projection-based method is proposed to reduce the contact problem under small deformations. In [40], an application of the hyper-reduction technique is presented for the contact problem under small deformations. We also mention [12] where a new dual basis construction is proposed for the RBM applied to the unilateral contact problem under large deformations. Finally, the recent work [84] proposes a stable and efficient model reduction method for the unilateral contact problem.

In contrast to the mixed formulation approach, there are other methods to approximate the mechanical contact problem which are purely primal, *i.e.*, they do not require the introduction of additional unknowns. These methods have the advantage of leading to unconstrained minimization problems (thus easier to solve) but do not guarantee that the contact and friction conditions are strictly satisfied. One example are penalty methods [99]. Here, we focus on another primal approach based on Nitsche's method [85]. This method was originally introduced for the reformulation of Dirichlet boundary conditions and extended in [27] to the frictionless contact problem in the framework of the finite element method. The main characteristic of Nitsche's method is that it is consistent, in contrast to classical penalty methods. In the last few

years, many contributions have been made to this approach. For example, in [24], the method is extended to the case of contact with Tresca's friction; in [29], symmetric and nonsymmetric variants are presented; in [77], an extension to Coulomb's friction and large deformations is discussed; in [25], a nonconforming high-order discretization is considered; in [28], existence results for the contact problem with Coulomb friction are given in the context of static and dynamic finite element formulations. A state of the art on recent advances on Nitsche's method can be found in [26]. To the best of our knowledge, there is no previous work on model reduction for the contact problem formulated with Nitsche's method.

In this paper, we propose to fill this gap. The main challenge is that the classical RBM leads to an inefficient reduced model owing to the nonlinearity of Nitsche's formulation (even with small deformations). To overcome this problem, we propose a combination of the RBM with the Empirical Interpolation Method (EIM) [10, 75]. The realization of this idea is by no means straightforward since one needs to consider at the same time the parameter value and the iteration counter in the nonlinear iterative solver. The second important point addressed in this work is the comparison of the present approach with the inf-sup stable mixed formulation in terms of accuracy and efficiency. The two key advantages offered by Nitsche's method are the handling of unconstrained minimization problems and a higher effectiveness of the RBM since it is well-known that the dual basis is particularly hard to compress.

The rest of this paper is organized as follows. In Section 4.2, we briefly recall the unilateral contact problem with friction and its variational formulation under the assumption of small deformations. In Section 4.3, we derive the formulation of this problem using Nitsche's method in a form suitable to the RBM. In Section 4.4, we present our main result, namely the procedure for building the reduced model with Nitsche's method using the RBM and the EIM. In Section 4.5, we provide numerical results showcasing the efficiency and the robustness of the proposed procedure and comparing it to the mixed formulation. We consider as test case the Hertz contact problem between two half-disks with parameter-dependent radius.

4.2 Model problems

Let $\mathcal{D} \subset \mathbb{R}^m, m \in \mathbb{N}^* := \mathbb{N} \setminus \{0\}$, be the parameter domain. For all $\mu \in \mathcal{D}$, we consider an elastic body whose reference configuration is the domain $\Omega(\mu) \subset \mathbb{R}^d$, with $d \in \{2, 3\}$. The boundary $\Gamma(\mu) := \partial\Omega(\mu)$ is partitioned as $\Gamma(\mu) = \Gamma^{\mathrm{D}}(\mu) \cup \Gamma^{\mathrm{N}}(\mu) \cup \Gamma^{\mathrm{c}}(\mu)$. The body is clamped at the boundary $\Gamma^{\mathrm{D}}(\mu)$, free of traction at the boundary $\Gamma^{\mathrm{N}}(\mu)$, and $\Gamma^{\mathrm{c}}(\mu)$ denotes the potential contact boundary with a given rigid support. We denote by $\boldsymbol{n}(\mu)$ the unit outward normal on $\Gamma(\mu)$ and by $\boldsymbol{\tau}(\mu) := \left[\boldsymbol{\tau}_1(\mu) \cdots \boldsymbol{\tau}_{d-1}(\mu)\right] \in \mathbb{R}^{d\times(d-1)}$ an orthonormal basis of the hyperplane orthogonal to $\boldsymbol{n}(\mu)$ in $\mathbb{R}^d$. For simplicity, we just write $\boldsymbol{n}$ and $\boldsymbol{\tau}$ whenever there is no ambiguity. The body in its reference configuration is located at some distance from a rigid support and we denote by $g(\mu) \in L^2(\Gamma^{\mathrm{c}}(\mu); \mathbb{R}_+)$ the corresponding gap function. An external load $\boldsymbol{\ell}(\mu) : \Omega(\mu) \to \mathbb{R}^d$ is applied to the body, and we assume to be in the case of small deformations. For a generic $\mathbb{R}^d$-valued displacement field $\boldsymbol{v}$, the $\mathbb{R}^{d\times d}$-valued linearized strain tensor $\varepsilon(\boldsymbol{v})$ and the $\mathbb{R}^{d\times d}$-valued

stress tensor $\sigma(\boldsymbol{v})$ are given by

$$\varepsilon(\boldsymbol{v}) := \frac{1}{2}\Big(\nabla \boldsymbol{v} + \nabla \boldsymbol{v}^{\top}\Big), \quad \sigma(\boldsymbol{v}) := \mathbb{C}\varepsilon(\boldsymbol{v}), \tag{4.1}$$

with $\mathbb{C}$ the elastic coefficient tensor. At the boundary, we decompose the displacement field, $\boldsymbol{v}$, and the normal component of the stress tensor, $\sigma(\boldsymbol{v})\boldsymbol{n}$, in normal and tangential components as follows:

$$\boldsymbol{v} = v_{\boldsymbol{n}}\boldsymbol{n} + \boldsymbol{\tau}\boldsymbol{v}_{\boldsymbol{\tau}}, \quad \sigma(\boldsymbol{v})\boldsymbol{n} = \sigma_{\boldsymbol{nn}}(\boldsymbol{v})\boldsymbol{n} + \boldsymbol{\tau}\boldsymbol{\sigma}_{\boldsymbol{n\tau}}(\boldsymbol{v}), \tag{4.2}$$

with $v_{\boldsymbol{n}} \in \mathbb{R}$, $\boldsymbol{v}_{\boldsymbol{\tau}} \in \mathbb{R}^{d-1}$, $\sigma_{\boldsymbol{nn}}(\boldsymbol{v}) \in \mathbb{R}$ and $\boldsymbol{\sigma}_{\boldsymbol{n\tau}}(\boldsymbol{v}) \in \mathbb{R}^{d-1}$.

The frictionless contact problem (also called Signorini problem) consists in finding the displacement field $\boldsymbol{u}(\mu) : \Omega(\mu) \to \mathbb{R}^d$ satisfying, for all $\mu \in \mathcal{D}$,

$$-\mathrm{div}(\sigma(\boldsymbol{u}(\mu))) = \boldsymbol{\ell}(\mu), \quad \text{in } \Omega(\mu), \tag{4.3a}$$
$$\boldsymbol{u}(\mu) = \boldsymbol{0}, \quad \text{on } \Gamma^{\mathrm{D}}(\mu), \tag{4.3b}$$
$$\sigma(\boldsymbol{u}(\mu))\boldsymbol{n} = \boldsymbol{0}, \quad \text{on } \Gamma^{\mathrm{N}}(\mu), \tag{4.3c}$$
$$u_{\boldsymbol{n}}(\mu) \le g(\mu),\ \sigma_{\boldsymbol{nn}}(\boldsymbol{u}(\mu)) \le 0,\ \sigma_{\boldsymbol{nn}}(\boldsymbol{u}(\mu))(u_{\boldsymbol{n}}(\mu) - g(\mu)) = 0, \quad \text{on } \Gamma^{\mathrm{c}}(\mu), \tag{4.3d}$$
$$\boldsymbol{\sigma}_{\boldsymbol{n\tau}}(\boldsymbol{u}(\mu)) = \boldsymbol{0}, \quad \text{on } \Gamma^{\mathrm{c}}(\mu). \tag{4.3e}$$

In the case of contact problems with friction, the condition (4.3e) on $\Gamma^{\mathrm{c}}(\mu)$ has to be replaced by a condition depending on the considered friction law [64, 77]:

- Tresca conditions:

$$\begin{cases} \|\boldsymbol{\sigma}_{\boldsymbol{n\tau}}(\boldsymbol{u}(\mu))\| \le s, & \text{if } \boldsymbol{u}_{\boldsymbol{\tau}}(\mu) = \boldsymbol{0}, \\ \boldsymbol{\sigma}_{\boldsymbol{n\tau}}(\boldsymbol{u}(\mu)) = -s\dfrac{\boldsymbol{u}_{\boldsymbol{\tau}}(\mu)}{\|\boldsymbol{u}_{\boldsymbol{\tau}}(\mu)\|}, & \text{otherwise}, \end{cases} \tag{4.4}$$

  where $\|\cdot\|$ denotes the Euclidean norm in $\mathbb{R}^{d-1}$ and $s > 0$ is a given threshold, taken to be constant for simplicity (units in Pa).

- Coulomb conditions:

$$\begin{cases} \|\boldsymbol{\sigma}_{\boldsymbol{n\tau}}(\boldsymbol{u}(\mu))\| \le \nu_{\mathcal{F}}|\sigma_{\boldsymbol{nn}}(\boldsymbol{u}(\mu))|, & \text{if } \boldsymbol{u}_{\boldsymbol{\tau}}(\mu) = \boldsymbol{0}, \\ \boldsymbol{\sigma}_{\boldsymbol{n\tau}}(\boldsymbol{u}(\mu)) = -\nu_{\mathcal{F}}|\sigma_{\boldsymbol{nn}}(\boldsymbol{u}(\mu))|\dfrac{\boldsymbol{u}_{\boldsymbol{\tau}}(\mu)}{\|\boldsymbol{u}_{\boldsymbol{\tau}}(\mu)\|}, & \text{otherwise}, \end{cases} \tag{4.5}$$

  where $\nu_{\mathcal{F}} > 0$ is a given nondimensional coefficient, taken to be constant for simplicity.

The model problem consisting of equations (4.3a)-(4.3b)-(4.3c)-(4.3d) and (4.4) (resp. (4.5)) is called Tresca (resp. Coulomb) frictional contact problem.

We introduce the finite-dimensional space $\boldsymbol{\mathcal{V}}(\mu)$ and the admissible set $\boldsymbol{\mathcal{K}}(\mu)$ such that

$$\boldsymbol{\mathcal{V}}(\mu) \subset \Big\{\boldsymbol{v} \in H^1(\Omega(\mu); \mathbb{R}^d) \mid \boldsymbol{v} = \boldsymbol{0} \text{ on } \Gamma^{\mathrm{D}}(\mu)\Big\}, \tag{4.6a}$$
$$\boldsymbol{\mathcal{K}}(\mu) := \Big\{\boldsymbol{v} \in \boldsymbol{\mathcal{V}}(\mu) \mid v_{\boldsymbol{n}} \le g(\mu) \text{ on } \Gamma^{\mathrm{c}}(\mu)\Big\}. \tag{4.6b}$$

We notice that $\boldsymbol{\mathcal{K}}(\mu)$ is a non-empty convex set. The space $\boldsymbol{\mathcal{V}}(\mu)$ is typically built using finite elements on a fine mesh of $\Omega(\mu)$. The bilinear form $a(\mu;\cdot,\cdot) : \boldsymbol{\mathcal{V}}(\mu) \times \boldsymbol{\mathcal{V}}(\mu) \to \mathbb{R}$ associated with the equilibrium equation (4.3a) in $\Omega(\mu)$ is defined as

$$a(\mu;\boldsymbol{u},\boldsymbol{v}) := \int_{\Omega(\mu)} \sigma(\boldsymbol{u}) : \varepsilon(\boldsymbol{v})\, d\Omega(\mu), \tag{4.7}$$

and the linear form $f(\mu;\cdot) : \boldsymbol{\mathcal{V}}(\mu) \to \mathbb{R}$ associated with the external load $\boldsymbol{\ell}(\mu)$ as

$$f(\mu;\boldsymbol{v}) := \int_{\Omega(\mu)} \boldsymbol{\ell}(\mu) \cdot \boldsymbol{v}\, d\Omega(\mu). \tag{4.8}$$

The weak formulation of the Signorini contact problem (4.3) consists of solving the following variational inequality of the first kind: For all $\mu \in \mathcal{D}$, find $\boldsymbol{u}(\mu) \in \boldsymbol{\mathcal{K}}(\mu)$ such that

$$a(\mu;\boldsymbol{u}(\mu),\boldsymbol{v}-\boldsymbol{u}(\mu)) \geq f(\mu;\boldsymbol{v}-\boldsymbol{u}(\mu)), \quad \forall \boldsymbol{v} \in \boldsymbol{\mathcal{K}}(\mu). \tag{4.9}$$

For all $\mu \in \mathcal{D}$, Stampacchia's theorem [100] ensures that there is a unique solution to (4.9) which is also the unique solution to the following constrained minimization problem: Find $\boldsymbol{u}(\mu) \in \boldsymbol{\mathcal{K}}(\mu)$ such that

$$\boldsymbol{u}(\mu) = \underset{\boldsymbol{v}\in\boldsymbol{\mathcal{K}}(\mu)}{\operatorname{argmin}}\ \mathcal{J}(\mu;\boldsymbol{v}), \tag{4.10}$$

where the energy functional $\mathcal{J}(\mu;\cdot) : \boldsymbol{\mathcal{V}}(\mu) \to \mathbb{R}$ is defined as follows:

$$\mathcal{J}(\mu;\boldsymbol{v}) := \frac{1}{2} a(\mu;\boldsymbol{v},\boldsymbol{v}) - f(\mu;\boldsymbol{v}). \tag{4.11}$$

In the case of the Tresca or Coulomb frictional contact problem, we need to consider the friction functional $\mathcal{F}$ defined as follows:

$$\mathcal{F}(\mu;\boldsymbol{w},\boldsymbol{v}) := \begin{cases} \int_{\Gamma^c(\mu)} -s\|\boldsymbol{v}_{\boldsymbol{\tau}}\|\, d\Gamma(\mu), & \text{(Tresca friction)}, \\ \int_{\Gamma^c(\mu)} -\nu_{\mathcal{F}}|\sigma_{\boldsymbol{nn}}(\boldsymbol{w})|\|\boldsymbol{v}_{\boldsymbol{\tau}}\|\, d\Gamma(\mu), & \text{(Coulomb friction)}. \end{cases} \tag{4.12}$$

This leads to the following variational inequality: For all $\mu \in \mathcal{D}$, find $\boldsymbol{u}(\mu) \in \boldsymbol{\mathcal{K}}(\mu)$ such that

$$a(\mu;\boldsymbol{u}(\mu),\boldsymbol{v}-\boldsymbol{u}(\mu)) + \mathcal{F}(\mu;\boldsymbol{u}(\mu),\boldsymbol{v}) - \mathcal{F}(\mu;\boldsymbol{u}(u),\boldsymbol{u}(\mu)) \geq f(\mu;\boldsymbol{v}-\boldsymbol{u}(\mu)), \quad \forall \boldsymbol{v} \in \boldsymbol{\mathcal{K}}(\mu). \tag{4.13}$$

4.3 Nitsche's method

The main idea in the original Nitsche method [85] is the enforcement of Dirichlet boundary conditions by means of a consistent penalty method. As shown in [27, 29, 26], it is possible to generalize this idea to frictional contact problems. The main advantage of Nitsche's method is that the problem to be solved is unconstrained. Hence, in contrast to the mixed formulation, one does not need any additional unknowns such as Lagrange multipliers. Moreover, a higher effectivity of the RBM is expected since it is

well-known that the dual basis is particularly hard to compress. The price to be paid, though, is that the constraint is not exactly enforced.

To derive Nitsche's method, we are going to assume that all the considered functions are smooth enough so that the associated normal stress tensor can be defined pointwise at the boundary. Recall that, for all $\mu \in \mathcal{D}$, the HF finite-dimensional space $\boldsymbol{\mathcal{V}}(\mu)$ in (4.6a) results from the finite element discretization of the Hilbert space $H^1(\Omega(\mu);\mathbb{R}^d)$. Hence, the above assumption is indeed met.

4.3.1 Frictionless case

Following [31], the starting observation is that the Signorini conditions (4.3d) can be equivalently reformulated as follows:

$$\sigma_{\boldsymbol{nn}}(\boldsymbol{u}(\mu)) = \Big[\sigma_{\boldsymbol{nn}}(\boldsymbol{u}(\mu)) - \gamma\Big(u_{\boldsymbol{n}}(\mu) - g(\mu)\Big)\Big]_-, \tag{4.14}$$

where $\big[z\big]_- := \min\big(z,0\big)$ denotes the negative part of a generic real number z and where $\gamma > 0$ is a user-defined parameter (taken to be constant for simplicity). In practice, the parameter γ should be chosen large enough (see Section 4.5 for further discussion).

For all $\mu \in \mathcal{D}$, one introduces the energy functional $J^{\text{Nitsche}}(\mu;\cdot) : \boldsymbol{\mathcal{V}}(\mu) \to \mathbb{R}$ such that

$$\begin{aligned} J^{\text{Nitsche}}(\mu;\boldsymbol{v}) := \mathcal{J}(\mu;\boldsymbol{v}) &- \frac{1}{2}\int_{\Gamma^{\text{c}}(\mu)} \frac{1}{\gamma}|\sigma_{\boldsymbol{nn}}(\boldsymbol{v})|^2 d\Gamma(\mu) \\ &+ \frac{1}{2}\int_{\Gamma^{\text{c}}(\mu)} \frac{1}{\gamma}\Big[\sigma_{\boldsymbol{nn}}(\boldsymbol{v}) - \gamma\Big(v_{\boldsymbol{n}} - g(\mu)\Big)\Big]_-^2 d\Gamma(\mu), \end{aligned} \tag{4.15}$$

recalling that the energy functional $\mathcal{J}$ is defined in (4.11). Nitsche's method consists in finding $\boldsymbol{u}(\mu) \in \boldsymbol{\mathcal{V}}(\mu)$ solution to the following unconstrained minimization problem: Find $\boldsymbol{u}(\mu) \in \boldsymbol{\mathcal{V}}(\mu)$ such that

$$\boldsymbol{u}(\mu) = \underset{\boldsymbol{v}\in\boldsymbol{\mathcal{V}}(\mu)}{\operatorname{argmin}}\ J^{\text{Nitsche}}(\mu;\boldsymbol{v}). \tag{4.16}$$

The first-order optimality condition associated with (4.16) reads

$$a_\gamma^{\boldsymbol{n}}(\mu;\boldsymbol{u}(\mu),\boldsymbol{v}) + \int_{\Gamma^{\text{c}}(\mu)} \frac{1}{\gamma}\Big[P_{\gamma,g}^{\boldsymbol{n}}(\mu;\boldsymbol{u}(\mu))\Big]_- P_{\gamma,0}^{\boldsymbol{n}}(\mu;\boldsymbol{v})\, d\Gamma(\mu) = f(\mu;\boldsymbol{v}), \quad \forall \boldsymbol{v} \in \boldsymbol{\mathcal{V}}(\mu), \tag{4.17}$$

with the bilinear form $a_\gamma^{\boldsymbol{n}}(\mu;\cdot,\cdot) : \boldsymbol{\mathcal{V}}(\mu)\times\boldsymbol{\mathcal{V}}(\mu) \to \mathbb{R}$ defined as

$$a_\gamma^{\boldsymbol{n}}(\mu;\boldsymbol{u},\boldsymbol{v}) := a(\mu;\boldsymbol{u},\boldsymbol{v}) - \int_{\Gamma^{\text{c}}(\mu)} \frac{1}{\gamma}\sigma_{\boldsymbol{nn}}(\boldsymbol{u})\sigma_{\boldsymbol{nn}}(\boldsymbol{v})\, d\Gamma(\mu), \quad \forall \boldsymbol{u},\boldsymbol{v} \in \boldsymbol{\mathcal{V}}(\mu), \tag{4.18}$$

and the operators $P_{\gamma,g}^{\boldsymbol{n}}(\mu;\cdot)$, $P_{\gamma,0}^{\boldsymbol{n}}(\mu;\cdot) : \boldsymbol{\mathcal{V}}(\mu) \to L^2(\Gamma^{\text{c}}(\mu))$ defined as

$$P_{\gamma,g}^{\boldsymbol{n}}(\mu;\boldsymbol{v}) := \sigma_{\boldsymbol{nn}}(\boldsymbol{v}) - \gamma(v_{\boldsymbol{n}} - g(\mu)), \tag{4.19a}$$

$$P_{\gamma,0}^{\boldsymbol{n}}(\mu;\boldsymbol{v}) := \sigma_{\boldsymbol{nn}}(\boldsymbol{v}) - \gamma v_{\boldsymbol{n}}. \tag{4.19b}$$

With this notation, we can rewrite the energy functional $J^{\text{Nitsche}}(\mu;\cdot)$ as

$$J^{\text{Nitsche}}(\mu;\boldsymbol{v}) := \mathcal{J}(\mu;\boldsymbol{v}) - \frac{1}{2}\int_{\Gamma^{\text{c}}(\mu)} \frac{1}{\gamma}|\sigma_{\boldsymbol{nn}}(\boldsymbol{v})|^2 d\Gamma(\mu) + \frac{1}{2}\int_{\Gamma^{\text{c}}(\mu)} \frac{1}{\gamma}\Big[P_{\gamma,g}^{\boldsymbol{n}}(\boldsymbol{v})\Big]_-^2 d\Gamma(\mu). \tag{4.20}$$

The problem (4.17) is nonlinear. To solve it, we use an iterative method. Given $\boldsymbol{u}_0(\mu) \in \boldsymbol{\mathcal{V}}(\mu)$ and a tolerance $\delta_{\boldsymbol{u}} \in \mathbb{R}_+$, we look, for all $k \geq 0$, for the solution $\boldsymbol{u}_{k+1}(\mu)$ in the form $\boldsymbol{u}_{k+1}(\mu) = \boldsymbol{u}_k(\mu) + \boldsymbol{\delta u}_k(\mu)$. Ideally, we seek $\boldsymbol{\delta u}_k(\mu) \in \boldsymbol{\mathcal{V}}(\mu)$ such that

$$\begin{cases} a_\gamma^{\boldsymbol{n}}(\mu; \boldsymbol{u}_k(\mu) + \boldsymbol{\delta u}_k(\mu), \boldsymbol{v}) \\ + \displaystyle\int_{\Gamma^{\mathrm{c}}(\mu)} \frac{1}{\gamma} \Big[P_{\gamma,g}^{\boldsymbol{n}}(\mu; \boldsymbol{u}_k(\mu) + \boldsymbol{\delta u}_k(\mu)) \Big]_- P_{\gamma,0}^{\boldsymbol{n}}(\mu; \boldsymbol{v}) \, d\Gamma(\mu) = f(\mu; \boldsymbol{v}), \quad \forall \boldsymbol{v} \in \boldsymbol{\mathcal{V}}(\mu). \end{cases} \tag{4.21}$$

However, since the problem (4.21) is nonlinear, it is expensive to solve it directly. Therefore, we approximate the solution $\boldsymbol{\delta u}_k(\mu)$ by linearizing the problem. In order to do this, we observe that $P_{\gamma,g}^{\boldsymbol{n}}(\mu; \boldsymbol{u}_k(\mu) + \boldsymbol{\delta u}_k(\mu)) = P_{\gamma,g}^{\boldsymbol{n}}(\mu; \boldsymbol{u}_k(\mu)) + P_{\gamma,0}^{\boldsymbol{n}}(\mu; \boldsymbol{\delta u}_k(\mu))$ and approximate the term $\Big[P_{\gamma,g}^{\boldsymbol{n}}(\mu; \boldsymbol{u}_k(\mu) + \boldsymbol{\delta u}_k(\mu)) \Big]_-$ as follows:

$$\Big[P_{\gamma,g}^{\boldsymbol{n}}(\mu; \boldsymbol{u}_k(\mu) + \boldsymbol{\delta u}_k(\mu)) \Big]_- \approx \Big[P_{\gamma,g}^{\boldsymbol{n}}(\mu; \boldsymbol{u}_k(\mu)) \Big]_- + H(-P_{\gamma,g}^{\boldsymbol{n}}(\mu; \boldsymbol{u}_k(\mu))) P_{\gamma,0}^{\boldsymbol{n}}(\mu; \boldsymbol{\delta u}_k(\mu)), \tag{4.22}$$

where $H(\cdot)$ denotes the Heaviside function. Using this approximation in (4.21) (for simplicity, we keep the same notation for the unknown $\boldsymbol{\delta u}_k(\mu)$), we consider the following sequence of problems: For all $k \geq 0$, find $\boldsymbol{\delta u}_k(\mu) \in \boldsymbol{\mathcal{V}}(\mu)$ such that

$$a_\gamma^{\boldsymbol{n}}(\mu; \boldsymbol{\delta u}_k(\mu), \boldsymbol{v}) + b_\gamma^{\boldsymbol{n}}(\mu; \boldsymbol{u}_k(\mu); \boldsymbol{\delta u}_k(\mu), \boldsymbol{v}) = -r_\gamma^{\boldsymbol{n}}(\mu; \boldsymbol{u}_k(\mu); \boldsymbol{v}), \quad \forall \boldsymbol{v} \in \boldsymbol{\mathcal{V}}(\mu), \tag{4.23}$$

where

$$b_\gamma^{\boldsymbol{n}}(\mu; \boldsymbol{w}; \boldsymbol{u}, \boldsymbol{v}) := \int_{\Gamma^{\mathrm{c}}(\mu)} \frac{1}{\gamma} H(-P_{\gamma,g}^{\boldsymbol{n}}(\mu; \boldsymbol{w})) P_{\gamma,0}^{\boldsymbol{n}}(\mu; \boldsymbol{u}) P_{\gamma,0}^{\boldsymbol{n}}(\mu; \boldsymbol{v}) \, d\Gamma(\mu), \tag{4.24a}$$

$$r_\gamma^{\boldsymbol{n}}(\mu; \boldsymbol{w}; \boldsymbol{v}) := a_\gamma^{\boldsymbol{n}}(\mu; \boldsymbol{w}, \boldsymbol{v}) + \theta_\gamma^{\boldsymbol{n}}(\mu; \boldsymbol{w}; \boldsymbol{v}) - f(\mu; \boldsymbol{v}), \tag{4.24b}$$

(4.24c)

with

$$\theta_\gamma^{\boldsymbol{n}}(\mu; \boldsymbol{w}, \boldsymbol{v}) := \int_{\Gamma^{\mathrm{c}}(\mu)} \frac{1}{\gamma} \Big[P_{\gamma,g}^{\boldsymbol{n}}(\mu; \boldsymbol{w}) \Big]_- P_{\gamma,0}^{\boldsymbol{n}}(\mu; \boldsymbol{v}) \, d\Gamma(\mu). \tag{4.25}$$

We iterate on k until the following convergence criterion is reached:

$$\frac{\|\boldsymbol{u}_{k+1}(\mu) - \boldsymbol{u}_k(\mu)\|_{\boldsymbol{\mathcal{V}}(\mu)}}{\|\boldsymbol{u}_{k+1}(\mu)\|_{\boldsymbol{\mathcal{V}}(\mu)}} \leq \delta_{\boldsymbol{u}}. \tag{4.26}$$

In what follows, we denote by $k^{\mathrm{cv}}(\mu) \in \mathbb{N}^*$ the number of iterations required to solve (4.23) for all $\mu \in \mathcal{D}$. We denote the converged solution to the sequence of problems (4.23) as $\boldsymbol{u}_{\mathrm{cv}}(\mu) \in \boldsymbol{\mathcal{V}}(\mu)$.

To introduce the algebraic formulation, we assume that for all $\mu \in \mathcal{D}$, the HF (finite-dimensional) space $\boldsymbol{\mathcal{V}}(\mu)$ is such that

$$\boldsymbol{\mathcal{V}}(\mu) := \boldsymbol{Span}\Big(\{\boldsymbol{\varphi}_n(\mu)\}_{n \in \{1:\mathcal{N}\}} \Big). \tag{4.27}$$

Notice that the dimension $\mathcal{N}^{\mathrm{HF}}$ of $\boldsymbol{\mathcal{V}}(\mu)$ is parameter-independent. We illustrate in Section 4.4.1 how to accomplish this property. Furthermore, we adopt the following

decompositions for the sequence of solutions to (4.23):

$$\boldsymbol{u}_k(\mu) := \sum_{n\in\{1:\mathcal{N}^{\mathrm{HF}}\}} \boldsymbol{u}_k^n(\mu)\boldsymbol{\varphi}_n(\mu), \qquad \boldsymbol{U}_k(\mu) := (\boldsymbol{u}_k^n(\mu))_{n\in\{1:\mathcal{N}^{\mathrm{HF}}\}} \in \mathbb{R}^{\mathcal{N}^{\mathrm{HF}}}, \tag{4.28a}$$

$$\boldsymbol{\delta u}_k(\mu) := \sum_{n\in\{1:\mathcal{N}^{\mathrm{HF}}\}} \boldsymbol{\delta u}_k^n(\mu)\boldsymbol{\varphi}_n(\mu), \quad \boldsymbol{\Delta U}_k(\mu) := (\boldsymbol{\delta u}_k^n(\mu))_{n\in\{1:\mathcal{N}^{\mathrm{HF}}\}} \in \mathbb{R}^{\mathcal{N}^{\mathrm{HF}}}. \tag{4.28b}$$

The algebraic formulation of the sequence of problems (4.23) then reads as follows: For all $k \geq 0$, find $\boldsymbol{\Delta U}_k(\mu) \in \mathbb{R}^{\mathcal{N}^{\mathrm{HF}}}$ such that

$$A_\gamma^{\boldsymbol{n}}(\mu)\boldsymbol{\Delta U}_k(\mu) + B_\gamma^{\boldsymbol{n}}(\mu, \boldsymbol{u}_k(\mu))\boldsymbol{\Delta U}_k(\mu) = -R_\gamma^{\boldsymbol{n}}(\mu, \boldsymbol{u}_k(\mu)), \tag{4.29}$$

where for all $n, m \in \{1:\mathcal{N}^{\mathrm{HF}}\}$,

$$(A_\gamma^{\boldsymbol{n}}(\mu))_{mn} := a_\gamma^{\boldsymbol{n}}(\mu; \varphi_n(\mu), \varphi_m(\mu)), \tag{4.30a}$$

$$(B_\gamma^{\boldsymbol{n}}(\mu, \boldsymbol{u}_k(\mu)))_{mn} := b_\gamma^{\boldsymbol{n}}(\mu; \boldsymbol{u}_k(\mu); \varphi_n(\mu), \varphi_m(\mu)), \tag{4.30b}$$

$$(R_\gamma^{\boldsymbol{n}}(\mu, \boldsymbol{u}_k(\mu)))_m := r_\gamma^{\boldsymbol{n}}(\mu; \boldsymbol{u}_k(\mu); \varphi_m(\mu)). \tag{4.30c}$$

The convergence criterion for (4.29) is still (4.26) using the reconstructed functions (see (4.28)). We denote the converged solution to the sequence of problems (4.29) as $\boldsymbol{U}_{\mathrm{cv}}(\mu) \in \mathbb{R}^{\mathcal{N}^{\mathrm{HF}}}$. Furthermore, let us denote by $\Theta_\gamma^{\boldsymbol{n}}(\mu, \boldsymbol{w})$ (resp. $F(\mu)$) the algebraic representation of the operator $\theta_\gamma^{\boldsymbol{n}}(\mu; \boldsymbol{w}; \cdot)$ (resp. $f(\mu; \cdot)$) such that for all $m \in \{1:\mathcal{N}^{\mathrm{HF}}\}$,

$$(\Theta_\gamma^{\boldsymbol{n}}(\mu, \boldsymbol{w}))_m := \theta_\gamma^{\boldsymbol{n}}(\mu; \boldsymbol{w}; \varphi_m(\mu)), \qquad (F(\mu))_m := f(\mu; \varphi_m(\mu)). \tag{4.31}$$

With this notation, we have the following decomposition:

$$R_\gamma^{\boldsymbol{n}}(\mu, \boldsymbol{u}_k(\mu)) := A_\gamma^{\boldsymbol{n}}(\mu)\boldsymbol{U}_k(\mu) + \Theta_\gamma^{\boldsymbol{n}}(\mu, \boldsymbol{u}_k(\mu)) - F(\mu). \tag{4.32}$$

4.3.2 Friction case

4.3.2.1 Tresca friction

Let us first consider the Tresca frictional contact problem. We use the following reformulation of the friction conditions given in [26]:

$$\boldsymbol{\sigma}_{\boldsymbol{n\tau}}(\boldsymbol{u}(\mu)) = \Big[\boldsymbol{\sigma}_{\boldsymbol{n\tau}}(\boldsymbol{u}(\mu)) - \gamma \boldsymbol{u}_{\boldsymbol{\tau}}(\mu)\Big]_s, \tag{4.33}$$

where, for a positive real number r, the notation

$$\Big[\boldsymbol{x}\Big]_r := \begin{cases} \boldsymbol{x}, & \text{if } \|\boldsymbol{x}\| \leq r, \\ r\frac{\boldsymbol{x}}{\|\boldsymbol{x}\|}, & \text{otherwise,} \end{cases} \tag{4.34}$$

defines the projection of $\boldsymbol{x} \in \mathbb{R}^{d-1}$ onto the ball centered at the origin and of radius r. Let us introduce the operator $P_\gamma^{\boldsymbol{\tau}}(\mu; \cdot) : \boldsymbol{\mathcal{V}}(\mu) \to L^2(\Gamma^{\mathrm{c}}(\mu); \mathbb{R}^{d-1})$ such that

$$P_\gamma^{\boldsymbol{\tau}}(\mu; \boldsymbol{v}) := \boldsymbol{\sigma}_{\boldsymbol{n\tau}}(\boldsymbol{v}) - \gamma \boldsymbol{v}_{\boldsymbol{\tau}}. \tag{4.35}$$

We start from the energy functional $J_{\mathcal{F}}^{\text{Nitsche}}(\mu;\cdot) : \boldsymbol{\mathcal{V}}(\mu) \to \mathbb{R}$ defined as

$$\begin{aligned} J_{\mathcal{F}}^{\text{Nitsche}}(\mu;\boldsymbol{v}) := J^{\text{Nitsche}}(\mu;\boldsymbol{v}) - \frac{1}{2}\int_{\Gamma^c(\mu)} \frac{1}{\gamma}\|\boldsymbol{\sigma}_{\boldsymbol{n\tau}}(\boldsymbol{v})\|^2 \, d\Gamma(\mu) \\ + \frac{1}{2}\int_{\Gamma^c(\mu)} \frac{1}{\gamma}\|P_\gamma^{\boldsymbol{\tau}}(\boldsymbol{v})\|^2 \, d\Gamma(\mu) - \frac{1}{2}\int_{\Gamma^c(\mu)} \frac{1}{\gamma}\|P_\gamma^{\boldsymbol{\tau}}(\boldsymbol{v}) - \Big[P_\gamma^{\boldsymbol{\tau}}(\boldsymbol{v})\Big]_s\|^2 \, d\Gamma(\mu). \end{aligned} \tag{4.36}$$

Nitsche's method consists in solving to the following unconstrained minimization problem: Find $\boldsymbol{u}(\mu) \in \boldsymbol{\mathcal{V}}(\mu)$ such that

$$\boldsymbol{u}(\mu) = \underset{\boldsymbol{v}\in\boldsymbol{\mathcal{V}}(\mu)}{\operatorname{argmin}} \; J_{\mathcal{F}}^{\text{Nitsche}}(\mu;\boldsymbol{v}). \tag{4.37}$$

Let us consider the functional $J : \mathbb{R}^{d-1} \to \mathbb{R}$ defined as follows:

$$J(\boldsymbol{x}) = \frac{1}{2}\|\boldsymbol{x} - \Big[\boldsymbol{x}\Big]_s\|^2. \tag{4.38}$$

One easily verifies that this functional is Gâteaux-differentiable and that its differential is given by $DJ(\boldsymbol{x}) = \boldsymbol{x} - \Big[\boldsymbol{x}\Big]_s$ for all $\boldsymbol{x} \in \mathbb{R}^{d-1}$. Therefore, using the same approach as for the frictionless contact problem, we obtain the following Nitsche's formulation for the Tresca frictional contact problem: Find $\boldsymbol{u}(\mu) \in \boldsymbol{\mathcal{V}}(\mu)$ such that

$$\begin{cases} a_\gamma^{\boldsymbol{n\tau}}(\mu;\boldsymbol{u}(\mu),\boldsymbol{v}) + \displaystyle\int_{\Gamma^c(\mu)} \frac{1}{\gamma}\Big[P_{\gamma,g}^{\boldsymbol{n}}(\mu;\boldsymbol{u}(\mu))\Big]_- P_{\gamma,0}^{\boldsymbol{n}}(\mu;\boldsymbol{v}) \, d\Gamma(\mu) \\ \quad + \displaystyle\int_{\Gamma^c(\mu)} \frac{1}{\gamma}\Big[P_\gamma^{\boldsymbol{\tau}}(\mu;\boldsymbol{u}(\mu))\Big]_s P_\gamma^{\boldsymbol{\tau}}(\mu;\boldsymbol{v}) \, d\Gamma(\mu) = f(\mu;\boldsymbol{v}), \quad \forall \boldsymbol{v} \in \boldsymbol{\mathcal{V}}(\mu), \end{cases} \tag{4.39}$$

where the bilinear form $a_\gamma^{\boldsymbol{n\tau}}(\mu;\cdot,\cdot) : \boldsymbol{\mathcal{V}}(\mu) \times \boldsymbol{\mathcal{V}}(\mu) \to \mathbb{R}$ is defined as

$$a_\gamma^{\boldsymbol{n\tau}}(\mu;\boldsymbol{u},\boldsymbol{v}) := a(\mu;\boldsymbol{u},\boldsymbol{v}) - \int_{\Gamma^c(\mu)} \frac{1}{\gamma}\sigma(\boldsymbol{u})\boldsymbol{n}\cdot\sigma(\boldsymbol{v})\boldsymbol{n} \, d\Gamma(\mu). \tag{4.40}$$

The linearization of the problem (4.39) leads to the following sequence of problems: For all $k \geq 0$, find $\boldsymbol{\delta u}_k(\mu) \in \boldsymbol{\mathcal{V}}(\mu)$ such that

$$a_\gamma^{\boldsymbol{n\tau}}(\mu;\boldsymbol{\delta u}_k(\mu),\boldsymbol{v}) + b_\gamma^{\boldsymbol{n\tau}}(\mu;\boldsymbol{u}_k(\mu);\boldsymbol{\delta u}_k(\mu),\boldsymbol{v}) = -r_\gamma^{\boldsymbol{n\tau}}(\mu;\boldsymbol{u}_k(\mu);\boldsymbol{v}), \quad \forall \boldsymbol{v} \in \boldsymbol{\mathcal{V}}(\mu), \tag{4.41}$$

with

$$b_\gamma^{\boldsymbol{n\tau}}(\mu;\boldsymbol{w};\boldsymbol{u},\boldsymbol{v}) := b_\gamma^{\boldsymbol{n}}(\mu;\boldsymbol{w};\boldsymbol{u},\boldsymbol{v}) + b_\gamma^{\boldsymbol{\tau}}(\mu;\boldsymbol{w};\boldsymbol{u},\boldsymbol{v}), \tag{4.42a}$$

$$r_\gamma^{\boldsymbol{n\tau}}(\mu;\boldsymbol{w};\boldsymbol{v}) := a_\gamma^{\boldsymbol{n\tau}}(\mu;\boldsymbol{w},\boldsymbol{v}) + \theta_\gamma^{\boldsymbol{n}}(\mu;\boldsymbol{w},\boldsymbol{v}) + \theta_\gamma^{\boldsymbol{\tau}}(\mu;\boldsymbol{w},\boldsymbol{v}) - f(\mu;\boldsymbol{v}), \tag{4.42b}$$

where

$$b_\gamma^{\boldsymbol{\tau}}(\mu;\boldsymbol{w};\boldsymbol{u},\boldsymbol{v}) := \int_{\Gamma^c(\mu)} \frac{1}{\gamma}\Big(\mathbb{G}_s(P_\gamma^{\boldsymbol{\tau}}(\mu;\boldsymbol{w})) \cdot P_\gamma^{\boldsymbol{\tau}}(\mu;\boldsymbol{u})\Big) P_\gamma^{\boldsymbol{\tau}}(\mu;\boldsymbol{v}) \, d\Gamma(\mu), \tag{4.43a}$$

$$\theta_\gamma^{\boldsymbol{\tau}}(\mu;\boldsymbol{w},\boldsymbol{v}) := \int_{\Gamma^c(\mu)} \frac{1}{\gamma}\Big[P_\gamma^{\boldsymbol{\tau}}(\mu;\boldsymbol{w})\Big]_s P_\gamma^{\boldsymbol{\tau}}(\mu;\boldsymbol{v}) \, d\Gamma(\mu), \tag{4.43b}$$

and $\mathbb{G}_s(\cdot)$, the differential of $\left[\,\cdot\,\right]_s$, is given by

$$\mathbb{G}_s(\boldsymbol{x}) := \begin{cases} \mathbb{I}_{d-1}, & \text{if } \|\boldsymbol{x}\| \leq s, \\ \frac{s}{\|\boldsymbol{x}\|}\left(\mathbb{I}_{d-1} - \frac{\boldsymbol{x}\otimes\boldsymbol{x}}{\|\boldsymbol{x}\|^2}\right), & \text{otherwise,} \end{cases} \tag{4.44}$$

with $\mathbb{I}_{d-1}$ the identity matrix of order $d-1$. The convergence criterion for (4.41) is still (4.26). We denote the converged solution to the sequence of problems (4.41) as $\boldsymbol{u}_{\mathrm{cv}}(\mu) \in \boldsymbol{\mathcal{V}}(\mu)$.

The algebraic formulation of the sequence of problems (4.41) reads as follows: For all $k \geq 0$, find $\boldsymbol{\Delta U}_k(\mu) \in \mathbb{R}^{\mathcal{N}^{\mathrm{HF}}}$ such that

$$A_\gamma^{n\tau}(\mu)\boldsymbol{\Delta U}_k(\mu) + B_\gamma^{n\tau}(\mu, \boldsymbol{u}_k(\mu))\boldsymbol{\Delta U}_k(\mu) = -R_\gamma^{n\tau}(\mu, \boldsymbol{u}_k(\mu)), \tag{4.45}$$

where for all $n, m \in \{1{:}\mathcal{N}^{\mathrm{HF}}\}$,

$$(A_\gamma^{n\tau}(\mu))_{mn} := a_\gamma^{n\tau}(\mu; \varphi_n(\mu), \varphi_m(\mu)), \tag{4.46a}$$
$$(B_\gamma^{n\tau}(\mu, \boldsymbol{u}_k(\mu)))_{mn} := b_\gamma^{n\tau}(\mu; \boldsymbol{u}_k(\mu); \varphi_n(\mu), \varphi_m(\mu)), \tag{4.46b}$$
$$(R_\gamma^{n\tau}(\mu, \boldsymbol{u}_k(\mu)))_m := r_\gamma^{n\tau}(\mu; \boldsymbol{u}_k(\mu); \varphi_m(\mu)). \tag{4.46c}$$

The convergence criterion for (4.45) is still (4.26) using the reconstructed functions. We denote the converged solution to the sequence of problems (4.45) as $\boldsymbol{U}_{\mathrm{cv}}(\mu) \in \mathbb{R}^{\mathcal{N}^{\mathrm{HF}}}$. Furthermore, let us denote by $B_\gamma^\tau(\mu, \boldsymbol{w})$ (resp. $\Theta_\gamma^\tau(\mu, \boldsymbol{w})$) the algebraic representation of the operator $b_\gamma^\tau(\mu; \boldsymbol{w}; \cdot, \cdot)$ (resp. $\theta_\gamma^\tau(\mu; \boldsymbol{w}; \cdot)$) such that for all $n, m \in \{1{:}\mathcal{N}^{\mathrm{HF}}\}$,

$$(B_\gamma^\tau(\mu, \boldsymbol{w}))_{mn} := b_\gamma^\tau(\mu; \boldsymbol{w}; \varphi_n(\mu), \varphi_m(\mu)), \qquad (\Theta_\gamma^\tau(\mu, \boldsymbol{w}))_m := \theta_\gamma^\tau(\mu; \boldsymbol{w}; \varphi_m(\mu)). \tag{4.47}$$

With this notation, we have the following decompositions:

$$B_\gamma^{n\tau}(\mu, \boldsymbol{u}_k(\mu)) := B_\gamma^n(\mu, \boldsymbol{u}_k(\mu)) + B_\gamma^\tau(\mu, \boldsymbol{u}_k(\mu)), \tag{4.48a}$$
$$R_\gamma^{n\tau}(\mu, \boldsymbol{u}_k(\mu)) := A_\gamma^{n\tau}(\mu)\boldsymbol{U}_k(\mu) + \Theta_\gamma^n(\mu, \boldsymbol{u}_k(\mu)) + \Theta_\gamma^\tau(\mu, \boldsymbol{u}_k(\mu)) - F(\mu). \tag{4.48b}$$

4.3.2.2 Coulomb friction

Let us now consider the Coulomb frictional contact problem. We use the following reformulation of the friction conditions given in [28]:

$$\boldsymbol{\sigma}_{n\tau}(\boldsymbol{u}(\mu)) = \Big[\boldsymbol{\sigma}_{n\tau}(\boldsymbol{u}(\mu)) - \gamma \boldsymbol{u}_\tau(\mu)\Big]_{(\nu_{\mathcal{F}}|\sigma_{nn}(\boldsymbol{u}(\mu))|)}. \tag{4.49}$$

Using the reformulation of the Signorini contact conditions given in (4.14), (4.49) can be rewritten as follows:

$$\boldsymbol{\sigma}_{n\tau}(\boldsymbol{u}(\mu)) = \Big[\boldsymbol{\sigma}_{n\tau}(\boldsymbol{u}(\mu)) - \gamma \boldsymbol{u}_\tau(\mu)\Big]_{s^{\mathrm{c}}(\mu;\boldsymbol{u}(\mu))}, \tag{4.50}$$

where for a generic displacement field $\boldsymbol{v} \in \boldsymbol{\mathcal{V}}(\mu)$, we have introduced the Tresca-like threshold

$$s^{\mathrm{c}}(\mu; \boldsymbol{v}) := \nu_{\mathcal{F}}\Big|\Big[P_{\gamma,g}^n(\mu; \boldsymbol{v})\Big]_-\Big|. \tag{4.51}$$

Then, Nitsche's formulation for the Coulomb frictional contact problem reads as follows: Find $\boldsymbol{u}(\mu) \in \boldsymbol{\mathcal{V}}(\mu)$ such that

$$\begin{cases} a_\gamma^{n\tau}(\mu;\boldsymbol{u}(\mu),\boldsymbol{v}) + \displaystyle\int_{\Gamma^c(\mu)} \frac{1}{\gamma}\Big[P_{\gamma,g}^n(\mu;\boldsymbol{u}(\mu))\Big]_- P_{\gamma,0}^n(\mu;\boldsymbol{v})\,d\Gamma(\mu) \\ + \displaystyle\int_{\Gamma^c(\mu)} \frac{1}{\gamma}\Big[P_\gamma^\tau(\mu;\boldsymbol{u}(\mu))\Big]_{s^c(\mu;\boldsymbol{u}(\mu))} P_\gamma^\tau(\mu;\boldsymbol{v})\,d\Gamma(\mu) = f(\mu;\boldsymbol{v}), \quad \forall \boldsymbol{v} \in \boldsymbol{\mathcal{V}}(\mu). \end{cases} \tag{4.52}$$

The problem (4.52) is nonlinear. A possible way to solve it would be to do as for the Tresca problem by linearizing the problem. However, there is an additional difficulty due to the fact that the term $\Big[P_\gamma^\tau(\mu;\boldsymbol{u}(\mu))\Big]_{s^c(\mu;\boldsymbol{u}(\mu))}$ depends on the displacement in two ways, and the dependency through the threshold in the projection operator is particularly delicate. As an alternative, we propose to solve the Coulomb frictional contact problem by directly using the iterative scheme (4.41) designed for the Tresca frictional contact problem where, at iteration k, we use the Tresca-like threshold $s_k := s^c(\mu;\boldsymbol{u}_k(\mu))$. The proposed iterative algorithm to solve (4.52) then leads to the following sequence of problems: For all $k \geq 0$, find $\boldsymbol{\delta u}_k(\mu) \in \boldsymbol{\mathcal{V}}(\mu)$ such that

$$a_\gamma^{n\tau}(\mu;\boldsymbol{\delta u}_k(\mu),\boldsymbol{v}) + b_\gamma^{n\tau^c}(\mu;\boldsymbol{u}_k(\mu);\boldsymbol{\delta u}_k(\mu),\boldsymbol{v}) = -r_\gamma^{n\tau^c}(\mu;\boldsymbol{u}_k(\mu);\boldsymbol{v}), \quad \forall \boldsymbol{v} \in \boldsymbol{\mathcal{V}}(\mu), \tag{4.53}$$

with

$$b_\gamma^{n\tau^c}(\mu;\boldsymbol{w};\boldsymbol{u},\boldsymbol{v}) := b_\gamma^n(\mu;\boldsymbol{w};\boldsymbol{u},\boldsymbol{v}) + b_\gamma^{\tau^c}(\mu;\boldsymbol{w};\boldsymbol{u},\boldsymbol{v}), \tag{4.54a}$$

$$r_\gamma^{n\tau^c}(\mu;\boldsymbol{w};\boldsymbol{v}) := a_\gamma^{n\tau}(\mu;\boldsymbol{w},\boldsymbol{v}) + \theta_\gamma^n(\mu;\boldsymbol{w};\boldsymbol{v}) + \theta_\gamma^{\tau^c}(\mu;\boldsymbol{w};\boldsymbol{v}) - f(\mu;\boldsymbol{v}), \tag{4.54b}$$

where

$$b_\gamma^{\tau^c}(\mu;\boldsymbol{w};\boldsymbol{u},\boldsymbol{v}) := \int_{\Gamma^c(\mu)} \frac{1}{\gamma}\Big(\mathbb{G}_{s^c(\mu;\boldsymbol{w})}(P_\gamma^\tau(\mu;\boldsymbol{w})) \cdot P_\gamma^\tau(\mu;\boldsymbol{u})\Big) P_\gamma^\tau(\mu;\boldsymbol{v})\,d\Gamma(\mu), \tag{4.55a}$$

$$\theta_\gamma^{\tau^c}(\mu;\boldsymbol{w};\boldsymbol{v}) := \int_{\Gamma^c(\mu)} \frac{1}{\gamma}\Big[P_\gamma^\tau(\mu;\boldsymbol{w})\Big]_{s^c(\mu;\boldsymbol{w})} P_\gamma^\tau(\mu;\boldsymbol{v})\,d\Gamma(\mu). \tag{4.55b}$$

The convergence criterion for (4.53) is still (4.26). We denote the converged solution to the sequence of problems (4.53) as $\boldsymbol{u}_{\mathrm{cv}}(\mu) \in \boldsymbol{\mathcal{V}}(\mu)$.

The algebraic formulation of the sequence of problems (4.53) reads as follows: For all $k \geq 0$, find $\boldsymbol{\Delta U}_k(\mu) \in \mathbb{R}^{\mathcal{N}^{\mathrm{HF}}}$ such that

$$A_\gamma^{n\tau}(\mu)\boldsymbol{\Delta U}_k(\mu) + B_\gamma^{n\tau^c}(\mu,\boldsymbol{u}_k(\mu))\boldsymbol{\Delta U}_k(\mu) = -R_\gamma^{n\tau^c}(\mu,\boldsymbol{u}_k(\mu)), \tag{4.56}$$

where for all $n, m \in \{1{:}\mathcal{N}^{\mathrm{HF}}\}$,

$$(A_\gamma^{n\tau}(\mu))_{mn} := a_\gamma^{n\tau}(\mu;\varphi_n(\mu),\varphi_m(\mu)), \tag{4.57a}$$

$$(B_\gamma^{n\tau^c}(\mu,\boldsymbol{u}_k(\mu)))_{mn} := b_\gamma^{n\tau^c}(\mu;\boldsymbol{u}_k(\mu);\varphi_n(\mu),\varphi_m(\mu)), \tag{4.57b}$$

$$(R_\gamma^{n\tau^c}(\mu,\boldsymbol{u}_k(\mu)))_m := r_\gamma^{n\tau^c}(\mu;\boldsymbol{u}_k(\mu);\varphi_m(\mu)). \tag{4.57c}$$

The convergence criterion for (4.56) is still (4.26) using the reconstructed functions. We denote the converged solution to the sequence of problems (4.56) as $\boldsymbol{U}_{\mathrm{cv}}(\mu) \in \mathbb{R}^{\mathcal{N}^{\mathrm{HF}}}$.

Furthermore, let us denote by $B_\gamma^{\tau^c}(\mu, \boldsymbol{w})$ (resp. $\Theta_\gamma^{\tau^c}(\mu, \boldsymbol{w})$) the algebraic representation of the form $b_\gamma^{\tau^c}(\mu; \boldsymbol{w}; \cdot, \cdot)$ (resp. $\theta_\gamma^{\tau^c}(\mu; \boldsymbol{w}; \cdot)$) such that for all $n, m \in \{1{:}\mathcal{N}^{\mathrm{HF}}\}$,

$$(B_\gamma^{\tau^c}(\mu, \boldsymbol{w}))_{mn} := b_\gamma^{\tau^c}(\mu; \boldsymbol{w}; \varphi_n(\mu), \varphi_m(\mu)), \qquad (\Theta_\gamma^{\tau^c}(\mu, \boldsymbol{w}))_m := \theta_\gamma^{\tau^c}(\mu; \boldsymbol{w}; \varphi_m(\mu)). \tag{4.58}$$

With this notation, we have the following decompositions:

$$B_\gamma^{\boldsymbol{n}\boldsymbol{\tau}^c}(\mu, \boldsymbol{u}_k(\mu)) := B_\gamma^{\boldsymbol{n}}(\mu, \boldsymbol{u}_k(\mu)) + B_\gamma^{\boldsymbol{\tau}^c}(\mu, \boldsymbol{u}_k(\mu)), \tag{4.59a}$$

$$R_\gamma^{\boldsymbol{n}\boldsymbol{\tau}^c}(\mu, \boldsymbol{u}_k(\mu)) := A_\gamma^{\boldsymbol{n}\boldsymbol{\tau}}(\mu)\boldsymbol{U}_k(\mu) + \Theta_\gamma^{\boldsymbol{n}}(\mu, \boldsymbol{u}_k(\mu)) + \Theta_\gamma^{\boldsymbol{\tau}^c}(\mu, \boldsymbol{u}_k(\mu)) - F(\mu). \tag{4.59b}$$

Remark 4.3.1 (Energy). The formulation (4.52) is directly obtained from the weak formulation of equations (4.3a)-(4.3b)-(4.3c)-(4.3d) and (4.5), and not from an energy minimization as for the Tresca frictional contact problem.

One can also solve the Coulomb frictional contact problem using a fixed-point method on the Tresca frictional contact problem. For this purpose, we introduce the mapping $\boldsymbol{\phi}(\mu; \cdot) : \boldsymbol{\mathcal{V}}(\mu) \to \boldsymbol{\mathcal{V}}(\mu)$ defined for all $\boldsymbol{v} \in \boldsymbol{\mathcal{V}}(\mu)$ by requiring that $\boldsymbol{\phi}(\mu; \boldsymbol{v})$ solves (4.52) with the threshold $s^c(\mu; \boldsymbol{v})$. With this definition, one can see that the solution to (4.52) is a fixed-point of the mapping $\boldsymbol{\phi}(\mu; \cdot)$. It is shown in [28, Thm 4.3] that, under certain conditions, the mapping $\boldsymbol{\phi}(\mu; \cdot)$ is contractive so that (4.52) admits a solution according to the Banach fixed-point theorem. The fixed-point algorithm to solve (4.52) then reads as follows: Given $\boldsymbol{u}^0(\mu) \in \boldsymbol{\mathcal{V}}(\mu)$ and a tolerance $\delta_{\boldsymbol{u}}^{\mathrm{ct}}$, for all $n \in \mathbb{N}$, find $\boldsymbol{u}^{n+1}(\mu) \in \boldsymbol{\mathcal{V}}(\mu)$ solution to (4.39) with the Tresca-like threshold $s_n := s^c(\mu; \boldsymbol{u}^n(\mu))$. We iterate on n until the following convergence criterion is reached:

$$\frac{\|\boldsymbol{u}^{n+1}(\mu) - \boldsymbol{u}^n(\mu)\|_{\boldsymbol{\mathcal{V}}(\mu)}}{\|\boldsymbol{u}^{n+1}(\mu)\|_{\boldsymbol{\mathcal{V}}(\mu)}} \leq \delta_{\boldsymbol{u}}^{\mathrm{ct}}. \tag{4.60}$$

Let us introduce the following notation:

$$b_\gamma^{\boldsymbol{n}\boldsymbol{\tau}^{\mathrm{ct}}}(\mu; \boldsymbol{z}; \boldsymbol{w}; \boldsymbol{u}, \boldsymbol{v}) := b_\gamma^{\boldsymbol{n}}(\mu; \boldsymbol{w}; \boldsymbol{u}, \boldsymbol{v}) + b_\gamma^{\boldsymbol{\tau}^{\mathrm{ct}}}(\mu; \boldsymbol{z}; \boldsymbol{w}; \boldsymbol{u}, \boldsymbol{v}), \tag{4.61a}$$

$$r_\gamma^{\boldsymbol{n}\boldsymbol{\tau}^{\mathrm{ct}}}(\mu; \boldsymbol{z}; \boldsymbol{w}; \boldsymbol{v}) := a_\gamma^{\boldsymbol{n}\boldsymbol{\tau}}(\mu; \boldsymbol{w}, \boldsymbol{v}) + \theta_\gamma^{\boldsymbol{n}}(\mu; \boldsymbol{w}; \boldsymbol{v}) + \theta_\gamma^{\boldsymbol{\tau}^{\mathrm{ct}}}(\mu; \boldsymbol{z}; \boldsymbol{w}; \boldsymbol{v}) - f(\mu; \boldsymbol{v}), \tag{4.61b}$$

with

$$b_\gamma^{\boldsymbol{\tau}^{\mathrm{ct}}}(\mu; \boldsymbol{z}; \boldsymbol{w}; \boldsymbol{u}, \boldsymbol{v}) := \int_{\Gamma^c(\mu)} \frac{1}{\gamma}\Big(\mathbb{G}_{s^c(\mu;\boldsymbol{z})}(P_\gamma^{\boldsymbol{\tau}}(\mu; \boldsymbol{w})) \cdot P_\gamma^{\boldsymbol{\tau}}(\mu; \boldsymbol{u})\Big) P_\gamma^{\boldsymbol{\tau}}(\mu; \boldsymbol{v})\, d\Gamma(\mu), \tag{4.62a}$$

$$r_\gamma^{\boldsymbol{n}\boldsymbol{\tau}^{\mathrm{ct}}}(\mu; \boldsymbol{z}; \boldsymbol{w}; \boldsymbol{v}) := \int_{\Gamma^c(\mu)} \frac{1}{\gamma}\Big[P_\gamma^{\boldsymbol{\tau}}(\mu; \boldsymbol{w})\Big]_{s^c(\mu;\boldsymbol{z})} P_\gamma^{\boldsymbol{\tau}}(\mu; \boldsymbol{v})\, d\Gamma(\mu). \tag{4.62b}$$

It is important to observe that there is an additional argument $\boldsymbol{z}$ in the forms $b_\gamma^{\boldsymbol{n}\boldsymbol{\tau}^{\mathrm{ct}}}(\mu; \cdot; \cdot; \cdot, \cdot)$ and $r_\gamma^{\boldsymbol{n}\boldsymbol{\tau}^{\mathrm{ct}}}(\mu; \cdot; \cdot; \cdot)$. Since $\boldsymbol{u}^{n+1}(\mu)$ solves (4.39) with the Tresca-like threshold s_n, $\boldsymbol{u}^{n+1}(\mu)$ is computed as the limit $\boldsymbol{u}_{\mathrm{cv}}^{n+1}(\mu)$ obtained by solving the following sequence of problems: For all $k \geq 0$, find $\boldsymbol{\delta u}_k^{n+1}(\mu) \in \boldsymbol{\mathcal{V}}(\mu)$ such that

$$\begin{cases} a_\gamma^{\boldsymbol{n}\boldsymbol{\tau}}(\mu; \boldsymbol{\delta u}_k^{n+1}(\mu), \boldsymbol{v}) + b_\gamma^{\boldsymbol{n}\boldsymbol{\tau}^{\mathrm{ct}}}(\mu; \boldsymbol{u}^n(\mu); \boldsymbol{u}_k^{n+1}(\mu); \boldsymbol{\delta u}_k^{n+1}(\mu), \boldsymbol{v}) \\ \quad = -r_\gamma^{\boldsymbol{n}\boldsymbol{\tau}^{\mathrm{ct}}}(\mu; \boldsymbol{u}^n(\mu); \boldsymbol{u}_k^{n+1}(\mu); \boldsymbol{v}), \quad \forall \boldsymbol{v} \in \boldsymbol{\mathcal{V}}(\mu). \end{cases} \tag{4.63}$$

We iterate on k until the following convergence criterion is reached:

$$\frac{\|\boldsymbol{u}_{k+1}^{n+1}(\mu) - \boldsymbol{u}_k^{n+1}(\mu)\|_{\boldsymbol{\mathcal{V}}(\mu)}}{\|\boldsymbol{u}_{k+1}^{n+1}(\mu)\|_{\boldsymbol{\mathcal{V}}(\mu)}} \leq \delta_{\boldsymbol{u}}. \tag{4.64}$$

Thus, we obtain a nested loop for the Coulomb frictional contact problem: the superscript n refers to the fixed-point iteration for the Coulomb problem and the subscript k refers to the iteration of the underlying Tresca problem. The nested loop structure makes this second approach more expensive than the iterative scheme (4.53). A way to see (4.53) is actually to consider the nested algorithm (4.63) and perform only one iteration in the underlying Tresca frictional contact problem. Our numerical experiments indicate that the nested-loop approach is actually more robust than the iterative scheme (4.53).

4.4 Reduced-basis formulation

In this section, we derive the RBM. We describe the problem in detail for the frictionless contact problem, and briefly highlight the (simple) adaptations needed to account for friction.

4.4.1 Geometric mapping

We recall that the dimension $\mathcal{N}^{\mathrm{HF}}$ of the HF (finite-dimensional) space $\boldsymbol{\mathcal{V}}(\mu)$ is parameter-independent. This is important since, in order to compress the space generated by the snapshots, it is necessary that all the snapshots live in the same space. For this purpose, since the geometry is parameter-dependent, we use a parameter-independent reference domain $\widehat{\Omega}$. We assume that for all $\mu \in \mathcal{D}$, there is a smooth invertible geometric mapping $h(\mu) : \widehat{\Omega} \to \Omega(\mu)$. We denote by $\widehat{\Gamma} := \partial\widehat{\Omega}$ the boundary of $\widehat{\Omega}$ and we assume that it can be partitioned as $\widehat{\Gamma} = \widehat{\Gamma}^{\mathrm{D}} \cup \widehat{\Gamma}^{\mathrm{N}} \cup \widehat{\Gamma}^{\mathrm{c}}$ in such a way that, for all $\mu \in \mathcal{D}$,

$$\widehat{\Gamma}^{\mathrm{D}} := h_d^{-1}(\mu)(\Gamma^{\mathrm{D}}(\mu)), \quad \widehat{\Gamma}^{\mathrm{N}} := h_n^{-1}(\mu)(\Gamma^{\mathrm{N}}(\mu)), \quad \widehat{\Gamma}^{\mathrm{c}} := h_c^{-1}(\mu)(\Gamma^{\mathrm{c}}(\mu)), \tag{4.65}$$

with $h_d(\mu) := h(\mu)_{|\widehat{\Gamma}^{\mathrm{D}}}$, $h_n(\mu) := h(\mu)_{|\widehat{\Gamma}^{\mathrm{N}}}$ and $h_c(\mu) := h(\mu)_{|\widehat{\Gamma}^{\mathrm{c}}}$. Then, the mesh of $\Omega(\mu)$ is generated by generating a mesh of $\widehat{\Omega}$ matching the partition of the boundary $\widehat{\Gamma}$ and applying the mapping $h(\mu)$ to the mesh of the reference domain $\widehat{\Omega}$. The finite element basis functions are generated from the reference basis functions by using a pullback.

4.4.2 Naive approach

The goal of this section is to present the naive reduced model resulting from the application of a plain RBM to the contact problem formulated with Nitsche's method and highlight the problem of computational inefficiency raised by such a formulation. This problem will be circumvented in the next section eventually leading to a computationally effective RBM. The major difficulty comes from the nonlinearity of Nitsche's formulation.

To build the reduced basis (RB), the starting point is to compute (in the offline phase) a family $\{\boldsymbol{U}_{\mathrm{cv}}(\mu_p)\}_{p\in\{1:P\}} \subset \mathbb{R}^{\mathcal{N}^{\mathrm{HF}}}$ of HF solutions to the frictionless contact problem (4.29) by using a training subset $\mathcal{D}_{\mathtt{train}} := \{\mu_p\}_{p\in\{1:P\}} \subset \mathcal{D}$ of cardinality $P \in \mathbb{N}^*$. Using the Proper Orthogonal Decomposition (POD) [54, 69] based on the inner product of $H^1(\widehat{\Omega}; \mathbb{R}^d)$ and the geometric mapping $h(\mu)$, one can then construct

an orthonormal family $\{\boldsymbol{\Xi}_n\}_{n\in\{1:N\}} \subset \mathbb{R}^{\mathcal{N}^{\mathrm{HF}}}$ of $N \in \mathbb{N}^*$ ($N \leq P$) vectors. Let us denote by $\boldsymbol{V}_N$ the reduced space generated by the family $\{\boldsymbol{\Xi}_n\}_{n\in\{1:N\}}$, *i.e.*,

$$\boldsymbol{V}_N := \boldsymbol{Span}\Big(\{\boldsymbol{\Xi}_n\}_{n\in\{1:N\}}\Big) \subset \mathbb{R}^{\mathcal{N}^{\mathrm{HF}}}. \tag{4.66}$$

In algebraic form, the RB formulation of the sequence of HF problems (4.29) reads as follows: For all $k \geq 0$, find $\boldsymbol{\Delta U}_{N,k}(\mu) \in \mathbb{R}^N$ such that

$$A^{\boldsymbol{n}}_{\gamma,N}(\mu)\boldsymbol{\Delta U}_{N,k}(\mu) + B^{\boldsymbol{n}}_{\gamma,N}(\mu,k)\boldsymbol{\Delta U}_{N,k}(\mu) = -R^{\boldsymbol{n}}_{\gamma,N}(\mu,k), \tag{4.67}$$

where

$$A^{\boldsymbol{n}}_{\gamma,N}(\mu) := Z^\top A^{\boldsymbol{n}}_{\gamma}(\mu) Z \in \mathbb{R}^{N\times N}, \tag{4.68a}$$

$$B^{\boldsymbol{n}}_{\gamma,N}(\mu,k) := Z^\top B^{\boldsymbol{n}}_{\gamma}(\mu,\boldsymbol{u}_{N,k}(\mu)) Z \in \mathbb{R}^{N\times N}, \quad R^{\boldsymbol{n}}_{\gamma,N}(\mu,k) := Z^\top R^{\boldsymbol{n}}_{\gamma}(\mu,\boldsymbol{u}_{N,k}(\mu)) \in \mathbb{R}^N, \tag{4.68b}$$

with $Z := \Big[\boldsymbol{\Xi}_1 \cdots \boldsymbol{\Xi}_N\Big] \in \mathbb{R}^{\mathcal{N}^{\mathrm{HF}}\times N}$. The convergence criterion for (4.67) is still (4.26) using the reconstructed functions (see Remark 4.4.1 for more details).

At this stage, the RBM basically consists of the following two stages:

— Offline stage

1. Select a training subset $\mathcal{D}_{\texttt{train}} := \{\mu_p\}_{p\in\{1:P\}} \subset \mathcal{D}$.
2. Compute the snapshots $\{\boldsymbol{U}_{\mathrm{cv}}(\mu_p)\}_{p\in\{1:P\}} \subset \mathbb{R}^{\mathcal{N}^{\mathrm{HF}}}$ by solving (4.29).
3. Compute the reduced space $\boldsymbol{V}_N$ by using POD on snapshots.

— Online stage: For any $\mu \in \mathcal{D} \setminus \mathcal{D}_{\texttt{train}}$,

1. Compute $A^{\boldsymbol{n}}_{\gamma,N}(\mu)$ using (4.68a).
2. Loop on $k \geq 0$,
   (a) Compute $B^{\boldsymbol{n}}_{\gamma,N}(\mu,k)$ and $R^{\boldsymbol{n}}_{\gamma,N}(\mu,k)$ using (4.68b).
   (b) Solve (4.67).
   (c) Check convergence; if not, set $k \leftarrow k+1$ and go back to (2a).

It is crucial to derive a reduced problem that is independent of the high-fidelity dimension $\mathcal{N}^{\mathrm{HF}}$ in order to obtain an inexpensive online stage. This condition is not yet satisfied with the current formalism. The main issue is the manipulation of large-dimensional arrays in (4.67). We propose in Section 4.4.3 a procedure to overcome this issue in order to construct a computationally efficient RBM.

Remark 4.4.1 (Reconstructed functions). Let us introduce the following reconstructed functions:

$$\boldsymbol{\xi}_n(\mu) := \sum_{i\in\{1:\mathcal{N}^{\mathrm{HF}}\}} \boldsymbol{\Xi}^i_n \boldsymbol{\varphi}_i(\mu) \in \boldsymbol{\mathcal{V}}(\mu), \quad \forall n \in \{1{:}N\}. \tag{4.69}$$

With this notation, solving the RB problem (4.67) in algebraic form leads to the following reconstructed solutions:

$$\boldsymbol{u}_{N,k}(\mu) := \sum_{n\in\{1:N\}} \boldsymbol{u}^n_{N,k}(\mu)\boldsymbol{\xi}_n(\mu) \in \boldsymbol{\mathcal{V}}(\mu), \qquad \boldsymbol{U}_{N,k}(\mu) := (\boldsymbol{u}^n_{N,k}(\mu))_{n\in\{1:N\}} \in \mathbb{R}^N, \tag{4.70a}$$

$$\boldsymbol{\delta u}_{N,k}(\mu) := \sum_{n\in\{1:N\}} \boldsymbol{\delta u}^n_{N,k}(\mu)\boldsymbol{\xi}_n(\mu) \in \boldsymbol{\mathcal{V}}(\mu), \quad \boldsymbol{\Delta U}_{N,k}(\mu) := (\boldsymbol{\delta u}^n_{N,k}(\mu))_{n\in\{1:N\}} \in \mathbb{R}^N. \tag{4.70b}$$

4.4.3 Computationally efficient approach

In this section, we describe the strategy to avoid the manipulation of large-dimensional arrays in the problem (4.67). The idea consists in introducing appropriate affine parametric decompositions of the parameter-dependent and "parameter/iteration"-dependent operators involved in the problem by using the Empirical Interpolation Method (EIM) [10, 75].

Specifically, our goal is to separate the dependence on μ and k from the dependence on the indices in the large-dimensional arrays $A^{\boldsymbol{n}}_\gamma(\mu)$, $B^{\boldsymbol{n}}_\gamma(\mu, \boldsymbol{u}_{N,k}(\mu))$ and $R^{\boldsymbol{n}}_\gamma(\mu, \boldsymbol{u}_{N,k}(\mu))$. This operation is performed during the offline stage. For this purpose, using the EIM, we obtain the following approximations:

$$A^{\boldsymbol{n}}_\gamma(\mu) \approx \quad E^{a^{\boldsymbol{n}}}(\mu) := \sum_{s\in\{1:S^{a^{\boldsymbol{n}}}\}} \alpha^{a^{\boldsymbol{n}}}_s(\mu) A^{\boldsymbol{n}}_{\gamma,s}, \qquad A^{\boldsymbol{n}}_{\gamma,s} \in \mathbb{R}^{\mathcal{N}^{\mathrm{HF}}\times\mathcal{N}^{\mathrm{HF}}},\ \alpha^{a^{\boldsymbol{n}}}_s(\mu) \in \mathbb{R}, \tag{4.71a}$$

$$B^{\boldsymbol{n}}_\gamma(\mu, \boldsymbol{u}_k(\mu)) \approx E^{b^{\boldsymbol{n}}}(\mu, k) := \sum_{s\in\{1:S^{b^{\boldsymbol{n}}}\}} \alpha^{b^{\boldsymbol{n}}}_s(\mu, k) B^{\boldsymbol{n}}_{\gamma,s}, \quad B^{\boldsymbol{n}}_{\gamma,s} \in \mathbb{R}^{\mathcal{N}^{\mathrm{HF}}\times\mathcal{N}^{\mathrm{HF}}},\ \alpha^{b^{\boldsymbol{n}}}_s(\mu, k) \in \mathbb{R}, \tag{4.71b}$$

$$\Theta^{\boldsymbol{n}}_\gamma(\mu, \boldsymbol{u}_k(\mu)) \approx E^{\theta^{\boldsymbol{n}}}(\mu, k) := \sum_{s\in\{1:S^{\theta^{\boldsymbol{n}}}\}} \alpha^{\theta^{\boldsymbol{n}}}_s(\mu, k) \Theta^{\boldsymbol{n}}_{\gamma,s}, \quad \Theta^{\boldsymbol{n}}_{\gamma,s} \in \mathbb{R}^{\mathcal{N}^{\mathrm{HF}}},\ \alpha^{\theta^{\boldsymbol{n}}}_s(\mu, k) \in \mathbb{R}, \tag{4.71c}$$

$$F(\mu) \approx \quad E^f(\mu) := \sum_{s\in\{1:S^f\}} \alpha^f_s(\mu) F_s, \qquad F_s \in \mathbb{R}^{\mathcal{N}^{\mathrm{HF}}},\ \alpha^f_s(\mu) \in \mathbb{R}, \tag{4.71d}$$

where the large-dimensional arrays $A^{\boldsymbol{n}}_{\gamma,s}$, $B^{\boldsymbol{n}}_{\gamma,s}$, $\Theta^{\boldsymbol{n}}_{\gamma,s}$ and F_s are now independent of the parameter μ and the iteration counter k, whereas the functions $\alpha^{a^{\boldsymbol{n}}}_s$ and α^f_s (resp., $\alpha^{b^{\boldsymbol{n}}}_s$ and $\alpha^{\theta^{\boldsymbol{n}}}_s$) only depend on μ (resp., (μ, k)). We obtain the following approximation of the residual:

$$R^{\boldsymbol{n}}_\gamma(\mu, \boldsymbol{u}_k(\mu)) \approx E^{r^{\boldsymbol{n}}}(\mu, k) := E^{a^{\boldsymbol{n}}}(\mu)\boldsymbol{U}_k(\mu) + E^{\theta^{\boldsymbol{n}}}(\mu, k) - E^f(\mu). \tag{4.72}$$

To build the large-dimensional arrays $A^{\boldsymbol{n}}_{\gamma,s}$, $B^{\boldsymbol{n}}_{\gamma,s}$, $\Theta^{\boldsymbol{n}}_{\gamma,s}$ and F_s , we respectively use the training sets $\mathcal{E}^{a^{\boldsymbol{n}}}_{\mathtt{train}}$, $\mathcal{E}^{b^{\boldsymbol{n}}}_{\mathtt{train}}$, $\mathcal{E}^{\theta^{\boldsymbol{n}}}_{\mathtt{train}}$ and $\mathcal{E}^f_{\mathtt{train}}$ defined as follows:

$$\mathcal{E}^{a^{\boldsymbol{n}}}_{\mathtt{train}} = \mathcal{E}^f_{\mathtt{train}} := \mathcal{D}_{\mathtt{train}}, \quad \mathcal{E}^{b^{\boldsymbol{n}}}_{\mathtt{train}} = \mathcal{E}^{\theta^{\boldsymbol{n}}}_{\mathtt{train}} := \Big\{(\mu, k) \mid \mu \in \mathcal{D}_{\mathtt{train}},\ k \in \{1{:}k^{\mathrm{cv}}(\mu)\}\Big\}. \tag{4.73}$$

Notice that a training set different (possibly richer) than $\mathcal{D}_{\texttt{train}}$ can be used. We introduce the index subsets $\{(n_s^{a^n}, m_s^{a^n})\}_{s\in\{1:S^{a^n}\}}, \{(n_s^{b^n}, m_s^{b^n})\}_{s\in\{1:S^{b^n}\}} \subset \{1{:}\mathcal{N}^{\mathrm{HF}}\} \times \{1{:}\mathcal{N}^{\mathrm{HF}}\}$, $\{m_s^{\theta^n}\}_{s\in\{1:S^{\theta^n}\}} \subset \{1{:}\mathcal{N}^{\mathrm{HF}}\}$ and $\{m_s^f\}_{s\in\{1:S^f\}} \subset \{1{:}\mathcal{N}^{\mathrm{HF}}\}$ of cardinality S^{a^n}, S^{b^n}, S^{θ^n}, and S^f respectively, corresponding to the indices selected by the EIM for the approximation of $A_\gamma^{\boldsymbol{n}}$, $B_\gamma^{\boldsymbol{n}}$, $\Theta_\gamma^{\boldsymbol{n}}$ and F. Then, the functions $\alpha_s^{a^n}$, $\alpha_s^{b^n}$, $\alpha_s^{\theta^n}$ and α_s^f are such that

$$\forall \mu \in \mathcal{E}_{\texttt{train}}^{a^n}, \qquad (E^{a^n}(\mu))_{n_s^{a^n} m_s^{a^n}} = (A_\gamma^{\boldsymbol{n}}(\mu))_{n_s^{a^n} m_s^{a^n}}, \qquad \forall s \in \{1{:}S^{a^n}\}, \tag{4.74a}$$

$$\forall (\mu, k) \in \mathcal{E}_{\texttt{train}}^{b^n}, \qquad (E^{b^n}(\mu,k))_{n_s^{b^n} m_s^{b^n}} = (B_\gamma^{\boldsymbol{n}}(\mu, \boldsymbol{u}_k(\mu)))_{n_s^{b^n} m_s^{b^n}}, \qquad \forall s \in \{1{:}S^{b^n}\}, \tag{4.74b}$$

$$\forall (\mu, k) \in \mathcal{E}_{\texttt{train}}^{\theta^n}, \qquad (E^{\theta^n}(\mu,k))_{m_s^{\theta^n}} = (\Theta_\gamma^{\boldsymbol{n}}(\mu, \boldsymbol{u}_k(\mu)))_{m_s^{\theta^n}}, \qquad \forall s \in \{1{:}S^{\theta^n}\}, \tag{4.74c}$$

$$\forall \mu \in \mathcal{E}_{\texttt{train}}^{f}, \qquad (E^{f}(\mu))_{m_s^{f}} = (F(\mu))_{m_s^{f}}, \qquad \forall s \in \{1{:}S^{f}\}, \tag{4.74d}$$

and $E^{a^n}(\mu)$, $E^{b^n}(\mu,k)$, $E^{\theta^n}(\mu,k)$ and $E^f(\mu)$ defined in (4.71). Notice that we use the HF solution $\boldsymbol{u}_k(\mu)$ instead of the RB solution $\boldsymbol{u}_{N,k}(\mu)$ to compute the functions $\alpha_s^{b^n}$ and $\alpha_s^{\theta^n}$.

In the online phase, for every new value of the parameter pair $(\mu, k) \in \mathcal{D} \times \mathbb{N}$, the functions $\alpha_s^{a^n}$, $\alpha_s^{b^n}$, $\alpha_s^{\theta^n}$ and α_s^f are approximated by functions $\alpha_{N,s}^{a^n}$, $\alpha_{N,s}^{b^n}$, $\alpha_{N,s}^{\theta^n}$ and $\alpha_{N,s}^f$ which solve the following linear systems:

$$Q^{a^n} \alpha_N^{a^n}(\mu) = T^{a^n}(\mu), \qquad T^{a^n}(\mu) := \left((A_\gamma^{\boldsymbol{n}}(\mu))_{n_s^{a^n} m_s^{a^n}}\right)_{s\in\{1:S^{a^n}\}} \in \mathbb{R}^{S^{a^n}}, \tag{4.75a}$$

$$Q^{b^n} \alpha_N^{b^n}(\mu,k) = T^{b^n}(\mu,k), \quad T^{b^n}(\mu,k) := \left((B_\gamma^{\boldsymbol{n}}(\mu, \boldsymbol{u}_{N,k}(\mu)))_{n_s^{b^n} m_s^{b^n}}\right)_{s\in\{1:S^{b^n}\}} \in \mathbb{R}^{S^{b^n}}, \tag{4.75b}$$

$$Q^{\theta^n} \alpha_N^{\theta^n}(\mu,k) = T^{\theta^n}(\mu,k), \quad T^{\theta^n}(\mu,k) := \left((\Theta_\gamma^{\boldsymbol{n}}(\mu, \boldsymbol{u}_{N,k}(\mu)))_{m_s^{\theta^n}}\right)_{s\in\{1:S^{\theta^n}\}} \in \mathbb{R}^{S^{\theta^n}}, \tag{4.75c}$$

$$Q^{f} \alpha_N^{f}(\mu) = T^{f}(\mu), \qquad T^{f}(\mu) := \left((F(\mu))_{m_s^{f}}\right)_{s\in\{1:S^{f}\}} \in \mathbb{R}^{S^{f}}, \tag{4.75d}$$

where the vector-valued functions $\alpha_N^{a^n}$, $\alpha_N^{b^n}$, $\alpha_N^{\theta^n}$ and α_N^f are such that

$$\alpha_N^{a^n}(\mu) := (\alpha_{N,s}^{a^n}(\mu))_{s\in\{1:S^{a^n}\}} \in \mathbb{R}^{S^{a^n}}, \tag{4.76a}$$

$$\alpha_N^{b^n}(\mu,k) := (\alpha_{N,s}^{b^n}(\mu))_{s\in\{1:S^{b^n}\}} \in \mathbb{R}^{S^{b^n}}, \tag{4.76b}$$

$$\alpha_N^{\theta^n}(\mu,k) := (\alpha_{N,s}^{\theta^n}(\mu))_{s\in\{1:S^{\theta^n}\}} \in \mathbb{R}^{S^{\theta^n}}, \tag{4.76c}$$

$$\alpha_N^{f}(\mu) := (\alpha_{N,s}^{f}(\mu))_{s\in\{1:S^{f}\}} \in \mathbb{R}^{S^{f}}. \tag{4.76d}$$

Notice that here, in the online phase, we use the RB solutions $\boldsymbol{u}_{N,k}(\mu)$. The parameter-independent interpolation matrices $Q^{a^n} \in \mathbb{R}^{S^{a^n}\times S^{a^n}}$, $Q^{b^n} \in \mathbb{R}^{S^{b^n}\times S^{b^n}}$, $Q^{\theta^n} \in \mathbb{R}^{S^{\theta^n}\times S^{\theta^n}}$

and $Q^f \in \mathbb{R}^{S^f \times S^f}$ are such that

$$(Q^{a^n})_{is} := (A^{\boldsymbol{n}}_{\gamma,s})_{n_i^{a^n} m_i^{a^n}}, \qquad \forall i, s \in \{1{:}S^{a^n}\}, \tag{4.77a}$$

$$(Q^{b^n})_{is} := (B^{\boldsymbol{n}}_{\gamma,s})_{n_i^{b^n} m_i^{b^n}}, \qquad \forall i, s \in \{1{:}S^{b^n}\}, \tag{4.77b}$$

$$(Q^{\theta^n})_{is} := (\Theta^{\boldsymbol{n}}_{\gamma,s})_{m_i^{\theta^n}}, \qquad \forall i, s \in \{1{:}S^{\theta^n}\}, \tag{4.77c}$$

$$(Q^f)_{is} := (F_s)_{m_i^f}, \qquad \forall i, s \in \{1{:}S^f\}. \tag{4.77d}$$

By construction, these matrices are lower-triangular with unit diagonal. Consequently, these matrices are invertible and their inverse can be easily computed once and for all during the offline phase. Combining (4.68) with (4.71), we obtain the following approximate decompositions:

$$A^{\boldsymbol{n}}_{\gamma,N}(\mu) \approx \quad E^{a^n}_N(\mu) := \sum_{s\in\{1:S^{a^n}\}} \alpha^{a^n}_{N,s}(\mu) A^{\boldsymbol{n}}_{\gamma,N,s}, \qquad A^{\boldsymbol{n}}_{\gamma,N,s} := Z^\top A^{\boldsymbol{n}}_{\gamma,s} Z \in \mathbb{R}^{N\times N}, \tag{4.78a}$$

$$B^{\boldsymbol{n}}_{\gamma,N}(\mu,k) \approx E^{b^n}_N(\mu,k) := \sum_{s\in\{1:S^{b^n}\}} \alpha^{b^n}_{N,s}(\mu,k) B^{\boldsymbol{n}}_{\gamma,N,s}, \quad B^{\boldsymbol{n}}_{\gamma,N,s} := Z^\top B^{\boldsymbol{n}}_{\gamma,s} Z \in \mathbb{R}^{N\times N}, \tag{4.78b}$$

$$\Theta^{\boldsymbol{n}}_{\gamma,N}(\mu,k) \approx E^{\theta^n}_N(\mu,k) := \sum_{s\in\{1:S^{\theta^n}\}} \alpha^{\theta^n}_{N,s}(\mu,k) \Theta^{\boldsymbol{n}}_{\gamma,N,s}, \quad \Theta^{\boldsymbol{n}}_{\gamma,N,s} := Z^\top \Theta^{\boldsymbol{n}}_{\gamma,s} \in \mathbb{R}^N, \tag{4.78c}$$

$$F_N(\mu) \approx \quad E^f_N(\mu) := \sum_{s\in\{1:S^f\}} \alpha^f_{N,s}(\mu) F_{N,s}, \qquad F_{N,s} := Z^\top F_s \in \mathbb{R}^N, \tag{4.78d}$$

which lead to an efficient offline/online decomposition since the parameter-independent arrays $A^{\boldsymbol{n}}_{\gamma,N,s}$, $B^{\boldsymbol{n}}_{\gamma,N,s}$, $\Theta^{\boldsymbol{n}}_{\gamma,N,s}$ and $F_{N,s}$ are small-dimensional and can be computed once and for all during the offline phase. Finally, using the approximations from (4.78) in (4.67) (for simplicity, we keep the same notation for the unknown $\boldsymbol{\Delta U}_{N,k}(\mu)$), we consider the following sequence of problems: For all $(\mu,k) \in \mathcal{D}\times\mathbb{N}$, find $\boldsymbol{\Delta U}_{N,k}(\mu) \in \mathbb{R}^N$ such that

$$E^{a^n}_N(\mu)\boldsymbol{\Delta U}_{N,k}(\mu) + E^{b^n}_N(\mu,k)\boldsymbol{\Delta U}_{N,k}(\mu) = -E^{r^n}_N(\mu,k), \tag{4.79}$$

where $E^{r^n}_N(\mu,k)$ is given by

$$E^{r^n}_N(\mu,k) := E^{a^n}_N(\mu)\boldsymbol{U}_{N,k}(\mu) + E^{\theta^n}_N(\mu,k) - E^f_N(\mu). \tag{4.80}$$

The convergence criterion for (4.79) is still (4.26) using the reconstructed functions. We denote the converged solution to the sequence of problems (4.79) as $\boldsymbol{U}_{N,\mathrm{cv}}(\mu) \in \mathbb{R}^R$ and the associated reconstructed solution as $\boldsymbol{u}_{N,\mathrm{cv}}(\mu) \in \boldsymbol{\mathcal{V}}(\mu)$.

To summarize, our RB procedure is organized as follows:

— Offline stage

1. Select a training subset $\mathcal{D}_{\texttt{train}} := \{\mu_p\}_{p\in\{1:P\}} \subset \mathcal{D}$.
2. Compute the HF snapshots $\{\boldsymbol{U}_{\mathrm{cv}}(\mu_p)\}_{p\in\{1:P\}} \subset \mathbb{R}^{\mathcal{N}^{\mathrm{HF}}}$ by solving (4.29).
3. Compute the reduced space $\boldsymbol{V}_N$ by using POD on the snapshots.
4. Compute the high-dimensional arrays $A^{\boldsymbol{n}}_{\gamma,s}$, $B^{\boldsymbol{n}}_{\gamma,s}$, $\Theta^{\boldsymbol{n}}_{\gamma,s}$ and F_s by using the EIM.

5. Invert the interpolation matrices Q^{a^n}, Q^{b^n}, Q^{θ^n} and Q^f.
6. Compute the small-dimensional arrays $A^{n}_{\gamma,N,s}$, $B^{n}_{\gamma,N,s}$, $\Theta^{n}_{\gamma,N,s}$ and $F_{N,s}$ by using (4.78).

— Online stage: For any $\mu \in \mathcal{D} \setminus \mathcal{D}_{\texttt{train}}$,

1. Evaluate $T^{a^n}(\mu)$ and $T^f(\mu)$ and compute $\alpha_N^{a^n}(\mu)$ and $\alpha_N^f(\mu)$ by using (4.75a) and (4.75d).
2. Evaluate $E_N^{a^n}(\mu)$ and $E_N^f(\mu)$ by using (4.78a) and (4.78d).
3. Loop on $k \geq 0$,
   (a) Evaluate $T^{b^n}(\mu,k)$ and $T^{\theta^n}(\mu,k)$ and compute $\alpha_N^{b^n}(\mu,k)$ and $\alpha_N^{\theta^n}(\mu,k)$ by using (4.75b) and (4.75c).
   (b) Evaluate $E_N^{b^n}(\mu,k)$ and $E_N^{\theta^n}(\mu,k)$ by using (4.78b) and (4.78c).
   (c) Solve (4.79).
   (d) Check convergence; if not, set $k \leftarrow k+1$ and go back to (3a).

For the contact problem with friction, the RB formulation is obtained in exactly the same way. We simply replace the forms $a_\gamma^{n}(\mu;\cdot,\cdot)$, $b_\gamma^{n}(\mu;\cdot;\cdot,\cdot)$ and $r_\gamma^{n}(\mu;\cdot;\cdot)$ by the forms $a_\gamma^{n\tau}(\mu;\cdot,\cdot)$, $b_\gamma^{n\tau}(\mu;\cdot;\cdot,\cdot)$ and $r_\gamma^{n\tau}(\mu;\cdot;\cdot)$ for Tresca's friction, and by the forms $a_\gamma^{n\tau}(\mu;\cdot,\cdot)$, $b_\gamma^{n\tau^c}(\mu;\cdot;\cdot,\cdot)$ and $r_\gamma^{n\tau^c}(\mu;\cdot;\cdot)$ for Coulomb's friction. Notice that for the EIM approximation, additional affine parametric decompositions are performed on the large-dimensional arrays $B_\gamma^{\tau}(\mu,k)$ and $\Theta_\gamma^{\tau}(\mu,k)$ (resp. $B_\gamma^{\tau^c}(\mu,k)$ and $\Theta_\gamma^{\tau^c}(\mu,k)$) for Tresca's friction (resp. Coulomb's friction). We notice that for Coulomb's friction, the realization of the nested algorithm (4.63) within the framework of the RBM is delicate since the affine parametric decomposition requires to separate the dependencies on the triple (μ,n,k). To overcome this difficulty, only converged solutions for the inner iteration (index k) are considered when computing the EIM decompositions of the tangent matrix and the residual.

4.5 Numerical results

We consider the Hertz contact problem between the two half-disks as represented in Figure 4.1. The upper half-disk occupies the deformable domain $\Omega_1(\mu) \subset \mathbb{R}^2$ of parametric radius

$$R_1 := \mu \in \mathcal{D} := \Big[0.7, 1.3\Big](\text{m}), \tag{4.81}$$

and the lower half-disk the rigid domain $\Omega_2 \subset \mathbb{R}^2$ of fixed radius $R_2 := 1\text{m}$. The initial gap between the two half-disks is equal to $g_0 > 0$. We impose a displacement of $-d$ on $\Gamma_1^{\texttt{top}}(\mu)$ of $\Omega_1(\mu)$ with $d \geq g_0$. The initial gap g_0 and the imposed displacement d are, respectively, set to $g_0 := 0.001\text{m}$ and $d := 0.09\text{m}$. This latter value, which is less than 10% of the maximum value of R_1 allows us to remain within the validity of the small deformation assumption. Notice that since Ω_2 is rigid and fixed, we only mesh the domain $\Omega_1(\mu)$ and set $\Omega(\mu) := \Omega_1(\mu)$ to build the HF space. The material parameters are $E := 15\text{Pa}$ for the Young modulus and $\nu := 0.35$ for the Poisson coefficient. The

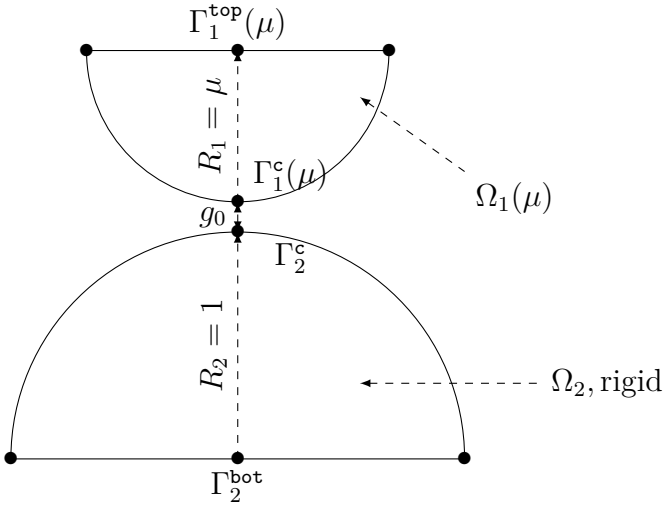

Figure 4.1 – Frictionless Hertz test case: Configuration.

training set is chosen as $\mathcal{D}_{\mathtt{train}} := \left\{0.7 + 0.0075i, 0 \leq i \leq 60\right\}$(m) (altogether 61 points), and the validation set $\mathcal{D}_{\mathtt{valid}}$ is generated by choosing 30 elements in $\mathcal{D}$ randomly with a uniform distribution.

We consider the reference domain $\widehat{\Omega}_1 := \Omega_1(1)$ and introduce the geometric mapping $h_1(\mu) : \widehat{\Omega}_1 \to \Omega_1(\mu)$ defined as $h_1(\mu)(\boldsymbol{x}) := \mu\boldsymbol{x}$, for all $\boldsymbol{x} \in \widehat{\Omega}_1$, with the origin located at the center of $\widehat{\Omega}_1$. We use a mesh composed of 1956 nodes with 633 nodes on the potential contact manifold $\widehat{\Gamma}_1^{\mathtt{c}}$ which is the part of the half circle $\widehat{\Gamma}_1^{\mathtt{c}}$ of angle $\theta \in [-\frac{5\pi}{8}, -\frac{3\pi}{8}]$ with respect to the horizontal axis. For all $\mu \in \mathcal{D}$, we equip the space $\boldsymbol{\mathcal{V}}(\mu)$ with the norm $\|\cdot\|_{\boldsymbol{\mathcal{V}}(\mu)}$ defined as follows:

$$\|\boldsymbol{v}\|_{\boldsymbol{\mathcal{V}}(\mu)} := \left(\|\boldsymbol{v}\|^2_{L^2(\Omega(\mu))} + \widehat{\ell}^2\|\nabla\boldsymbol{v}\|^2_{L^2(\Omega(\mu))}\right)^{\frac{1}{2}}, \quad \forall \boldsymbol{v} \in \boldsymbol{\mathcal{V}}(\mu), \tag{4.82}$$

where the characteristic length $\widehat{\ell}$ is the radius of $\widehat{\Omega}_1$ and is introduced for dimensional consistency. The HF and RB computations use the python library of the finite element software `getfem` [93].

4.5.1 Frictionless case

We first consider the frictionless Hertz contact problem.

4.5.1.1 Results using Nitsche's method

For the discretization, we use $\mathbb{P}_2$ Lagrange finite elements leading to $\mathcal{N}^{\mathrm{HF}} := 14918$ degrees of freedom. We choose $\gamma := \frac{\gamma_0}{h}$ with $\gamma_0 := 50\mu^{\mathrm{Lamé}}$, where $h := 2.5$mm refers to the mesh size and $\mu^{\mathrm{Lamé}} := \frac{E}{2(1+\nu)}$Pa refers to the second Lamé parameter.

Figure 4.2 displays the deformed configurations resulting from the HF displacement fields $\boldsymbol{u}(\mu)$ for $\mu = 0.7$m (left panel) and for $\mu = 1.3$m (right panel). We can see that we use a symmetric mesh. This is important because it guarantees the symmetry of the HF snapshots. Indeed, if the snapshots are not symmetric, the resulting POD modes will not be either. Consequently, the reduced model looses this symmetry

property, leading to reduced solutions of poorer quality. Moreover, we have discretized a complete half-disk instead of a quarter-disk to avoid some difficulties when enforcing the symmetry condition at the lowest point of $\Omega_1(\mu)$ in the case of the frictional contact problems (see Section 4.5.2).

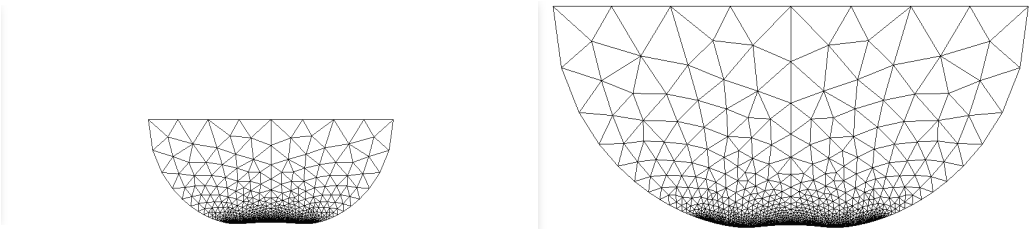

Figure 4.2 – Frictionless Hertz test case, Nitsche's method: $\boldsymbol{u}(\mu)$. Left: $\mu = 0.7$m; Right: $\mu = 1.3$m.

Figure 4.3 displays the superposition of the normal stress $\sigma_{\boldsymbol{nn}}(\boldsymbol{u}(\mu))$ and its Alart–Curnier reformulation $\left[P^{\boldsymbol{n}}_{\gamma,g}(\mu;\boldsymbol{u}(\mu))\right]_-$ (Row 1) and the gap on the deformed configuration $u_{\boldsymbol{n}}(\mu) - g(\mu)$ (Row 2) as a function of the abscissa along $\Gamma^{\mathrm{c}}(\mu)$ for $\mu = 0.7$m (Column 1), $\mu = 1$m (Column 2), and $\mu = 1.3$m (Column 3). We see that the normal

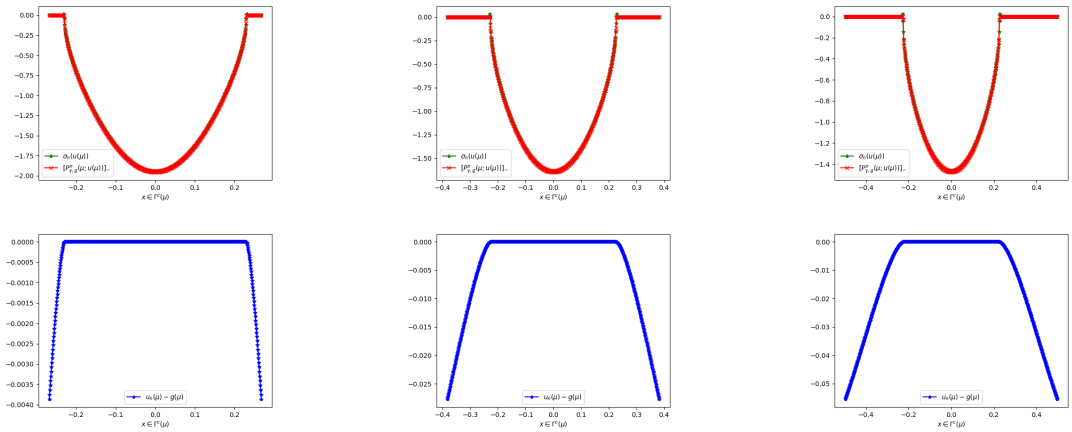

Figure 4.3 – Frictionless Hertz test case; Nitsche's method. Row 1: $\sigma_{\boldsymbol{nn}}(\boldsymbol{u}(\mu))$ and $[P^{\boldsymbol{n}}_{\gamma,g}(\mu;\boldsymbol{u}(\mu))]_-$. Row 2: $u_{\boldsymbol{n}}(\mu) - g(\mu)$. Column 1: $\mu = 0.7$m. Column 2: $\mu = 1.0$m. Column 3: $\mu = 1.3$m.

stress is of good quality (with almost no spurious oscillations) and matches very well with its counterpart $\left[P^{\boldsymbol{n}}_{\gamma,g}(\mu;\boldsymbol{u}(\mu))\right]_-$ resulting from the Alart–Curnier reformulation. We also see that the negativity condition on the gap $u_{\boldsymbol{n}}(\mu) - g(\mu)$ is satisfied on the whole potential contact manifold $\Gamma^{\mathrm{c}}(\mu)$. To have a better look at Signorini's contact conditions, we display in Table 4.1 the relative error on the Alart–Curnier reformulation of Signorini's contact conditions defined as follows:

$$e^{\boldsymbol{n}}_{\mathrm{AC}}(\mu) := \frac{\|\sigma_{\boldsymbol{nn}}(\boldsymbol{u}(\mu)) - [P^{\boldsymbol{n}}_{\gamma,g}(\mu;\boldsymbol{u}(\mu))]_-\|_{\ell^2(\Gamma^{\mathrm{c}}(\mu))}}{\|\sigma_{\boldsymbol{nn}}(\boldsymbol{u}(\mu))\|_{\ell^2(\Gamma^{\mathrm{c}}(\mu))}}, \tag{4.83}$$

where the discrete $\ell^2(\Gamma^{\mathrm{c}}(\mu))$-norms are sampled at the mesh nodes located on $\Gamma^{\mathrm{c}}(\mu)$. For the three values of the parameter $\mu \in \{0.7, 1, 1.3\}$(m), we consider three values of the

mesh size h, namely $h = 5$mm (coarse), $h = 2.5$mm (medium) and $h = 1.25$mm (fine). We notice that the relative error $e^{\boldsymbol{n}}_{\mathrm{AC}}(\mu)$ is smaller than 1.5% for the three parameters values and for the three mesh sizes. Moreover, we see that the error decreases when h decreases, thereby indicating the convergence of the approximation. More precisely, we observe a convergence of order 1 for the approximation of $\sigma_{\boldsymbol{nn}}(\boldsymbol{u}(\mu))$ (with a slight order reduction for the larger value of μ). Thus, we can say that the Signorini contact conditions are globally satisfied with a good accuracy although they are not strictly enforced.

μ(m)	0.7			1			1.3		
h(mm)	5	2.5	1.25	5	2.5	1.25	5	2.5	1.25
$e^{\boldsymbol{n}}_{\mathrm{AC}}(\%)$	1	0.52	0.28	1.45	0.72	0.33	1.17	1.1	0.43

Table 4.1 – Frictionless Hertz test case, Nitsche's method: Relative error $e^{\boldsymbol{n}}_{\mathrm{AC}}(\mu)$ for $\mu \in \{0.7, 1.0, 1.3\}$(m) and the mesh sizes $h \in \{5, 2.5, 1.25\}$(mm).

Let us consider the relative POD projection error defined as follows:

$$e_{\mathtt{POD}}(N) := \frac{\left(\sum\limits_{p\in\{1:P\}} \left\| \left(\mathbb{I}_{\mathbb{R}^{\mathcal{N}^{\mathrm{HF}}}} - \Pi_{\boldsymbol{V}_N} \right) (\boldsymbol{U}_{\mathrm{cv}}(\mu_p)) \right\|^2_{\mathbb{W}(\mu_p)} \right)^{\frac{1}{2}}}{\left(\sum\limits_{p\in\{1:P\}} \|\boldsymbol{U}_{\mathrm{cv}}(\mu_p)\|^2_{\mathbb{W}(\mu_p)} \right)^{\frac{1}{2}}}, \tag{4.84}$$

where $\Pi_{\boldsymbol{V}_N}$ denotes the orthogonal projection onto $\boldsymbol{V}_N \subset \mathbb{R}^{\mathcal{N}^{\mathrm{HF}}}$ and $\mathbb{W}(\mu_p)$ the Gram matrix of the inner product associated with $H^1(\Omega(\mu_p); \mathbb{R}^d)$. We consider two different training sets, the first with cardinality 61 and the second with cardinality 201. Figure 4.4 shows the relative projection error $e_{\mathtt{POD}}(N)$ produced by the POD algorithm as a function of the number of vectors composing the reduced basis for both training sets. In all cases, we notice that the projection error decreases sufficiently fast so that indeed the linear spaces generated by the snapshots can be approximated by small-dimensional subspaces. We also observe a fast decrease of the POD error for the first 15 modes before a slower decrease occurs at error levels between 10^{-5} and 10^{-6} (resp. 10^{-5} and 10^{-7}) for the first (resp. second) training set.

For the EIM approximation, the training sets $\mathcal{E}^{b^{\boldsymbol{n}}}_{\mathtt{train}}$ and $\mathcal{E}^{\theta^{\boldsymbol{n}}}_{\mathtt{train}}$ introduced in (4.73) are of cardinality 897. We fix a tolerance $\delta_{\mathtt{EIM}} := 10^{-6}$ to bound the errors resulting from (4.71). With this choice, we obtain $S^{b^{\boldsymbol{n}}} = 619 \ll \mathcal{N}^{\mathrm{HF}} \times \mathcal{N}^{\mathrm{HF}}$ and $S^{\theta^{\boldsymbol{n}}} = 281 \ll \mathcal{N}^{\mathrm{HF}}$. Notice that in the present test case, we do not need to perform an EIM decomposition on $A^{\boldsymbol{n}}_\gamma(\mu)$ since this matrix is already linearly dependent on μ; moreover, $F(\mu)$ vanishes since we only use an imposed displacement for the load. Figure 4.5 shows the relative EIM interpolation errors for the tangent matrix $B^{\boldsymbol{n}}_\gamma(\mu, \boldsymbol{u}_k(\mu))$ (left panel) and the residual vector $\Theta^{\boldsymbol{n}}_\gamma(\mu, \boldsymbol{u}_k(\mu))$ (right panel) as a function of the rank $S^{b^{\boldsymbol{n}}}$ or $S^{\theta^{\boldsymbol{n}}}$,

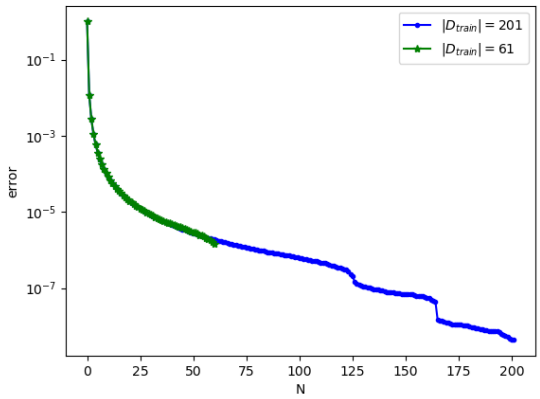

Figure 4.4 – Frictionless Hertz test case, Nitsche's method: Relative POD projection error $e_{\texttt{POD}}(N)$ as function of N, for $|\mathcal{D}_{\texttt{train}}| = 61$ and $|\mathcal{D}_{\texttt{train}}| = 201$.

i.e., we plot

$$e^{b^{\boldsymbol{n}}}_{\texttt{EIM}}(S^{b^{\boldsymbol{n}}}, \mathcal{D}_*) := \frac{\max\limits_{\mu\in\mathcal{D}_*} \max\limits_{k\in\{1:k^{\mathrm{cv}}(\mu)\}} \|B^{\boldsymbol{n}}_\gamma(\mu, \boldsymbol{u}_k(\mu)) - E^{b^{\boldsymbol{n}}}(\mu, k)\|_{\ell^\infty(ij)}}{\max\limits_{\mu\in\mathcal{D}_*} \max\limits_{k\in\{1:k^{\mathrm{cv}}(\mu)\}} \|B^{\boldsymbol{n}}_\gamma(\mu, \boldsymbol{u}_k(\mu))\|_{\ell^\infty(ij)}}, \tag{4.85a}$$

$$e^{\theta^{\boldsymbol{n}}}_{\texttt{EIM}}(S^{\theta^{\boldsymbol{n}}}, \mathcal{D}_*) := \frac{\max\limits_{\mu\in\mathcal{D}_*} \max\limits_{k\in\{1:k^{\mathrm{cv}}(\mu)\}} \|\Theta^{\boldsymbol{n}}_\gamma(\mu, \boldsymbol{u}_k(\mu)) - E^{\theta^{\boldsymbol{n}}}(\mu, k)\|_{\ell^\infty(j)}}{\max\limits_{\mu\in\mathcal{D}_*} \max\limits_{k\in\{1:k^{\mathrm{cv}}(\mu)\}} \|\Theta^{\boldsymbol{n}}_\gamma(\mu, \boldsymbol{u}_k(\mu))\|_{\ell^\infty(j)}}, \tag{4.85b}$$

where for a generic matrix (resp. vector) $M \in \mathbb{R}^{\mathcal{N}^{\mathrm{HF}}\times\mathcal{N}^{\mathrm{HF}}}$ (resp. $V \in \mathbb{R}^{\mathcal{N}^{\mathrm{HF}}}$),

$$\|M\|_{\ell^\infty(ij)} := \max_{(i,j)\in\{1:\mathcal{N}^{\mathrm{HF}}\}\times\{1:\mathcal{R}^{\mathrm{HF}}\}} |M_{ij}|, \tag{4.86a}$$

$$\|V\|_{\ell^\infty(j)} := \max_{j\in\{1:\mathcal{N}^{\mathrm{HF}}\}} |V_j|, \tag{4.86b}$$

and with $\mathcal{D}_*$ either equal to $\mathcal{D}_{\texttt{train}}$ or to $\mathcal{D}_{\texttt{valid}}$. Let us first consider the training set $\mathcal{D}_{\texttt{train}}$. We observe that both errors decrease fast enough to allow accurate approximations. For the tangent matrix $B^{\boldsymbol{n}}_\gamma(\mu, \boldsymbol{u}_k(\mu))$, we notice a quasi-uniform decrease of the relative error $e^{b^{\boldsymbol{n}}}_{\texttt{EIM}}(S^{b^{\boldsymbol{n}}}, \mathcal{D}_{\texttt{train}})$ with an acceleration at error levels between 10^{-3} and 10^{-6}. For the residual vector $\Theta^{\boldsymbol{n}}_\gamma(\mu, \boldsymbol{u}_k(\mu))$, we observe a fast decrease of the relative error $e^{\theta^{\boldsymbol{n}}}_{\texttt{EIM}}(S^{\theta^{\boldsymbol{n}}}, \mathcal{D}_{\texttt{train}})$ for ranks $S^{\theta^{\boldsymbol{n}}}$ between 1 and 40 yielding errors between 1 down to 10^{-2}, and then a significant drop of the error at about $S^{\theta^{\boldsymbol{n}}} = 40$ before a slower decrease occurs at error levels between 10^{-3} and 10^{-6}. Considering the validation set $\mathcal{D}_{\texttt{valid}}$, we additionally plot the relative EIM approximation errors $e^{b^{\boldsymbol{n}},\mathrm{cv}}_{\texttt{EIM}}(S^{b^{\boldsymbol{n}}})$ and $e^{\theta^{\boldsymbol{n}},\mathrm{cv}}_{\texttt{EIM}}(S^{\theta^{\boldsymbol{n}}})$ defined as

$$e^{b^{\boldsymbol{n}},\mathrm{cv}}_{\texttt{EIM}}(S^{b^{\boldsymbol{n}}}) := \frac{\max\limits_{\mu\in\mathcal{D}_{\texttt{valid}}} \|B^{\boldsymbol{n}}_\gamma(\mu, \boldsymbol{u}_{\mathrm{cv}}(\mu)) - E^{b^{\boldsymbol{n}}}(\mu, k^{\mathrm{cv}}(\mu))\|_{\ell^\infty(ij)}}{\max\limits_{\mu\in\mathcal{D}_{\texttt{valid}}} \|B^{\boldsymbol{n}}_\gamma(\mu, \boldsymbol{u}_{\mathrm{cv}}(\mu))\|_{\ell^\infty(ij)}}, \tag{4.87a}$$

$$e^{\theta^{\boldsymbol{n}},\mathrm{cv}}_{\texttt{EIM}}(S^{\theta^{\boldsymbol{n}}}) := \frac{\max\limits_{\mu\in\mathcal{D}_{\texttt{valid}}} \|\Theta^{\boldsymbol{n}}_\gamma(\mu, \boldsymbol{u}_{\mathrm{cv}}(\mu)) - E^{\theta^{\boldsymbol{n}}}(\mu, k^{\mathrm{cv}}(\mu))\|_{\ell^\infty(j)}}{\max\limits_{\mu\in\mathcal{D}_{\texttt{valid}}} \|\Theta^{\boldsymbol{n}}_\gamma(\mu, \boldsymbol{u}_{\mathrm{cv}}(\mu))\|_{\ell^\infty(j)}}. \tag{4.87b}$$

These errors correspond to the relative EIM approximation error at convergence of the iterative algorithm, *i.e.*, when $k = k^{\mathrm{cv}}(\mu)$. For the tangent matrix $B^{\boldsymbol{n}}_{\gamma}(\mu, \boldsymbol{u}_k(\mu))$, considering first $e^{b^{\boldsymbol{n}}}_{\mathtt{EIM}}(S^{b^{\boldsymbol{n}}}, \mathcal{D}_{\mathtt{valid}})$, we notice a quite modest decrease of the error for ranks $S^{b^{\boldsymbol{n}}}$ between 1 and 100 with errors values between 0.95 and 0.7, and then a stagnation of the error at around 0.65. Considering $e^{b^{\boldsymbol{n}},\mathrm{cv}}_{\mathtt{EIM}}(S^{b^{\boldsymbol{n}}})$, we observe instead a rather uniform decrease of the error, with values quite close to those of $e^{b^{\boldsymbol{n}}}_{\mathtt{EIM}}(S^{b^{\boldsymbol{n}}}, \mathcal{D}_{\mathtt{train}})$, before a stagnation occurs at a value of about 10^{-3}. For the residual vector $\Theta^{\boldsymbol{n}}_{\gamma}(\mu, \boldsymbol{u}_k(\mu))$, considering first $e^{\theta^{\boldsymbol{n}}}_{\mathtt{EIM}}(S^{\theta^{\boldsymbol{n}}}, \mathcal{D}_{\mathtt{valid}})$, we observe a stagnation of the error for ranks $S^{\theta^{\boldsymbol{n}}}$ between 1 and 80 with error values between 1 and 0.9, and then a slower decrease at error levels between 0.8 and $5 \cdot 10^{-2}$ with some stagnation phases. Considering $e^{\theta^{\boldsymbol{n}},\mathrm{cv}}_{\mathtt{EIM}}(S^{\theta^{\boldsymbol{n}}})$, we instead observe a stagnation at about 0.5 for ranks $S^{\theta^{\boldsymbol{n}}}$ between 2 and 80, and then a slower decrease with error values between 0.3 down to 10^{-2}. We conclude that the EIM approximation is not very accurate for $\mu \in \mathcal{D}_{\mathtt{valid}}$ and small values of k, whereas the accuracy becomes more satisfactory as $k \to k^{\mathrm{cv}}(\mu)$. Therefore, we may expect some difficulties in achieving convergence in the iterative solvers applied to reduced problems, but if convergence is indeed achieved, the accuracy should be reasonable.

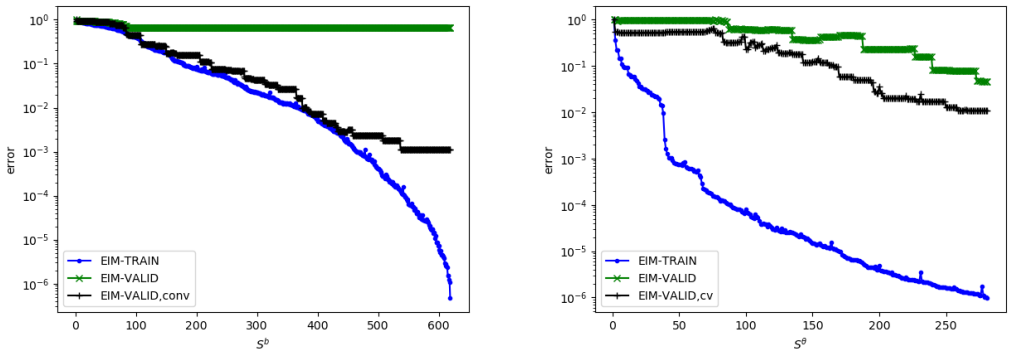

Figure 4.5 – Frictionless Hertz test case, Nitsche's method: Relative EIM approximation errors as a function of the rank $S^{b^{\boldsymbol{n}}}$ or $S^{\theta^{\boldsymbol{n}}}$ of the approximation. Left: $e^{b^{\boldsymbol{n}}}_{\mathtt{EIM}}(S^{b^{\boldsymbol{n}}}, \mathcal{D}_{\mathtt{train}})$, $e^{b^{\boldsymbol{n}}}_{\mathtt{EIM}}(S^{b^{\boldsymbol{n}}}, \mathcal{D}_{\mathtt{valid}})$ and $e^{b^{\boldsymbol{n}},\mathrm{cv}}_{\mathtt{EIM}}(S^{b^{\boldsymbol{n}}})$; Right: $e^{\theta^{\boldsymbol{n}}}_{\mathtt{EIM}}(S^{\theta^{\boldsymbol{n}}}, \mathcal{D}_{\mathtt{train}})$, $e^{\theta^{\boldsymbol{n}}}_{\mathtt{EIM}}(S^{\theta^{\boldsymbol{n}}}, \mathcal{D}_{\mathtt{valid}})$ and $e^{\theta^{\boldsymbol{n}},\mathrm{cv}}_{\mathtt{EIM}}(S^{\theta^{\boldsymbol{n}}})$.

We denote by $e^{\boldsymbol{u}}_N(\mu)$ (resp. $e^{\boldsymbol{nn}}_N(\mu)$) the relative RB approximation error on the displacement (resp. normal stress) defined as

$$e^{\boldsymbol{u}}_N(\mu) := \frac{\|\boldsymbol{u}_{\mathrm{cv}}(\mu) - \boldsymbol{u}_{N,\mathrm{cv}}(\mu)\|_{\boldsymbol{\mathcal{V}}(\mu)}}{\|\boldsymbol{u}_{\mathrm{cv}}(\mu)\|_{\boldsymbol{\mathcal{V}}(\mu)}}, \tag{4.88a}$$

$$e^{\boldsymbol{nn}}_N(\mu) := \frac{\|\sigma_{\boldsymbol{nn}}(\boldsymbol{u}_{\mathrm{cv}}(\mu)) - \sigma_{\boldsymbol{nn}}(\boldsymbol{u}_{N,\mathrm{cv}}(\mu))\|_{\ell^2(\Gamma^{\mathrm{c}}(\mu))}}{\|\sigma_{\boldsymbol{nn}}(\boldsymbol{u}_{\mathrm{cv}}(\mu))\|_{\ell^2(\Gamma^{\mathrm{c}}(\mu))}}, \tag{4.88b}$$

and introduce the relative error measures $e^{u}_{N,\max}$ and $e^{\boldsymbol{nn}}_{N,\max}$ defined as

$$e^{\boldsymbol{u}}_{N,\max} := \max_{\mu \in \mathcal{D}_{\mathtt{valid}}} e^{\boldsymbol{u}}_N(\mu), \qquad e^{\boldsymbol{nn}}_{N,\max} := \max_{\mu \in \mathcal{D}_{\mathtt{valid}}} e^{\boldsymbol{nn}}_N(\mu). \tag{4.89}$$

Figure 4.6 displays $e^{\boldsymbol{u}}_{N,\max}$ (left panel) and $e^{\boldsymbol{nn}}_{N,\max}$ (right panel) as a function of the number of vectors composing the reduced basis. We only consider RB dimensions N

larger than 10. Indeed, for smaller values, the iterative algorithm does not converge for some values of the parameter μ. This can be explained by the poor quality of the EIM approximation of the tangent matrix $B^{\boldsymbol{n}}_{\gamma,N}(\mu, k)$ for small values of N due to the fact that the RB solution at the first iterations of the iterative algorithm on the reduced model is quite far from the HF solution on which the training of the EIM is performed. We also observe some convergence difficulties for values of the parameter μ larger than 1.2m. For this reason, we consider a validation set $\mathcal{D}_{\texttt{valid}}$ restricted to the interval $[0.7, 1.18]$(m). In Figure 4.6, we superpose the plain RBM approximation error (without any EIM) and the RBM-EIM approximation error. We observe that similar errors are obtained for plain RBM and RBM-EIM. This confirms the good quality of the EIM approximations at convergence as claimed above. With both approaches, we notice a stagnation of the relative error at about 10^{-4} from about 40 modes, in agreement with the stagnation observed on the POD projection error.

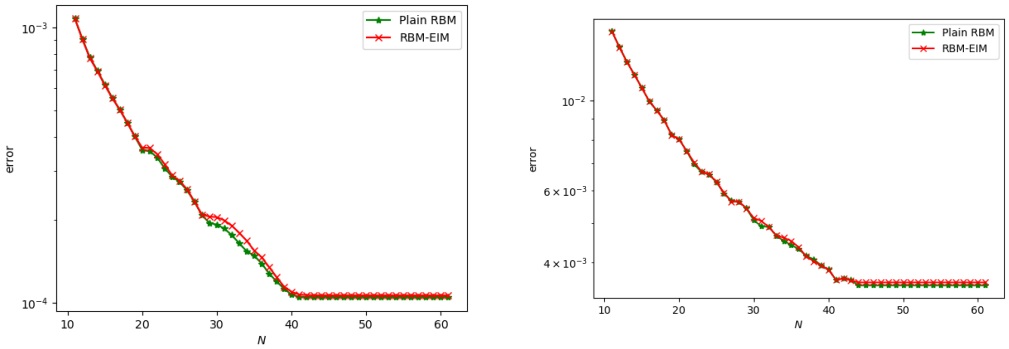

Figure 4.6 – Frictionless Hertz test case, Nitsche's method: RBM approximation errors for $|\mathcal{D}_{\texttt{train}}| = 61$. Left: $e^{\boldsymbol{u}}_{N,\max}$; Right: $e^{\boldsymbol{nn}}_{N,\max}$.

4.5.1.2 Comparison with the mixed formulation

For the comparison, we consider the primal-dual formulation employed in [84] with $\mathbb{P}_2$ finite elements for displacement and $\mathbb{P}_1$ finite elements for the Lagrange multiplier. With this choice of the discretization, we can compare on a fair basis the HF displacements obtained with the mixed formulation and with Nitsche's method. We display in Figure 4.7 the HF energy $\mathcal{J}(\mu; \boldsymbol{u}(\mu))$ (see (4.11)) for all $\mu \in \mathcal{D}_{\texttt{train}}$. We notice that we obtain (in the eyeball norm) the same values for the two methods for all $\mu \in \mathcal{D}_{\texttt{train}}$. Thus, although the constraints are not strictly imposed with Nitsche's method, we obtain a satisfactory accuracy for the quality of the solution in comparison with the mixed formulation. We can also see that the energy decreases with the parameter radius μ of the half-disk $\Omega(\mu)$. The complementary condition is not reported since it is on the order of the machine precision (10^{-14}N/m) as expected with the primal-dual formulation since the constraints are exactly enforced.

In contrast to Nitsche's method, in the mixed formulation, it is necessary to stabilize the RBM in order to ensure inf-sup stability for the pair of primal/dual reduced spaces. For this purpose, we use the Projected Greedy Algorithm (PGA) algorithm from [84] with a tolerance $\delta_{\texttt{PGA}} := \sup_{\mu \in \mathcal{D}_{\texttt{train}}} \frac{\beta_{\mathrm{HF}}(\mu)}{c_{\mathrm{HF}}(\mu)} = 0.047$ so that the stability condition

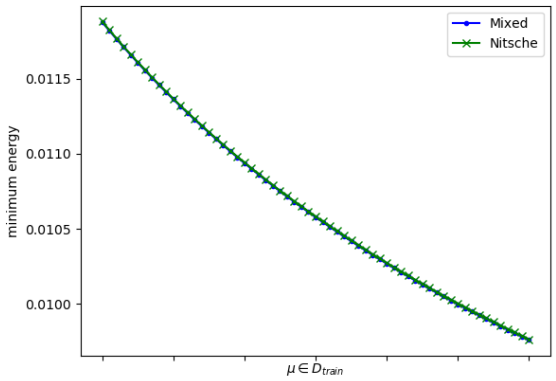

Figure 4.7 – Frictionless Hertz test case: Comparison of the HF energy $\mathcal{J}(\mu; \boldsymbol{u}(\mu))$ between the mixed formulation and Nitsche's method for all $\mu \in \mathcal{D}_{\texttt{train}}$.

established from [84, Prop 3.1] is fulfilled. We denote by $e^{\boldsymbol{u}}_{N,R}(\mu)$ (resp. $e^{\lambda}_{N,R}(\mu)$) the primal (resp. dual) relative RB approximation error defined as follows:

$$e^{\boldsymbol{u}}_{N,R}(\mu) := \frac{\|\boldsymbol{u}(\mu) - \boldsymbol{u}_N(\mu)\|_{\boldsymbol{\mathcal{V}}(\mu)}}{\|\boldsymbol{u}(\mu)\|_{\boldsymbol{\mathcal{V}}(\mu)}}, \quad e^{\lambda}_{N,R}(\mu) := \frac{\|\lambda(\mu) - \lambda_R(\mu)\|_{\ell^2(\Gamma^c(\mu))}}{\|\lambda(\mu)\|_{\ell^2(\Gamma^c(\mu))}}, \tag{4.90}$$

and introduce the relative primal (resp. dual) error measure $e^{\boldsymbol{u}}_{N,R,\max}$ (resp. $e^{\lambda}_{N,R,\max}$) defined as

$$e^{\boldsymbol{u}}_{N,R,\max} := \max_{\mu \in \mathcal{D}_{\texttt{valid}}} e^{\boldsymbol{u}}_{N,R}(\mu), \quad e^{\lambda}_{N,R,\max} := \max_{\mu \in \mathcal{D}_{\texttt{valid}}} e^{\lambda}_{N,R}(\mu). \tag{4.91}$$

Figure 4.8 displays the quantity $e^{\boldsymbol{u}}_{N,R,\max}$ (resp. $e^{\lambda}_{N,R,\max}$) on the left (resp. right) panel as a function of the dimension of the reduced primal basis (after stabilization) for three values of the dimension of the reduced dual basis R, namely $R = 10$, $R = 30$ and $R = 40$. In addition, we plot the relative error $e^{\boldsymbol{u}}_{N,\max}$ (resp. $e^{\boldsymbol{nn}}_{N,\max}$) in the left (resp. right) panel in order to compare the displacement (resp. normal stress) error between the mixed and Nitsche approaches. Considering the mixed approach, we notice a stagnation for all errors after a certain number of primal modes N. For the primal error, there is a clear decrease of the error as a function of the dimension of the dual basis R. However, for the dual error, although the error decreases, we observe some oscillations for certain values of the dimension of the primal basis N (compare the errors for $R = 30$ and $R = 40$). This can be explained by the fact that the dual basis obtained with the mCPG algorithm is not orthonormal (owing to the sign constraints on the Lagrange multiplier, since an orthonormalization process cannot be performed). Moreover, the higher the number of vectors in the dual basis, the more the orthogonality property is lost, and this fact introduces noise in the reduced model. In terms of accuracy, we observe that we have a better approximation for the primal variable (error of the order of 10^{-4}m) than for the dual variable (error of the order of 10^{-2}Pa) in the mixed formulation. These results illustrate the fact that it is very difficult to reduce the dual space, and therefore further motivate the use of purely primal methods like Nitsche's method in the RBM framework applied to contact problems. Finally, comparing the

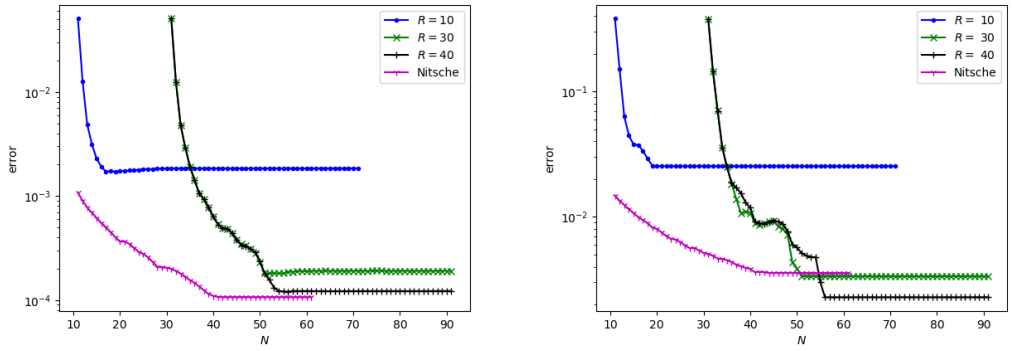

Figure 4.8 – Frictionless Hertz test case, mixed method: RBM approximation errors. Right: displacement errors $e^{\boldsymbol{u}}_{N,R,\max}$ and $e^{\boldsymbol{u}}_{N,\max}$; Left: normal stress errors $e^{\lambda}_{N,R,\max}$ and $e^{\boldsymbol{nn}}_{N,\max}$.

mixed and Nitsche formulations, we observe that the displacement error for the latter is better than for the former for the three values of the dimension of the dual reduced cone. Instead, comparing the error on the normal stress, we observe that the error for the former is slightly better when $R = 40$, but the dimension of the primal reduced space is much larger owing to the need to ensure inf-sup stability.

4.5.2 Friction case

Let us now consider the Tresca and Coulomb frictional Hertz contact problems. We choose a threshold $s = 0.1$ for Tresca's friction and a friction coefficient $\nu_{\mathcal{F}} = 0.1$ for Coulomb's friction. The parameter γ and the mesh size h are the same as for the frictionless case (see Section 4.5.1.1). For Coulomb's friction, we use the iterative algorithm based on the double-nested loop.

Figure 4.9 displays the superposition of the tangential stress $\boldsymbol{\sigma}_{\boldsymbol{n\tau}}(\boldsymbol{u}(\mu))$ and its Alart–Curnier reformulation $[P^{\boldsymbol{\tau}}_{\gamma}(\mu;\boldsymbol{u}(\mu))]_s$ (resp. $[P^{\boldsymbol{\tau}}_{\gamma}(\mu;\boldsymbol{u}(\mu))]_{s^{\mathrm{c}}(\mu;\boldsymbol{u}(\mu))}$) (Row 1) (resp. (Row 2)) for Tresca's (resp. Coulomb's) friction as a function of the abscissa along $\Gamma^{\mathrm{c}}(\mu)$ for $\mu = 0.7$m (Column 1), $\mu = 1$m (Column 2), and $\mu = 1.3$m (Column 3). For Tresca's friction, we observe that the tangential stress matches very well with its counterpart $[P^{\boldsymbol{\tau}}_{\gamma}(\mu;\boldsymbol{u}(\mu))]_s$ resulting from the Alart–Curnier reformulation. However, we observe some oscillations on $\boldsymbol{\sigma}_{\boldsymbol{n\tau}}(\boldsymbol{u}(\mu))$ at the end of the effective contact zone (contact/non-contact transition zone) and at the end of the potential contact zone. We also notice that the tangential stress is not zero outside the effective contact zone, which is consistent with a known (undesirable) feature of Tresca's model, namely to predict friction without contact. For Coulomb's friction, we observe that the tangential stress is of good quality (with almost no spurious oscillations) and matches very well with its counterpart $[P^{\boldsymbol{\tau}}_{\gamma}(\mu;\boldsymbol{u}(\mu))]_{s^{\mathrm{c}}(\mu;\boldsymbol{u}(\mu))}$ resulting from the Alart–Curnier reformulation. To have a better look at the friction conditions, we display in Table 4.2 the relative errors on the Alart–Curnier reformulation of the Tresca and Coulomb friction conditions

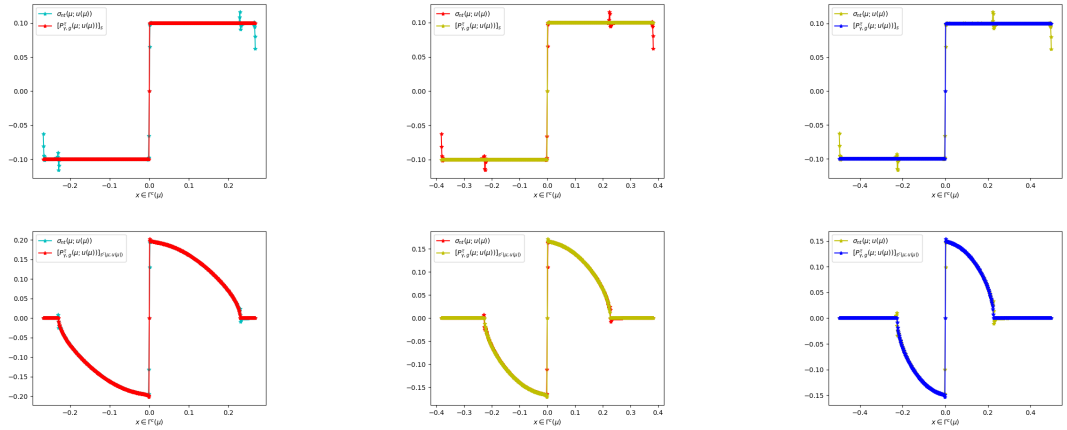

Figure 4.9 – Frictional Hertz test case; Nitsche's method. Row 1: $\boldsymbol{\sigma}_{\boldsymbol{n\tau}}(\boldsymbol{u}(\mu))$ and $[P_\gamma^{\boldsymbol{\tau}}(\mu;\boldsymbol{u}(\mu))]_s$. Row 2: $\boldsymbol{\sigma}_{\boldsymbol{n\tau}}(\boldsymbol{u}(\mu))$ and $[P_\gamma^{\boldsymbol{\tau}}(\mu;\boldsymbol{u}(\mu))]_{s^{\mathrm{c}}(\mu;\boldsymbol{u}(\mu))}$. Column 1: $\mu = 0.7$m. Column 2: $\mu = 1.0$m. Column 3: $\mu = 1.3$m.

defined as follows:

$$e_{\mathrm{AC}}^{\boldsymbol{n\tau},\mathrm{T}}(\mu) := \frac{\|\boldsymbol{\sigma}_{\boldsymbol{n\tau}}(\boldsymbol{u}(\mu)) - [P_\gamma^{\boldsymbol{\tau}}(\mu;\boldsymbol{u}(\mu))]_s\|_{\ell^2(\Gamma^{\mathrm{c}}(\mu))}}{\|\sigma_{\boldsymbol{nn}}(\boldsymbol{u}(\mu))\|_{\ell^2(\Gamma^{\mathrm{c}}(\mu))}}, \tag{4.92a}$$

$$e_{\mathrm{AC}}^{\boldsymbol{n\tau},\mathrm{C}}(\mu) := \frac{\|\boldsymbol{\sigma}_{\boldsymbol{n\tau}}(\boldsymbol{u}(\mu)) - [P_\gamma^{\boldsymbol{\tau}}(\mu;\boldsymbol{u}(\mu))]_{s^{\mathrm{c}}(\mu;\boldsymbol{u}(\mu))}\|_{\ell^2(\Gamma^{\mathrm{c}}(\mu))}}{\|\sigma_{\boldsymbol{nn}}(\boldsymbol{u}(\mu))\|_{\ell^2(\Gamma^{\mathrm{c}}(\mu))}}. \tag{4.92b}$$

For the three values of the parameter $\mu \in \{0.7, 1, 1.3\}$(m), we consider three values of the mesh size h, namely $h = 5$mm (coarse), $h = 2.5$mm (medium) and $h = 1.25$mm (fine). We notice that the relative error $e_{\mathrm{AC}}^{\boldsymbol{n\tau},\mathrm{T}}(\mu)$ (resp. $e_{\mathrm{AC}}^{\boldsymbol{n\tau},\mathrm{C}}(\mu)$) is smaller than 6% (resp. 7%) for the three parameters values and for the three mesh sizes. Moreover, we see that the errors decrease when h decreases, thereby indicating the convergence of the approximation. More precisely, we observe a convergence of order $\frac{1}{2}$ for the approximation of $\boldsymbol{\sigma}_{\boldsymbol{n\tau}}(\boldsymbol{u}(\mu))$ for both Tresca's and Coulomb's friction. Notice that this order is different from the one observed in the frictionless case (order 1). Thus, we can say that the friction conditions are globally satisfied with a good accuracy as for the Signorini contact conditions although they are not strictly enforced.

μ(m)	0.7			1			1.3		
h(m)	5	2.5	1.25	5	2.5	1.25	5	2.5	1.25
$e_{\mathrm{AC}}^{\boldsymbol{n\tau},\mathrm{T}}$(%)	5.49	3.33	2.36	5.5	3.35	2.33	5.76	3.4	2.37
$e_{\mathrm{AC}}^{\boldsymbol{n\tau},\mathrm{C}}$(%)	4.34	3.03	2.12	5.51	3.63	2.57	6.65	4.46	3.16

Table 4.2 – Frictional Hertz test case, Nitsche's method: Relative errors $e_{\mathrm{AC}}^{\boldsymbol{n\tau},\mathrm{T}}(\mu)$ and $e_{\mathrm{AC}}^{\boldsymbol{n\tau},\mathrm{C}}(\mu)$ for $\mu \in \{0.7, 1.0, 1.3\}$(m) and the mesh sizes $h \in \{5, 2.5, 1.25\}$(mm).

Figure 4.10 shows the relative projection error $e_{\mathtt{POD}}(N)$ produced by the POD algorithm (see (4.84)) as a function of the number of vectors composing the reduced

basis for Tresca's (left panel) and Coulomb's (right panel) friction. We see that similar errors are obtained for the two friction models. In both cases, we notice that the projection error decreases sufficiently fast so that indeed the linear spaces generated by the snapshots can be approximated by small-dimensional subspaces. We also observe a fast decrease of the POD error for the first 15 modes before a slower decrease occurs at relative error levels between 10^{-5} and 10^{-6}.

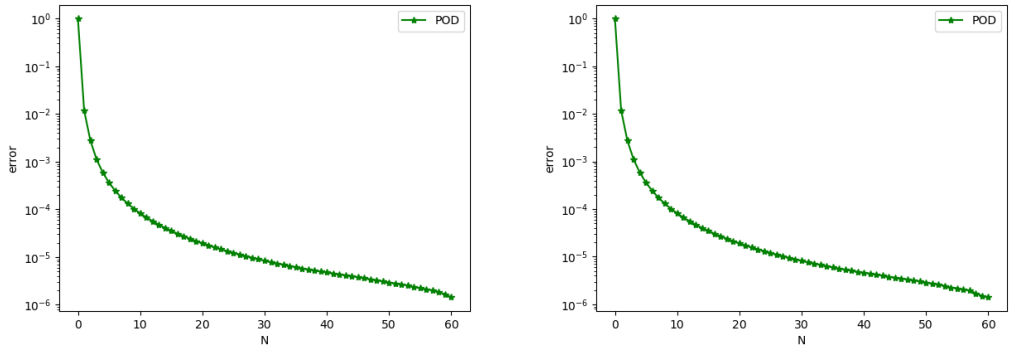

Figure 4.10 – Frictional Hertz test case, Nitsche's method: Relative POD projection error $e_{\texttt{POD}}(N)$ as function of N, for $|\mathcal{D}_{\texttt{train}}| = 61$. Left: Tresca; Right: Coulomb.

Let us first discuss Tresca's friction for which the training sets $\mathcal{E}^{b^{n\tau}}_{\texttt{train}}$, $\mathcal{E}^{\theta^n}_{\texttt{train}}$ and $\mathcal{E}^{\theta^\tau}_{\texttt{train}}$ are of cardinality 898. For the EIM approximation, we fix a tolerance $\delta_{\texttt{EIM}} := 10^{-6}$. With this choice, we obtain $S^{b^{n\tau}} = 630 \ll \mathcal{N}^{\mathrm{HF}} \times \mathcal{N}^{\mathrm{HF}}$, $S^{\theta^n} = 291 \ll \mathcal{N}^{\mathrm{HF}}$ and $S^{\theta^\tau} = 3 \ll \mathcal{N}^{\mathrm{HF}}$. For the same reason as for the frictionless case, we do not need to perform an EIM decomposition on $A^{n\tau}_\gamma(\mu)$ and on $F(\mu)$. Figure 4.11 shows the relative EIM interpolation errors for the tangent matrix $B^{n\tau}_\gamma(\mu, \boldsymbol{u}_k(\mu))$ (left panel) and the residual vector $\Theta^n_\gamma(\mu, \boldsymbol{u}_k(\mu))$ (right panel) as a function of the rank $S^{b^{n\tau}}$ or S^{θ^n}, *i.e.*, we plot $e^{\theta^n}_{\texttt{EIM}}(S^{\theta^n}, \mathcal{D}_*)$ defined in (4.85b) and

$$e^{b^{n\tau}}_{\texttt{EIM}}(S^{b^{n\tau}}, \mathcal{D}_*) := \frac{\max\limits_{\mu\in\mathcal{D}_*} \max\limits_{k\in\{1:k^{\mathrm{cv}}(\mu)\}} \|B^{n\tau}_\gamma(\mu, \boldsymbol{u}_k(\mu)) - E^{b^{n\tau}}(\mu, k)\|_{\ell^\infty(ij)}}{\max\limits_{\mu\in\mathcal{D}_*} \max\limits_{k\in\{1:k^{\mathrm{cv}}(\mu)\}} \|B^{n\tau}_\gamma(\mu, \boldsymbol{u}_k(\mu))\|_{\ell^\infty(ij)}}, \tag{4.93}$$

with $\mathcal{D}_*$ either equal to $\mathcal{D}_{\texttt{train}}$ or to $\mathcal{D}_{\texttt{valid}}$. For the validation set $\mathcal{D}_{\texttt{valid}}$, we additionally plot the relative EIM approximation errors

$$e^{b^{n\tau},\mathrm{cv}}_{\texttt{EIM}}(S^{b^{n\tau}}) := \frac{\max\limits_{\mu\in\mathcal{D}_{\texttt{valid}}} \|B^{n\tau}_\gamma(\mu, \boldsymbol{u}_{\mathrm{cv}}(\mu)) - E^{b^{n\tau}}(\mu, k^{\mathrm{cv}}(\mu))\|_{\ell^\infty(ij)}}{\max\limits_{\mu\in\mathcal{D}_{\texttt{valid}}} \|B^{n\tau}_\gamma(\mu, \boldsymbol{u}_{\mathrm{cv}}(\mu))\|_{\ell^\infty(ij)}}, \tag{4.94}$$

and $e^{\theta^n,\mathrm{cv}}_{\texttt{EIM}}(S^{\theta^n})$ defined in (4.87b). Notice that for Tresca friction, we perform the EIM on the tangent matrix $B^{n\tau}_\gamma(\mu; \boldsymbol{u}_k(\mu))$ instead of performing it separately on the tangent matrices $B^n_\gamma(\mu; \boldsymbol{u}_k(\mu))$ and $B^\tau_\gamma(\mu; \boldsymbol{u}_k(\mu))$. We see that the result is close to the one obtained for the frictionless case because the contribution of $B^\tau_\gamma(\mu; \boldsymbol{u}_k(\mu))$ is negligible. Indeed, as can be seen in Figure 4.9 (Row 1), the Alart–Curnier reformulation of the tangential stress is equal to $\pm s$ almost everywhere (except at 3 nodes) which results in the nullity of $\mathbb{G}_s(P^\tau_\gamma(\mu; \boldsymbol{u}_k(\mu)))$ almost everywhere. For the same reason, the dependence

of the residual vector $\Theta_\gamma^\tau(\mu, \boldsymbol{u}_k(\mu))$ on (μ, k) is almost of rank one and therefore its EIM approximation is very simple ($S^{\theta^\tau} = 3$); hence, its relative EIM approximation error is not reported. Altogether, the behaviour of the residual vector $\Theta_\gamma^n(\mu, \boldsymbol{u}_k(\mu))$ remains similar to that observed in the frictionless case.

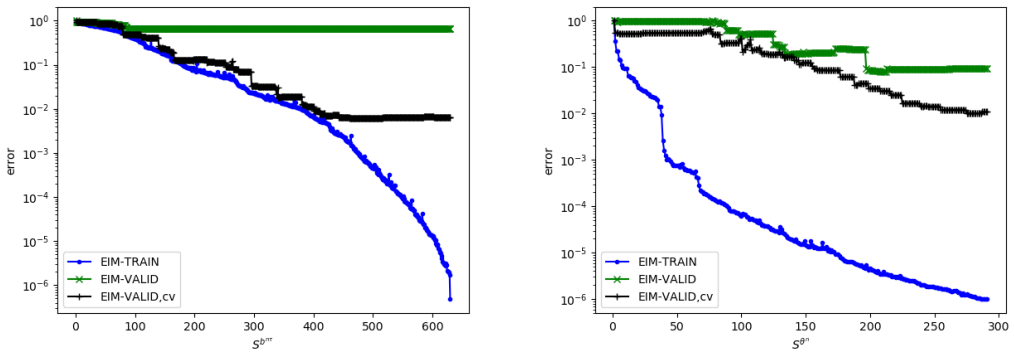

Figure 4.11 – Tresca frictional Hertz test case, Nitsche's method: Relative EIM approximation errors as a function of the rank $S^{b^{n\tau}}$ or S^{θ^n} of the approximation. Left: $e^{b^{n\tau}}_{\texttt{EIM}}(S^{b^{n\tau}}, \mathcal{D}_{\texttt{train}})$, $e^{b^{n\tau}}_{\texttt{EIM}}(S^{b^{n\tau}}, \mathcal{D}_{\texttt{valid}})$ and $e^{b^{n\tau},\text{cv}}_{\texttt{EIM}}(S^{b^{n\tau}})$; Right: $e^{\theta^n}_{\texttt{EIM}}(S^{\theta^n}, \mathcal{D}_{\texttt{train}})$, $e^{\theta^n}_{\texttt{EIM}}(S^{\theta^n}, \mathcal{D}_{\texttt{valid}})$ and $e^{\theta^n,\text{cv}}_{\texttt{EIM}}(S^{\theta^n})$.

Let us now discuss Coulomb's friction for which the training sets $\mathcal{E}^{b^n}_{\texttt{train}}$, $\mathcal{E}^{b^\tau}_{\texttt{train}}$, $\mathcal{E}^{\theta^n}_{\texttt{train}}$ and $\mathcal{E}^{\theta^\tau}_{\texttt{train}}$ are of cardinality 407. With the above choice for the tolerance $\delta_{\texttt{EIM}}$, we obtain $S^{b^n} = 126 \ll \mathcal{N}^{\text{HF}} \times \mathcal{N}^{\text{HF}}$, $S^{b^\tau} = 4 \ll \mathcal{N}^{\text{HF}} \times \mathcal{N}^{\text{HF}}$, $S^{\theta^n} = 214 \ll \mathcal{N}^{\text{HF}}$ and $S^{\theta^\tau} = 191 \ll \mathcal{N}^{\text{HF}}$. Figure 4.12 shows the relative EIM interpolation error for the tangent matrix $B^n_\gamma(\mu, \boldsymbol{u}_k(\mu))$ (Column 1), the residual vector $\Theta^n_\gamma(\mu, \boldsymbol{u}_k(\mu))$ (Column 2) and the residual vector $\Theta^\tau_\gamma(\mu, \boldsymbol{u}_k(\mu))$ (Column 3) as a function of the rank S^{b^n}, S^{θ^n} or S^{θ^τ}, *i.e.*, we plot $e^{b^n}_{\texttt{EIM}}(S^{b^n}, \mathcal{D}_*)$ defined in (4.85a), $e^{\theta^n}_{\texttt{EIM}}(S^{\theta^n}, \mathcal{D}_*)$ defined in (4.85b) and

$$e^{\theta^\tau}_{\texttt{EIM}}(S^{\theta^\tau}, \mathcal{D}_*) := \frac{\max\limits_{\mu\in\mathcal{D}_*} \max\limits_{k\in\{1:k^{\text{cv}}(\mu)\}} \|\Theta^\tau_\gamma(\mu, \boldsymbol{u}_k(\mu)) - E^{\theta^\tau}(\mu, k)\|_{\ell^\infty(j)}}{\max\limits_{\mu\in\mathcal{D}_*} \max\limits_{k\in\{1:k^{\text{cv}}(\mu)\}} \|\Theta^\tau_\gamma(\mu, \boldsymbol{u}_k(\mu))\|_{\ell^\infty(j)}}, \tag{4.95}$$

with $\mathcal{D}_*$ either equal to $\mathcal{D}_{\texttt{train}}$ or to $\mathcal{D}_{\texttt{valid}}$. For the validation set $\mathcal{D}_{\texttt{valid}}$, we additionally plot the relative EIM approximation errors $e^{b^n,\text{cv}}_{\texttt{EIM}}(b^n)$ (see (4.87a)), $e^{\theta^n,\text{cv}}_{\texttt{EIM}}(S^{\theta^n})$ (see (4.87b)) and $e^{\theta^\tau,\text{cv}}_{\texttt{EIM}}(S^{\theta^\tau})$ defined as

$$e^{\theta^\tau,\text{cv}}_{\texttt{EIM}}(S^{\theta^\tau}) := \frac{\max\limits_{\mu\in\mathcal{D}_{\texttt{valid}}} \|\Theta^\tau_\gamma(\mu, \boldsymbol{u}_{\text{cv}}(\mu)) - E^{\theta^\tau}(\mu, k^{\text{cv}}(\mu))\|_{\ell^\infty(j)}}{\max\limits_{\mu\in\mathcal{D}_{\texttt{valid}}} \|\Theta^\tau_\gamma(\mu, \boldsymbol{u}_{\text{cv}}(\mu))\|_{\ell^\infty(j)}}. \tag{4.96}$$

For Coulomb's friction, we perform the EIM separately on the tangent matrices $B^n_\gamma(\mu; \boldsymbol{u}_k(\mu))$ and $B^\tau_\gamma(\mu; \boldsymbol{u}_k(\mu))$. For the tangent matrix $B^\tau_\gamma(\mu; \boldsymbol{u}_k(\mu))$, the EIM approximation leads to a rather low-rank decomposition ($S^{b^\tau} = 4$) and therefore the EIM approximation errors are not reported. For the tangent matrix $B^n_\gamma(\mu; \boldsymbol{u}_k(\mu))$ (left panel), we do not report in Figure 4.12 the last value of the relative error $e^{b^n}_{\texttt{EIM}}(S^{b^n}, \mathcal{D}_{\texttt{train}})$ (corresponding to $S^{b^n} = 126$) since it is of the order of the machine precision (10^{-16}).

We observe that the relative error $e^{b^n}_{\texttt{EIM}}(S^{b^n}, \mathcal{D}_{\texttt{train}})$ decreases fast enough to allow accurate approximations. We actually notice a rather modest decrease for ranks S^{b^n} between 1 and 106 with errors values between 1 and 0.5, and then a significant drop at about $S^{b^n} = 106$. Instead, the relative errors $e^{b^n}_{\texttt{EIM}}(S^{b^n}, \mathcal{D}_{\texttt{valid}})$ and $e^{b^n,\mathrm{cv}}_{\texttt{EIM}}(S^{b^n})$ exhibit a similar behaviour characterized by two phases of stagnation. For the residual vector $\Theta^{\boldsymbol{n}}_{\gamma}(\mu, \boldsymbol{u}_k(\mu))$ (central panel), we observe that the relative error $e^{\theta^n}_{\texttt{EIM}}(S^{\theta^n}, \mathcal{D}_{\texttt{train}})$ decreases fast enough to allow accurate approximations. We observe a rather uniform decrease with values from 1 down to 10^{-6}. Instead, the relative errors $e^{\theta^n}_{\texttt{EIM}}(S^{\theta^n}, \mathcal{D}_{\texttt{valid}})$ and $e^{\theta^n,\mathrm{cv}}_{\texttt{EIM}}(S^{\theta^n})$ are almost similar with a slow decrease for S^{θ^n} between 1 and 56, and then a stagnation occurs at a value of about 10^{-2}. Finally, for the residual vector $\Theta^{\boldsymbol{\tau}}_{\gamma}(\mu, \boldsymbol{u}_k(\mu))$ (right panel), the relative errors $e^{\theta^\tau}_{\texttt{EIM}}(S^{\theta^\tau}, \mathcal{D}_{\texttt{train}})$, $e^{\theta^\tau}_{\texttt{EIM}}(S^{\theta^\tau}, \mathcal{D}_{\texttt{valid}})$ and $e^{\theta^\tau,\mathrm{cv}}_{\texttt{EIM}}(S^{\theta^\tau})$ exhibit almost the same behaviour as the one of the errors for the residual vector $\Theta^{\boldsymbol{n}}_{\gamma}(\mu, \boldsymbol{u}_k(\mu))$.

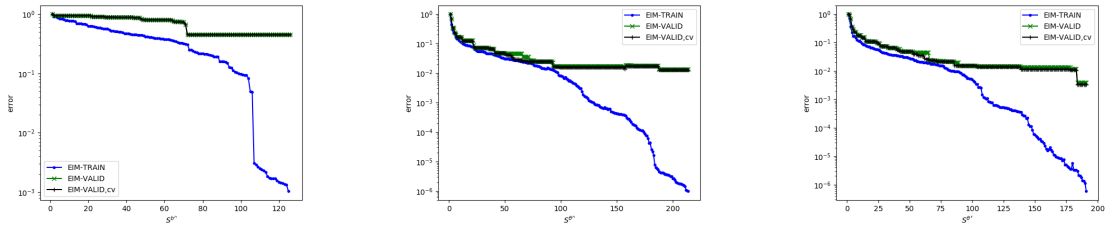

Figure 4.12 – Coulomb frictional Hertz test case, Nitsche's method: Relative EIM approximation errors as a function of the ranks S^{b^n}, S^{θ^n} or S^{θ^τ}. Left: $e^{b^n}_{\texttt{EIM}}(S^{b^n}, \mathcal{D}_{\texttt{train}})$, $e^{b^n}_{\texttt{EIM}}(S^{b^n}, \mathcal{D}_{\texttt{valid}})$ and $e^{b^n,\mathrm{cv}}_{\texttt{EIM}}(S^{b^n})$. Center: $e^{\theta^n}_{\texttt{EIM}}(S^{\theta^n}, \mathcal{D}_{\texttt{train}})$, $e^{\theta^n}_{\texttt{EIM}}(S^{\theta^n}, \mathcal{D}_{\texttt{valid}})$ and $e^{\theta^n,\mathrm{cv}}_{\texttt{EIM}}(S^{\theta^n})$. Right: $e^{\theta^\tau}_{\texttt{EIM}}(S^{\theta^\tau}, \mathcal{D}_{\texttt{train}})$, $e^{\theta^\tau}_{\texttt{EIM}}(S^{\theta^\tau}, \mathcal{D}_{\texttt{valid}})$ and $e^{\theta^\tau,\mathrm{cv}}_{\texttt{EIM}}(S^{\theta^\tau})$

We denote by $e^{\boldsymbol{n\tau}}_N(\mu)$ the relative RB approximation error on the tangential stress defined as

$$e^{\boldsymbol{n\tau}}_N(\mu) := \frac{\|\boldsymbol{\sigma}_{\boldsymbol{n\tau}}(\boldsymbol{u}_{\mathrm{cv}}(\mu)) - \boldsymbol{\sigma}_{\boldsymbol{n\tau}}(\boldsymbol{u}_{N,\mathrm{cv}}(\mu))\|_{\ell^2(\Gamma^c(\mu))}}{\|\boldsymbol{\sigma}_{\boldsymbol{n\tau}}(\boldsymbol{u}_{\mathrm{cv}}(\mu))\|_{\ell^2(\Gamma^c(\mu))}}, \tag{4.97}$$

and introduce the relative error measure $e^{\boldsymbol{n\tau}}_{N,\max}$ defined as

$$e^{\boldsymbol{n\tau}}_{N,\max} := \max_{\mu \in \mathcal{D}_{\texttt{valid}}} e^{\boldsymbol{n\tau}}_N(\mu). \tag{4.98}$$

Figure 4.13 displays for Tresca's friction the relative errors $e^{\boldsymbol{u}}_{N,\max}$ (left panel) and $e^{\boldsymbol{n\tau}}_{N,\max}$ (right panel) as a function of the number of vectors composing the reduced basis. As for the frictionless case, we only consider RB dimensions N larger than 10 and the validation set $\mathcal{D}_{\texttt{valid}}$ is restricted to the interval $[0.7, 1.18]$(m). In Figure 4.13, we superpose the plain RBM approximation error (without any EIM) and the RBM-EIM approximation error. As for the frictionless case, we observe that similar errors are obtained for plain RBM and RBM-EIM. This again confirms the satisfactory quality of the EIM approximations at convergence.

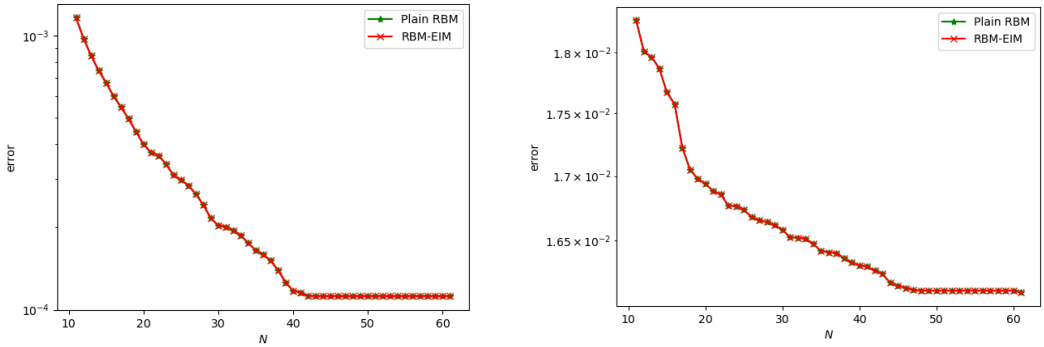

Figure 4.13 – Tresca frictional Hertz test case, Nitsche's method: RBM approximation errors for $|\mathcal{D}_{\texttt{train}}| = 61$. Left: $e^{\boldsymbol{u}}_{N,\max}$; Right: $e^{\boldsymbol{n\tau}}_{N,\max}$.

CHAPTER 5

CONCLUSIONS AND PERSPECTIVES

In this thesis, we have investigated several aspects of the application of the Reduced Basis Method (RBM) to variational inequalities in order to obtain robust and computationally efficient reduced models. The work has been carried out along three axes.

Firstly, we have addressed the problem of inf-sup stability of the reduced model in the framework of a primal-dual formulation and parameter-dependent constraints. The target model problem is here the frictionless contact problem. An greedy algorithm to guarantee inf-sup stability of the reduced model by enriching the primal basis according to the dual basis during the offline stage has been developed for this purpose. Furthermore, the difficulty of suitably compressing the dual basis due to the conical constraints on the Lagrange multiplier has been addressed by developing an algorithm generating a cone of larger aperture and thereby leading to a compressed dual basis with a better condition number. The robustness and efficiency of the methodology have been numerically confirmed on representative test cases. The contents of this chapter have been published in [84]. An extension to nonlinear variational inequalities is highlighted in Appendix A in the context of the frictionless contact problem with large deformations as an example of application.

Secondly, an effective method for reducing the contact problem with friction (Tresca or Coulomb) in the primal-dual formulation has been proposed. The tangential stress constraint has been treated by a collocation method. A greedy algorithm for the selection of collocation nodes for the reduced model has been developed to create an efficient reduced model. The stability of the latter is achieved by the use of the PGA algorithm developed in Chapter 2, here accounting at the same time for the normal and tangential dual bases. The stability and efficiency of the reduced model have been numerically illustrated.

Thirdly, an effective method for reducing the contact problem with and without friction formulated with Nitsche's method has been introduced. The inefficiency of the application of the classical RBM due to the nonlinearity of Nitsche's formulation was overcome by means of the Empirical Interpolation Method (EIM) [10, 75]. A comparison in terms of accuracy and efficiency of the Nitsche and primal-dual approaches for frictionless contact indicates the benefits of the former.

The present work can be pursued in several directions. Firstly, in terms of applica-

tions, it would be very interesting to use the methods developed so far for the following challenging and industrially relevant problems:

- **Friction in large deformations**: Although an extension to large deformations is given in the appendix for the problem of contact without friction, either in primal-dual formulation or with Nitsche's method, the problem of contact with friction has been treated only in the context of small deformations. Furthermore, an issue that could arise when using a primal-dual formulation is that the dimension of the reduced primal space obtained with the present approach in order to guarantee inf-sup stability becomes quite large. Indeed, an additional loop is needed to solve for the nonlinearity, and the collection of needed supremizers will depend not only on the parameter but also on the iteration number.

- **Hydromechanical coupling**: Within the ERMES department of EDF R&D, there is also an interest in seepage conditions for hydromechanical problems [88]. As for the contact problem, the weak formulation leads to a variational inequality with hybrid constraints on the pressure and the flow. This would open another field of application for the methods proposed in this Thesis.

- **Industrial test cases**: Although already tested on Taylor test cases and Hertz spheres in 3D with `code_aster`, an application to industrial study cases will highlight the bottlenecks in terms of efficiency for such problems. In practice, the use of High-Performance Computing (HPC) for snapshot generation can already help to considerably reduce the cost of the offline phase.

- **Beyond mechanics**: The generality of the ideas devised in Chapter 2 as well as the theoretical foundations behind it indicate that the methods proposed therein can be applied in the more general framework of variational inequalities, opening the door to applications, *e.g.* in finance or biology [82, 66].

Secondly, in terms of mathematical analysis and software development, the following points can be explored:

- **A posteriori error estimator**: The way the training space is generated (sampling using uniform laws) may not be optimal, especially if the number of parameters becomes large. An alternative would be to design an a posteriori error estimator and use it to build the reduced spaces in an optimal way by generating the snapshots in a greedy manner. One idea would be to extend the method proposed in [105] to the case of a non-invertible operator.

- **Precision/stability balance**: If an a posteriori error estimator is available, the generation of the reduced bases and the stabilization procedure can be deployed together. A unique algorithm that directly creates primal and dual bases satisfying an inf-sup stability condition could be implemented. The idea would be to use the estimator to check the accuracy (of both bases) and the stability condition given in Proposition 2.3.1 as a "stability estimator". Concretely, one would iteratively generate (in a greedy way) the primal and dual bases by testing at each iteration if the inf-sup stability condition is satisfied. If this is the case, one continues the generation of the bases; otherwise, one enriches the primal basis until the criteria on stability is satisfied.

- **Active-set strategy**: The current methods in `code_aster` for solving the contact problem are based on an active-set strategy [68, 33]. With this type of approach, contact status (active/inactive) is part of the unknowns in the problem. However, it can be very difficult to reduce the contact problem in this context. Indeed, considering a new parameter that encodes status but is not taken into account in the training phase is not a viable approach since, the reduced model may not converge to the correct solution or may even diverge. A solution could be a data-driven approach where one would combine the reduced basis method with a learning algorithm dedicated to contact status using snapshots or experimental data (if available) as training data.

APPENDIX A

EXTENSION TO NONLINEAR VARIATIONAL INEQUALITIES

This appendix proposes an extension of the stabilization method presented in Chapter 2 for linear variational inequalities to the case of nonlinear variational inequalities.

A.1 Model problem

Let $\mathcal{V}$ and $\mathcal{W}$ be two finite-dimensional high-fidelity (HF) spaces typically resulting from the finite element discretization of some Hilbert spaces. We denote by $\langle\cdot,\cdot\rangle_{\mathcal{V}}$ (resp. $\langle\cdot,\cdot\rangle_{\mathcal{W}}$) the inner product equipping $\mathcal{V}$ (resp. $\mathcal{W}$) and inducing the norm $\|\cdot\|_{\mathcal{V}}$ (resp. $\|\cdot\|_{\mathcal{W}}$). We denote by $\mathcal{V}'$ the dual space of $\mathcal{V}$ equipped with the duality product $\langle\cdot,\cdot\rangle_{\mathcal{V}',\mathcal{V}}$, and by $\|\cdot\|_{\mathcal{V}'}$ the associated norm. Let $\mathcal{W}^+ \subset \mathcal{W}$ be a positive convex cone containing 0. Let $\mathcal{D} \subset \mathbb{R}^m, m \in \mathbb{N}^* := \mathbb{N} \setminus \{0\}$, be the parameter domain. We consider a uniformly bounded, symmetric and coercive bilinear form $a(\mu;\cdot,\cdot) : \mathcal{V} \times \mathcal{V} \to \mathbb{R}$ and a uniformly bounded linear form $f(\mu;\cdot) : \mathcal{V} \to \mathbb{R}$ for all $\mu \in \mathcal{D}$. Let $b(\mu;\cdot;\cdot,\cdot) : \mathcal{V} \times \mathcal{V} \times \mathcal{W} \to \mathbb{R}$ and $g(\mu;\cdot;\cdot) : \mathcal{V} \times \mathcal{W} \to \mathbb{R}$ be two uniformly bounded nonlinear forms for all $\mu \in \mathcal{D}$. We assume that, for all $\mu \in \mathcal{D}$, $b(\mu;\cdot;\cdot,\cdot)$ is linear with respect to its last two arguments and that $g(\mu;\cdot;\cdot)$ is linear with respect to its last argument. We consider the following constrained minimization problem: For all $\mu \in \mathcal{D}$, find $u(\mu) \in \mathcal{V}$ such that

$$u(\mu) \in \underset{v \in \mathcal{K}(\mu)}{\operatorname{argmin}} \frac{1}{2} a(\mu; v, v) - f(\mu; v), \tag{A.1}$$

where the admissible set is defined as

$$\mathcal{K}(\mu) := \Big\{ v \in \mathcal{V} \;\Big|\; b(\mu; v; v, \eta) \leq g(\mu; v; \eta), \quad \forall \eta \in \mathcal{W}^+ \Big\}, \tag{A.2}$$

and is assumed to be non-empty for all $\mu \in \mathcal{D}$.

We denote by $c_{\mathrm{HF}}(\mu)$ the boundedness coefficient $b(\mu;\cdot;\cdot,\cdot)$ defined as follows:

$$c_{\mathrm{HF}}(\mu) := \sup_{\eta \in \mathcal{W}^+} \sup_{v \in \mathcal{V}} \frac{b(\mu; v; v, \eta)}{\|v\|_{\mathcal{V}} \|\eta\|_{\mathcal{W}}}. \tag{A.3}$$

By the above assumption on $b(\mu;\cdot;\cdot,\cdot)$, there exists a real number C_0 such that $c_{\mathrm{HF}}(\mu) \leq C_0$ for all $\mu \in \mathcal{D}$. We additionally assume that the HF pair $(\mathcal{V}, \mathcal{W}^+)$ ensures that there exists $\beta_0 > 0$ such that

$$\forall \mu \in \mathcal{D}, \quad \beta_{\mathrm{HF}}(\mu) := \inf_{w\in\mathcal{V}} \inf_{\eta\in\mathcal{W}^+} \sup_{v\in\mathcal{V}} \frac{b(\mu;w;v,\eta)}{\|v\|_{\mathcal{V}}\|\eta\|_{\mathcal{W}}} > \beta_0. \tag{A.4}$$

One possibility to solve the optimization problem (A.1) is to use a primal-dual formulation. Let $\mathcal{L}(\mu;\cdot;\cdot,\cdot) : \mathcal{V}\times\mathcal{V}\times\mathcal{W}^+ \to \mathbb{R}$ be the Lagrangian associated with (A.1) and defined as follows: For all $\mu \in \mathcal{D}$,

$$\mathcal{L}(\mu;w;v,\eta) := \frac{1}{2}a(\mu;v,v) - f(\mu;v) + b(\mu;w;v,\eta) - g(\mu;w;\eta). \tag{A.5}$$

Then, for all $\mu \in \mathcal{D}$, we can rewrite (A.1) as the following saddle-point problem: Find $(u(\mu),\lambda(\mu)) \in \mathcal{V}\times\mathcal{W}^+$ such that

$$(u(\mu),\lambda(\mu)) \in \arg\min_{v\in\mathcal{V}} \max_{\eta\in\mathcal{W}^+} \mathcal{L}(\mu;v;v,\eta). \tag{A.6}$$

The problem (A.6) being nonlinear, we solve it using the so-called Kačanov algorithm [45]. Concretely, for all $\mu \in \mathcal{D}$, given $\big(u_0(\mu),\lambda_0(\mu)\big) \in \mathcal{V}\times\mathcal{W}^+$, the linearized problem consists of solving at each iteration $k \in \mathbb{N}$ the following problem: find $(u_{k+1}(\mu),\lambda_{k+1}(\mu)) \in \mathcal{V}\times\mathcal{W}^+$ such that

$$(u_{k+1}(\mu),\lambda_{k+1}(\mu)) = \arg\min_{v\in\mathcal{V}} \max_{\eta\in\mathcal{W}^+} \tilde{\mathcal{L}}(\mu,k;v,\eta) := \mathcal{L}(\mu;u_k(\mu);v,\eta), \tag{A.7}$$

until the following convergence criterion is reached:

$$\frac{\|u_{k+1}(\mu)-u_k(\mu)\|_{\mathcal{V}}}{\|u_{k+1}(\mu)\|_{\mathcal{V}}} \leq \delta_u \quad \text{and} \quad \frac{\|\lambda_{k+1}(\mu)-\lambda_k(\mu)\|_{\mathcal{W}}}{\|\lambda_{k+1}(\mu)\|_{\mathcal{W}}} \leq \delta_\lambda, \tag{A.8}$$

for a pair of tolerances $(\delta_u,\delta_\lambda) \in \mathbb{R}_+\times\mathbb{R}_+$. Notice that under the above assumptions (in particular (A.4) and the coercivity of $a(\mu;\cdot,\cdot)$), the pair $(u_{k+1}(\mu),\lambda_{k+1}(\mu)) \in \mathcal{V}\times\mathcal{W}^+$ is uniquely defined for all $k \in \mathbb{N}$ and can be found as the critical point of the Lagrangian $\tilde{\mathcal{L}}(\mu,k;\cdot,\cdot)$ by solving

$$\begin{cases} a(\mu;u_{k+1}(\mu),v) + \tilde{b}(\mu,k;v,\lambda_{k+1}(\mu)) = f(\mu;v), & \forall v \in \mathcal{V}, \\ \tilde{b}(\mu,k;u_{k+1}(\mu),\eta) \leq \tilde{g}(\mu,k;\eta), & \forall \eta \in \mathcal{W}^+, \end{cases} \tag{A.9}$$

with

$$\tilde{b}(\mu,k;v,\eta) := b(\mu;u_k(\mu);v,\eta), \quad \tilde{g}(\mu,k;\eta) := g(\mu;u_k(\mu);\eta) \quad \forall (v,\eta) \in \mathcal{V}\times\mathcal{W}^+. \tag{A.10}$$

The convergence criterion for (A.9) is still (A.8). We denote the converged solution to the problem (A.9) as the pair $(u_{\mathrm{cv}}(\mu),\lambda_{\mathrm{cv}}(\mu)) \in \mathcal{V}\times\mathcal{W}^+$.

In what follows, we denote by $k^{\mathrm{cv}}(\mu) \in \mathbb{N}$ the number of iterations required to solve (A.9) for any $\mu \in \mathcal{D}$. We assume that the Kačanov algorithm converges sufficiently well so that $k^{\mathrm{cv}}(\mu)$ is uniformly bounded in μ, *i.e.*,

$$\exists K \in \mathbb{N}, \quad k^{\mathrm{cv}}(\mu) \leq K, \quad \forall \mu \in \mathcal{D}.$$

A.2 Stable reduced basis method

Let $P \in \mathbb{N}^*$ and let us consider a family $\{(u_{\mathrm{cv}}(\mu_p), \lambda_{\mathrm{cv}}(\mu_p))\}_{p\in\{1:P\}} \subset \mathcal{V} \times \mathcal{W}^+$ of Hf solutions to (A.9) which are computed by using a training subset $\mathcal{D}_{\mathtt{train}} := \{\mu_p\}_{p\in\{1:P\}} \subset \mathcal{D}$ of cardinality P. In practice, the sampling of the parameter domain can be driven by a posteriori error estimates, as in [55, 5, 105]. Let us set

$$V := \boldsymbol{Span}\Big(\{u_{\mathrm{cv}}(\mu_p)\}_{p\in\{1:P\}}\Big) \subset \mathcal{V}, \qquad W^+ := \boldsymbol{Span}^+\Big(\{\lambda_{\mathrm{cv}}(\mu_p)\}_{p\in\{1:P\}}\Big) \subset \mathcal{W}^+. \tag{A.11}$$

(Recalling that $\boldsymbol{Span}^+$ denotes the positive cone generated by the family of snapshots.) Notice that the space V and the cone W^+ are built using snapshots obtained at convergence of the Kačanov algorithm.

Given a positive real number $\delta_{\mathtt{POD}} > 0$, one can construct using POD [54, 69] an orthonormal family of $N \in \mathbb{N}^*$ ($N \leq P$) elements of V,

$$\{v_n\}_{n\in\{1:N\}} := \mathtt{POD}\Big(\{u_{\mathrm{cv}}(\mu_p)\}_{p\in\{1:P\}};\ \mathcal{V},\ \delta_{\mathtt{POD}}\Big),$$

such that

$$V_N := \boldsymbol{Span}\Big(\{v_n\}_{n\in\{1:N\}}\Big) \subset V, \tag{A.12}$$

$$e_{\mathtt{POD}}(N) := \frac{\displaystyle\left(\sum_{p\in\{1:P\}} \|(\mathbb{I}^{\mathcal{V}} - \Pi^{\mathcal{V}}_{V_N})(u_{\mathrm{cv}}(\mu_p))\|^2_{\mathcal{V}}\right)^{\frac{1}{2}}}{\displaystyle\left(\sum_{p\in\{1:P\}} \|u_{\mathrm{cv}}(\mu_p)\|^2_{\mathcal{V}}\right)^{\frac{1}{2}}} \leq \delta_{\mathtt{POD}}, \tag{A.13}$$

where $\Pi^{\mathcal{H}}_Z$ denotes the projection onto a generic closed convex subset Z of the generic Hilbert space $\mathcal{H}$ ($\Pi^{\mathcal{H}}_Z$ is the orthogonal projection if $\mathcal{Z}$ is a linear subspace) and $\mathbb{I}^{\mathcal{H}}$ denotes the identity operator in $\mathcal{H}$. Moreover, given a positive real number $\delta_{\mathtt{mCPG}} > 0$, one can construct using the mCPG algorithm [12, 84] a family $\{\chi_r\}_{r\in\{1:R\}}$ of $R \in \mathbb{N}^*$ ($R \leq P$) vectors of W^+,

$$\{\chi_r\}_{r\in\{1:R\}} := \mathtt{mCPG}\Big(\{\lambda_{\mathrm{cv}}(\mu_p)\}_{p\in\{1:P\}};\ \mathcal{W},\ \delta_{\mathtt{mCPG}}\Big),$$

satisfying

$$W^+_R := \boldsymbol{Span}^+\Big(\{\chi_r\}_{r\in\{1:R\}}\Big) \subset W^+, \tag{A.14}$$

$$e_{\mathtt{mCPG}}(R) := \frac{\displaystyle\max_{p\in\{1:P\}} \|(\mathbb{I}^{\mathcal{W}} - \Pi^{\mathcal{W}}_{W^+_R})(\lambda_{\mathrm{cv}}(\mu_p))\|_{\mathcal{W}}}{\displaystyle\max_{p\in\{1:P\}} \|\lambda_{\mathrm{cv}}(\mu_p)\|_{\mathcal{W}}} \leq \delta_{\mathtt{mCPG}}. \tag{A.15}$$

For all $\mu \in \mathcal{D}$ and all $k \in \mathbb{N}$, we define

$$\beta^{\mathrm{dec}}_{N,R}(\mu, k) := \inf_{\eta\in W^+_R} \sup_{v\in V_N} \frac{\tilde{b}(\mu, k; v, \eta)}{\|v\|_{\mathcal{V}}\|\eta\|_{\mathcal{W}}}, \tag{A.16}$$

where the superscript refers to the decorrelated construction of the reduced bases. Recalling that $\tilde{b}(\mu,k;\cdot,\cdot)$ is defined in (A.10) for all $k \in \{0{:}k^{\mathrm{cv}}(\mu)\}$, we conventionally set $\tilde{b}(\mu,k;\cdot,\cdot) := b(\mu;u_{\mathrm{cv}}(\mu);\cdot,\cdot)$ for all $k \geq k^{\mathrm{cv}}(\mu)$. Since the primal reduced space V_N and the dual reduced cone W_R^+ are constructed in a decorrelated manner, we cannot guarantee that $\beta_{N,R}^{\mathrm{dec}}(\mu,k) > 0$ for all $(\mu,k) \in \mathcal{D} \times \mathbb{N}$.

A strategy for enriching the reduced primal basis in order to achieve inf-sup stability has been initially proposed in Chapter 2 for linear variational inequalities with parameter-dependent constraints. Here, we can apply the same strategy at each step of the Kačanov's algorithm. To this purpose, we proceed as follows: For all $\mu \in \mathcal{D}$ and all $k \in \mathbb{N}$, we define the operator $\mathbb{T}^k(\mu) : \mathcal{W}^+ \to \mathcal{V}$ such that

$$\mathbb{T}^k(\mu) := J \circ \mathcal{B}_{\mathrm{HF}}^k(\mu), \tag{A.17}$$

where $J : \mathcal{V}' \to \mathcal{V}$ is the Riesz isomorphism between $\mathcal{V}'$ and $\mathcal{V}$ and where the operator $\mathcal{B}_{\mathrm{HF}}^k(\mu) : \mathcal{W}^+ \to \mathcal{V}'$ is defined such that

$$\langle \mathcal{B}_{\mathrm{HF}}^k(\mu)(\eta), v\rangle_{\mathcal{V}',\mathcal{V}} := \tilde{b}(\mu,k;v,\eta), \quad \forall (v,\eta) \in \mathcal{V} \times \mathcal{W}^+. \tag{A.18}$$

Then, for all $\mu \in \mathcal{D}$ and all $k \in \mathbb{N}$, we define the enriched reduced primal space $V_{N,R}^{\mathrm{on}}(\mu,k)$ as follows :

$$V_{N,R}^{\mathrm{on}}(\mu,k) := V_N + S_R(\mu,k) \subset \mathcal{V}, \quad S_R(\mu,k) := \boldsymbol{Span}(\{\mathbb{T}^k(\mu)\chi_r\}_{r\in\{1:R\}}). \tag{A.19}$$

The superscript refers to the online construction of the enriched basis. Proceeding as in Chapter 2, one readily sees that the bilinear form $\tilde{b}(\mu,k;\cdot,\cdot)$ is uniformly inf-sup stable with respect to the pair $(V_{N,R}^{\mathrm{on}}(\mu,k), W_R^+)$, *i.e.*, we have

$$\forall (\mu,k) \in \mathcal{D} \times \mathbb{N}, \quad \beta_{N,R}^{\mathrm{on}}(\mu,k) := \inf_{\eta\in W_R^+} \sup_{v\in V_{N,R}^{\mathrm{on}}(\mu)} \frac{\tilde{b}(\mu,k;v,\eta)}{\|v\|_{\mathcal{V}}\|\eta\|_{\mathcal{W}}} \geq \beta_{\mathrm{HF}}(\mu,k) \geq \beta_0 > 0. \tag{A.20}$$

Notice that in addition to depending on the parameter, the enriched space $V_{N,R}^{\mathrm{on}}(\mu,k)$ also depends on the iteration counter. Thus, this space has to be reconstructed at each iteration of the Kačanov algorithm in the online phase, which is computationally inefficient.

To overcome this problem, we adapt the ideas of Chapter 2. The goal is to construct a "parameter/iteration"-independent subspace of $\mathcal{V}$ that provides a sufficiently accurate approximation of $V_{N,R}^{\mathrm{on}}(\mu,k)$ for all $(\mu,k) \in \mathcal{D} \times \mathbb{N}$ to preserve inf-sup stability. The crucial advantage is that this "parameter/iteration"-independent subspace can be constructed once and for all in the offline phase. The idea is to approximate the linear space S_R defined as

$$S_R := \sum_{\substack{\mu\in\mathcal{D} \\ k\in\{0:k^{\mathrm{cv}}(\mu)\}}} S_R(\mu,k), \tag{A.21}$$

by a subspace $S_R^{\mathrm{red}} \subset S_R$, so that the bilinear form $\tilde{b}(\mu,k;\cdot,\cdot)$ is inf-sup stable with respect to the pair $(V_N + S_R^{\mathrm{red}}, W_R^+)$ for all $\mu \in \mathcal{D}_{\mathtt{train}}$ and all $k \in \{1,\cdots,k^{\mathrm{cv}}(\mu)\}$. To this purpose, given a tolerance $\delta_{\mathtt{PGA}} > 0$ small enough, we can construct a proper subspace $S_R^{\mathrm{red}} \subset S_R$ using the Projected Greedy Algorithm (PGA) from Chapter 2,

$$S_R^{\mathrm{red}} := \mathtt{PGA}\Big(\mathcal{D}_{\mathtt{train}}, V_N, \delta_{\mathtt{PGA}}\Big) \subset S_R \subset \mathcal{V}. \tag{A.22}$$

APPENDIX B
METHODS AND ALGORITHMS

This appendix is dedicated to a brief presentation of some methods and algorithms used in this thesis. For simplicity, the presentation is given in the context of an algebraic formulation.

B.1 Proper Orthogonal Decomposition

In this section, we present the Proper Orthogonal Decomposition (POD) [54, 69] method which is used for vector space compression. Let $\mathcal{V}$ be a finite-dimensional (high-fidelity) subspace of dimension $\mathcal{N}^{\text{HF}} \in \mathbb{N}^*$ (typically resulting from the finite element discretization of a Hilbert space) such that

$$\mathcal{V} := \boldsymbol{Span}\Big(\{\varphi_n\}_{n\in\{1:\mathcal{N}^{\text{HF}}\}}\Big). \tag{B.1}$$

We denote by $\langle\cdot,\cdot\rangle_{\mathcal{V}}$ the inner product equipping $\mathcal{V}$ and inducing the norm $\|\cdot\|_{\mathcal{V}}$. Let us consider a family $\{u_p\}_{p\in\{1:P\}}$ of $P \in \mathbb{N}^*$ ($P \ll \mathcal{N}^{\text{HF}}$) elements of $\mathcal{V}$ (typically snapshots computed on a training subset of the parametric domain) and let us set

$$V := \boldsymbol{Span}\Big(\{u_p\}_{p\in\{1:P\}}\Big) \subset \mathcal{V}. \tag{B.2}$$

Given a positive real number $\delta_{\texttt{POD}} > 0$, the aim of the POD is to construct an orthonormal family of $N \in \mathbb{N}^*$ ($N \leq P$) elements of V,

$$\{\xi_n\}_{n\in\{1:N\}} := \texttt{POD}\Big(\{u_p\}_{p\in\{1:P\}};\ \mathcal{V},\ \delta_{\texttt{POD}}\Big), \tag{B.3}$$

such that

$$V_N := \boldsymbol{Span}\Big(\{\xi_n\}_{n\in\{1:N\}}\Big) \subset V, \tag{B.4a}$$

$$e_{\texttt{POD}}(N) := \frac{\Big(\sum\limits_{p\in\{1:P\}} \|(\mathbb{I}^{\mathcal{V}} - \Pi^{\mathcal{V}}_{V_N})(u_p)\|^2_{\mathcal{V}}\Big)^{\frac{1}{2}}}{\Big(\sum\limits_{p\in\{1:P\}} \|u_p\|^2_{\mathcal{V}}\Big)^{\frac{1}{2}}} \leq \delta_{\texttt{POD}}, \tag{B.4b}$$

where $\Pi_Z^{\mathcal{H}}$ denotes the projection onto a generic closed convex subset Z of the generic Hilbert space $\mathcal{H}$ ($\Pi_Z^{\mathcal{H}}$ is the orthogonal projection if $\mathcal{Z}$ is a linear subspace) and $\mathbb{I}^{\mathcal{H}}$ denotes the identity operator in $\mathcal{H}$. For the algebraic formulation of the POD, we adopt the following decomposition:

$$u_p := \sum_{n\in\{1:\mathcal{N}^{\mathrm{HF}}\}} \boldsymbol{U}_p^n \varphi_n, \quad \boldsymbol{U}_p := (\boldsymbol{U}_p^n)_{n\in\{1:\mathcal{N}^{\mathrm{HF}}\}} \in \mathbb{R}^{\mathcal{N}^{\mathrm{HF}}}. \tag{B.5}$$

Let us set

$$\boldsymbol{V} := \boldsymbol{Span}\Big(\{\boldsymbol{U}_p\}_{p\in\{1:P\}}\Big) \subset \mathbb{R}^{\mathcal{N}^{\mathrm{HF}}}. \tag{B.6}$$

The algebraic counterpart of (B.3) is that given the family $\{\boldsymbol{U}_p\}_{p\in\{1:P\}} \subset \mathbb{R}^{\mathcal{N}^{\mathrm{HF}}}$, the POD constructs an orthonormal family of $N \in \mathbb{N}^*$ elements of $\boldsymbol{V}$,

$$\{\boldsymbol{\Xi}_n\}_{n\in\{1:N\}} := \mathtt{POD}\Big(\{\boldsymbol{U}_p\}_{p\in\{1:P\}};\ \mathcal{V},\ \delta_{\mathtt{POD}}\Big), \tag{B.7}$$

such that

$$\boldsymbol{V}_N := \boldsymbol{Span}\Big(\{\boldsymbol{\Xi}_n\}_{n\in\{1:N\}}\Big) \subset \boldsymbol{V}, \tag{B.8a}$$

$$e_{\mathtt{POD}}(N) := \frac{\Big(\sum\limits_{p\in\{1:P\}} \|(\mathbb{I}_{\mathcal{N}^{\mathrm{HF}}} - \Pi_{\boldsymbol{V}_N})(\boldsymbol{U}_p)\|_{\mathbb{V}}^2\Big)^{\frac{1}{2}}}{\Big(\sum\limits_{p\in\{1:P\}} \|\boldsymbol{U}_p\|_{\mathbb{V}}^2\Big)^{\frac{1}{2}}} \leq \delta_{\mathtt{POD}}, \tag{B.8b}$$

where $\Pi_{\boldsymbol{V}_N}$ denotes the orthogonal projection onto $\boldsymbol{V}_N \subset \mathbb{R}^{\mathcal{N}^{\mathrm{HF}}}$ and $\mathbb{V} \in \mathbb{R}^{\mathcal{N}^{\mathrm{HF}}\times\mathcal{N}^{\mathrm{HF}}}$ denotes the Gram matrix associated with the inner product $\langle\cdot,\cdot\rangle_{\mathcal{V}}$.

Let us now describe the procedure for the construction of $\boldsymbol{V}_N$. Let us set $\boldsymbol{S} := \Big[\boldsymbol{U}_1 \cdots \boldsymbol{U}_P\Big] \in \mathbb{R}^{\mathcal{N}^{\mathrm{HF}}\times P}$ and $\boldsymbol{M} := \boldsymbol{S}^\top \mathbb{V} \boldsymbol{S} \in \mathbb{R}^{P\times P}$. Since $\boldsymbol{M}$ is symmetric and positive-definite, computing its eigendecomposition, one obtains an orthonormal family of eigenvectors $\{\boldsymbol{\Psi}_n\}_{n\in\{1:P\}} \subset \mathbb{R}^P$ and a family of associated eigenvalues $\{\theta_n\}_{n\in\{1:P\}} \subset \mathbb{R}_+$. Then, for all $n \in \{1{:}P\}$, one defines the vectors $\boldsymbol{\Xi}_n$ as

$$\boldsymbol{\Xi}_n := \frac{1}{\sqrt{\theta_n}} \boldsymbol{S}\boldsymbol{\Psi}_n \in \boldsymbol{V}. \tag{B.9}$$

The family of vectors $\{\boldsymbol{\Xi}_n\}_{n\in\{1:P\}} \subset \boldsymbol{V}$ thus defined is orthonormal. Indeed, for all $p, q \in \{1{:}P\}$, one has

$$\boldsymbol{\Xi}_p^\top \mathbb{V} \boldsymbol{\Xi}_q = \frac{1}{\sqrt{\theta_p\theta_q}} \boldsymbol{\Psi}_p^\top \boldsymbol{M} \boldsymbol{\Psi}_q = \frac{\sqrt{\theta_q}}{\sqrt{\theta_p}} \boldsymbol{\Psi}_p^\top \boldsymbol{\Psi}_q = \begin{cases} 1, & \text{if } p = q, \\ 0, & \text{otherwise.} \end{cases} \tag{B.10}$$

Assuming that the eigenvalues are sorted so that $\theta_1 \geq \cdots \geq \theta_P$, the dimension N is obtained as

$$N := \min\{p \in \{1{:}P\} \mid e_{\mathtt{POD}}(p) \leq \delta_{\mathtt{POD}}\}. \tag{B.11}$$

Finally, for all $n \in \{1{:}N\}$, the basis functions ξ_n are defined as follows:

$$\xi_n := \sum_{m\in\{1:\mathcal{N}^{\mathrm{HF}}\}} \boldsymbol{\Xi}_n^m \varphi_m \in V. \tag{B.12}$$

B.2 Cone Projected Greedy

In this section, we present the Cone Projected Greedy (CPG) [12] algorithm which is used for positive cone compression. Let $\mathcal{W}$ be a finite-dimensional (high-fidelity) subspace of dimension $\mathcal{R}^{\mathrm{HF}}$ (typically resulting from the finite element discretization of a Hilbert space) such that

$$\mathcal{W} := \boldsymbol{Span}\Big(\{\psi_r\}_{r\in\{1:\mathcal{R}^{\mathrm{HF}}\}}\Big). \tag{B.13}$$

We denote by $\langle\cdot,\cdot\rangle_{\mathcal{W}}$ the inner product equipping $\mathcal{W}$ and inducing the norm $\|\cdot\|_{\mathcal{W}}$. Let $\mathcal{W}^+ \subset \mathcal{W}$ be the positive cone defined as

$$\mathcal{W}^+ := \boldsymbol{Span}^+\Big(\{\psi_r\}_{r\in\{1:\mathcal{R}^{\mathrm{HF}}\}}\Big), \tag{B.14}$$

where, for an arbitrary family $\{\theta_q\}_{q\in\{1:Q\}} \subset \mathcal{W}^+$ with $Q \in \mathbb{N}^*$, $\boldsymbol{Span}^+\Big(\{\theta_q\}_{q\in\{1:Q\}}\Big)$ denotes the positive cone generated by setting

$$\boldsymbol{Span}^+\Big(\{\theta_q\}_{q\in\{1:Q\}}\Big) := \left\{ \sum_{q\in\{1:Q\}} \alpha_q\theta_q,\ (\alpha_1,\cdots,\alpha_Q) \in \mathbb{R}^Q_+ \right\}. \tag{B.15}$$

Let us consider a family $\{\lambda_p\}_{p\in\{1:P\}}$ of $P \in \mathbb{N}^*$ ($P \ll \mathcal{R}^{\mathrm{HF}}$) elements of $\mathcal{W}^+$ (typically snapshots computed on a training subset of the parametric domain) and let us set

$$W^+ := \boldsymbol{Span}^+\Big(\{\lambda_p\}_{p\in\{1:P\}}\Big) \subset \mathcal{W}^+. \tag{B.16}$$

Given a positive real number $\delta_{\texttt{CPG}} > 0$, the aim of the CPG algorithm is to select a subset $\{\upsilon_r\}_{r\in\{1:R\}}$ of $\{\lambda_p\}_{p\in\{1:P\}}$ composed of $R \in \mathbb{N}^*$ ($R \leq P$) vectors of W^+,

$$\{\upsilon_r\}_{r\in\{1:R\}} := \texttt{CPG}\Big(\{\lambda_p\}_{p\in\{1:P\}};\ \mathcal{W},\ \delta_{\texttt{CPG}}\Big) \tag{B.17}$$

satisfying

$$W^+_R := \boldsymbol{Span}^+\Big(\{\upsilon_r\}_{r\in\{1:R\}}\Big) \subset W^+, \tag{B.18a}$$

$$e_{\texttt{CPG}}(R) := \frac{\max\limits_{p\in\{1:P\}} \|(\mathbb{I}^{\mathcal{W}} - \Pi^{\mathcal{W}}_{W^+_R})(\lambda_p)\|_{\mathcal{W}}}{\max\limits_{p\in\{1:P\}} \|\lambda_p\|_{\mathcal{W}}} \leq \delta_{\texttt{CPG}}. \tag{B.18b}$$

For the algebraic formulation of the CPG algorithm, we adopt the following decomposition:

$$\lambda_p := \sum_{r\in\{1:\mathcal{R}^{\mathrm{HF}}\}} \boldsymbol{\Lambda}^r_p \psi_r, \quad \boldsymbol{\Lambda}_p := (\boldsymbol{\Lambda}^r_p)_{r\in\{1:\mathcal{R}^{\mathrm{HF}}\}} \in \mathbb{R}^{\mathcal{R}^{\mathrm{HF}}}_+. \tag{B.19}$$

Let us set

$$\boldsymbol{W}^+ := \boldsymbol{Span}^+\Big(\{\boldsymbol{\Lambda}_p\}_{p\in\{1:P\}}\Big) \subset \mathbb{R}^{\mathcal{R}^{\mathrm{HF}}}_+. \tag{B.20}$$

The algebraic counterpart of (B.17) is that given the family $\{\boldsymbol{\Lambda}_p\}_{p\in\{1:P\}} \subset \mathbb{R}^{\mathcal{R}^{\mathrm{HF}}}_+$, the CPG algorithm selects a subset $\{\boldsymbol{\Upsilon}_r\}_{r\in\{1:R\}}$ of $\{\boldsymbol{\Lambda}_p\}_{p\in\{1:P\}}$ composed of $R \in \mathbb{N}^*$ ($R \leq P$) vectors of $\boldsymbol{W}^+$,

$$\{\boldsymbol{\Upsilon}_r\}_{r\in\{1:R\}} := \texttt{CPG}\Big(\{\boldsymbol{\Lambda}_p\}_{p\in\{1:P\}};\ \mathcal{W},\ \delta_{\texttt{CPG}}\Big) \tag{B.21}$$

satisfying

$$\boldsymbol{W}_R^+ := \boldsymbol{Span}^+\Big(\{\boldsymbol{\Upsilon}_r\}_{r\in\{1:R\}}\Big) \subset \mathbb{R}_+^{\mathcal{R}^{\mathrm{HF}}}, \tag{B.22a}$$

$$e_{\mathtt{CPG}}(R) := \frac{\max\limits_{p\in\{1:P\}} \|(\mathbb{I}_{\mathcal{R}^{\mathrm{HF}}} - \Pi_{\boldsymbol{W}_R^+})(\boldsymbol{\Lambda}_p)\|_{\mathbb{W}}}{\max\limits_{p\in\{1:P\}} \|\boldsymbol{\Lambda}_p\|_{\mathbb{W}}} \leq \delta_{\mathtt{CPG}}, \tag{B.22b}$$

where $\mathbb{W} \in \mathbb{R}^{\mathcal{R}^{\mathrm{HF}}\times\mathcal{R}^{\mathrm{HF}}}$ denotes the Gram matrix associated with the inner product $\langle\cdot,\cdot\rangle_{\mathcal{W}}$.

Let us now describe the procedure for the construction of $\boldsymbol{W}_R^+$. The idea is to order the vectors $\boldsymbol{\Lambda}_p$ depending on their relevance to represent the entire family $\{\boldsymbol{\Lambda}_p\}_{p\in\{1:P\}}$. First, one chooses the vector $\boldsymbol{\Upsilon}_1 \in \{\boldsymbol{\Lambda}_p\}_{p\in\{1:P\}}$ such that

$$\boldsymbol{\Upsilon}_1 := \operatorname*{argmax}_{\boldsymbol{\Lambda}_p\in\{\boldsymbol{\Lambda}_p\}_{p\in\{1:P\}}} \|\boldsymbol{\Lambda}_p\|_{\mathbb{W}}. \tag{B.23}$$

Afterwards, at the iteration $r \geq 2$, one defines the positive cone

$$\boldsymbol{W}_r^+ := \boldsymbol{Span}^+\Big(\{\boldsymbol{\Upsilon}_k\}_{k\in\{1:r-1\}}\Big)$$

and selects the new vector using the following criterion:

$$\boldsymbol{\Upsilon}_r \in \operatorname*{argmax}_{p\{1:P\}} \|(\mathbb{I}_{\mathcal{R}^{\mathrm{HF}}} - \Pi_{\boldsymbol{W}_r^+})(\boldsymbol{\Lambda}_p)\|_{\mathbb{W}}. \tag{B.24}$$

One iterates until the following stopping criterion is fulfilled:

$$\frac{\max\limits_{p\in\{1:P\}} \|(\mathbb{I}_{\mathcal{R}^{\mathrm{HF}}} - \Pi_{\boldsymbol{W}_r^+})(\boldsymbol{\Lambda}_p)\|_{\mathbb{W}}}{\max\limits_{p\in\{1:P\}} \|\boldsymbol{\Lambda}_p\|_{\mathbb{W}}} \leq \delta_{\mathtt{CPG}}, \tag{B.25}$$

and, the dimension R is set as the final iteration number. Finally, for all $r \in \{1{:}R\}$, the basis functions υ_r are defined as follows:

$$\upsilon_r := \sum_{s\in\{1:\mathcal{R}^{\mathrm{HF}}\}} \boldsymbol{\Upsilon}_r^s \psi_s \in \mathcal{W}. \tag{B.26}$$

B.3 Empirical Interpolation Method

In this section, we present the Empirical Interpolation Method (EIM) [10, 75] which is used for the so-called affine parametric decomposition of parameter-dependent applications. Originally, the EIM was introduced to approximate a continuous bivariate function. Here, we present the method in the context of the affine decomposition of a large-dimensional parameter-dependent matrix (typically resulting from the algebraic representation of a high-fidelity, parameter-dependent operator). The objective is to separate in a progressive way the dependency on the parameter from the dependency on the indices of the matrix. Let $\mathcal{D} \subset \mathbb{R}^m, m \in \mathbb{N}^*$, be the parameter domain. We consider a matrix $A(\mu) \in \mathbb{R}^{\mathcal{N}^{\mathrm{HF}}\times\mathcal{R}^{\mathrm{HF}}}$ for all $\mu \in \mathcal{D}$. Given a positive real number $\delta_{\mathtt{EIM}} > 0$, the EIM approximates the matrix $A(\mu)$ by a matrix $E^a(\mu)$ such that

$$A(\mu) \approx E^a(\mu) := \sum_{j\in\{1:J^a\}} \alpha_j^a(\mu) A_j, \quad A_j \in \mathbb{R}^{\mathcal{N}^{\mathrm{HF}}\times\mathcal{R}^{\mathrm{HF}}},\ \alpha_j^a(\mu) \in \mathbb{R},\ J^a \in \mathbb{N}^*, \tag{B.27}$$

satisfying

$$e^a_{\texttt{EIM}}(J^a) := \frac{\max\limits_{\mu\in\mathcal{D}_{\texttt{train}}} \|A(\mu) - E^a(\mu)\|_{\ell^\infty(ij)}}{\max\limits_{\mu\in\mathcal{D}_{\texttt{train}}} \|A(\mu)\|_{\ell^\infty(ij)}} \leq \delta_{\texttt{EIM}}, \tag{B.28}$$

where for a generic matrix $K \in \mathbb{R}^{\mathcal{N}^{\rm HF}\times\mathcal{R}^{\rm HF}}$,

$$\|K\|_{\ell^\infty(nm)} := \max_{(n,m)\in\{1:\mathcal{N}^{\rm HF}\}\times\{1:\mathcal{R}^{\rm HF}\}} |K_{nm}|. \tag{B.29}$$

The order (rank) of the approximation J^a is the number of iterations performed by the EIM when the stopping criterion is satisfied. The functions $\alpha^a_j : \mathcal{D} \to \mathbb{R}$ only depend on μ. The large-dimensional parameter-independent matrices A_j are obtained from the family of matrices $\{A(\mu)\}_{\mu\in\mathcal{D}_{\texttt{train}}}$, where $\mathcal{D}_{\texttt{train}} \subset \mathcal{D}$ is a training subset of relatively small cardinality.

Let us now described the procedure for the construction of the interpolation operator E^a. Let us denote by E^a_j the interpolation operator constructed at iteration $j \geq 0$ of the EIM with the convention $E^a_0 := 0 \in \mathbb{R}^{\mathcal{N}^{\rm HF}\times\mathcal{R}^{\rm HF}}$. At iteration $j \geq 1$, one first selects the parameter $\mu_j \in \mathcal{D}_{\texttt{train}}$ such that

$$\mu_j \in \operatorname*{argmax}_{\mu\in\mathcal{D}_{\texttt{train}}} \|A(\mu) - E^a_{j-1}(\mu)\|_{\ell^\infty(nm)}. \tag{B.30}$$

Once the parameter μ_j is selected, one seeks the pair of indices $(n_j, m_j) \in \{1{:}\mathcal{N}^{\rm HF}\} \times \{1{:}\mathcal{R}^{\rm HF}\}$ such that

$$(n_j, m_j) \in \operatorname*{argmax}_{(n,m)\in\{1:\mathcal{N}^{\rm HF}\}\times\{1:\mathcal{R}^{\rm HF}\}} |(A(\mu_j) - E^a_{j-1}(\mu_j))_{nm}|. \tag{B.31}$$

One then checks whether or not the stopping criterion $e^a_{\texttt{EIM}}(j) \leq \delta_{\texttt{EIM}}$ is satisfied, where the interpolation error $e^a_{\texttt{EIM}}(j)$ is defined as

$$e^a_{\texttt{EIM}}(j) := \frac{|(A(\mu_j) - E^a_{j-1}(\mu_j))_{m_j n_j}|}{|(A(\mu_1))_{m_1 n_1}|}. \tag{B.32}$$

If this criterion is not satisfied, one enriches the interpolation basis with the matrix

$$A_j := \frac{A(\mu_j) - E^a_{j-1}(\mu_j)}{(A(\mu_j) - E^a_{j-1}(\mu_j))_{m_j n_j}} \in \mathbb{R}^{\mathcal{N}^{\rm HF}\times\mathcal{R}^{\rm HF}}, \tag{B.33}$$

and computes an additional row of the interpolation matrix $Q^a_j \in \mathbb{R}^{j\times j}$ by setting

$$(Q^a_j)_{ji} := (A_i)_{m_j n_j}, \quad \forall i \in \{1{:}j\}. \tag{B.34}$$

Afterwards, the new interpolation matrix E^a_j is defined as

$$E^a_j(\mu) := \sum_{i\in\{1:j\}} \alpha^a_i(\mu) A_i, \quad \forall \mu \in \mathcal{D}_{\texttt{train}}, \tag{B.35}$$

where the interpolation coefficients α^a_i solve the linear system

$$Q^a_j(\alpha^a_i(\mu))_{i\in\{1:j\}} = \Big((A(\mu))_{m_i n_i}\Big)_{i\in\{1:j\}} \in \mathbb{R}^j, \quad \forall \mu \in \mathcal{D}_{\texttt{train}}. \tag{B.36}$$

The construction of the EIM approximation described above satisfies two properties:

1. The matrices $\{A_i\}_{i\in\{1:j\}}$ are linearly independent.
2. The interpolation matrices Q^a_j are lower-triangular with unit diagonal and therefore invertible.

BIBLIOGRAPHY

[1] M. Abbas, G. Drouet, and P. Hild. The local average contact (LAC) method. *Comput. Methods Appl. Mech. Engrg.*, 339:488–513, 2018.

[2] S. Ali, F. Ballarin, and G. Rozza. Stabilized reduced basis methods for parametrized steady Stokes and Navier-Stokes equations. *Comput. Math. Appl.*, 80(11):2399–2416, 2020.

[3] D. Amsallem and C. Farhat. An online method for interpolating linear parametric reduced-order models. *SIAM J. Sci. Comput.*, 33(5):2169–2198, 2011.

[4] M. S. Andersen, J. Dahl, and L. Vandenberghe. Cvxopt: A python package for convex optimization. Open source on `http://www.abel.ee.ucla.edu/cvxopt`, 2008.

[5] E. Bader, Z. Zhang, and K. Veroy. An empirical interpolation approach to reduced basis approximations for variational inequalities. *Math. Comput. Model. Dyn. Syst.*, 22(4):345–361, 2016.

[6] L. Baillet and T. Sassi. Mixed finite element methods for the Signorini problem with friction. *Numer. Methods Partial Differential Equations*, 22(6):1489–1508, 2006.

[7] A. Bakhta, T. Boiveau, Y. Maday, and O. Mula. Epidemiological forecasting with model reduction of compartmental models. Application to the covid-19 pandemic. *Biology*, 10(1):22, 2020.

[8] M. Balajewicz, D. Amsallem, and C. Farhat. Projection-based model reduction for contact problems. *Internat. J. Numer. Methods Engrg.*, 106(8):644–663, 2016.

[9] F. Ballarin, A. Manzoni, A. Quarteroni, and G. Rozza. Supremizer stabilization of POD-Galerkin approximation of parametrized steady incompressible Navier-Stokes equations. *Internat. J. Numer. Methods Engrg.*, 102(5):1136–1161, 2015.

[10] M. Barrault, Y. Maday, N. C. Nguyen, and A. T. Patera. An 'empirical interpolation' method: application to efficient reduced-basis discretization of partial differential equations. *C. R. Math. Acad. Sci. Paris*, 339(9):667–672, 2004.

[11] A. Benaceur. *Réduction de modèles en thermo-mécanique*. PhD thesis, University Paris Est, 2018.

[12] A. Benaceur, A. Ern, and V. Ehrlacher. A reduced basis method for parametrized variational inequalities applied to contact mechanics. *Internat. J. Numer. Methods Engrg.*, 121(6):1170–1197, 2020.

[13] P. Binev, A. Cohen, W. Dahmen, R. DeVore, G. Petrova, and P. Wojtaszczyk. Convergence rates for greedy algorithms in reduced basis methods. *SIAM J. Math. Anal.*, 43(3):1457–1472, 2011.

[14] D. Braess. *Finite Elements*. Cambridge University Press, Cambridge, 1997.

[15] S. C. Brenner and L. R. Scott. *The Mathematical Theory of Finite Element Methods*, volume 15 of *Texts in Applied Mathematics*. Springer, New York, third edition, 2008.

[16] H. Brézis. Problèmes unilatéraux. *J. Math. Pures Appl. (9)*, 51:1–168, 1972.

[17] F. Brezzi, W. W. Hager, and P.-A. Raviart. Error estimates for the finite element solution of variational inequalities. II. Mixed methods. *Numer. Math.*, 31(1):1–16, 1978/79.

[18] A. Buffa, Y. Maday, A. T. Patera, C. Prud'homme, and G. Turinici. *A priori* convergence of the greedy algorithm for the parametrized reduced basis method. *ESAIM Math. Model. Numer. Anal.*, 46(3):595–603, 2012.

[19] O. Burkovska, B. Haasdonk, J. Salomon, and B. Wohlmuth. Reduced basis methods for pricing options with the Black-Scholes and Heston models. *SIAM J. Financial Math.*, 6(1):685–712, 2015.

[20] A. Capatina. *Variational Inequalities and Frictional Contact Problems*, volume 31 of *Advances in Mechanics and Mathematics*. Springer, Cham, 2014.

[21] K. Carlberg, C. Bou-Mosleh, and C. Farhat. Efficient non-linear model reduction via a least-squares Petrov-Galerkin projection and compressive tensor approximations. *Internat. J. Numer. Methods Engrg.*, 86(2):155–181, 2011.

[22] A. Chatterjee. An introduction to the proper orthogonal decomposition. *Current Science*, pp. 808–817, 2000.

[23] F. Chinesta, P. Ladeveze, and E. Cueto. A short review on model order reduction based on proper generalized decomposition. *Arch. Comput. Methods Eng.*, 18(4):395–404, 2011.

[24] F. Chouly. An adaptation of Nitsche's method to the Tresca friction problem. *J. Math. Anal. Appl.*, 411(1):329–339, 2014.

[25] F. Chouly, A. Ern, and N. Pignet. A hybrid high-order discretization combined with Nitsche's method for contact and Tresca friction in small strain elasticity. *SIAM J. Sci. Comput.*, 42(4):A2300–A2324, 2020.

[26] F. Chouly, M. Fabre, P. Hild, R. Mlika, J. Pousin, and Y. Renard. An overview of recent results on Nitsche's method for contact problems. volume 121 of *Lect. Notes Comput. Sci. Eng.*, pp. 93–141. Springer, Cham, 2017.

[27] F. Chouly and P. Hild. A Nitsche-based method for unilateral contact problems: numerical analysis. *SIAM J. Numer. Anal.*, 51(2):1295–1307, 2013.

[28] F. Chouly, P. Hild, V. Lleras, and Y. Renard. Nitsche method for contact with Coulomb friction: existence results for the static and dynamic finite element formulations. *J. Comput. Appl. Math.*, 416, 2022.

[29] F. Chouly, P. Hild, and Y. Renard. Symmetric and non-symmetric variants of Nitsche's method for contact problems in elasticity: theory and numerical experiments. *Math. Comp.*, 84(293):1089–1112, 2015.

[30] P. G. Ciarlet. *The Finite Element Method for Elliptic Problems*, volume 40 of *Classics in Applied Mathematics*. Society for Industrial and Applied Mathematics (SIAM), Philadelphia, PA, 2002.

[31] A. Curnier and P. Alart. A generalized Newton method for contact problems with friction. *J. Méc. Théor. Appl.*, 7(suppl. 1):67–82, 1988.

[32] W. Dahmen, C. Plesken, and G. Welper. Double greedy algorithms: Reduced basis methods for transport dominated problems. *ESAIM Math. Model. Numer. Anal.*, 48(3):623–663, 2014.

[33] G. Drouet. *Méthode locale de type mortar pour le contact dans le cas de maillages incompatibles de degré élevé*. PhD thesis, University Toulouse 3, 2015.

[34] G. Duvaut. Problèmes unilatéraux en mécanique des milieux continus. In *Actes du Congrès International des Mathématiciens (Nice, 1970), Tome 3*, pp. 71–77. 1971.

[35] G. Duvaut and J.-L. Lions. *Les inéquations en mécanique et en physique*. Travaux et Recherches Mathématiques, No. 21. Dunod, Paris, 1972.

[36] I. Ekeland and R. Temam. *Convex Analysis and Variational Problems*, volume 28 of *Classics in Applied Mathematics*. Society for Industrial and Applied Mathematics (SIAM), Philadelphia, PA, 1999.

[37] D. F. Enns. Model reduction with balanced realizations: An error bound and a frequency weighted generalization. In *The 23rd IEEE conference on decision and control*, pp. 127–132. IEEE, 1984.

[38] A. Ern and J.-L. Guermond. *Theory and Practice of Finite Elements*, volume 159 of *Applied Mathematical Sciences*. Springer-Verlag, New York, 2004.

[39] R. S. Falk. Error estimates for the approximation of a class of variational inequalities. *Math. Comput.*, 28:963–971, 1974.

[40] J. Fauque, I. Ramière, and D. Ryckelynck. Hybrid hyper-reduced modeling for contact mechanics problems. *Internat. J. Numer. Methods Engrg.*, 115(1):117–139, 2018.

[41] G. Fichera. Problemi elastostatici con vincoli unilaterali: Il problema di Signorini con ambigue condizioni al contorno. *Atti Accad. Naz. Lincei Mem. Cl. Sci. Fis. Mat. Natur. Sez. Ia (8)*, 7:91–140, 1963/64.

[42] G. Fichera. Elastostatics problems with unilateral constraints: The Signorini problem with ambiguous boundary conditions. pp. 613–679. Ediz. Cremonese, Rome, 1965.

[43] G. Fichera. The Italian contribution to the mathematical theory of elasticity. *Meccanica–J. Italian Assoc. Theoret. Appl. Mech.*, 19(4):259–268, 1984.

[44] M. Fortin and R. Glowinski. *Augmented Lagrangian methods*, volume 15 of *Studies in Mathematics and its Applications*. North-Holland Publishing Co., Amsterdam, 1983. Applications to the numerical solution of boundary value problems, Translated from the French by B. Hunt and D. C. Spicer.

[45] S. Fučík, A. Kratochvíl, and J. Nečas. Kačanov-Galerkin method and its application. *Acta Univ. Carolin. Math. Phys.*, 15(1-2):31–33, 1974.

[46] A.-L. Gerner and K. Veroy. Certified reduced basis methods for parametrized saddle point problems. *SIAM J. Sci. Comput.*, 34(5):A2812–A2836, 2012.

[47] A. Giacoma, D. Dureisseix, and A. Gravouil. An efficient quasi-optimal space-time PGD application to frictional contact mechanics. *Adv. Model. Simul. Eng. Sci.*, 3(1):12, 2016.

[48] A. Giacoma, D. Dureisseix, A. Gravouil, and M. Rochette. A multiscale LATIN/-FAS algorithm with time-space model reduction for frictional contact problems. *Internat. J. Numer. Methods Engrg.*, 97(3):207–230, 2014.

[49] S. Glas and K. Urban. On noncoercive variational inequalities. *SIAM J. Numer. Anal.*, 52(5):2250–2271, 2014.

[50] S. Glas and K. Urban. Numerical investigations of an error bound for reduced basis approximations of noncoercice variational inequalities. *IFAC-PapersOnLine*, 48:721–726, 2015.

[51] R. Glowinski. *Numerical Methods for Nonlinear Variational Problems*. Scientific Computation. Springer-Verlag, Berlin, 2008.

[52] R. Glowinski, J.-L. Lions, and R. Trémolières. *Numerical Analysis of Variational Inequalities*, volume 8 of *Studies in Mathematics and its Applications*. North-Holland Publishing Co., Amsterdam-New York, 1981.

[53] R. J. Guyan. Reduction of stiffness and mass matrices. *AIAA journal*, 3(2):380–380, 1965.

[54] B. Haasdonk. Convergence rates of the POD-greedy method. *ESAIM Math. Model. Numer. Anal.*, 47(3):859–873, 2013.

[55] B. Haasdonk, J. Salomon, and B. Wohlmuth. A reduced basis method for parametrized variational inequalities. *SIAM J. Numer. Anal.*, 50(5):2656–2676, 2012.

[56] F. Hecht. New development in freefem++. *J. Numer. Math.*, 20(3-4):251–265, 2012.

[57] H. Hertz. Ueber die Berührung fester elastischer Körper. *J. Reine Angew. Math.*, 92:156–171, 1882.

[58] J. S. Hesthaven, G. Rozza, and B. Stamm. *Certified Reduced Basis Methods for Parametrized Partial Differential Equations*. SpringerBriefs in Mathematics. Springer, Cham; BCAM Basque Center for Applied Mathematics, Bilbao, 2016.

[59] P. Hild and Y. Renard. Local uniqueness and continuation of solutions for the discrete Coulomb friction problem in elastostatics. *Quart. Appl. Math.*, 63(3):553–573, 2005.

[60] I. Hlaváček, J. Haslinger, J. Nečas, and J. Lovíšek. *Solution of Variational Inequalities in Mechanics*, volume 66 of *Applied Mathematical Sciences*. Springer-Verlag, New York, 1988.

[61] K. Ito and K. Kunisch. *Lagrange Multiplier Approach to Variational Problems and Applications*, volume 15 of *Advances in Design and Control*. Society for Industrial and Applied Mathematics (SIAM), Philadelphia, PA, 2008.

[62] K. L. Johnson. *Contact mechanics*. Cambridge University Press, 1987.

[63] M. Jünger, G. Reinelt, and S. Thienel. Practical problem solving with cutting plane algorithms in combinatorial optimization. In *Combinatorial optimization (New Brunswick, NJ, 1992–1993)*, volume 20 of *DIMACS Ser. Discrete Math. Theoret. Comput. Sci.*, pp. 111–152. Amer. Math. Soc., Providence, RI, 1995.

[64] N. Kikuchi and J. T. Oden. *Contact Problems in Elasticity: A Study of Variational Inequalities and Finite Element Methods*, volume 8 of *SIAM Studies in Applied Mathematics*. Society for Industrial and Applied Mathematics (SIAM), Philadelphia, PA, 1988.

[65] D. Kinderlehrer and G. Stampacchia. *An Introduction to Variational Inequalities and their Applications*, volume 31 of *Classics in Applied Mathematics*. Society for Industrial and Applied Mathematics (SIAM), Philadelphia, PA, 2000.

[66] I. V. Konnov. *Equilibrium Models and Variational Inequalities*, volume 210 of *Mathematics in Science and Engineering*. Elsevier B. V., Amsterdam, 2007.

[67] A. S. Kravchuk and P. J. Neittaanmäki. *Variational and Quasi-Variational Inequalities in Mechanics*, volume 147 of *Solid Mechanics and its Applications*. Springer, Dordrecht, 2007.

[68] A. D. Kudawoo. *Problèmes industriels de grande dimension en mécanique numérique du contact : performance, fiabilité et robustesse.* PhD thesis, University Aix-Marseille, 2012.

[69] K. Kunisch and S. Volkwein. Galerkin proper orthogonal decomposition methods for parabolic problems. *Numer. Math.*, 90(1):117–148, 2001.

[70] P. Ladevèze, J.-C. Passieux, and D. Néron. The LATIN multiscale computational method and the proper generalized decomposition. *Comput. Methods Appl. Mech. Engrg.*, 199(21-22):1287–1296, 2010.

[71] T. A. Laursen. *Computational Contact and Impact Mechanics*. Springer-Verlag, Berlin, 2002. Fundamentals of modeling interfacial phenomena in nonlinear finite element analysis.

[72] D. D. Lee and H. S. Seung. Algorithms for nn-negative matrix factorization. NIPS'00, pp. 535–541. MIT Press, Cambridge, MA, USA, 2000.

[73] J.-L. Lions. *Quelques Méthodes de Résolution des Problèmes aux Limites Non Linéaires*. Dunod, Paris; Gauthier-Villars, Paris, 1969.

[74] J.-L. Lions and G. Stampacchia. Variational inequalities. *Comm. Pure Appl. Math.*, 20:493–519, 1967.

[75] Y. Maday, N. C. Nguyen, A. T. Patera, and G. S. H. Pau. A general multipurpose interpolation procedure: the magic points. *Commun. Pure Appl. Anal.*, 8(1):383–404, 2009.

[76] Y. Maday, A. T. Patera, and G. Turinici. A priori convergence theory for reduced-basis approximations of single-parameter elliptic partial differential equations. volume 17, pp. 437–446, 2002.

[77] R. Mlika, Y. Renard, and F. Chouly. An unbiased Nitsche's formulation of large deformation frictional contact and self-contact. *Comput. Methods Appl. Mech. Engrg.*, 325:265–288, 2017.

[78] R. Monneau. A brief overview on the obstacle problem. volume 202 of *Progr. Math.*, pp. 303–312. Birkhäuser, Basel, 2001.

[79] B. C. Moore. Principal component analysis in linear systems: controllability, observability, and model reduction. *IEEE Trans. Automat. Control*, 26(1):17–32, 1981.

[80] U. Mosco. An introduction to the approximate solution of variational inequalities. In *Constructive Aspects of Functional Analysis*, volume Erice 1971, pp. 497–684. Ed. Cremonese, 1973.

[81] U. Mosco. Implicit variational problems and quasi variational inequalities. pp. 83–156. Lecture Notes in Math., Vol. 543. 1976.

[82] A. Nagurney. Finance and variational inequalities. *Quant. Finance*, 1(3):309–317, 2001.

[83] D. Néron and P. Ladevèze. Proper generalized decomposition for multiscale and multiphysics problems. *Arch. Comput. Methods Eng.*, 17(4):351–372, 2010.

[84] I. Niakh, G. Drouet, V. Ehrlacher, and A. Ern. Stable model reduction for linear variational inequalities with parameter-dependent constraints. M2AN, to appear, `https://hal.archives-ouvertes.fr/hal-03611982`, March 2022.

[85] J. Nitsche. Über ein Variationsprinzip zur Lösung von Dirichlet-Problemen bei Verwendung von Teilräumen, die keinen Randbedingungen unterworfen sind. *Abh. Math. Sem. Univ. Hamburg*, 36:9–15, 1971.

[86] P. D. Panagiotopoulos. *Inequality Problems in Mechanics and Applications*. Birkhäuser Boston, Inc., Boston, MA, 1985.

[87] J. S. Peterson. The reduced basis method for incompressible viscous flow calculations. *SIAM J. Sci. Statist. Comput.*, 10(4):777–786, 1989.

[88] R. Plassart. *Modélisation hydromécanique du comportement des ouvrages souterrains avec un modèle élastoviscoplastique*. PhD thesis, Institut National Polytechnique de Lorraine, 2011, 2011.

[89] T. A. Porsching. Estimation of the error in the reduced basis method solution of nonlinear equations. *Math. Comp.*, 45(172):487–496, 1985.

[90] C. Prud'homme, D. V. Rovas, K. Veroy, L. Machiels, Y. Maday, A. T. Patera, and G. Turinici. Reliable real-time solution of parametrized partial differential equations: Reduced-basis output bound methods. *J. Fluids Eng.* , 124(1):70–80, 2001.

[91] Z.-Q. Qu. *Model Order Reduction Techniques*. Springer-Verlag London, Ltd., London, 2004.

[92] A. Quarteroni, A. Manzoni, and F. Negri. *Reduced Basis Methods for Partial Differential Equations*, volume 92 of *Unitext*. Springer, Cham, 2016.

[93] Y. Renard and K. Poulios. GetFEM: Automated FE modeling of multiphysics problems based on a generic weak form language. 2020.

[94] A. Ribes and C. Caremoli. Salomé platform component model for numerical simulation. volume 2, pp. 553–564, 2007.

[95] G. Rozza, D. B. P. Huynh, and A. Manzoni. Reduced basis approximation and a posteriori error estimation for Stokes flows in parametrized geometries: roles of the inf-sup stability constants. *Numer. Math.*, 125(1):115–152, 2013.

[96] G. Rozza and K. Veroy. On the stability of the reduced basis method for Stokes equations in parametrized domains. *Comput. Methods Appl. Mech. Engrg.*, 196(7):1244–1260, 2007.

[97] W. H. A. Schilders, H. A. van der Vorst, and J. Rommes, editors. *Model Order Reduction: Theory, Research Aspects and Applications*, volume 13 of *Mathematics in Industry*. Springer-Verlag, Berlin, 2008.

[98] A. Signorini. Sopra alcune questioni di statica dei sistemi continui. *Ann. Scuola Norm. Super. Pisa Cl. Sci. (2)*, 2(2):231–251, 1933.

[99] M. Sofonea and A. Matei. *Mathematical models in contact mechanics*, volume 398. Cambridge University Press, 2012.

[100] G. Stampacchia. Formes bilinéaires coercitives sur les ensembles convexes. *C. R. Acad. Sci. Paris*, 258:4413–4416, 1964.

[101] G. Stampacchia. Variational Inequalities. pp. 101–192. Edizioni "Oderisi", Gubbio, 1969.

[102] K. Willcox and J. Peraire. Balanced model reduction via the proper orthogonal decomposition. *AIAA Journal*, 40(11):2323–2330, 2002.

[103] P. Wriggers. Finite element algorithms for contact problems. *Arch. Comput. Methods Engrg.*, 2(4):1–49, 1995.

[104] P. Wriggers. *Computational Contact Mechanics*, volume 2. Springer Berlin, Heidelberg, 2006.

[105] Z. Zhang, E. Bader, and K. Veroy. A slack approach to reduced-basis approximation and error estimation for variational inequalities. *C. R. Math. Acad. Sci. Paris*, 354(3):283–289, 2016.